

**ENGINEERING OF POLY(2-OXAZOLINE)S
FOR A POTENTIAL USE IN
BIOMEDICAL APPLICATIONS**

by

Camille Legros

A thesis
presented to the University of Waterloo,
Université de Liege and Université de Bordeaux
in fulfillment of the
thesis requirement for the degree of
Doctor of Philosophy
in
Chemical Engineering (Nanotechnology)

Waterloo, Ontario, Canada, 2015

© Camille Legros 2015

'I hereby declare that I am the sole author of this thesis. This is a true copy of the thesis, including any required final revisions, as accepted by my examiners.

I understand that my thesis may be made electronically available to the public.'

Abstract

Résumé: Ce travail décrit d'abord l'élaboration de nanogels hydrophiles stimulables, sensibles à un changement de pH et à un environnement où les propriétés d'oxydo-réduction peuvent varier. Ils ont été synthétisés en milieu dilué, d'une part, et en émulsion inverse, d'autre part; dans les deux cas à partir d'un copolymère statistique composé d'unités 2-éthyl-2-oxazoline et éthylène imine. Ces nanogels n'ont pas montré d'interactions spécifiques avec des protéines telles que la BSA et se sont avérés non-toxiques *in vitro*. Une plateforme à base d'un copolymère POx statistique porteur de fonctions aldéhydes a par ailleurs permis d'accéder à une librairie de POx, incluant des structures greffées et réticulées. Enfin, l'auto-assemblage en solution d'un copolymère à blocs de type poly(2-méthyl-oxazoline)-*b*-poly(2-isopropyl-2-oxazoline) (PMeOx-*b*-PiPrOx), a été étudié en détail. Des micelles ont été observées à des temps courts au-dessus du point trouble du PiPrOx. Pour des temps plus longs, la formation de fibres et de micelles réticulées physiquement ont été mise en évidence, comportement expliqué par la cristallisation des chaînes de PiPrOx stabilisées par les blocs PMeOx hydrophiles.

Mots clés: poly(2-oxazoline), nanogel, hydrogel, stimuable, cristallisation, point trouble, aldéhyde, cytotoxicité.

Abstract: This PhD work is based on the design of poly(2-oxazoline) (POx) hydrogels and nanogels, by chemical or physical cross-linking, aimed to be used for biomedical applications. Nanogels were first prepared in dilute media and in inverse emulsion based on a statistical copolymer made of 2-ethyl-2-oxazoline and ethylene imine units. These stimuli-responsive nanogels were swelling in acidic media and were cleaved in reductive environment. They proved to be non-cytotoxic and act as protein repellent. Second, a reactive platform based on a statistical POx polymer bearing aldehyde functionalities was engineered, enabling the synthesis of graft and cross-linked POx. Last, a block copolymer made of 2-methyl- and 2-isopropyl-2-oxazoline units, proved to self-assemble into micelles when heated above its LCST, for a short period of time (< 1h30). When annealed for a longer time (> 1h30), crystallization-driven self-assembly led to the formation of different morphologies (fiber rods and cross-linked micelles).

Keywords : poly(2-oxazoline), nanogel, hydrogel, responsive, crystallization, LCST, post-polymerization modification, aldehyde, cytotoxicity, protein repellent.

Université de Bordeaux, Laboratoire de chimie des polymères organiques (LCPO), UMR 5629, 16 avenue Pey Berland, 33607 Pessac Cedex, France // University of Waterloo, 200 University Avenue West, Waterloo, Ontario, N2L 3G1, Canada // Université de Liège, Mammalian Cell Culture Laboratory, Allée de la Chimie 3 Sart Tilman, 4000 Liège, Belgique

ACKNOWLEDGMENTS/REMERCIEMENTS

This PhD project has been realized within the frame of the IDS FunMat program and was funded by the Erasmus Mundus Program of the European Union. It gave me the opportunity to work at three different universities, in three different countries: the University of Bordeaux, France, where I worked at the « Laboratoire de Chimie des polymères Organiques » (LCPO), the University of Waterloo, Canada and the University of Liège, Belgium.

First, I would like to thank the jury members, Pr. Catherine Amiel, Pr. Richard Hoogenboom, Pr. Mario Gauthier and Pr. Stéphane Carlotti for accepting to go through my work so carefully and for the fruitful discussion we had during my defense.

I would like to express my sincere gratitude and appreciation to Pr. Daniel Taton, Pr. Sébastien Lecommandoux, Pr. Michael Tam and Dr. Marie-Claire Gillet de Pauw for trusting me by giving me the opportunity to lead this PhD project. Each of you had a different way to support and direct me during these four years, which were all very complementary and key for me.

Lors de cette thèse, j'ai tout d'abord été accueillie au LCPO, à Bordeaux. Je tiens à remercier chaleureusement le Pr. Henri Cramail, directeur du LCPO, pour m'avoir permis d'intégrer cette grande famille qu'est le LCPO, et pour le regard bienveillant qu'il porte sur l'ensemble des doctorants. Daniel, Sébastien, je suis simplement heureuse d'avoir pu travailler avec vous durant ces 4 années. Vous étiez toujours à la bonne place : m'aidant énormément à définir mon sujet de thèse au début, puis me donnant des coups de pouce réguliers qui ont permis de débloquer beaucoup de choses et d'ouvrir énormément ce projet grâce à vos connaissances très complémentaires et votre rigueur scientifique commune. J'ai été très sensible à votre implication totale dans un projet qui n'était pas au départ le Coeur de votre recherche, ainsi qu'à votre disponibilité, votre optimisme et votre bienveillance. Daniel, merci de m'avoir donné goût à cette chimie, c'était une belle découverte que je ne regrette pas. Sébastien, merci d'entretenir cette atmosphère si familiale et amicale qui règne au N2, cette cohésion que tu arrives à créer rend le travail au quotidien tellement agréable et a été pour moi une vraie source d'épanouissement autant du point de vue scientifique qu'humain. Merci à tous les deux d'avoir cru en moi. J'ai grandi pendant cette thèse et c'est en majeure partie grâce à vous.

Michael, I want to thank you for your support while I was in Canada. I learnt a lot during my time there, discovering a new work environment and new ways to grasp what a PhD is about. Thank you for your patience and time. You were always paying attention to the small details in order to get to « the big picture », which gave value to my work and also made me more confident. I am also really thankful for the

scientific freedom you let me have, to choose the direction of my work and I really appreciated it.

Marie-Claire, je vous remercie pour votre enthousiasme et votre efficacité. Vous aviez très gentiment accepté de faire partie de cette aventure, et vous vous y êtes pleinement impliquée à chacun de mes passages à Liège ! Vous étiez toujours extrêmement disponible ce qui m'a permis d'être très efficace. Merci également d'avoir pris le temps de me faire découvrir et comprendre une partie de ce qui se cache derrière les « sciences biomédicales ». J'ai été profondément heureuse de pouvoir mener mon projet jusque là, et de le faire avec votre aide. Je vous remercie pour la confiance et le soutien que vous m'avez apportés.

Je tiens également à remercier différents acteurs du programme IDS FunMat : Laurent Servant, Thierry Tassaing, Stéphane Carlotti, Audrey Sidobre. Vous étiez toujours à veiller sur nous, et prêts à trouver des solutions pour nous rendre la vie de « doctorant mobile » plus facile.

Durant ces travaux de thèse, j'ai eu la chance de collaborer au LCPO avec des personnes indispensables: Nico, the « SECs master », je te remercie pour ton aide précieuse et pour ta bonne humeur permanente! Anne-Laure, Manu, merci de m'avoir fait profiter respectivement de votre expertise en RMN et en imagerie AFM. Merci à Catherine, Corinne, Bernadette, Nicole et Loïc qui travaillent « dans l'ombre », s'assurant du bon fonctionnement quotidien du labo et nous permettant d'être au top de l'efficacité !

Je tiens également à remercier Colin, qui a su me transmettre sa curiosité débordante et me redonner espoir plus d'une fois ! Nos discussions étaient précieuses. Enfin, un très grand merci à tous ceux qui ont participé au bonheur de ces 4 années, partageant les galères, les pauses café et lunchs au CAES, les soirées déguisées et conf à l'autre bout du monde : Charlotte (the one and only !), Lise (« découverte » tardive mais profonde. Merci pour ton soutien et ton amitié), Annie & An (you both were the energy of my last year ! « Thuck you ! »), Silvia (ah, ce sourire, cette bonne humeur et ce calme m'ont fait du bien plus d'une fois, merci !), Aurélien (mon premier soutien !), Maïté (Merci de nous avoir pris sous ton aile dès notre arrivée). Je remercie également nos post-docs en or : Julie, Hugo, Colin, Yannick, Karine (Merci pour ton aide précieuse pour tous ces gels SDS-PAGE) mais aussi Floraine, Loïc et plus récemment Kevin, Hélène et Cony. Merci à la « DT team »: Maréva (l'indispensable pionnière), Paul & Winnie (j'ai été ravie de partager cette dernière ligne droite avec vous, et vive San Francisco !). *Special thanks to my IDS « traveller » friends: Dan (Thank you for this awesome year in Canada, without you the story would have been completely different), Edgar (thank you for paying so much attention to others), Uyxing (on peut dire que l'on se sera bien serré les coudes !), Mathilde (je garde un très bon souvenir de ces quelques moments à Liège et à Roubaix !), Deniz, Yi-shang. Merci aux anciens: Laure, Romain, Antoine, Katerina, Chantal, Stéphanie, Maud, Audrey, Jules, Carine, Samira, et bon vent à ceux pour qui ce n'est pas fini:*

Rosine, Ariane, Gauvin, Blandine, Estelle, Elise, Mathilde, Tuyen, Vusala, Marie, Déborah, Océane, Geoffrey, Mikael, Alex, Olivia, Kevin et à tous ceux que j'ai pu oublier, c'était une formidable aventure.

Je tiens à remercier mes amis de longue date, « Les jeunes », leur soutien précieux m'apportait toujours la bouffée d'oxygène nécessaire et me permettait de décompresser le temps d'un court séjour à Paris ou Bergerac. J'espère que mon nouveau quotidien en sera plus amplement rythmé!

Enfin, je remercie profondément mes parents, Marie et Jean-philippe et ma soeur, Pauline. Votre soutien indéfectible pendant ces 4 ans (et bien avant!) m'a été très cher et je sais que sans votre amour je n'en serais pas là aujourd'hui. Romain, merci d'être à mes côtés depuis toutes ces années, de me soutenir et de m'encourager. Merci de m'avoir laissé ma liberté dans mes choix (une thèse entre 3 pays ce n'était pas un cadeau!), et maintenant voyageons !

Camille

TABLE OF CONTENT

GENERAL INTRODUCTION.....	1
Chapter 1. LITTERATURE OVERVIEW: SCOPE AND APPLICATION OF ENGINEERED POLY(2-OXAZOLINE)S	
INTRODUCTION	9
I. ADVANTAGEOUS PROPERTIES OF POLY(2-OXAZOLINE)S FOR BIOMEDICAL	10
I.1. Biocompatibility studies	10
I.2. Stealth behavior and protein repellent action of poly(2-oxazoline)s	12
II. SYNTHESIS OF POLY(2-OXAZOLINE)S	15
II.1. Polymerization mechanism: initiation and propagation	16
II.2. Polymerization mechanism: transfer and termination by coupling	18
II.3. Optimization of the reaction parameters	19
III. POLY(2-OXAZOLINE)S: A VERSATILE POLYMER CLASS	22
III.1. Taking advantage of the living polymerization: copolymers synthesis	22
III.2. Introduction of functionalities	23
III.2.1. In-chain functionalization through the use of functional monomers	24
III.2.2. Functionalization of the α -chain end	27
III.2.3. Functionalization of the ω -chain end	30
III.3. Poly(2-oxazoline)s hydrogels	32
III.3.1. Hydrogels prepared by polymerization with a bis-oxazoline monomer	33
III.3.2. Hydrogels prepared by direct post-polymerization reaction	34
III.3.3. Hydrogels prepared by 2 step post-polymerization reaction	36
III.4. Structure-property relationships	39
IV. POLY(2--OXAZOLINE)S AS POLYMER THERAPEUTICS	43
IV.1. Overview of the drug delivery problematic	43
IV.2. Poly(2-oxazoline) conjugation to biological molecules	46
IV.3. Self- assembly of poly(2-oxazoline)s and their use in biomedical applications	49
IV.4. Poly(2-oxazoline)s cross-linked nanostructures	55
IV.4.1. Brief overview of nanogels	55
IV.4.2. Synthetic methods to nanogels	56
IV.4.3. Poly(2-oxazoline)s cross-linked nanostructures/nanogels	57
V. CONCLUSIONS	59
List of Figures	xiv
List of Tables	xviii
List of Illustrations.....	xix

Chapter 2. pH AND REDOX RESPONSIVE HYDROGELS AND NANOGELS MADE FROM POLY(2-ETHYL-2-OXAZOLINE)

INTRODUCTION	67
I. SYNTHESIS AND PARTIAL HYDROLYSIS OF PETOX	69
II. HYDROGEL FORMATION AND CLEAVAGE	71
II.1. Cross-linker screening for the hydrogel formation	72
II.2. Hydrogel formation and cleavage with diglycidyl ether cross-linkers	75
III. SYNTHESIS OF PETOX NANOGELS	77
III.1. In dilute media	77
III.2. In inverse emulsion	78
CONCLUSIONS	80
EXPERIMENTAL SECTION	82
SUPPORTING INFORMATION	87
List of Figures	xiv
List of Tables	viii
List of Illustrations	xix

Chapter 3. CRYSTALLIZATION-DRIVEN SELF-ASSEMBLY OF POLY(2-ISOPROPYL-2-OXAZOLINE)-*BLOCK*-POLY(2-METHYL-2-OXAZOLINE) ABOVE THE LCST

INTRODUCTION	101
I. SYNTHESIS OF P(IPROX50-<i>B</i>-MEOX50) COPOLYMERS BY CATIONIC RING OPENING POLYMERIZATION	103
II. REVERSIBLE SELF-ASSEMBLY OF P(IPROX50-<i>B</i>-MEOX50) ABOVE THE LCST	104
III. MORPHOLOGY EVOLUTION BY CRYSTALLIZATION OF P(IPROX50-<i>B</i>-MEOX50)	105
IV. INFLUENCE OF EXTERNAL PARAMETERS ON THE CRYSTALLIZATION PROCESS	121
IV.1. Polymer concentration.....	121
IV.2. Heating rate.....	114
CONCLUSIONS	115
EXPERIMENTAL SECTION	117
SUPPORTING INFORMATION	119
List of Figures	xv

List of Tables	xviii
List of Illustrations.....	xix

Chapter 4. KETAL- AND ALDEHYDE-FUNCTIONAL COPOLYMERS BASED ON POLY(2-OXAZOLINE) FOR POSTPOLYMERIZATIONMODIFICATION

INTRODUCTION	131
I. SYNTHESIS OF PDPOX21 BY CATIONIC RING-OPENING POLYMERIZATION	132
II. CONJUGATION OF POBOX WITH AMINO-CONTAINING REAGENTS	133
III. COPOLYMER SYNTHESIS AND DEPROTECTION OF P(MEOX41- <i>STAT</i> -DPOX9)OH	135
IV. HYDROGEL FORMATION BETWEEN P(MEOX93- <i>STAT</i> -OBOX11)PIP & ADIPIC ACID DIHYDRAZIDE	138
V. TRANSACETALIZATION REACTION FROM P(MEOX41- <i>STAT</i> -DPOX9)OH WITH AN EXCESS OF PEG300	139
CONCLUSIONS	142
EXPERIMENTAL SECTION	143
SUPPORTING INFORMATION	149
List of Figures	xvi
List of Tables	xviii
List of Illustrations.....	xix

Chapter 5. POLY(2-OXAZOLINE) BASED NANOGELS AS BIOCOMPATIBLE PSEUDO-POLYPEPTIDE DRUG DELIVERY SYSTEM

INTRODUCTION	167
I. PETOX SYNTHESIS AND PARTIAL HYDROLYSIS	168
II. NANOGEL FORMATION IN AQUEOUS DILUTE MEDIA	169
III. NANOGEL CHARACTERIZATION	172
IV. CYTOTOXICITY TEST AND EVALUATION OF NANOGEL-PROTEIN INTERACTIONS	174
V. COMPLEMENT SYSTEM ACTIVATION	177
V.1. Measurement principles	177
V.2. EIA and LIA results	178
V.3. Discussion	180

CONCLUSIONS	181
EXPERIMENTAL SECTION	183
SUPPORTING INFORMATION	190
List of Figures	xvii
List of Tables	xviii
List of Illustrations.....	xx
BIBLIOGRAPHY	201

LIST OF FIGURES

Chapter 1

Page 13 : Figure 1 A) Blood circulation time and B) Biodistribution of liposomes coated with poly(ethylene glycol) (PEG), poly(2-ethyl-2-oxazoline) (PEtOx), poly(2-methyl-2-oxazoline) (PMeOx) and of uncoated liposomes, egg phosphatidylglycerol (EPG). Adapted from ref. 27

Page 20: Figure 2 SEC traces of poly(2-isopropyl-2-oxazoline) prepared at different temperatures. Reprinted from ref. 61

Page 24 : Figure 3 Possible ways to functionalize poly(2-oxazoline)s

Page 29 : Figure 4 (Macro-)initiators for the polymerization of 2-oxazolines

Page 32 : Figure 5 Termination agents used to quench the polymerization of 2-oxazolines

Page 34 : Figure 6 Hydrogel preparation by copolymerization of 2-alkyl-2-oxazoline and bis-oxazoline

Page 40: Figure 7 Structure-properties relationship for poly(2-oxazoline)s

Page 41 : Figure 8 Structure-properties relationship for poly(2-propyl-2-oxazoline)s isomers

Page 42 : Figure 9 Schematic representation of the changes in the conformation of PiPrOx in water as a function of temperature. Reprinted from ref. 204

Page 47 : Figure 10 A) Effect of the subcutaneous injection of insulin, insulin glargine, and poly(2-ethyl-2-oxazoline)-insulin on the blood glucose levels in male rats. B) 11 Relative immunogenicity of BSA, PEG-BSA, Poly(2-ethyl-2-oxazoline)-BSA in rabbits treated as measured by anti-BSA antibody levels. Treated on days 1, 14, 28 and 42. Adapted from ref. 14

Page 48 : Figure 11 Structure of the triblock copolymers used to form micelles. Reprinted from ref. 249

Page 51 : Figure 12 Schematic representation of enzyme- and temperature-induced self-assembly behavior of the polymer bio-conjugate. Reprinted from ref. 122

Page 52 : Figure 13 A) Biotinylated poly(2-methyl-2-oxazoline)-*b*-PDMS-*b*-poly(2-methyl-2-oxazoline) B) Functionalized polymersomes by streptavidin bridging. Reprinted from ref. 252

Page 58 : Figure 14 Strategy for the production of bisensitive nanogels and their supposed reaction to changes in stimuli like pH value and temperature. Red: side chains of poly(2-carboxyethyl-2-oxazoline); Blue: main chains of poly(N-isopropylacrylamide). Adapted from ref. 280

Chapter 2

Page 69: Figure 1 ¹H NMR spectra (400 MHz, D₂O) of poly(2-ethyl-2-oxazoline)₉₄

Page 70: Figure 2 SEC trace of poly(2-ethyl-2-oxazoline)₉₄ in DMF obtained with a laser light scattering detector

Page 71 : Figure 3 ¹H NMR spectra (400 MHz, D₂O) of poly((2-ethyl-2-oxazoline)₈₈-*stat*-(ethylene imine)₆)

Page 76 : Figure 4 Titration of the secondary amine by pH-metry and conductivity measurements A) of parent poly(2-ethyl-2-oxazoline)₉₄ and B) of poly((2-ethyl-2-oxazoline)₈₈-*stat*-(ethylene imine)₆) copolymer

Page 76 : Figure 5 A) Hydrogel formed by the reaction of ethylene imine groups on the polymer backbone with hydroxyethyl disulfide-*bis*-diglycidyl ether (2). B) Clear solution obtained after addition of DTT to the hydrogel.

Page 78 : Figure 6 DLS analysis and TEM of permanently cross-linked nanogels prepared in dilute media, using cross-linker (1). A) Variations of decay rate *versus* squared scattering vector with a linear fit. B) Relaxation time plot obtained at 90°. C) TEM micrograph (scale bar = 500 nm)

Page 79 : Figure 7 DLS and TEM analysis of the cleavable and non-cleavable nanogels. Panel A: Variations of decay rate *versus* squared scattering vector with linear fits at different pHs. Panel B: Relaxation time plot obtained at 90° at different pHs. Panel C: TEM micrographs at neutral pH

Page 87 : Figure S1 SEC traces of poly(2-ethyl-2-oxazoline)₉₄ and poly((2-ethyl-2-oxazoline)-*stat*-(ethylene imine)) copolymer obtained after 6.5 h of hydrolysis in DMF

Page 88 : Figure S2 SEC traces of poly(2-ethyl-2-oxazoline)₉₄ and poly((2-ethyl-2-oxazoline)₈₈-*stat*-(ethylene imine)₆) statistic copolymer after 2 h of hydrolysis in DMF

Page 88 : Figure S3 Determination of the intrinsic viscosity of poly(2-ethyl-2-oxazoline)₉₄ by plotting the reduced viscosity as a function of the concentration.

Page 89 : Figure S4 FT-IR spectrum of poly((2-ethyl-2-oxazoline)₈₈-*stat*-(ethylene imine)₆)

Page 89 : Figure S5 FT-IR spectrum of the dry hydrogel made with poly((2-ethyl-2-oxazoline)₈₈-*stat*-(ethylene imine)₆) and 1,6-hexanediol-diglycidyl ether

Page 90 : Figure S6 FT-IR spectrum of the dry hydrogel made up of poly((2-ethyl-2-oxazoline)₈₈-*stat*-(ethylene

Page 98 : Figure S7 ¹H NMR spectrum (400 MHz, CDCl₃) of hydroxyethyl disulfide-*bis*-diglycidyl ether (cross-linker 2)imine)₆) and hydroxyethyl disulfide-*bis*-diglycidyl ether (2)

Page 91 : Figure S8 HSQC NMR spectrum (400 MHz, CDCl₃) of hydroxyethyl disulfide-*bis*-diglycidyl ether (cross-linker 2)

Page 91 : Figure S9 Decrease in relative count rate (%) measured by DLS at 90°, after addition of DTT or DI water.

Chapter 3

Page 104 : Figure 1 P(iPrOx₅₀-*b*-MeOx₅₀) micelle characterization at 65 °C A) DLS analysis with correlogram and size distribution obtained at 90°, B) TEM micrograph C) distribution of micelle size by TEM, determined by Image J.

Page 105 : Figure 2 P(iPrOx₅₀-*b*-MeOx₅₀) micelles size evolution with temperature measured by DLS

Page 106: Figure 3 *in situ* DLS measurements of P(iPrOx₅₀-*b*-MeOx₅₀) in water at 10 mg/mL and 65 °C

Page 107 : Figure 4 TEM micrographs of 10 mg/mL of P(iPrOx₅₀-*b*-MeOx₅₀) solution in water heated at 65 °C for 1h30, 3h, 4h30, 7h and 24h

Page 109 : Figure 5 DSC thermograms of P(iPrOx₅₀-*b*-MeOx₅₀) without any further post-treatment and after 24 h heating in aqueous solution at 65 °C

Page 110: Figure 6 A) WAXS patterns of P(iPrOx₅₀-*b*-MeOx₅₀) after 1h40, 3h, 4h30, 7h and 24h of annealing at 65 °C. Peaks assignment according to ref. 35 B) Crystal structure adapted from ref. 35

Page 111: Figure 7 Schematic representation of the changes in the conformation of PiPrOx in water as a function of temperature. Reprinted from ref. 33

Page 112 : Figure 8 *In situ* DLS measurements of P(iPrOx₅₀-*b*-MeOx₅₀) in water at 1 mg/mL and 65 °C

Page 113 : Figure 9 TEM micrographs of 10 mg/mL of P(iPrOx₅₀-*b*-MeOx₅₀) solution in water heated at 65 °C for 1h30, 3h, 4h30, 7h and 24h.

Page 114 : Figure 10 *In situ* DLS measurements of a 10 mg/mL P(iPrOx₅₀-*b*-MeOx₅₀) solution in water heated at 0.1 °C/min from 25 °C up to 65 °C.

Page 119 : Figure S1 ¹H NMR spectrum (400 MHz, CDCl₃) of 2-isopropyl-2-oxazoline (iPrOx)

Page 120 : Figure S2 ¹H NMR spectrum (400 MHz, CDCl₃) of poly[(2-isopropyl-2-oxazoline)-*b*-(2-methyl-2-oxazoline)] (P(iPrOx-*b*-MeOx))

Page 120 : Figure S3 SEC trace of A) poly[(2-methyl-2-oxazoline)-*b*-(2-isopropyl-2-oxazoline)] and B) poly[(2-isopropyl-2-oxazoline)-*b*-(2-methyl-2-oxazoline)] in DMF

Page 121 : Figure S4 DLS measurements determining the cloud point of P(iPrOx-*b*-MeOx) (cloud point = 57 °C)

Page 122 : Figure S5 WAXS patterns of P(iPrOx₅₀-*b*-MeOx₅₀) after 1h40, 3 h, 4h30, 7 h and 24 h of annealing at 65°C. Peak assignment according to ref. 35

Page 123 : Figure S6 DSC thermograms of the first heat ramp of P(iPrOx₅₀-*b*-MeOx₅₀), non-treated and kept under storage condition (blue) and after 24 h of heating in aqueous solution at 65 °C (red)

Page 123 : Figure S7 Appearance of P(iPrOx₅₀-*b*-MeOx₅₀) in water/trifluoroacetic acid mixture (1/5 v/v) and in pure water

Page 124 : Figure S8 Illustration of constructive and destructive interferences. Adapted from ref. 62

Chapter 4

Page 134 Figure 1 Post-polymerization modification of POBOx₂₁ with benzylamine, Jeffamine D400 and adipic acid dihydrazide

Page 135 Figure 2 SEC traces in Tris buffer of P(MeOx₄₁-*stat*-DPOx₉)OH before and after deprotection

Page 136 : Figure 3 Solid state ¹³CNMR of the self-cross-linked P(MeOx₄₁-*stat*-OBOx₉)OH, rotation speed = 10000 Hz, ns = 160000

Page 138 : Figure 4 Solubility in Tris buffer, after 4 ½ months, of A) P(MeOx₆₃-*stat*-DPOx₁₄) pip B) P(MeOx₁₂₄-*stat*-DPOx₁₂)OH C) P(MeOx₉₃-*stat*-DPOx₁₁)pip

Page 139 : Figure 5 Gel formation and cleavage between P(MeOx₉₃-*stat*-OBOx₁₁)pip and adipic acid dihydrazide

Page 141 : Figure 6 ¹H NMR spectrum after transacetalization between P(MeOx₄₁-*stat*-DPOx₉)OH and PEG₃₀₀

Page 149 : Figure S1 ¹H and ¹³C NMR spectra (400 MHz, CDCl₃) of 2-[3-(1,3)-dioxolan-2-ylpropyl]-2-oxazoline (DPOx)

Page 150 : Figure S2 ¹H NMR spectrum (400 MHz, CDCl₃) of *N*-methyl-2-methyl-2-oxazolinium triflate

Page 150 : Figure S3 ¹H NMR spectrum (400 MHz, CDCl₃) of poly(2-[3-(1,3)-dioxolan-2-ylpropyl]-2-oxazoline)₂₁ (PDPOx₂₁)

Page 151 : Figure S4 ¹H NMR spectrum (400 MHz, CDCl₃) of PDPOx₂₁ after deprotection (POBOx₂₁)

Page 151 : Figure S5 FTIR spectrum of PDPOx₂₁

Page 152 : Figure S6 FTIR spectrum of POBOx₂₁

Page 152 : Figure S7 FTIR spectrum of POBOx₂₁ after reaction with benzylamine

Page 153 : Figure S9 FTIR spectrum of POBOx₂₁ after reaction with adipic acid dihydrazide

Page 153 : Figure S8 FTIR spectrum of POBOx₂₁ after reaction with Jeffamine D400

Page 154: Figure S10 ¹H and ¹³C NMR spectra (400 MHz, CDCl₃) of P(MeOx₄₁-*stat*-DPOx₉)OH

Page 155 : Figure S11 SEC trace of P(MeOx₄₁-*stat*-DPOx₉)OH in DMF

Page 155 : Figure S12 ¹H NMR spectrum (400 MHz, CDCl₃) of P(MeOx₄₁-*stat*-DPOx₉)OH after deprotection (P(MeOx₄₁-*stat*-OBOx₉)OH)

Page 156 : Figure S13 ¹H NMR spectrum (400 MHz, CDCl₃) of P(MeOx₁₀₁-*stat*-DPOx₁₀)pip

Page 156 : Figure S14 ¹H NMR spectrum (400 MHz, CDCl₃) of P(MeOx₁₀₁-*stat*-OBOx₁₀)pip

Page 157 : Figure S15 Solid ¹³C NMR spectrum of the self cross-linked P(MeOx₄₀-*stat*-OBOx₁₀)OH, rotation speed = 8000 Hz, ns = 7000

Page 157 : Figure S16 Evolution with time of the SEC traces in Tris buffer of P(MeOx₁₂₄-*stat*-OBOx₁₂)OH

Page 158 : Figure S17 Evolution with time of the SEC traces in Tris buffer of P(MeOx₉₃-*stat*-OBOx₁₁)pip

Page 158 : Figure S18 Evolution with time of the SEC traces in Tris buffer of P(MeOx₆₃-stat-OBOx₁₄)pip

Page 159 : Figure S19 DOSY spectrum after transacetalization between P(MeOx₄₁-stat-DPOx₉)OH and PEG₃₀₀

Chapter 5

Page 171 : Figure 1 HSQC NMR spectra of the nanogel formation a) T₀, b) T_{6h} at 80 °C

Page 172 : Figure 2 Nanogel characterization. Top: DLS analysis; left: variation of decay rate versus squared scattering vector with linear fits; right: relaxation time plot obtained at 90°. Bottom, left: TEM micrograph. Bottom, right: Taping mode AFM image and section profile of the AFM imaging

Page 175 : Figure 3 MTS assay conducted on mouse fibroblast-like L929 cells.

Page 176 : Figure 4 Native gels run for BSA and nanogels-BSA mixture at different incubation concentrations

Page 179: Figure 5 Results for complement activation by A) the EIA method, B) the LIA method

Page 188 : Figure 6 Enzyme immunoassay (EIA) principle (adapted from ref. ⁹⁶)

Page 189 : Figure 7 Principle of the LIA assay (adapted from ref. ⁹⁷)

Page 190 : Figure S1 ¹H NMR spectrum (400 MHz, D₂O) of PEtOx₁₀₀

Page 191 : Figure S2 SEC trace of PEtOx₁₀₀ in DMF

Page 191 : Figure S3 FT-IR spectrum of PEtOx₁₀₀

Page 192 : Figure S4 ¹H NMR spectrum (400 MHz, D₂O) of P(EtOx₇₄-stat-EI₂₆)

Page 192 : Figure S5 SEC trace of P(EtOx₇₄-stat-EI₂₆) in DMF

Page 193 : Figure S6 FT-IR spectrum of P(EtOx₇₄-stat-EI₂₆)

Page 193 : Figure S7 HSQC NMR spectrum of nanogel formation after 2 h at 80 °C

Page 194 : Figure S8 HSQC NMR spectrum of nanogel formation after 5 h at 80 °C

Page 195 : Figure S9 TEM micrograph of nanogels with size measurements

Page 195 : Figure S10 Statistical distributions of TEM particle hydrodynamic radii

Page 196 : Figure S11 Titration of the secondary amine by pH-metry and conductivity measurements

Page 196 : Figure S12 Variation of the zeta potential of nanogels with pH

Page 197: Figure S13 Images obtained on inverted IX81 microscope of fibroblast-like L929 cells after 72 h exposure to nanogel solutions

Page 198: Figure S14 Measurement of isoelectric point of BSA by zetametry

LIST OF TABLES

Chapter 1

Page 23 : Table 1 Example of copolymers synthesized in the literature

Page 26 : Table 2 R side groups of 2-R-2-oxazolines allowing for functionalization of POx pendant chains

Page 28 : Table 3 Initiators with reactive functionalities for the CROP of 2-oxazolines

Page 30 : Table 4 Termination agents with reactive functionalities for the polymerization of 2-oxazolines

Page 33 : Table 5 Different strategies to synthesize POx hydrogels

Page 44 : Table 6 List of polymers commonly used in biomedical applications. Adapted from ref. 222

Page 54 : Table 7 Self-assembled nanostructures made from poly(2-oxazoline)s

Chapter 2

Page 71 : Table 1 Evolution of the degree of hydrolysis of poly(2-ethyl-2-oxazoline)₉₄ with time

Page 73 : Table 2 Cross-linkers used to form hydrogel with partially hydrolyzed poly(2-ethyl-2-oxazoline) and conditions used for the hydrogel formation

Page 92 : Table S1 Determination of the critical concentration c^* of poly(2-ethyl-2-oxazoline)₉₄

Chapter 3

Page 121 : Table S1 DLS measurements determined at 65 and 25 °C of aliquots taken at a various annealing times after annealing at 65 °C

Page 122 : Table S2 WAXS scattering angles and corresponding spacing between the crystallographic planes obtained from Bragg's law

Chapter 4

Page 145: Table 1 Characteristics of DPOx-based copolymers

Chapter 5

Page 170 : Table 1 DLS measurements confirming nanogel formation

Page 174 : Table 2 Nanogel characteristics calculated from NanoSight results

Page 188 : Table 3 Characteristics of the control nanoparticles used for the complement system activation assay

Page 198 : Table S1 NanoSight measurements on the nanogel solution, $c = 4.7$ mg/mL

LIST OF ILLUSTRATIONS

Chapter 1

Page 9: Scheme 1 Poly(2-oxazoline)s general structure

Page 10: Scheme 2 Analogy between poly(2-oxazoline)s and synthetic or naturally occurring polypeptides

Page 11: Scheme 3 Poly(2-ethyl-2-oxazoline) degradation by Proteinase K

Page 15 : Scheme 4 Polymerization of 2-substitued-2-oxazolines

Page 16 : Scheme 5 Examples of 2-oxazoline monomer synthesis

Page 17 : Scheme 6 Polymerization mechanisms

Page 18 : Scheme 7 Mechanism of chain transfer

Page 18 : Scheme 8 Extent of chain transfer depending on the monomer side-chain

Page 19: Scheme 9 Mechanism of chain coupling

Page 37 : Scheme 10 Strategies adopted by Saegusa's research group to form hydrogels with partially-hydrolyzed poly(2-methyl-2-oxazoline)

Page 38 : Scheme 11 Schematic of the thermosensitive hydrogel formed by Diels-Alder reaction

Chapter 2

Page 72 : Scheme 1 Synthesis of hydrogels made from poly(2-ethyl-2-oxazoline): (a) Cationic ring-opening polymerization (CROP) of 2-ethyl-2-oxazoline. (b) Partial hydrolysis of the poly(2-ethyl-2-oxazoline). (c)-(e) Formation of hydrogels by reaction with cross-linker (c) *N*-hydroxysuccinimide ester (d) diepoxide/diglycidyl ether (e) diacrylate.

Page 75 : Scheme 2 Synthesis of hydrogels made from poly(2-ethyl-2-oxazoline): (a) Formation of non-cleavable hydrogels by reaction with 1,6-hexanediol diglycidyl ether (1). (b) Formation of cleavable hydrogels by reaction with hydroxyethyl disulfide-*bis*-diglycidyl ether (2). (c) Hydrogel cleavage under reducing environment.

Page 80 : Scheme 3 Schematic illustration of the dual-responsiveness of PEtOx-based nanogels: swelling in acidic environment and chemical cleavage in reducing environment.

Page 84 : Scheme 4 Synthesis of cross-linker (2), hydroxyethyl disulfide-*bis*-diglycidyl ether

Chapter 3

Page 103 : Scheme 1 Synthesis of P(iPrOx₅₀-*b*-MeOx₅₀) BCP by sequential cationic ring-opening polymerization

Page 116 : Scheme 2 Schematic representation of the nano-structures formed depending on the annealing time

Page 118 : Scheme 3 Synthesis of 2-isopropyl-2-oxazoline

Chapter 4

Page 133 : Scheme 1 Cationic ring opening polymerization of 2-[3-(1,3)-dioxolan-2-ylpropyl]-2-oxazoline and subsequent deprotection (inspired from ref. 17)

Page 136 Scheme 2 Aldol condensation and subsequent dehydration resulting in α,β -unsaturated aldehydes

Page 140 : Scheme 3 Transacetalization reaction from P(MeOx₄₁-*stat*-DPOx₉)OH with an excess of PEG₃₀₀ and its schematic representation

Page 144 : Scheme 4 Synthesis of 2-[3-(1,3)-dioxolan-2-ylpropyl]-2-oxazoline

Page 145 : Scheme 5 Synthesis of N-methyl-2-methyl-2-oxazolinium triflate

Chapter 5

Page 168 : Scheme 1 Cationic ring opening polymerization of 2-ethyl-2-oxazoline followed by partial hydrolysis

LIST OF ABBREVIATIONS

AFM	Atomic force microscopy
Ara-C	Cytosine arabinose, 1-(B-D-arabinofuranosyl)cytosine
ATR	Attenuated total reflection
ATRP	Atom-transfer radical-polymerization
BB	Benzyl bromide
BCP	Block copolymers
BIC	Bordeaux Imaging center
BOC	<i>tert</i> -butyloxycarbonyl group
BSA	Bovine serum albumin
BuOx	2-Butyl-2-oxazoline
CA	Complement activation
CH ₅₀	50% complement hemolytic unit
CPMAS	Cross polarization magic angle spinning
CROP	Cationic ring opening polymerization
CRPP	Centre de recherche Paul Pascal
\bar{D}	Dispersity = $\overline{Mw/Mn}$
DBU	1,8-Diazabicycloundec-7-ene
DDA	<i>N, N</i> -Dimethyldodecylamine
DDS	Drug delivery system
DecOx	2-Decenyl-2-oxazoline
DI	Deionized
DLS	Dynamic light scattering
DMAc	Dimethylacetamide
DMEM	Dulbecco's Modified Eagle's Medium
DMF	Dimethylformamide
DNP	Dinitrophenyl

DOSY Diffusion ordered spectroscopy
DOTA *N,N',N'',N'''*-Tetraazacyclododecane-1,4,7,10-tetra-acetic acid
DOX Doxorubicin
DP Degree of polymerization
DPOx 2-[3-(1,3)-Dioxolan-2-ylpropyl]-2-oxazoline
DPPC Dipalmitoylphosphatidylcholine
DSC Differential scanning calorimetry
DTT Dithiothreitol
EIA Enzyme immunoassay
EPG Egg phosphatidylglycerol
EPR Enhanced permeability and retention effect
EtOx 2-Ethyl-2-oxazoline
FBS Fetal bovine serum
FDA Food and drug administration
Fmoc-*p*Y Fluorenylmethoxycarbonyl-tyrosine phosphate
FTIR Fourier transform infrared spectroscopy
G6P Glucose-6-phosphate
G6PDH Glucose-6-phosphate dehydrogenase
GSH Glutathione
HEMA 2-Hydroxyethyl methacrylate
HRP Horseradish peroxidase
HSA Human serum albumin
HSQC Heteronuclear single quantum coherence
Hya Hyaluronan
IC Incubation concentration
IP Isoelectric point
iPOx 2-Isopropyl-2-oxazoline
LCPO Laboratoire de chimie des polymères

LCST Low critical solution temperature
 LIA Liposome immunoassay
 MALLS Multi-angle laser light scattering
 MeI Methyl iodide
 MeOTf Methyl trifluoromethanesulfonate
 MeOTs Methyl *p*-toluenesulfonate
 MeOx 2-Methyl-2-oxazoline
 MeOxOTf *N*-methyl-2-methyl-2-oxazolinium triflate
 \overline{Mn} Average number molecular weight
 MPS Mononuclear phagocytic system
 MTD Maximum tolerated dose
 MTS 3-(4,5-Dimethylthiazol-2-yl)-5-(3-carboxymethoxyphenyl)-2-(4-sulfophenyl)-2H-tetrazolium
 \overline{Mw} Molecular weight
 NAD Nicotinamide adenine dinucleotide
 NHS *N*-hydroxysuccinimide
 NMR Nuclear magnetic resonance
 NonOx 2-Nonyl-2-oxazoline
 NVP *N*-vinyl-2-pyrrolidone
 OTf Trifluoromethanesulfonate
 OTs *p*-Toluenesulfonate
 NP Nanoparticle
 nPOx 2-*N*-propyl- 2-oxazoline
 PAA Poly(acrylic acid)
 PBLG Poly(γ -benzyl-L-glutamate)
 PBS Phosphate buffer saline
 PCL Poly(ϵ -caprolactone)
 PcPOx Poly(2-cyclopropyl-2-oxazoline)
 Pdl Polydispersity

PDMS Polydimethylsiloxane

PDPOx Poly(2-[3-(1,3)-dioxolan-2-ylpropyl]-2-oxazoline)

PEG Poly(ethylene glycol)

PEI Poly(ethylene imine)

PEtOx Poly(2-ethyl-2-oxazoline)

PFS Polyferrocenylsilane

PhOx 2-Phenyl-2-oxazoline

PHPMA Poly(N-(2-hydroxypropyl) methacrylamide)

Pid Piperidine

Pip Piperazine

PiPOx Poly(2-isopropyl-2-oxazoline)

PLA Poly(lactic acid)

PLGA Poly(D,L-lactide-co-glycolide)

PLL Poly(L-lysine)

PMeOx Poly(2-methyl-2-oxazoline)

PMMA Poly(methyl methacrylate)

PNIPAAm Poly(N-isopropylacrylamide)

PnPOx Poly(2-n-propyl-2-oxazoline)

PNonOx Poly(2-nonyl-2-oxazoline)

POBOx Poly[2-(4-oxobutyl)-2-oxazoline]

POx Poly(oxazoline)

PTSA *p*-Toluene sulfonic acid

PTX Paclitaxel

PVP Poly(vinyl pyrrolidone)

RAFT Reversible addition-fragmentation chain-transfer

RCC Radical cross-linking copolymerization

RES Reticuloendothelial system

R_g Radius of gyration

R _H	Hydrodynamic radius
RI	Refractive index
ROS	Reactive oxygen species
RSH	Mercaptant
SEC	Size exclusion chromatography
SFM	Scanning force microscopy
SI	Supporting information
SoyOx	Unsaturated soybean fatty acid based 2-oxazoline monomer
TEM	Transmission electron microscopy
TFA	Trifluoroacetic acid
T _g	Glass transition temperature
UCST	Upper critical solution temperature
WAXS	Wide angle X-ray scattering
w/o	Water-in-oil
XRD	X-ray diffraction

GENERAL INTRODUCTION

Hydrogels are a broad class of cross-linked polymeric networks, which often extensively swell in water or biological fluids while maintaining their three-dimensional (3D) structure.¹ Because of their high water content, hydrogels are most of the time biocompatible and have been widely developed and used in biomaterial sciences. Since the first biocompatible hydrogel reported in 1960,² Their use as biomaterials has evolved from static implants and devices to dynamic, bio-responsive scaffolds, drug delivery vehicles and cell culture platforms for regenerative medicine. As for nanogels, they are defined as soluble polymer networks with a dimension smaller than 100 nm,³ and display the same structural features as hydrogels. Nanogels have been proposed as robust drug delivery systems (DDS);⁴ the current trend in the field being to introduce both responsiveness and targeting properties in these nanocarriers.

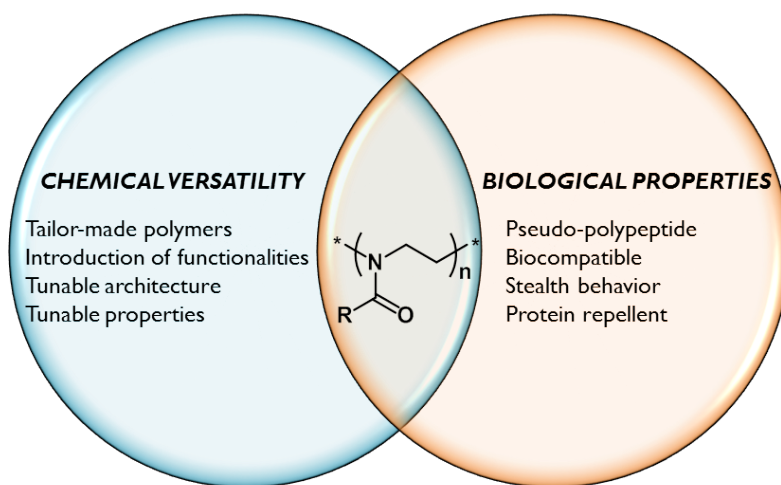
Thanks to the increasing knowledge in polymer engineering, environment-stimuli responsive hydrogels and nanogels are now accessible.^{5,6} Depending on the polymer and cross-linker used, hydrogels/nanogels can, for example, be made responsive to pH or temperature changes. They can also exhibit an “on and off” response, depending on fluctuating properties, in order to answer to more precise and specialized needs, as it is the case to glucose concentration.⁷⁻¹⁰

In the past decades, the use of polymeric materials has increased dramatically for biomedical applications. The main used polymers – polyether,¹¹ polyesters,¹² polycarbonates¹³ and polypeptides¹⁴ - are biocompatible, the unconditional properties for biomedical applications. Another important feature in this field is the will to develop synthetic polymers with chemical structures as close as possible to natural polypeptides and proteins, in order to obtain bio-mimicking functional biomaterials. Synthetic peptide-based polymers are actually not new,¹⁵ but one of the current trend is to go towards increasingly complex polymer sequences that would display tunable properties, while presenting excellent biocompatibility and offering some potential biofunctionalities.

The major goal of this PhD thesis work was to design responsive hydrogels and nanogels made from a specific class of polymers - poly(2-oxazoline)s (POx) - for biomedical applications. POx are, however, still relatively new in comparison to other polymers already established for such a use, but they definitely fall within this approach. POx are synthesized by living cationic ring opening polymerization, and are described as pseudo-polypeptides because of their similar structure. Nevertheless, the presence of tertiary amides in POx makes them more chemically and enzymatically stable than polypeptides, while having a similar biocompatibility.¹⁶

POx prove fully competitive as biocompatible hydrophilic polymer alternatives of poly(ethylene glycol) (PEG), poly(vinyl pyrrolidone) (PVP), and poly(*N*-(2-hydroxypropyl) methacrylamide) (PHPMA) for biomedical uses.¹⁷ More especially poly(2-methyl-2-oxazoline) (PMeOx) and poly(2-ethyl-2-oxazoline) (PEtOx) are often compared to PEG because they present the same stealth behavior towards plasmatic protein.

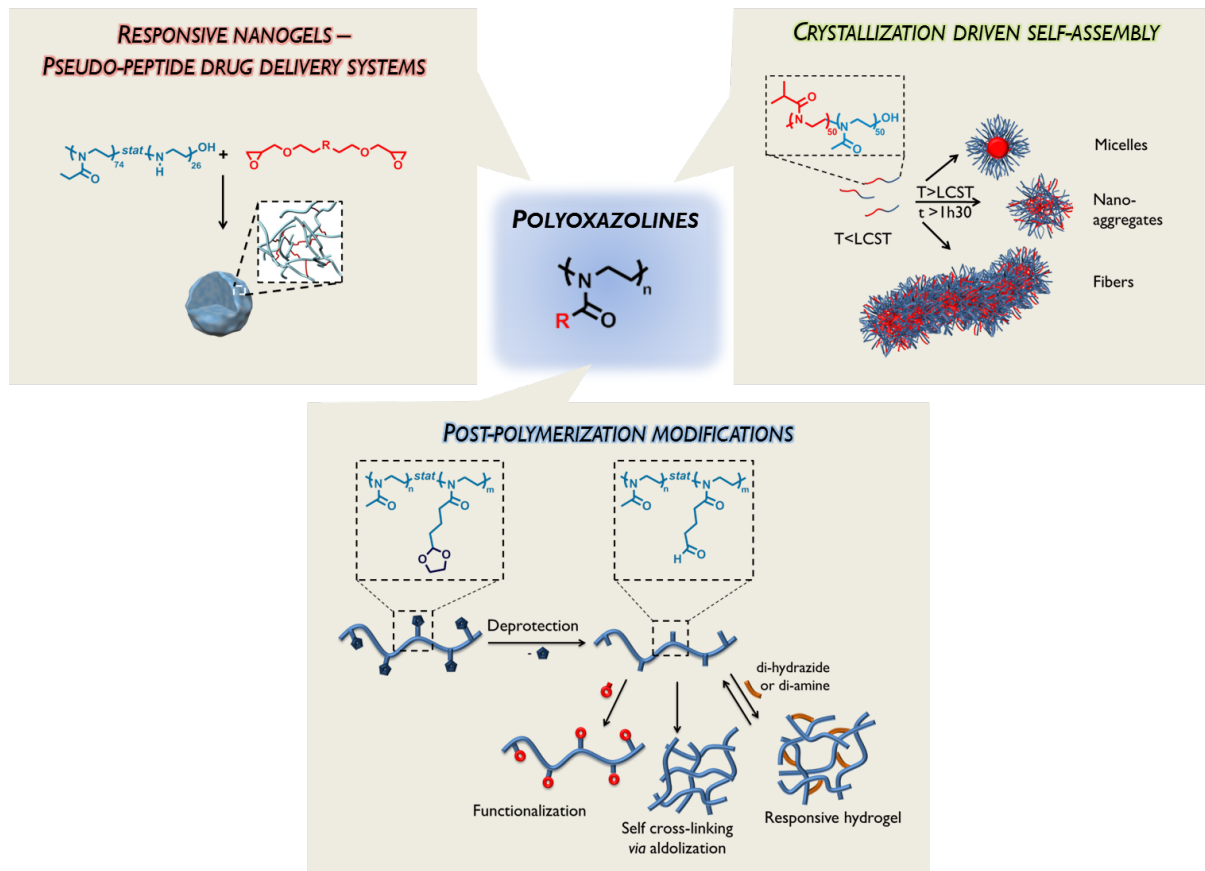
In addition to their advantageous biological properties, POx are chemically versatile allowing the synthesis of tailor-made polymers and copolymers with tunable properties. Finally, POx interests are not only recognized by researchers in Academia but also by the chemical industry: a pharmaceutical company, Serina therapeutics, is currently creating new pharmaceutical candidates using poly(2-oxazoline)s for Parkinson's disease, cancer, inflammation, pain and metabolic disorders.¹⁸



In this context, we propose, in this work, to expand the POx toolbox towards the design of functional POx-based hydrogels and nanogels that are chemically or physically cross-linked, for possible biomedical applications. Different oxazoline monomers will be used, yielding (co)polymers with various chemical handles and/or properties.

This manuscript is composed of five chapters. First, a literature review on engineering of POx and their use in biomedical applications is presented. The second chapter will describe the design of dual-stimuli responsive hydrogels and nanogels made from partially hydrolyzed POx. The third chapter is devoted to the crystallization driven self-assembly of a particular diblock copolymer, namely poly(2-isopropyl-2-oxazoline)-*block*-(2-methyl-2-oxazoline) copolymer; the manipulation of which can lead to the formation of different nanostructures. In the fourth chapter, the expansion of the POx toolbox by post-polymerization modification of ketal and aldehyde-functionalized POx, which could be further used to

prepare hydrogels, so as will be exploited. In the last chapter, the optimization of POx nanogels presented in the first chapter to meet the specific needs of a drug delivery system, and their evaluation in term of cytotoxicity and interactions with proteins will be discussed.



This PhD work was carried out in the framework of a collaboration between three universities: the University of Bordeaux in the Laboratoire de chimie des polymères organiques (LCPO, France), the University of Waterloo (Canada) and the University of Liège (Belgium). It was part of the International Doctoral Programme in Functional Materials (IDS FunMat), with an Erasmus Mundus scholarship.

CHAPTER 1

LITERATURE OVERVIEW:

SCOPE AND APPLICATIONS OF ENGINEERED POLY(2-OXAZOLINE)S

CHAPTER 1

LITERATURE OVERVIEW: SCOPE AND APPLICATIONS OF ENGINEERED POLY(2-OXAZOLINE)S

INTRODUCTION	9
I. ADVANTAGEOUS PROPERTIES OF POLY(2-OXAZOLINE)S FOR BIOMEDICAL APPLICATIONS	10
I.1. Biocompatibility studies.....	10
I.2. Stealth behavior and protein repellent action of poly(2-oxazoline)s	12
II. SYNTHESIS OF POLY(2-OXAZOLINE)S.....	15
II.1. Polymerization mechanism: initiation and propagation.....	16
II.2. Polymerization mechanism: transfer and termination by coupling.....	18
II.3. Optimization of the reaction parameters	19
III. POLY(2-OXAZOLINE)S: A VERSATILE POLYMER CLASS	22
III.1. Taking advantage of the living polymerization: copolymers synthesis.....	22
III.2. Introduction of functionalities	23
III.2.1. In-chain functionalization through the use of functional monomers	24
III.2.2. Functionalization of the α -chain end.....	27
III.2.3. Functionalization of the ω -chain end	30

III.3.	Poly(2-oxazoline)s hydrogels	32
III.3.1.	Hydrogels prepared by polymerization with a bis-oxazoline monomer	33
III.3.2.	Hydrogels prepared by direct post-polymerization reaction.....	34
III.3.3.	Hydrogels prepared by 2 step post-polymerization reaction	36
III.4.	Structure-property relationships	39
IV.	POLY(2-OXAZOLINE)S AS POLYMER THERAPEUTICS	43
IV.1.	Overview of the drug delivery problematic	43
IV.2.	Poly(2-oxazoline) conjugation to biological molecules.....	46
IV.3.	Self-assembly of poly(2-oxazoline)s and their use in biomedical applications	49
IV.4.	Poly(2-oxazoline)s cross-linked nanostructures	55
IV.4.1.	Brief overview of nanogels	55
IV.4.2.	Synthetic methods to nanogels	56
IV.4.2.1.	Nanogel synthesis by cross-linking preformed polymers.....	56
IV.4.2.2.	Nanogel synthesis by polymerization in heterogeneous media.....	56
IV.4.3.	Poly(2-oxazoline)s cross-linked nanostructures/nanogels	57
V.	CONCLUSIONS	59

INTRODUCTION

The aim of this literature review is to give to the reader the key elements for a critical reading of this PhD manuscript. This chapter is dedicated to the scope and applications of engineered poly(2-oxazoline)s (POx, Scheme 1). The living cationic ring opening polymerization (CROP) leading to POx has been discovered more than 50 years ago by 4 different research teams simultaneously and since then, this special class of polymers has been studied meticulously, giving rise to versatile polymeric materials. However, it is only since 15 years, with the discovery of their remarkable properties for biomedical applications and their thermo-responsiveness, that POx arouse increasing interest by the scientific community. POx are now considered as smart bioinspired polymers,¹ with an ability to form functional materials and nanostructures with tunable properties,¹⁻³ leading to numerous applications.³ POx are claimed to be used in adhesives,⁴ coatings^{5,6} or ink formulations⁷ as well as in drug delivery applications.^{8,9} The reader should be advised that the former applications are out of the scope of this literature review but related information can be found elsewhere.⁴⁻⁹



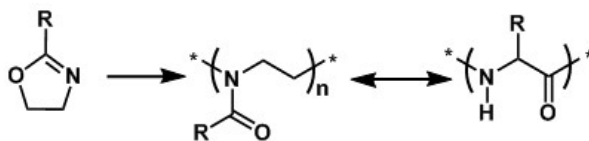
Scheme 1 Poly(2-oxazoline)s general structure

First, the remarkable properties of POx making them attractive candidates for biomedical applications will be presented. Second, a description of the polymerization mechanism, and potential issues which could be encountered, will be discussed. In the third part, the POx versatility in terms of chemistry and properties will be illustrated through selected examples. A special focus will also be placed on the design of POx-based hydrogels, as this category of materials has been the main topic of this PhD thesis. In the last part, the use of POx as polymer therapeutics will be briefly reviewed, with a special emphasis on both self-assembled nano-structures (micelles, polymer vesicles and polyplexes) and nanogels.

I. ADVANTAGEOUS PROPERTIES OF POLY(2-OXAZOLINE)S FOR BIOMEDICAL APPLICATIONS

I.1. BIOCOMPATIBILITY STUDIES

POx are often viewed as amino-acid analogues³ or as pseudo-polypeptides, where each repeating unit contains a peptide bond, albeit on the side instead of the main chain (Scheme 2). One can thus expect POx to be biocompatible. In addition, poly(2-ethyl-2-oxazoline) (PEtOx) has been approved by the Food and Drug Administration (FDA) as an indirect additive used in food contact substances,¹⁰ which was the case for poly(ethylene glycol) (PEG) before being accepted in pharmaceutical formulations.



Scheme 2 Analogy between poly(2-oxazoline)s and synthetic or naturally occurring polypeptides³

In order to evaluate the biocompatibility of both homopolymers and block copolymers based on POx, a series of studies has to be conducted. First, *in vitro* studies should be carried out, in order to check the cytotoxicity of POx on different cell lines as well as their hemocompatibility and cell internalization. If *in vitro* tests are conclusive, *in vivo* evaluation should be realized with a pharmacokinetic study (*i.e.* the study of the fate of the polymer in the body), and the biodistribution evaluation.

First, an *in vitro* cytotoxicity study was conducted on a library of homopolymers and block copolymers based on POx, showing that POx were well tolerated at polymer concentrations up to 20 mg/mL,¹¹ and even up to 80 mg/mL for PEtOx.¹²

The POx molar mass also influenced cytotoxicity: the higher the molar mass, the lower the cell toxicity.^{12,13} POx purity matters too, as monomers appeared to be toxic.¹³

Hemocompatibility evaluation of PEtOx with molar masses of 5, 10, and 20 kDa, at a polymer concentration up to 10 mg/mL, showed no adverse effect on red blood cells.¹⁴ Other studies reported even better blood compatibility with no damaging effect on red blood cells, regardless of the poly(2-methyl-2-oxazoline) (PMeOx) and PEtOx molar mass, and up to a concentration higher than that typically used in biomedical application (up to 80 mg/mL).^{12,15} More recently, zwitterionic POx (*i.e.* a globally neutral POx polymer but with positive and negative electrical charges along the

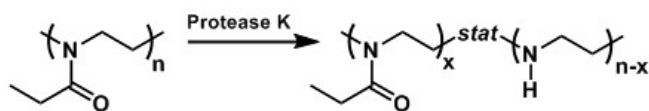
chain) were reported to not only exhibit high hemocompatibility and low cytotoxicity, but also a beneficial anticoagulant activity.¹⁶

A cellular uptake study was also conducted on a POx library, at a polymer concentration below the critical micellar concentration.¹¹ The results suggested that amphiphilic POx could efficiently enter cells. All polymers studied were water-soluble (> 100 g/L), but the more hydrophobic the polymer, the more readily it could enter the cell.^{11,12} PEtOx, which is one of the most water-soluble systems, displayed a low endocytosis (molecules absorption by the cells by engulfing them). Moreover, it was observed that the length of the hydrophilic block had no influence on cellular uptake, but it depended on the polymer concentration and on temperature (cellular uptake decreased when the temperature was increased).

In vivo studies were conducted on PMeOx and PEtOx that were radio-labelled and injected into mice and both polymers were rapidly cleared from the body.^{17,18} PEtOx was safe when administered intravenously, and the maximum tolerated dose corresponding to a unique injection (MTD) was greater than 2 g/kg.¹⁴ However, in case of multiple intravenous injections, 20 kDa PEtOx appeared to be safe and non-toxic if injected every 2 days at doses of up to 50 mg/kg over a period of 2 weeks.^{19,20}

In terms of biodistribution and cytotoxicity, POx were compared to other commonly used polymers, such as poly(*N*-(2-hydroxypropyl)methacrylamide) (PHPMA) or PEG.^{18,21}

In vivo POx pharmacokinetics have not been studied yet, but some *in vitro* studies suggested that PEtOx was not subjected to enzymatic degradation. First, a biodegradation study of PEtOx by Proteinase K, a non-human enzyme, was achieved *via* incubation.²² A partial hydrolysis reaction occurred at the amide bond, leading to the formation of a statistical copolymer made of PEtOx and poly(ethylene imine) (PEI, Scheme 3) and ultimately to linear PEI.



Scheme 3 Poly(2-ethyl-2-oxazoline) degradation by Proteinase K

Nevertheless, *in vitro* studies showed that the lower the percentage of linear PEI, the lower the cationic charge density.^{23,24} In such cases, a better cell viability was also observed,^{23,24} and even until 10% of hydrolysis no cytotoxicity was detected.²⁵ More recently, PEtOx degradation in presence of digestive enzymes and in an acidic environment, mimicking physiological conditions, revealed that PEtOx did not undergo hydrolysis.²⁵ As a consequence, POx are most often described as non-biodegradable polymers because only hydrolytic and proteolytic (enzymatic) degradation are

considered. However, a recent study by Luxenhofer *et al.* showed that POx were prone to oxidative degradation under physiologically relevant conditions.²⁶ The generation of reactive oxygen species (ROS) led to a pronounced time and concentration dependent degradation, and *in vivo* degradability seemed feasible. In addition, there is a plethora of ROS in the body (mainly produced in mitochondria, a special sub-units found within eukaryotic cells), which could lead to oxidative stimuli system.

I.2. STEALTH BEHAVIOR AND PROTEIN REPELLENT ACTION OF POLY(2-OXAZOLINE)S

PMeOx and PEtOx are not only compared to PEG because of their similar properties in the therapeutic relevant dosage range (*i.e.* non-toxicity and hemocompatibility properties), but most importantly because all these polymers exhibit a stealth behavior. “Stealth” nanoparticles are defined as possessing properties that allow them to evade clearance by the body and remain in circulation for extended periods of time. Their extended presence in the bloodstream allows for a greater percentage of compound cargo to reach target tissue, as well as to provide more consistent dosing of the tissue.

The stealth behavior of PMeOx and PEtOx was first reported in 1994 by Woodle *et al.*²⁷ who studied the fate of PMeOx or PEtOx coated liposomes injected into rats. The coated liposomes showed dramatic reticuloendothelial system (RES)-evasion and prolonged blood circulation effects compared to uncoated liposomes, which had a short blood lifetime and accumulated in the RES (Figure 1).

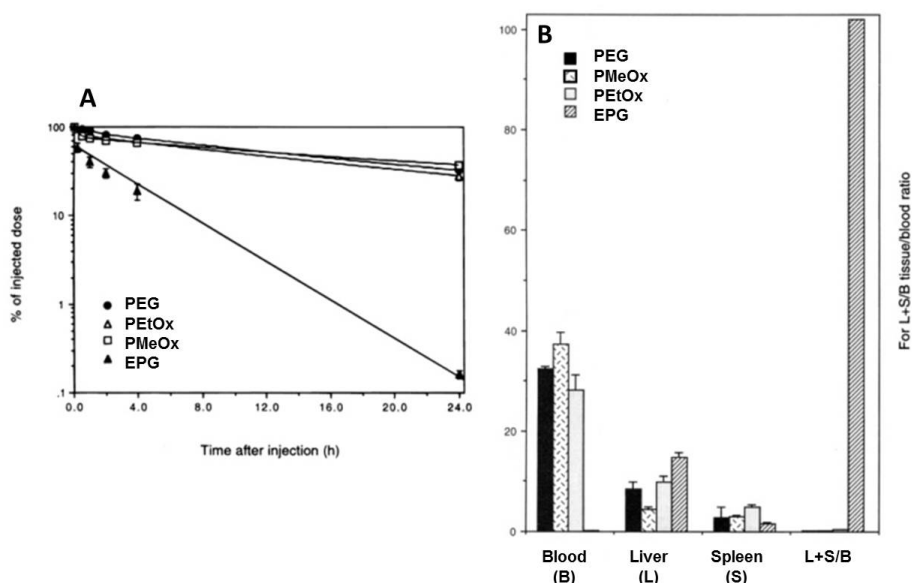


Figure 1 A) Blood circulation time and B) Biodistribution of liposomes coated with poly(ethylene glycol) (PEG), poly(2-ethyl-2-oxazoline) (PEtOx), poly(2-methyl-2-oxazoline) (PMeOx) and of uncoated liposomes, egg phosphatidylglycerol (EPG). Adapted from ref. 27

Moreover, with the POx coated liposomes, the pharmacokinetics were dose-independent. The blood circulation time and biodistribution were compared between POx and PEG coated liposomes. The results showed that both systems presented the same stealth behavior, as confirmed by another study by Zalipsky *et al.*²⁸

The stealth behavior of PEG is due to a steric stabilization effect because PEG chains are mobile, present conformational flexibility and water binding ability.²⁸ PMeOx and PEtOx possess similar solution properties and flexibility, the chain backbone of both polymers being composed of carbon-carbon bonds featuring one heteroatom.²⁸

As a consequence, POx are increasingly regarded as a good alternative to PEG.^{12,29–31} PEGylated systems have been in the market for more than 20 years,²⁰ mainly with protein PEGylation applications (*i.e.* attachment of PEG to a protein), as it enhances the permeability and retention effect, increases the biodistribution, the cellular targeting and the solubility of insoluble drugs in water or of enzymes in organic solvents due to its amphipatic properties.³² The new challenge is to be able to have site-selective PEGylation to increase the degree of homogeneity and to preserve the bioactivity.³³ However, because of this intensive use of PEG, PEGylated systems lose their function when placed *in vivo* because of specific and nonspecific recognition of PEG by the immune system. Specific antibodies were detected in the serum of patients treated with PEG-asparaginase and PEG-uricane. Anti-PEG antibodies were also identified in the case of patients who never received treatment based on PEG, due to the presence of PEG in food products.³⁴ These antibodies have a neutralizing effect and cause the loss of therapeutic efficacy.³⁵

Similarly to POx, PEG is described as a non-biodegradable (hydrolytic and enzymatic wise) polymer, but it is actually more sensitive to oxidative degradation than POx and the products resulting from the oxidative degradation of PEG were found to be toxic in humans.²⁰

Another disadvantage of PEG is its low drug content when used as a bioconjugate, as the only way to attach a drug molecule to a PEG chain is through the end functionalities. In contrast, due to the versatility of 2-oxazolines, such as in 2-oxazoline monomers bearing a functional group on their side chain, several drug molecules can eventually be coupled to the polymer chain. In addition, the end functionality can even be used to attach another active compound such as targeting moieties. POx functionalization will be discussed in greater details in section III of this chapter.

Last but not least, POx are less viscous than PEG, which makes the pharmaceutical formulation easier.³⁶

The protein repellent action of POx is a direct consequence of their stealth behavior. It has been studied for comb-polymers made from a poly(L-lysine) backbone and PMeOx side chains (PLL-g-PMeOx),³⁵ deposited on negatively charged surfaces, forming a polymer coating. This coating was then exposed to human serum albumin (HSA), and the adsorption of protein was monitored by optical spectroscopy that allowed *in situ* measurement of the surface immobilization of biomolecules in an aqueous environment. Even after several exposure cycles to HSA, no mass uptake was observed, indicating that protein adsorption was below the detection limit of the instrument (< 2 ng/cm²). Similar results were obtained for PEG-based systems. These results were corroborated with other POx architectures, such as polymer brushes,²⁹ bottle-brush brushes copolymers,³⁷ capsules,³⁸ hydrogels,^{39,40} or amphiphilic POx-based block copolymers⁴¹ where POx always presented a protein repellent character. Some compounds also showed an antimicrobial activity (*i.e.* bacteria repellent)²⁹ and were even cell repellent,^{37,39} leading to low or non-fouling systems.

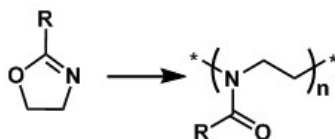
POx brushes were compared to the equivalent PEG brushes, and it appeared that the coating made of POx brushes had a better stability under physiological conditions, especially in an oxidative environment. In addition, the degradation of PEG surfaces under oxidation conditions led to protein adsorption.²⁹

Both POx architecture and composition are also of great importance: PLL-g-PMeOx brushes prevented protein adsorption and suppressed bacterial surface adhesion,²⁹ whereas linear PEtOx and poly(2-nonyl-2-oxazoline) (PNonOx) showed no antimicrobial activity.⁴² Concerning the composition, it was shown that the more hydrophilic the system (*i.e.* the POx used), the better the non-fouling properties.³⁷ Anti-microbial activities were also increased with the POx percentage of hydrolysis.⁴²

To summarize, POx, and especially PMeOx and PEtOx, proved non-toxic to cells, hemocompatible and internalized by cells. *In vivo*, they presented the same stealth behavior as PEG and could also be used as protein repellent. Last, studies on their *in vitro* degradation showed that POx were not sensitive to hemolytic or enzymatic degradation under physiological conditions, but could be cleaved by oxidative degradation under the same conditions leading to a possible degradable polymer. POx thus appears as valuable competitors in terms of biological properties compared not only to PEG, but also to other hydrophilic polymers used in biomedical applications, such as poly(vinyl pyrrolidone) (PVP), or polymethacrylamides.⁴³

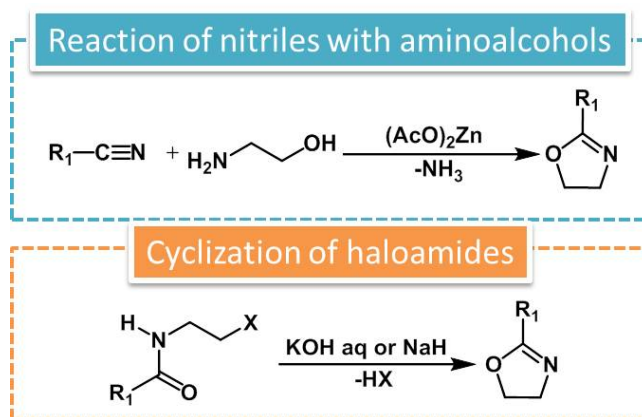
II. SYNTHESIS OF POLY(2-OXAZOLINE)S

2-Oxazolines represent a special class of 5 membered cyclic imino-ethers. Their “controlled/living” polymerization was discovered in 1966 by four different research groups simultaneously.^{44–47} Since then, their ring-opening polymerization (ROP) has been described in several reviews^{48–50} and book chapters.⁵¹ Scheme 4 shows the general scheme of such a ROP of 2-substituted-2-oxazolines.



Scheme 4 Polymerization of 2-substitued-2-oxazolines

The first monomers studied in polymerization reactions were 2-methyl-2-oxazoline (MeOx) and 2-phenyl-2-oxazoline (PhOx).⁴⁴ These monomers, now with 2-ethyl-2-oxazoline (EtOx), are still the most commonly used because of their commercial availability. However a wide variety of 2-substituted-2-oxazolines can be synthesized through various reaction schemes, such as the reaction of nitrile or isocyanides with amino-alcohols, the cyclization of haloamides, etc (Scheme 5). The different synthetic ways to 2-substituted-oxazolines were previously reviewed.^{48,49}



Scheme 5 Examples of 2-oxazoline monomer synthesis

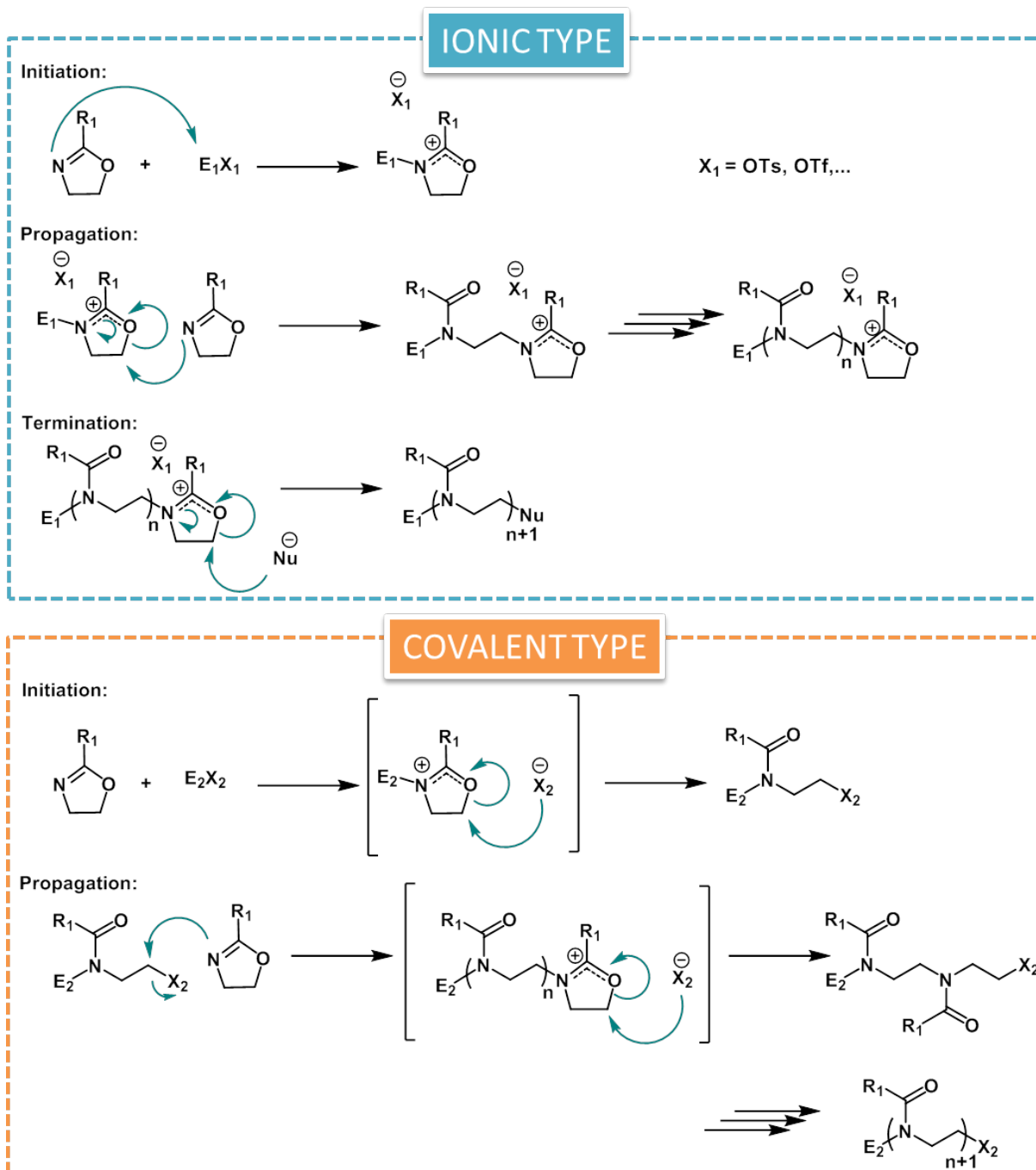
II.1. POLYMERIZATION MECHANISM: INITIATION AND PROPAGATION

The ROP of 2-oxazolines can be initiated by various reagents including Lewis acids (BF_3 , $AlCl_3$), strong protic acids ($HClO_4$, HBr , H_2SO_4), oxazolinium salts,⁵¹ strong cationic Bronsted acids,⁵² or more generally X of an electrophile RX , where the X typically stands for *p*-toluenesulfonate (OTs), trifluoromethanesulfonate (OTf), or Br, Cl or I. Polymerization can be conducted in relatively polar aprotic solvents, such as dimethylformamide (DMF), dimethylacetamide (DMAc) or in bulk, but the most commonly used solvent is acetonitrile (CH_3CN).

The termination agent has to be a nucleophilic species possessing a greater electron donating capacity than that of the monomer. Most common nucleophiles are water, alcohols or secondary amines (like piperidine).

The choice of initiator and termination agent will thus determine the end functionalization of the polymer chain and will be discussed in greater detail in section III.

Depending on the nucleophilic reactivity of the counter anion arising from the initiator, two different mechanisms, namely, the cationic and the covalent mechanism, can operate (Scheme 6).^{49,53} In the case of a cationic ROP, an electrophile species initiates the reaction, creating a cationic oxazolinium propagating species. The polymerization reaction corresponds to the nucleophilic attack of the subsequent monomer resulting in a ring opening step. Termination can be achieved by the addition of an external nucleophilic species. However, when an initiator generating a stronger nucleophile is used, the polymerization proceeds *via* covalent-bonded species. In this case, the 2-oxazolinium ring is eventually opened by the counter anion that has a higher nucleophilicity than the monomer. Last, when the nucleophilicity of the monomer and of the counter anion of the initiator are comparable both mechanisms can coexist.



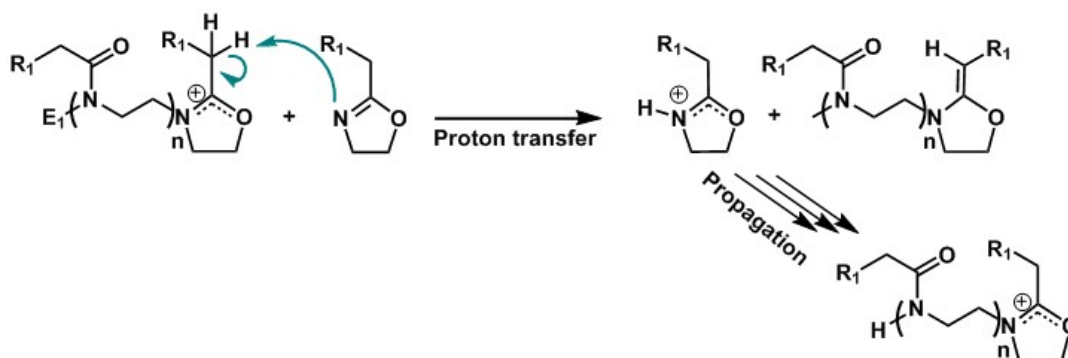
Scheme 6 Polymerization mechanisms

The reaction of the oxazolinium salt with the counter ion in the covalent mechanism is comparable to the termination reaction of the cationic mechanism. However, the covalent species proceed to react with the monomer and propagation continues.

Most of the initiators used currently, such as methyl *p*-toluenesulfonate (MeOTs) and methyl trifluoromethanesulfonate (MeOTf), lead to a true cationic polymerization pathway because they give rise to stable (less nucleophilic) tosylate and triflate anions, respectively.

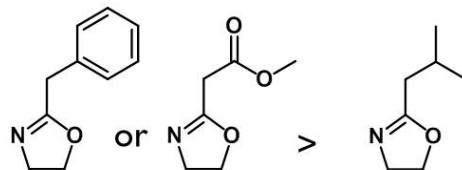
II.2. POLYMERIZATION MECHANISM: TRANSFER AND TERMINATION BY COUPLING

In the ideal case, the ROP of 2-oxazolines can be controlled, but one has to be aware that some side reactions can occur. For instance, a transfer reaction takes place by the abstraction of a proton from the R_1 -carbon atom of the propagating species, by the nitrogen atom of a monomer.⁵⁴ Consequently, a positively charged “activated” monomer and a non-charged polymer with a C=C double-bond are formed (Scheme 7).



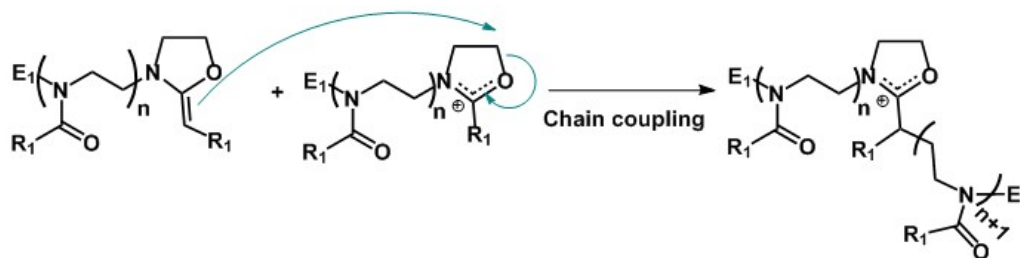
Scheme 7 Mechanism of chain transfer

This mechanism has been highlighted by Litt *et al.* in 1975.⁵⁴ They demonstrated that the major site of chain transfer is the carbon in α -position from the ring. A greater chain transfer is observed for POx with activated methylene groups such as 2-benzyl or 2-acetoxymethyl, whereas for polymers such as poly(2-isobutyl-2-oxazoline) where the α -methylene group is shielded, the chain transfer is reduced (Scheme 8). A greater chain transfer is also observed for PMeOx than for the polymerization of other 2-alkyl-2-oxazolines.



Scheme 8 Extent of chain transfer depending on the monomer side-chain

Once this chain transfer reaction has occurred, the dormant ene-terminated POx chain can act as a nucleophilic species *via* a process called chain coupling, which increases the molecular weight (Scheme 9). Nevertheless, the dormant chain being less nucleophilic than the monomer, it reacts more slowly, and most of the coupling reaction occurs during the last phase of the polymerization reaction.^{54,55} The mechanism of chain transfer and coupling has been confirmed by Warakowski *et al.*⁵⁶



Scheme 9 Mechanism of chain coupling

In order to control the polymerization and to avoid such side reactions, specific conditions have to be fulfilled, *i.e.* high purity of monomer, solvent and initiator, low $[M]/[I]$ ratio, a monomer with no α -hydrogen, and a solvent with no protic hydrogen atoms.⁵⁶ Another hindrance of the polymerization of 2-oxazolines is the rather long reaction time (reactions could last up to several days at 85 °C). Consequently, the optimization of the polymerization reaction conditions has been the subject of numerous studies, in order to reduce the reaction time. All parameters have to be considered to reach the optimum conditions: temperature, solvent, initiator and monomer used, monomer concentration, $[M]/[I]$ ratio, and heating process.

If chain transfer and coupling can be excluded, the polymerization proceeds in a “controlled/living” manner, which can be exploited in the design of well-defined systems and for block copolymer synthesis as well. In such a case, the concentration of propagating species is constant and the polymerization proceeds *via* a first order kinetic. As a matter of fact, the size exclusion chromatography (SEC) trace should be a narrow peak with no shoulder (coupling) or tail (transfer). One has to be aware, however, that the nitrogen atoms present on the backbone of the polymer can interact with the SEC column materials, and this may also contribute to the tail observed in the SEC traces. With the choice of a suitable solvent, such as DMF, most of the interactions with the column material can be suppressed.⁵⁷

Another interesting parameter that can be used to examine and elucidate the transfer and coupling reactions is the color of the reaction medium; it turns from clear to yellowish when chain transfer and/or coupling are occurring.⁵⁸

II.3. OPTIMIZATION OF THE REACTION PARAMETERS

In order to study the influence of each parameter, systematic studies (*i.e.* by varying one parameter at a time) have been conducted, mainly by Hoogenboom *et al.*, using an automated synthesizer (Chemspeed ASW200)⁵⁹ allowing to conduct 16 experiments simultaneously and with high reproducibility.

First, the influence of temperature was studied.⁵⁸ Sixteen PEtOx were synthesized under the same conditions (in DMAc using benzyl bromide as an initiator, with a $[M]/[I]$ ratio of 60 and a reaction time of 16h), but the temperature varied between 80 °C to 130 °C. As expected, the reaction rate increased with temperature due to the activation energy. The number-average molecular weight (\overline{M}_n) obtained from SEC increased linearly at 90 °C and 100 °C. Below 90 °C, no polymerization occurred and above 100 °C, it was not well-controlled.

The influence of temperature was also studied for the CROP of PhOx under the same conditions.⁶⁰ Its polymerization was more difficult to initiate than EtOx. With benzyl bromide as the initiator, polymerization was observed only at 140 °C and 150 °C and not in a quantitative manner. When using MeOTs as the initiator, linear first-order kinetics were obtained with an optimal temperature reaction of 130 °C. At lower temperature, the initiation was too slow and not all the polymer chains were growing at the same time (dispersity $\mathcal{D} > 1.40$); at higher temperature, side reactions were observed.

In addition, Park *et al.* used 2-isopropyl-2-oxazoline (iPrOx) and EtOx to synthesize homopolymers and gradient copolymers in acetonitrile, using MeOTs as initiator. They showed that mild temperature conditions, *i.e.* 42 °C, were optimum to avoid chain transfer and coupling (Figure 2).⁶¹

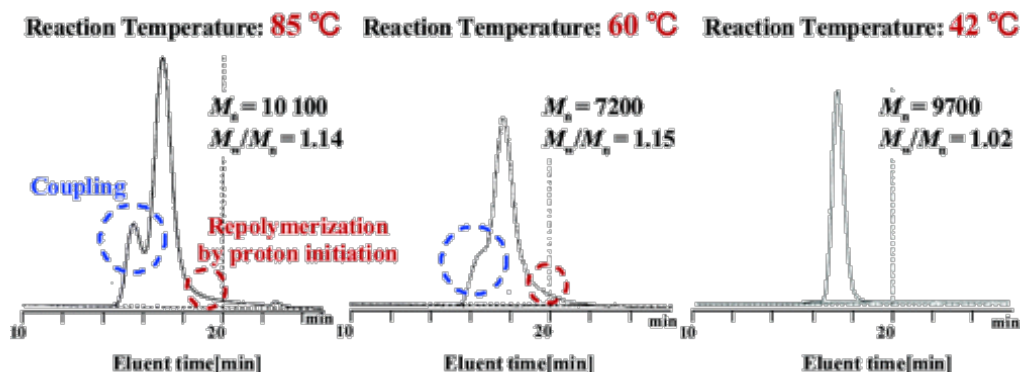


Figure 2 SEC traces of poly(2-isopropyl-2-oxazoline) prepared at different temperatures. Reprinted from ref. 61

The different POx obtained had a low dispersity ($\mathcal{D} = 1.02$) showing that the polymerizations were well controlled. However, as the temperature was decreased, reaction times were longer: up to 476.5h to get a PiPrOx with a degree of polymerization (DP) of 86, which represents a severe limitation.

The influence of the initiator was also studied for the CROP of MeOx, EtOx, PhOx and NonOx. The polymerization rate matched well with the decrease in nucleophilicity of the counter-ion: methyl

triflate (MeOTf) > MeOTs > methyl iodide (MeI) > benzyl bromide (BB).⁶² However, polymerizations initiated with MeOTf or MeOTs exhibited a loss of control, as indicated by a curved first-order kinetic behavior. This was ascribed to the fact that more active initiators were more sensitive to moisture and other contaminations.

Monomer concentration was optimized for the CROP of EtOx. The optimal monomer concentration was between 4 and 7M when polymerization was conducted at 100 °C in DMAc, using BB as the initiator, with a $[M]/[I]$ ratio of 60.⁵⁷ At lower concentration indeed, a deviation from the theoretical molecular weight was observed, and the dispersity values were high (between 1.6 and 1.9) with a tail at lower molecular weight, due to chain transfer reactions. At higher concentration, a shoulder characteristic of chain transfer and coupling was observed on the SEC trace. These differences were attributed to differences in the initiation process at low and high monomer concentration, but the exact mechanism is still being debated.⁵⁵

The reactions were also dependent on the solvent used: polymerization at 80 °C in acetonitrile was faster than at 90 °C in DMAc, but lower than at 100 °C in DMAc. This difference could be explained by the slightly higher dipole moment of acetonitrile that led to better solvation of the propagating oxazolinium rings.⁶²

The substituent group of the monomer has also a direct influence on the kinetics of the reaction and the occurrence of side reactions. The monomer reactivity increases with its nucleophilicity, but it also becomes more prone to side reactions.^{54,63} The higher nucleophilicity of MeOx resulted in a slightly faster polymerization rate compared to other monomers (EtOx, PhOx, NonOx). By copolymerizing monomers with different reactivities, side reactions could be avoided. For example, when MeOx was polymerized at 80 °C in acetonitrile, with MeOTs as an initiator, no polymer with a DP superior to 100 could be obtained without the occurrence of chain transfer. When MeOx and EtOx were copolymerized, EtOx being less susceptible to side reactions than MeOx, copolymers with DP up to 500 were obtained in a controlled manner.⁶⁴

Optimal conditions for a better control on the polymerization are thus different from one system to another, and the reaction times are still quite long, between 10h and a few days. In 2004, PEtOx was synthesized for the first time in a single mode microwave synthesizer, in acetonitrile, using MeOTs as the initiator and with a $[M]/[I]$ ratio of 60.⁶⁵ The reaction rate was significantly increased with temperature, as observed in conventional syntheses, but under microwave irradiation the solvent boiling point (82 °C for acetonitrile) was no longer a limiting factor as the pressure inside the vial also increased (up to 1 bar). Hence, the reaction could be performed even at 200 °C,⁶⁵ with a reaction rate up to 350 faster. Nevertheless, below 100 °C and above 160 °C side reactions were still present; the optimal temperature was 140 °C, at which PEtOx synthesis was completed in 10

minutes, with a dispersity below 1.10. The living character of the polymerization was also retained at all studied temperatures (between 80 and 190°C). A control experiment at 140°C under conventional heating in a high pressure vial revealed the same reaction speed, meaning that the increase in reaction rate was eventually not linked to any “microwave effect”, the microwave reactor being only used as an efficient heating device. The fast and direct heating applied without contact and the use of a good microwave absorbing solvent like acetonitrile are thus the keys factors. The efficiency of the polymerization under microwave irradiation was later confirmed for other homopolymer syntheses (PMeOx, PPhOx, PNonOx), where polymerization was still controlled ($\bar{D} < 1.2$) while being up to 400 faster.⁶⁶ Block copolymer synthesis was also possible under such conditions.⁶⁷

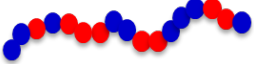
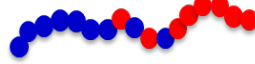
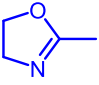
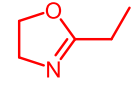
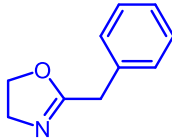
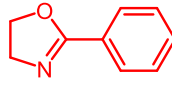
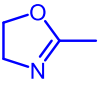
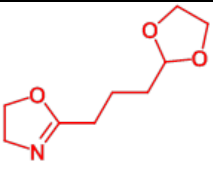
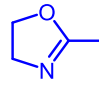
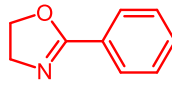
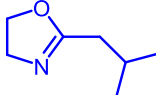
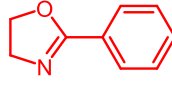
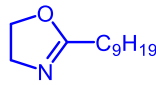
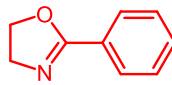
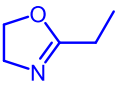
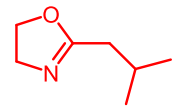
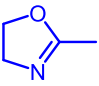
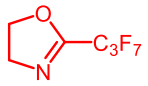
Thus microwave synthesizers seem to be powerful devices, overcoming the long reaction times necessary under conventional heating conditions, while producing polymers in a well-controlled manner and yielding products with lower dispersity values.⁶⁸ This new synthetic approach has brought POx to the fore front, and since then, POx research is mainly focused on POx engineering and applications.

III. POLY(2-OXAZOLINE)S: A VERSATILE POLYMER CLASS

III.1. TAKING ADVANTAGE OF THE LIVING POLYMERIZATION: COPOLYMERS SYNTHESIS

By taking advantage of the “controlled/living” character of the polymerization, statistical and block copolymers or even more complex architectures can be readily synthesized. The easiest and widely used method to obtain block copolymers is *via* the “one pot two stages” method where the second monomer is added once the first one is consumed.^{69,70} This method is also referred to as the sequential polymerization method. When two different monomers are added simultaneously, the composition of the copolymer can be predicted thanks to the reaction rate of each monomer: if the reactivities of both monomers are comparable, statistical copolymers are expected⁶⁴ whereas if one monomer is less reactive than the other, gradient copolymers are obtained.^{61,71} In some cases, block copolymers can also be obtained by this method, as it was demonstrated for the synthesis of PMeOx-*b*-(2-heptafluoropropyl-2-oxazolines), on the basis of highly different reactivity between the two parent monomers.⁵³ Some examples of statistical, block and gradient copolymers are given in Table I.

Table I Example of copolymers synthesized in the literature

Statistical			Gradient		
$r_{M1} \approx r_{M2}$			$r_{M1} > r_{M2}$		
					
M ₁	M ₂	Ref.	M ₁	M ₂	Ref.
		72			71
		73			71
Diblock					71
$r_{M1} \gg r_{M2}$					74
M ₁	M ₂	Ref.			61
		53			

III.2. INTRODUCTION OF FUNCTIONALITIES

By varying the initiator and termination agents, both α - and ω -chain ends of POx can be functionalized. The synthesis of POx with functional handles can also be achieved by resorting to specific functional 2-oxazoline monomers (Figure 3).

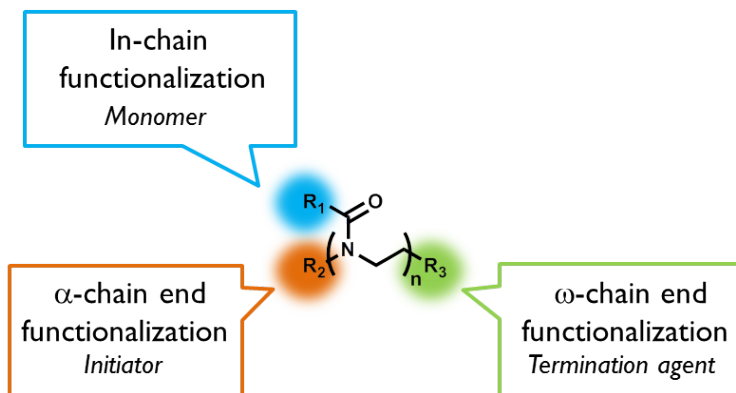


Figure 3 Possible ways to functionalize poly(2-oxazoline)s

For the scope of this PhD thesis, recent examples of such functionalized POx will be presented. This list may not be exhaustive, but synthetic strategies to functionalized POx have been recently reviewed.^{1,43,75} In addition, a patent about chain-end POx functionalization has been filed,⁷⁶ whereas the synthesis of monomers with various substituents was reported in papers.^{77,78}

III.2.1. IN-CHAIN FUNCTIONALIZATION THROUGH THE USE OF FUNCTIONAL MONOMERS

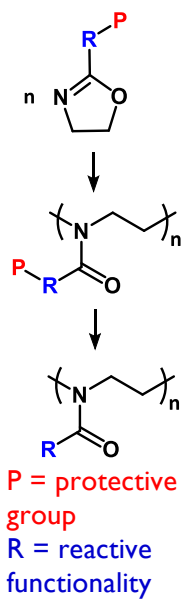
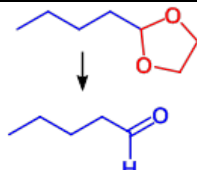
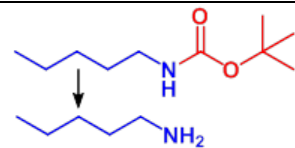
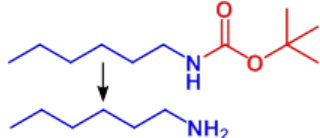
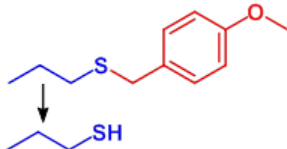
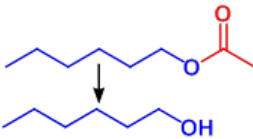
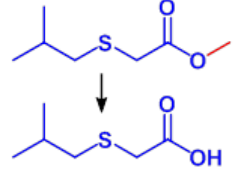
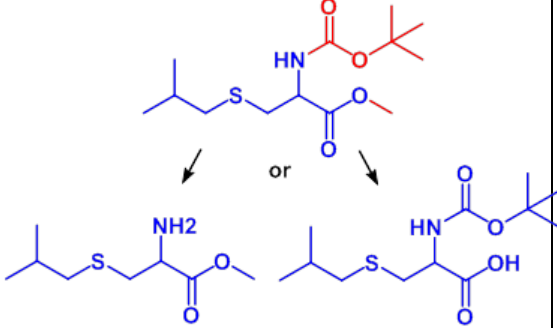
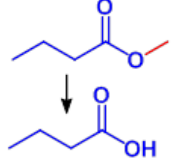
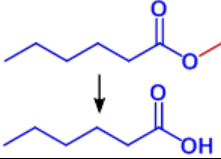
The first option to functionalize POx is to directly polymerize a monomer bearing a reactive handle (R). Whatever the R group is, the side chain of the monomer may not interfere during the CROP process. Consequently, a protecting group has often to be used to avoid any side-reaction of the R group with the propagating species. For example, monomers with an unprotected hydroxyl⁷⁹ or amino group⁸⁰ gave rise to chain transfer leading to the synthesis of branched polymers of high dispersity. As illustrated in Table 2, monomers containing alcohol,⁷⁹ carboxylic acid,^{79,81,82} amine,^{83,84} aldehyde⁷³ or thiol⁸⁵ functionalities thus require protection in the form of ester groups, *tert*-butyloxycarbonyl groups (BOC), ketal rings or methoxybenzyl groups, respectively. The resulting polymers were deprotected, most of the time in the presence of trifluoroacetic acid (TFA), before any post-polymerization modification.^{86–88} For example, POx with the aldehyde functionality (obtained from monomer 1, Table 2) further reacted in a quantitative way with amino-oxy compounds forming the corresponding oxime. POx with amino functionalities (from monomers 2 and 3) were able to react with different isocyanate compounds such as a fluorescence dye (tetramethylrhodamine isothiocyanate), or bifunctional isothiocyanates in order to form hydrogels.⁸³ Hydrogels were also formed from POx with pendant amino functionalities (monomer 2) in reaction with epichlorohydrin.^{84,89}

On the other hand, alkene and alkyne functionalities are increasingly being used because they are compatible with the living cationic polymerization, consequently no protecting group is needed, and because of the possible coupling reactions by further “click chemistry”.^{90,91} For example, 2-(pent-4-

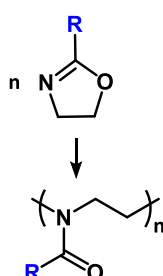

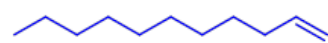
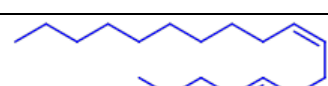
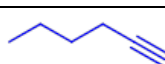
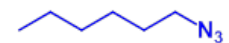
nyl)-2-oxazoline (monomer 13) could be copolymerized with MeOx and EtOx⁹² and pendant alkyne moieties could quantitatively yield triazoles by copper-catalyzed coupling. A monomer bearing an azide functionality has also been reported (monomer 14).⁹³

The synthesis of a 2-oxazoline monomer bearing an alkyl chain with alkene functions from renewable raw materials, such as unsaturated fatty acids present in vegetable oils, was reported (monomer 11).^{94,95} Thiol-ene chemistry could be performed on related POx using different mercaptans (RSH), resulting in the binding of protected glucose, fluorinated compounds,⁹⁶ dodecane chain⁹⁵ or 2-mercaptoethanol (monomer 10 and 11).⁹⁴ Diehl *et al.* synthesized thermoresponsive poly(2-oxazoline)s with a wide range of tunable low critical solution temperature (LCST, *i.e.* the critical temperature below which the components of a mixture are miscible for all compositions⁹⁷) by “clicking” different α -functionalized thiols to a statistical poly[2-(isopropyl/3-butenyl)-2-oxazoline] copolymer.⁹⁸ POx with aryl, ester, amine, and carboxylic acid side chains were synthesized using the thiol-ene coupling between a thiol and the pendant alkene of 2-isopropenyl-2-oxazoline before the polymerization (monomers 6 and 7).⁸¹ Apart from the classic azide-alkyne and thiol-ene coupling reactions, a reaction between a POx with an alkene side group with different functional acrylates, by cross-metathesis, was also reported.⁹⁹

Table 2 R side groups of 2-R-2-oxazolines allowing for functionalization of POx pendant chains

		Monomer side functionality	Post-polymerization reaction	Ref.
Monomer with protected functionalities  P = protective group R = reactive functionality	1		With amino-oxy compound	73
	2		With epichlorhydrin	84,89
	3		With (di)isocyanates	83
	4		With acrylamide or maleimide	85
	5		n.i.	79
	6		n.i.	81
	7		n.i.	81
	8		n.i.	79
	9		With a secondary amine	82

n.i.: not investigated

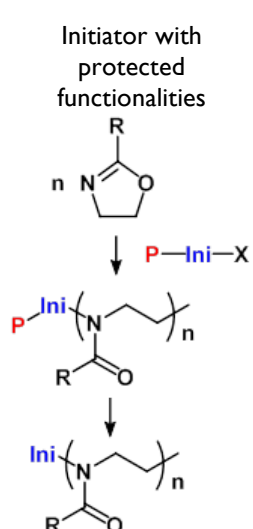
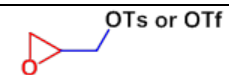
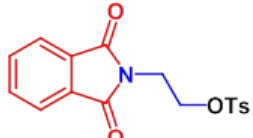
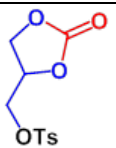
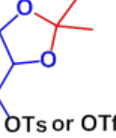
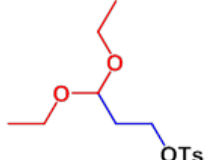
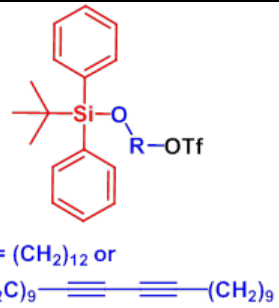
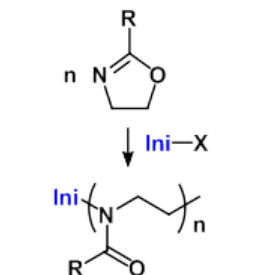
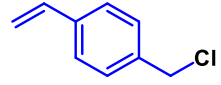

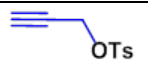
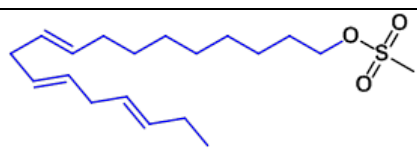
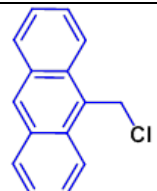
		Monomer side functionality	Post-polymerization reaction	Ref.
Monomer with unprotected functionalities 	10		Thiol-ene	16,96,98, 100–104
	11		Epoxidation with 3-chloroperoxybenzoic acid	105,106
			Thiol-ene	38,39,94, 95,107,108
			Cross-metathesis with functional acrylates	99
	12		Cross-linking under UV-radiation	2,106,109–111
	13		Azide-alkyne	92
14		Azide-alkyne	93	

In comparison to PEG, the ability to introduce various functionalities along the polymer backbone that could be involved in post-polymerization reactions to covalently attach, for instance a drug, represents a major advantage of POx.³⁰

III.2.2. FUNCTIONALIZATION OF THE α -CHAIN END

As illustrated in section II.1, a wide variety of initiators can be used to polymerize 2-oxazolines *via* either a cationic or a covalent mechanism. More recently, an array of initiators with reactive functionalities has been reported. Major examples are given in Table 3. As with functionalized monomers, if the initiator functionality is suspected to interfere with the polymerization process, it has to be protected (e.g. alcohol, amine or aldehyde functionalities). In addition, most of the designed initiators are oxygenated bases, with *p*-toluene sulfonate (OTs) or trifluoromethanesulfonate (OTf) functionalities operating in a true CROP process.

Table 3 Initiators with reactive functionalities for the CROP of 2-oxazolines

		Initiator	Deprotected function	Post-polymerization reaction	Ref.
<p>Initiator with protected functionalities</p>  <p>P = protective group X = OTs, OTf, Br, Cl or I.</p>	1		Diol	Acylation	112
	2		Amine	Reductive amination	113
	3		Diol	Reaction with isocyanate and carbonate compounds	114
	4		Diol	Acylation	112
	5		Aldehyde	-	115
	6	 R = (CH₂)₁₂ or (H₂C)₉-C≡C-C≡C-(CH₂)₉	Alcohol	-	116
<p>Initiator with unprotected functionalities</p> 	7		-	Polymerization of the vinyl unit	117
	8		-	Azide-alkyne reaction	118
	9		-	Azide-alkyne reaction	118-124
	10		-	-	125
	11		-	Diels-Alder reaction	107

Most of the initiators presented in Table 3 were involved in post-polymerization reactions leading to more complex polymer structures. For instance, the azide-alkyne click chemistry reaction involving POx initiated by propargyl tosylate (initiator 9, Table 3) was extensively used. Propargyl tosylate initiated the CROP of MeOx and the polymer chain was further coupled to polydimethylsiloxane (PDMS) to produce an amphiphilic copolymer.¹²¹ Initiator 9 was also used to polymerize iPrOx, and subsequent coupling on fluorenylmethoxycarbonyl-tyrosine phosphate (Fmoc-pY) allowed forming a phosphatase/temperature responsive diblock copolymer.¹²² Last, Fijten *et al.* polymerized different 2-oxazolines (MeOx, EtOx, PhOx, NonOx) with propargyl tosylate and clicked the acetylene-functionalized PEtOx to heptakis-azido- β -dextrin giving rise to the formation of a star polymer.¹²⁶

Some initiators were not designed purposely for post-polymerization modification, but still illustrate the versatility of POx, as shown in Figure 4.

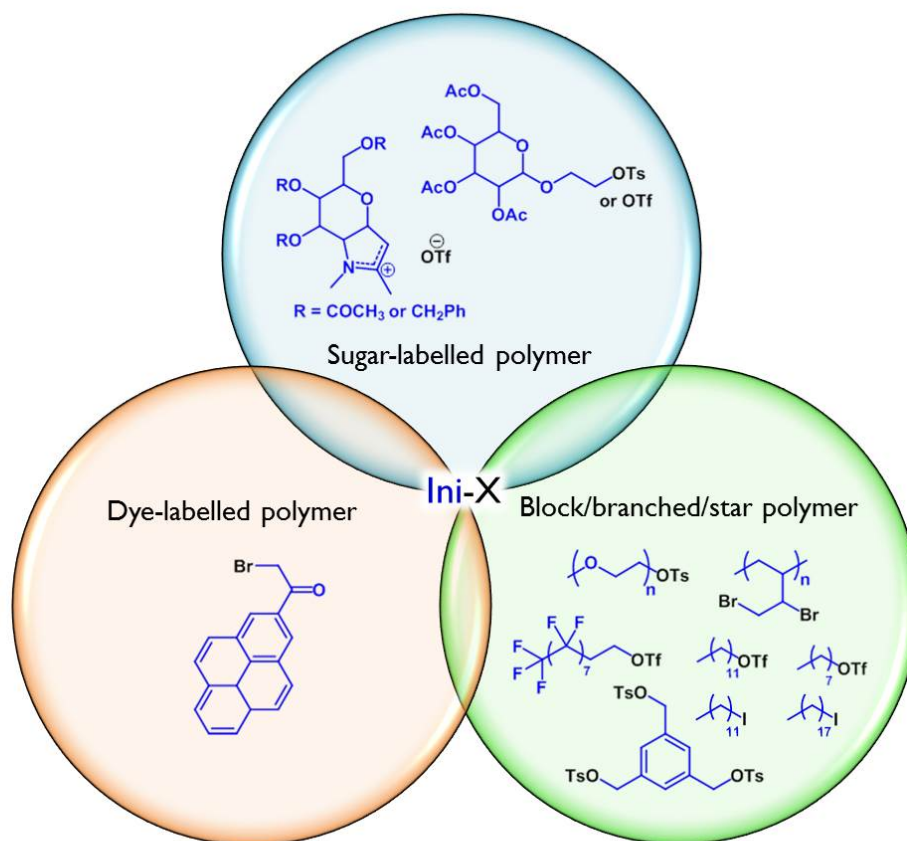


Figure 4 (Macro-)initiators for the polymerization of 2-oxazolines

Macro-initiators like fully brominated 1,2-polybutadiene,¹²⁷ polyethylene glycol-tosylate,⁶⁴ lipo-triflates,^{128,129} lipo-tosylates,^{129,130} lipo-iodine^{131,132} or tris(triflate)benzene¹³³ were used to initiate the polymerization of 2-oxazolines, resulting in graft, diblock and star copolymers, respectively. The capability of a range of protected glucose-, galactose-, and fructose-based tosylates and triflates to

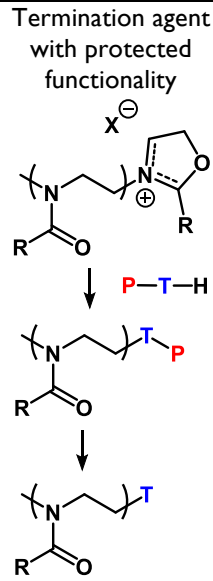
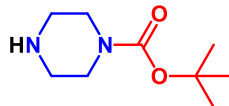

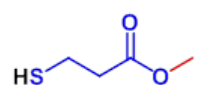
initiate the CROP of EtOx was also investigated, leading to sugar-containing polymers.^{134,135} Last, EtOx polymerization was initiated by a fluorescent tosylate derivative.¹³

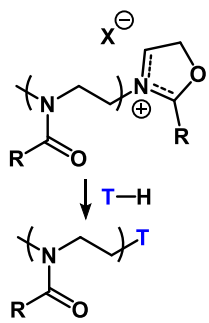

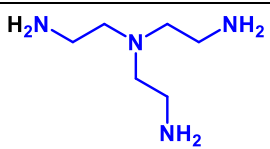
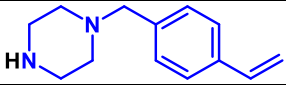
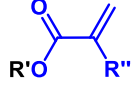
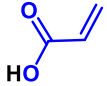
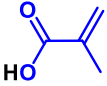
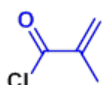
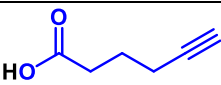
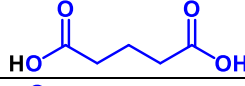
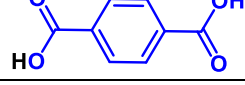
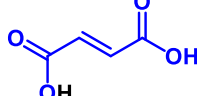
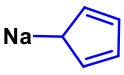
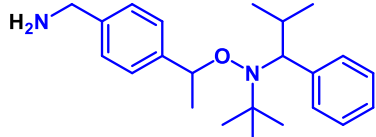
Besides triflate and tosylate derivatives, EtOx was polymerized using acetyl bromide, acetyl chloride and acetyl iodide as initiator.¹³⁶ This study broadened the range of possible acid halide initiators, which can be easily obtained from different commercially available carboxylic acid compounds.

III.2.3. FUNCTIONALIZATION OF THE ω -CHAIN END

Termination at the completion of CROP of 2-oxazolines proceeds *via* the addition of a compound with a higher nucleophilic power than the monomer. The most commonly used nucleophile is simply water, leading to a polymer with an alcohol terminal functionality. As a consequence, variation of the polymer chain end can either be achieved by post-polymerization modification of the terminal –OH group, or by direct attack of nucleophiles bearing a functionality, on the cationic polyoxazolinium species. In Table 4, an overview of the termination agents with protected or unprotected functionalities is provided.

Table 4 Termination agents with reactive functionalities for the polymerization of 2-oxazolines

	Termination agent	Possible available function after deprotection	Post-polymerization reaction	Ref.
Termination agent with protected functionality  P = protective group T = termination group		Amine	-	116
			With carboxylic acid	18
			With methacrylamide chloroformate	137
			With carboxylic acid compound	18
2		Silanol	Intermolecular condensation	138
3		Carboxylic acid	With amine compounds	139

		Termination agent	Possible available function	Post-polymerization reaction	Ref.
Termination agent with unprotected functionalities 	4	$\text{H}_2\text{O}/$ $\text{KOH aqueous solution}/$ $\text{Na}_2\text{CO}_3 \text{ aqueous solution}$	Alcohol	- With phthalimide compound	116 115
	5		Amine	With anhydride compound	140
	6		Amine	Cross-linking with dibromo, dialdehyde or diisocyanate compound	141
	7		Alkene	Polymerization of the vinyl unit	117
	8	 $\text{R}' = \text{Na, K, Ag, NR}_4, \text{NHR}_3, \text{SiR}_3$ $\text{R}'' = \text{H, CH}_3$	Acrylate/ methacrylate	-	142
	9		Acrylate	-	143
	10		Methacrylate	- Polymerization of the methacrylate units by ATRP	143 21,38,134, 144
	11		Methacrylate	Hydrogel formation with a trimethacrylate cross-linker	145
	12		Alkyne	Azide-alkyne	146
	13		Carboxylic acid	-	143
	14		Carboxylic acid	-	143
	15		Carboxylic acid	-	147
	16	Na-N_3	Azide	Azide-alkyne	107,148
	17		Cyclopentadienyl	Diels-Alder reaction with N-substituted maleimides	149
	18		Alkoxyamine	Radical polymerization of styrene	150

Another common termination agent is *N*-*tert*-butyloxycarbonylpiperazine (*N*-BOC-piperazine) (termination agent 1, Table 4), that leads to an amine functionality after treatment with TFA.¹⁸ The as-formed amine end-function was coupled with a common chelator (*N,N',N'',N'''*-tetraazacyclododecane-1,4,7,10-tetra-acetic acid (DOTA)), leading to a radio-labelled polymer after chelation of ¹¹¹In, and used for *in vivo* imaging studies.¹⁸ Alternatively, methacrylamide chloroformate was employed for post chemical modification and the methacrylamide function was further polymerized by free-radical polymerization, leading to brush-like polymers.¹³⁷ Clickable functions were also introduced by quenching the polymerization with sodium azide (termination agent 16),¹⁴⁸ sodium cyclopentadienide (termination agent 17)¹⁴⁹ or hexynoic acid (termination agent 12).¹⁴⁶

Some of these termination agents directly imparted a specific property to the POx. A dye, such as fluorescein, could for instance terminate the polymerization, leading to a fluorescent polymer. Quaternary ammonium groups, like *N,N*-dimethyldodecylamine (DDA), known as a biocide functional group, led to polymer with antimicrobial properties (Figure 5).^{151–153}

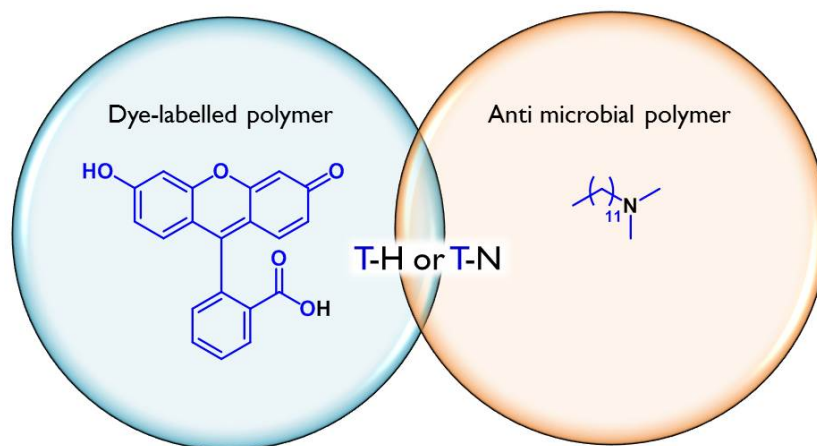


Figure 5 Termination agents used to quench the polymerization of 2-oxazolines

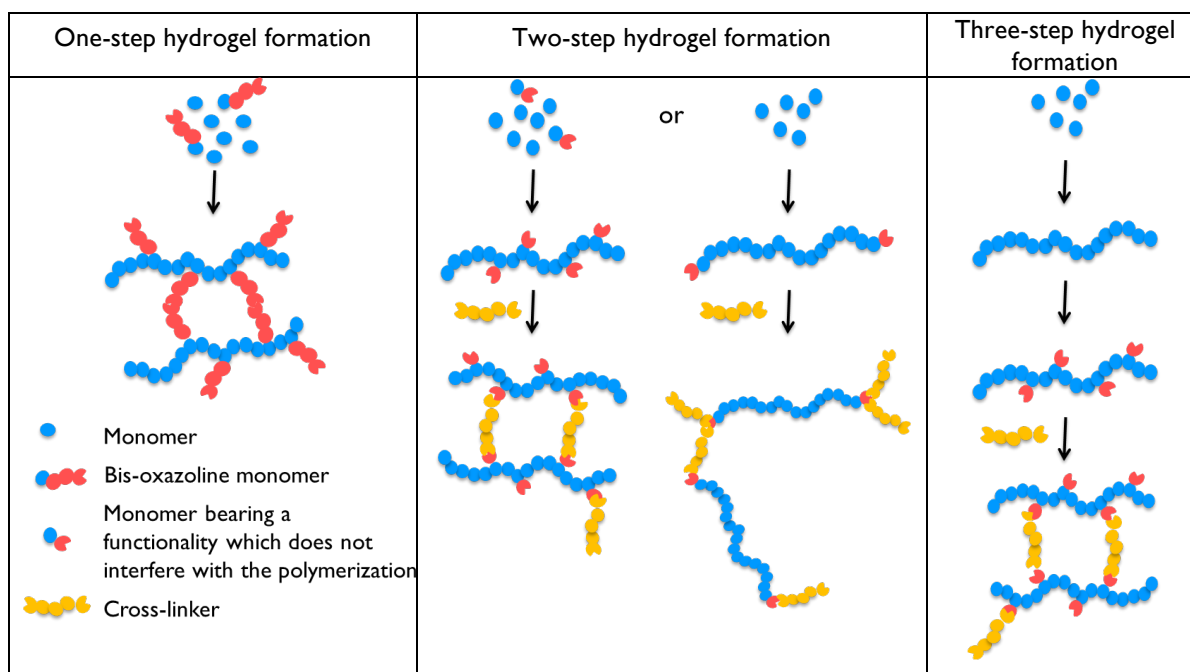
In summary, a plethora of chemical functionalities can be introduced into the POx structure, either within the polymer backbone or at both chain ends, giving rise to a versatile POx toolbox, which may be used to achieve polymers with various architectures and properties.

III.3. POLY(2-OXAZOLINE)S HYDROGELS

A hydrogel is one specific architecture that could be obtained thanks to the introduction of specific functionalities into the POx chemical structure. A hydrogel is defined as a cross-linked network of hydrophilic polymer chains.¹⁵⁴ To be able to form this network, the polymer chains need to bear reactive functionalities. Different routes can be used to produce POx hydrogels, depending on the

way functionalities are introduced on the POx chains. All these strategies have been recently reviewed.¹⁵⁵ Hydrogels could be produced by one-, two- or three-step reactions. The most straightforward way to synthesize a hydrogel is to directly copolymerize a 2-alkyl-2-oxazoline monomer with a bis-oxazoline comonomer serving as a cross-linking coupling agent. The hydrogel will be synthesized *in situ* as the polymerization proceeds. As presented in the last section, functionalities can also be introduced on the monomer or polymer chain end, in which case hydrogels will be obtained by post-polymerization reaction with a specific cross-linker. Last, functionalities can be introduced on the polymer chain by post polymerization functionalization, followed by a cross-linking reaction. These different strategies are illustrated in Table 5.

Table 5 Different strategies to synthesize POx hydrogels



In this PhD work, we will provide a novel synthetic strategy to POx hydrogels and nanogels (chapter 2).

III.3.1. HYDROGELS PREPARED BY POLYMERIZATION WITH A BIS-OXAZOLINE MONOMER

The first hydrogel prepared by copolymerization with a bis-oxazoline monomer was reported by Chujo *et al.* in 1989. They performed the ter-polymerization of MeOx with 2-alkyl-2-oxazoline (alkyl = n-butyl, n-octyl or n-dodecyl) and 2,2'-tetramethylenebis(2-oxazoline) (Figure 6),^{156,157} where they combined, respectively, hydrophilic, lipophilic and bifunctional monomers. By varying the monomer ratio, they thus tuned the hydrophilicity and the swelling properties of the resulting hydrogels.

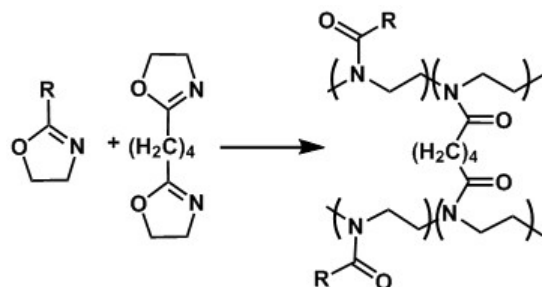


Figure 6 Hydrogel preparation by copolymerization of 2-alkyl-2-oxazoline and bis-oxazoline¹⁵⁶

The respective monomer reactivities were determined and it appeared that the bis-oxazoline monomer had a higher reactivity than MeOx and than the other 2-alkyl-2-oxazolines. As a consequence, the bis-oxazoline was incorporated more rapidly into the gel and the chain length between two cross-linking points could be varied.¹⁴⁴

More recently, this technique was used to synthesize a library of hydrogels from EtOx, PhOx and phenylene-1,3-bis-2-oxazoline monomers.¹⁵⁸ Again, the ratio of hydrophilic, lipophilic and bifunctional monomers was varied allowing for the comparison of the swelling degree of the gels. The authors showed that swelling in water was enhanced for lower degrees of cross-linking, and when a lower amount of PhOx was used. Moreover, dye molecules could be trapped into the hydrogels and released in a controlled way by solvent exchange (diffusion-mediated release), or by pH change, leading to slow degradation-mediated release. As the solvent exchange did not degrade the hydrogels, they were well-suited for repeated release/loading cycles.

III.3.2. HYDROGELS PREPARED BY DIRECT POST-POLYMERIZATION REACTION

Another way to prepare hydrogels is by a post-polymerization reaction between a POx bearing functionalities and a cross-linker. Functionalities could be introduced on the polymer backbone or at both chain ends, as presented in Section III.2.

If a polymer with side chain functionalities is used, a reaction with a difunctional cross-linker leads to hydrogel formation. For example, a hydrogel was prepared from a statistical copolymer with MeOx and 2-(dec-9-enyl)-2-oxazoline (monomer 11, Table 2) followed by thiol-ene coupling with different dithiol molecules.^{39,108} 2-3'-Butenyl-2-oxazoline (monomer 10) was also used as one of the building block of a copolymer, and post-polymerization by thio-ene coupling was conducted with a tetrathiol under UV irradiation.¹⁰⁴ Copolymers with amine side chain functionalities (monomer 2) also formed hydrogels when reacting with epichlorohydrin.^{84,89} Such hydrogels had the ability to absorb and release DNA thanks to electrostatic interactions. Hoogenboom also polymerized an unsaturated soybean fatty acid-based 2-oxazoline monomer (SoyOx) (monomer 12) using microwave irradiation.²

The unsaturated fatty acid side chains of the resulting polymer were then cross-linked under UV irradiation, without the need of any cross-linker, leading to hydrogel formation.

Functionalities can also be introduced at the polymer chain-ends by using functionalized initiators and termination agents already presented (respectively in Table 3 and 4). Most of the time, a difunctional initiator is used and functionalities are only introduced at the termination step. By this way, hydrogels were prepared from telechelic PMeOx bearing trimethoxy-silyl end-functionalities (termination agent 2, Table 4), followed by deprotection of silanol groups and further intermolecular condensation reaction.¹³⁸ The swelling degree was found directly dependent on the $[M]/[I]$ ratio. Telechelic PMeOx was also functionalized at both chain ends with hydroxy groups (termination agent 4). Reaction with pluri-isocyanates led to hydrogels.¹⁵⁹

The synthesis of block copolymers made from MeOx and BuOx was terminated by the addition of *N,N*-bis(2-aminoethyl)ethylenediamine (termination agent 6), and hydrogel formation occurred by reaction with 1,4-dibromo-2-butene.¹⁴¹ Last, dimethacrylate-functionalized PEtOx (termination agent 11) was reacted with a 3-arm poly(*D,L*-lactide) trimethacrylate under UV irradiation.¹⁴⁵ The hydrogel swelling/deswelling behavior was tuned by varying both the temperature and pH. When the temperature was increased, the PEtOx chains became dehydrated, as the hydrogen-bonds previously formed with water were disrupted, hence the gel shrunk. The pH effect was linked to the presence of amide groups on the polymer backbone. The amide groups were ionized at low pH leading to swelling of the gel. As PEtOx is hydrophilic, whereas poly(*D,L*-lactide) is hydrophobic, the hydrophilicity of the gel could be manipulated, by varying the ratio of each macro-monomer.

Hydrogels were also prepared from a star-shaped PMeOx.¹³³ A trifunctional initiator was used (*i.e.* 1,3,5-tris(iodomethyl)benzene or 1,3,5-tris(*p*-toluenesulfonyloxymethyl)benzene, Figure 4) leading to a 3-arm POx with amine end functionalities. The hydrogel was then formed in the presence of a difunctional isocyanate.

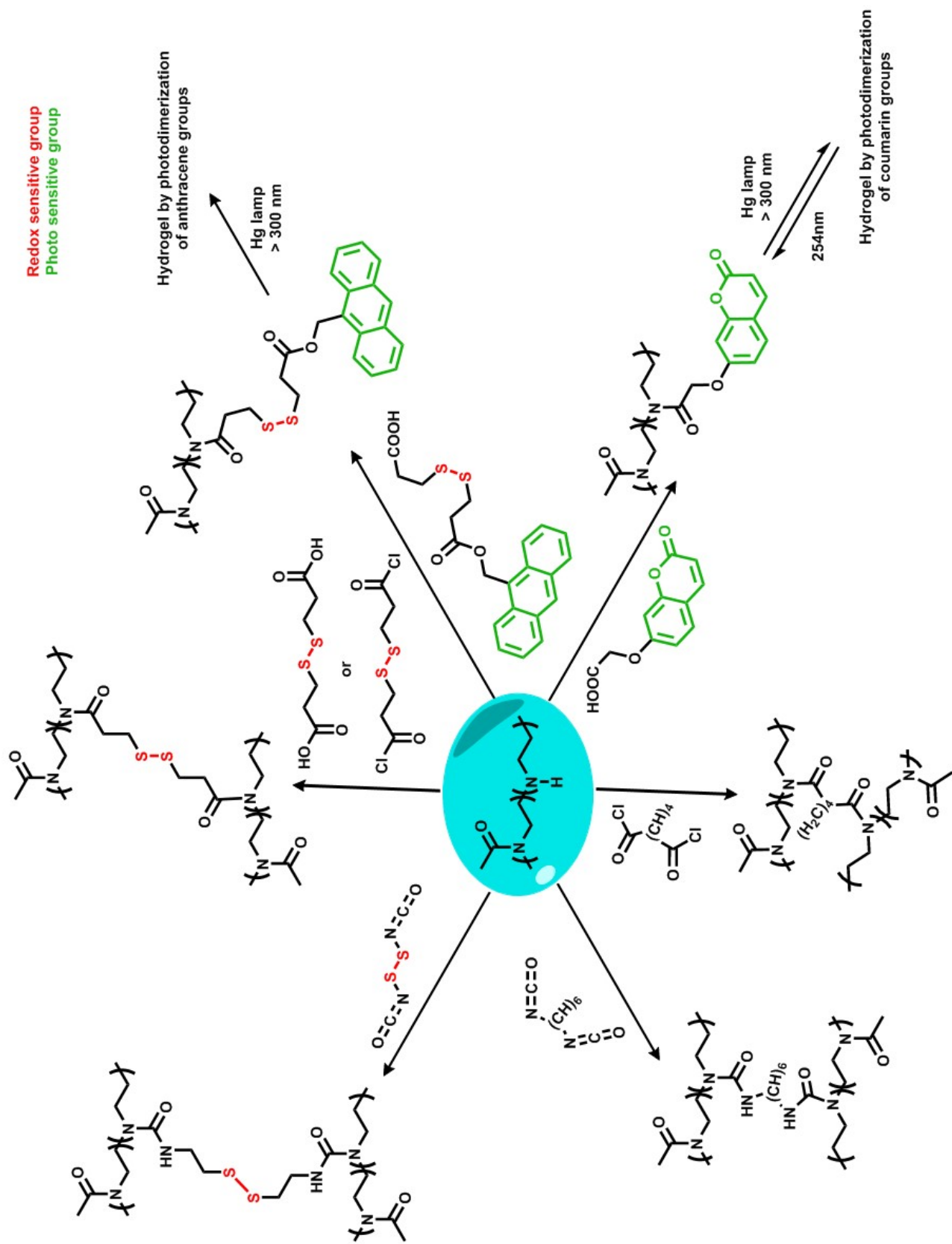
Vinyl-functionalized PMeOx was also synthesized, but the functionalities were introduced thanks to both the initiator and termination agent to produce a bis-macromonomer (initiator 7, Table 3 and termination agent 7, Table 4).¹¹⁷ The hydrogel was formed either by free radical polymerization of the bis-macromonomer or by copolymerization with *N*-vinyl-2-pyrrolidone (NVP). The density of the network and swelling characteristics were controlled by the degree of polymerization of the PMeOx and by the molar ratio between the bis-macromonomer and NVP as well.

III.3.3. HYDROGELS PREPARED BY 2 STEP POST-POLYMERIZATION REACTION

The third synthetic method used to prepare POx hydrogels involves a three-step reaction. First, MeOx or EtOx is polymerized, and second, the polymer is partially hydrolyzed to introduce amine functionalities on the polymer backbone leading to a statistical copolymer. Last, the hydrogels is obtained by reaction of a cross-linker with amine functionalities.

In biomedical applications, POx were first used as a source for linear PEI obtained after hydrolysis and which was further used to form polyplexes with DNA and used as gene-vector (see further and see also Scheme 10).^{24,160} The hydrolysis rate of POx could be easily controlled, leading to randomly distributed amine functions along the POx chain. As mentioned in section I, when the polymer backbone is hydrolyzed up to 10%, no cytotoxicity is observed.²⁵ The hydrolysis reaction was studied for different monomers (mainly MeOx and EtOx), under different conditions (base, acid or in a water-ethanol mixture); more information can be found in the literature.^{70,161-168}

Hydrogels were prepared by reaction of the amine functions of partially hydrolyzed POx with different cross-linkers. Most of this work was carried out in the 1990s, by the group of Saegusa, on the basis of a partially hydrolyzed PMeOx, as illustrated in Scheme 10.

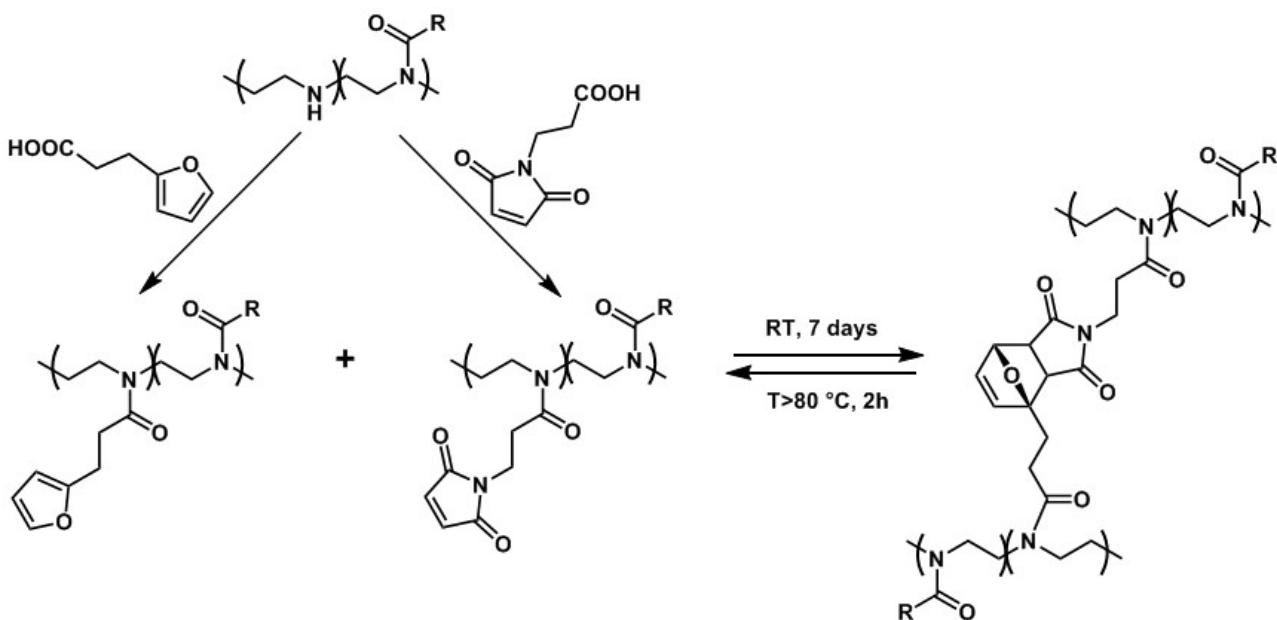


Scheme 10 Strategies adopted by Saegusa's research group to form hydrogels with partially-hydrolyzed poly(2-methyl-2-oxazoline)

A hydrogel was produced under mild conditions, at room temperature, using hexamethylene diisocyanate in the presence of 1,8-diazabicycloundec-7-ene (DBU) as an organic catalyst in DMF (Scheme 10).¹⁶⁹ With a diisocyanate cross-linker bearing a disulfide bridge, a hydrogel that was cleavable in a reductive environment was synthesized (Scheme 10).¹⁷⁰ Photo-responsive hydrogels were also prepared when the amine functionalities were reacted with coumarin moieties ((7-coumaryloxy)acetic acid). The hydrogel was formed by photo-dimerization of the coumarin moieties, by exposing the polymer to mercury lamp irradiation at a wavelength greater than 300 nm (Scheme 10).¹⁷¹ The photosensitive gel obtained could be cleaved by exposing it again to irradiation at a wavelength lower than 300 nm; the cyclobutane ring was thus cleaved and the coumarin moieties were regenerated, thereby reversing the process.

Partially hydrolyzed PMeOx were also modified with (9-anthracenyl)methyl hydrogen 3,3'-dithiodipropionate, in the presence of dicyclohexylcarbodiimide as a condensing agent (Scheme 10),¹⁷² leading to a modified PMeOx bearing disulfide and anthracene functions. As in the previous example with coumarin moieties, a hydrogel was formed by the dimerization of anthracene moieties, when the modified PMeOx was irradiated with a mercury lamp at a wavelength greater than 300 nm. This system proved to be photo- and redox-sensitive by means of reversible conversion between disulfides and thiols and the photo-dimerization of anthracene moieties.

Temperature sensitive-hydrogels were also prepared using a maleimide modified PMeOx that reacted with an antagonistic furan-modified PMeOx, *via* a Diels-Alder reaction (Scheme 11).¹⁷³



Scheme 11 Schematic of the thermosensitive hydrogel formed by Diels-Alder reaction¹⁷³

The gelification process was reversible: if the hydrogel was heated at 80 °C for 2h, the retro Diels-alder reaction occurred thereby regenerating the starting compounds. Without heating, the hydrogel only swelled in water.

Some of the hydrogels presented in this section are potential candidates for drug delivery applications, but only one paper reported on the evaluation of a POx hydrogel for such an application.¹⁷⁴ An ABA triblock copolymer, prepared from PEOx-*b*-PCL-*b*-PEOx, was used to encapsulate Bevacizumab, an antibody used to cure intra-ocular diseases, known to be efficient but with a short half-life. The triblock copolymer was subjected to a sol-gel transition when the temperature was increased. At room temperature and in a balanced salt solution (standard saline for intraocular use), it existed as a “sol”, but when temperature was increased to the physiological temperature, it turned into a “gel”. When the temperature was further increased, PEOx segments became dehydrated and formed micellar aggregates. The Bevacizumab release *in vitro* was slow, with no burst release, and lasted for up to 20 days. The release was achieved first by diffusion and when the equilibrium concentration was reached, the release was controlled by gel degradation. *In vitro* cytotoxicity studies were conducted by co-culturing hydrogels with cells at 37 °C. After 24h, more than 90 % of cell viability was observed. The *in vivo* cytotoxicity study performed on rabbit eyes showed that the hydrogel and its degradation products were not toxic to neuroretinal tissues for at least two months. This hydrogel thus exhibited a good *in vitro* and *in vivo* biocompatibility for neuronal tissues with extended drug release.

To summarize, numerous synthetic strategies leading to POx hydrogels have been described in the literature. *In situ* cross-linking can be conducted by the addition of bisfunctional 2-oxazolines to the polymerization mixture, but hydrogels can also be synthesized by post-polymerization reactions. Cross-linking reaction can alternatively involve functionalization of ethylene imine repeating units obtained by partial hydrolysis, or by the direct introduction of reactive handles to the POx backbone.

III.4. STRUCTURE-PROPERTY RELATIONSHIPS

By taking advantage of the POx versatility, *i.e.* the living ROP combined with the potential for functionalization at both chain ends and/or in the polymer side chains, not only POx chemistry allows designing polymers with different architectures, but also tuning their physico-chemical properties such as thermal transitions, mechanical properties, solubility and surface energy. All these properties are obviously linked together. For example, mechanical and thermal properties depend directly on the presence of crystalline phases. Herein, only thermal transitions correlated to the polymer behavior in solution will be discussed. This is because this aspect has been investigated in the context

of this PhD work, from specific POx-based copolymers (see Chapter 3). Additional information on the mechanical properties and surface energy of POx can be found elsewhere.^{2,175,176}

The nature of the substituent (R) on the polymer side chain determines its hydrophilicity: PMeOx is water-soluble in the entire temperature range of liquid water under atmospheric pressure, PEtOx and poly(2-n-propyl-2-oxazoline) (PnPrOx) exhibit a LCST behavior in aqueous solution, whereas longer substituents result in hydrophobic polymers (Figure 7).¹⁷⁷ PMeOx and PEtOx are also known to be hygroscopic and the effect of the water uptake has an influence on their mechanical properties.^{178,179} Due to the current trend in the use of renewable resources, many of the hydrophobic POx reported in the literature are based on fatty acids as mentioned in section III.2.1.¹⁰⁶

The polymer behavior in solution is greatly affected by the solvent used, and in water-ethanol solvent mixtures, some POx also present an upper critical solution temperature (UCST).¹⁸⁰⁻¹⁸²

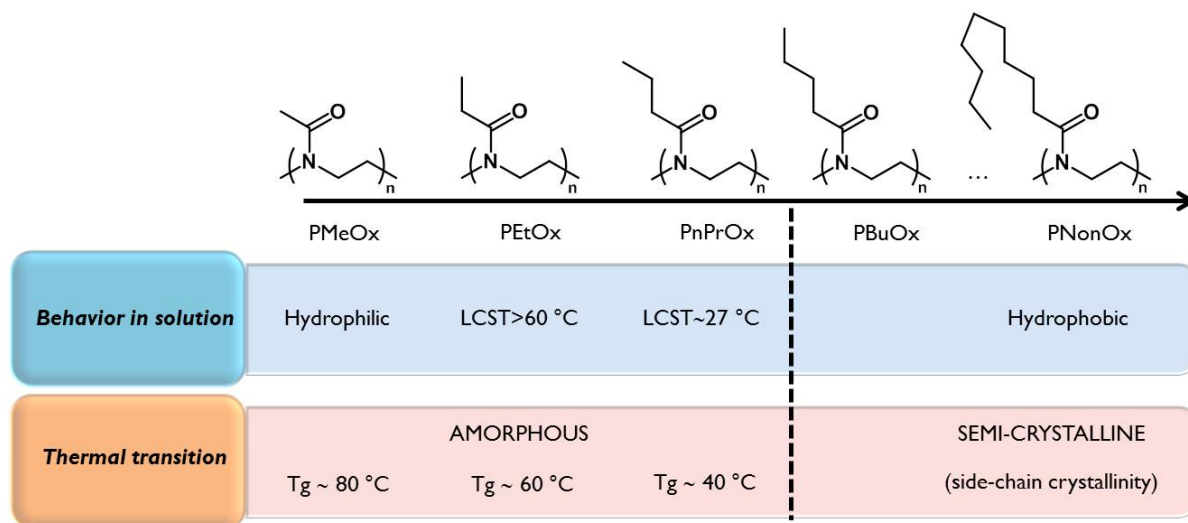


Figure 7 Structure-properties relationship for poly(2-oxazoline)s

The LCST values given in Figure 7 varied with the polymer molecular weight,¹⁸³ polymer concentration and the presence of salt (salting-in or salting-out effect)¹⁸⁴ or surfactant in the solution.¹⁷⁷ The polymer chain-end functionality also influences the LCST: the LCST increases with the hydrophilicity of the chain-end.¹⁸⁵

By post-polymerization modification, a poly(benzyl ether) dendrimer with carboxylic acid functions at the periphery was coupled to PiPrOx by one of its chain-end, leading to a hybrid copolymer with a pH-tunable LCST.¹²³

Last, when the polymer contains branching in its side chains, the branching position has an important influence on the glass transition temperature (T_g)¹⁸⁶ and on the LCST as well.

Numerous studies on the modulation of POx LCST and T_g by synthesizing block,^{67,175,187} gradient,⁶¹ random¹⁷⁵ or brush/graft^{188–190} copolymers have been also reported. Tuning the LCST by post-polymerization modification is also an option.^{98,191}

The state of the polymer in bulk will also change drastically, from amorphous to semi-crystalline, depending on the length of the alkyl side chain. Polymers with short side chains such as PMeOx, PEtOx, and PnPOx are amorphous, whereas POx with 4 and more carbons on the side chains show a semi-crystalline behavior.^{176,192,193} Some POx have the ability to crystallize also when annealed in dilute solution. For example poly(2-isobutyl-2-oxazoline) and PNonOx form crystalline self-assembled structures, in a water-ethanol mixture, below their UCST.¹⁹⁴ PEtOx forms crystalline fiber visible with the naked eyes within a few weeks, when kept above its LCST in water.¹⁹⁵ The crystallization of comb-like POx copolymers¹⁴⁴ or chiral POx¹⁹⁶ have also been reported.

A closer look should be given to PnPrOx and its two different isomers, PiPrOx and poly(2-cyclopropyl-2-oxazoline) (PcPrOx) (Figure 8).¹⁹⁷ It is interesting to highlight the key role played by the side chain architecture on the polymer properties: the three polymers have a LCST, but PnPrOx and PcpPrOx are amorphous, with a T_g of 40 and 80 °C, respectively, whereas PiPrOx is semi-crystalline.

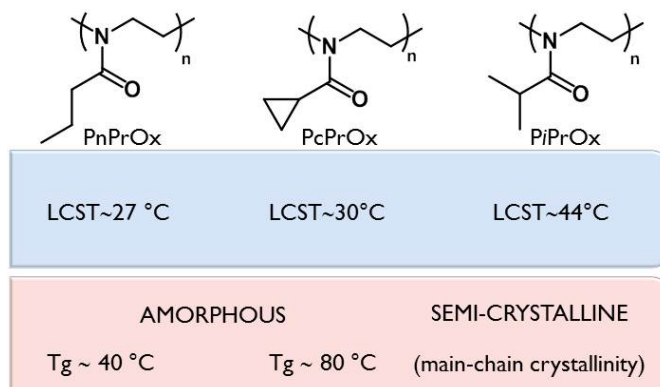


Figure 8 Structure-properties relationship for poly(2-propyl-2-oxazoline)s isomers

PiPrOx has been more extensively studied than its other two isomers because of its remarkable properties. On one hand, it is a structural isomer of poly(*N*-isopropylacrylamide) (PNIPAAm) and poly(*L*-leucine)¹⁹⁸ and like PNIPAAm, it has an LCST close to body temperature making it a particularly interesting candidate for biomedical applications.^{199,200} The phase transition for PiPrOx is reported to be sharper, with almost no hysteresis compared to PNIPAAm, due to the weaker H-bonding capacity of PiPrOx.²⁰¹

But on the other hand, when PiPrOx is annealed above its LCST (at 65 °C) for 3 hours or more, it forms crystalline structures in an irreversible manner.^{1,177,202,203} The crystal structure evolves with the

annealing time, from a network-like structure to a micron-size assembly composed of fibers mesh. The crystal structure has been identified by X-Ray Diffraction (XRD),²⁰³ and crystallization is driven by hydrophobic and dipolar interactions. Thanks to vibrational spectroscopy analysis and molecular orbital calculation, Winnik *et al.* were able to associate the crystallization of PiPrOx to a change in the conformation of the polymer chains, from trans and gauche to all trans (Figure 9).²⁰⁴

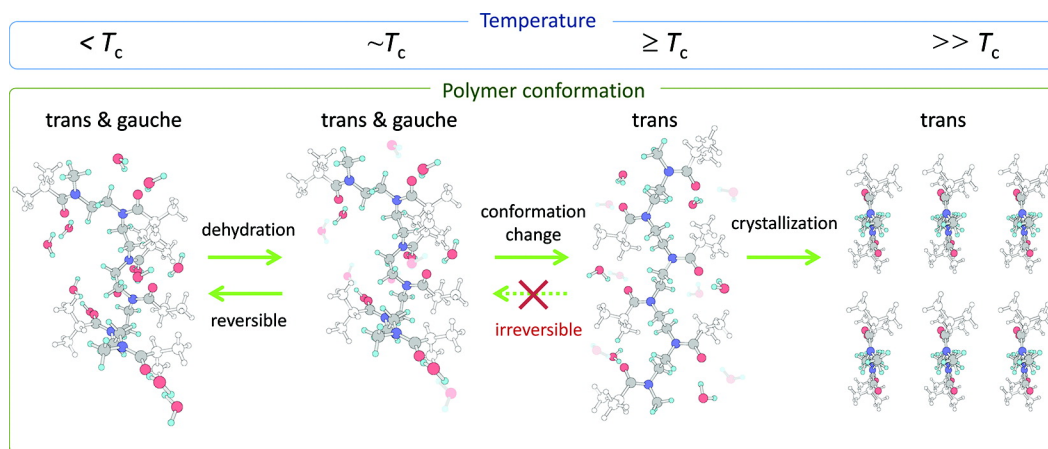


Figure 9 Schematic representation of the changes in the conformation of PiPrOx in water as a function of temperature. Reprinted from ref. 204

At a specific temperature, the PiPrOx solution undergoes first liquid/liquid phase separation and PiPrOx then crystallizes in the polymer-rich phase by changing its conformation.²⁰⁴ In contrast to POx with long alkyl side chains, PiPrOx crystallinity appears in the main chain and not in the side chains. Last, solvation appears to be especially important in lowering the kinetic barriers in the crystallization process, similarly to the self-organization of polypeptides and proteins.²⁰³

PiPrOx crystallization was further exploited in copolymer systems. A statistical copolymer made of iPrOx and 2-(3-butenyl)-2-oxazoline units was also synthesized and found to self-assemble and crystallize above its LCST into spherical micron-size structures, which was further used for carbohydrate protein recognition.²⁰⁵ The self-assembly and crystallization of a PiPrOx-grafted pullulan copolymer were also reported.²⁰⁶ Micron-sized ring-like structures with short fibrils emanating from the ring circumference or “sea urchin”-like morphology were obtained, but other morphologies were also observed depending on the experimental conditions (addition of salts, with/without stirring).

In chapter 4, we will describe how to take advantage of this specific property of PiPrOx to crystallize in water, by arranging the polymer into a block copolymer architecture.

These systematic studies on libraries of POx (co)polymers revealed several structure–property relationships for the thermal properties as well as solubility and crystallization. This allows moving forward toward POx engineering in order to meet defined properties.

IV. POLY(2-OXAZOLINE)S AS POLYMER THERAPEUTICS

POx is an interesting platform for biomaterials development and especially for polymer therapeutics because it meets some specific needs, such as biocompatibility, stealth behavior, but also in terms of tunable thermo-responsiveness and variation of architecture and functionalities. The use of POx as polymer therapeutics has been recently reviewed.^{207,208}

Except for one paper reporting on the use of a PEtOx matrix as an excipient in the formulation of oral tablets,²⁰⁹ POx are most often involved in the design of drug nanocarriers. POx could be conjugated to biological molecules, such as proteins or drugs, or be part of self-assembled structures, such as micelles, polymer vesicles or polyplexes. Serina Therapeutics, a pharmaceutical company based in Huntsville, Alabama, is currently advancing novel therapeutics for Parkinson's disease, cancer, inflammation, pain and metabolic disorders based on POx nanocarriers.²¹⁰

IV.1. OVERVIEW OF THE DRUG DELIVERY PROBLEMATIC

One of the major challenges that needs to be addressed in current nanomedicine research is to deliver drugs at a controlled place and time in order to improve the drug efficacy, while decreasing the side effects. In oncology for example, current chemotherapeutic treatments are administered intravenously and their biodistribution and pharmacokinetics are not well-controlled.²¹¹ The majority of anti-cancer drugs being hydrophobic, their circulation in body fluids is challenging and requires a large volume for distribution. In addition, when drugs are hydrophilic, it is difficult for them to cross membrane barriers and to reach their final target site. Because the size of drug molecules is small (< 10 nm), they are rapidly cleared from the bloodstream by renal filtration before being able to reach the tumor site. As a consequence, drug accumulation at the tumor site is difficult to achieve. Moreover, due to their small size and molecular weight, drug molecules penetrate not only to the diseased tissues but also to healthy ones, thereby damaging these tissues and resulting in a significant number of side effects.

By using polymeric nanostructures as drug carriers, a balance between efficacy and toxicity can be achieved, opening a wide range of new opportunities for cancer treatment. The use of polymer

nanotechnologies holds enormous promise for various reasons: they can improve the solubility of hydrophobic drugs, and drug cell penetration. Because of their larger size, nanocarriers would not be cleared as rapidly as free drugs from the blood stream. The drug delivery can also be targeted to specific tissues or even cells, improving drug efficacy. It can allow the delivery of drug cocktails and also of therapeutic and diagnostic agents, leading to a “theranostic” platform.^{212–214} For example, imaging agents can be delivered at the same time as a drug, making possible the visualization of the drug delivery site. Lastly, the release can be triggered in a controlled manner.^{215,216}

Nanocarriers can be made from inorganic or organic compounds. Inorganic nanocarriers are out of the scope of this literature review, but some additional information can be found elsewhere.²¹⁷ Organic structures made from polymeric systems²¹⁸ can be prepared by self-assembly, leading to the formation of polymer vesicles (polymersomes) or micelles.²¹⁹ They can alternatively be highly branched and shape-persistent as in the case of dendrimers²²⁰ or chemically cross-linked as in the case of nanogels.²²¹ For all these structures, the polymers used should fulfill some specific requirements: they should be biocompatible and approved by FDA for use in biomedical applications. They may also be biodegradable and readily cleared by the body.

All these nanocarriers end up being made from the main polymers presented in Table 6, depending on the properties needed.^{218,222}

Table 6 List of polymers commonly used in biomedical applications. Adapted from ref. 222

Polymers	Acronyms	Properties
Poly(ethylene glycol)	PEG	Biocompatible, hydrophilic, stealth, FDA approved
Poly(D,L-lactide-co-glycolide)	PLGA	Biodegradable, hydrophobic, FDA approved
Poly(acrylic acid)	PAA	Hydrophilic, pH-responsive
Poly(lactic acid)	PLA	Biodegradable, hydrophobic
Poly(caprolactone)	PCL	Biodegradable, hydrophobic, FDA approved
Poly(N-isopropylacrylamide)	PNIPAAm	Thermo-responsive
Poly(ethyleneimine)	PEI	Cationic, pH-responsive
Poly(amino acids)	-	Biodegradable, anionic
Polysaccharides cellulose, chitin, pullulan	-	Hydrophilic, natural polymers

Research is not only conducted on the cargo itself, but also on improving the targeting of the drug delivery system (DDS) which could be passive or active. All currently approved nanotechnology platforms in cancer treatment deliver cancer drugs to the tumor site *via* passive targeting that relies on the properties of the delivery system and the disease pathology, in order to selectively

accumulate the drug at the site of interest, thereby avoiding non-specific distribution.²²³ In the case of cancer, tumor cells are growing faster than healthy tissues resulting in the development of a “permeable” vasculature that allows nanomaterials of up to several hundred nanometers to penetrate in the tumor site. In addition, tumor tissues are also characterized by poor lymphatic drainage, thus once nanocarriers reach the tumor site, they will not be rapidly cleared. For a treatment to be efficient, drug delivery carriers should be able to circulate in the body for an extended duration, hence they should possess stealth behavior to exploit the enhanced permeability and retention effect (EPR) that enables the accumulation of drug carriers at the tumor site. One has to be aware that this EPR effect is not specific to cancer. It is also present for other diseases, such as chronic inflammation and infections.²²³

So far, improvement of the circulation time was made possible by coating PEG on the surface of liposomes that prevents non-specific binding and avoids recognition by the phagocytic system, resulting in clearance from the body. As presented in section I, PEtOx and PMeOx are presented as alternatives to PEG for such applications. However, the accumulation level at the tumor site also depends on the inherent characteristics of the DDS, such as its size, hydrophilicity, charge, etc.^{222,224}

Nanotechnology platforms can also target specific tissues or cells by bearing ligands on their surface, such as antibodies, peptides or proteins, where the ligands can bind to receptors on the targeted site. However, the DDS must first reach the tumor cells, before being able to bind to them. Active targeting would not improve the accumulation at the tumor site due to the EPR effect. However, the drug carrier will definitely be more efficiently internalized by tumor cells as cell recognition and uptake by targeted cells will be improved.^{224,225} In addition, one should also take into account that the introduction of targeting moieties on the surface of nanocarriers will reduce their stealth behavior by increasing their immunogenicity and protein adsorption.²¹¹ Up to recently, only a few active targeting systems were at the clinical trial stage, and none has been approved for clinical use yet.²¹¹

In order to produce a successful nanoparticle-based DDS, once the nanoparticles have reached the targeted site, the drug should be released. The stability of the nanocarriers is a key factor, *i.e.* they have to be stable under physiological conditions while the drug must be released at the targeted site. The release can be achieved by diffusion through the nanoparticles wall or by erosion of nanoparticle matrices. Physiologically relevant stimuli can be used to trigger the release of the drug, and the factors chosen should vary between normal tissues and some pathological sites.^{226–228} Temperature is one of the most commonly used triggers since the temperature increases by 1-2 degrees at the inflammatory tissue site.²²⁹ As a consequence, polymers that exhibit temperature-dependent phase transitions around the physiological temperature, such as in the range 10–42 °C, are the ones used to construct drug carriers.

pH variations are also widely used as a trigger, especially in the case of cancer, because tumor tissues are known to possess a lower pH than healthy tissues.^{230,231} The release could be mediated by ligand exchange, by an enzymatic reaction, or even by a chemical reduction reaction,^{232–235} as certain biological molecules are produced in excess at a target site in comparison to healthy tissues. For example, glutathione (GSH) is the most abundant reducing agent in the body. In the cell, its concentration can reach 10 mM, whereas in the extracellular environment it only approaches 0.002 mM. This significant variation in concentration has been used to trigger intracellular delivery.²³⁶ Moreover, tumor tissues are known to be highly reductive compared to healthy tissues, with at least four-fold higher concentration of GSH in tumor tissues than in normal tissues, which makes a trigger release based on redox conditions even more relevant in the case of cancer treatments.²³⁵ The most popular method to obtain this reductive sensitivity is to introduce disulfide linkages in the nanocarrier. This can be achieved in the polymer main chain, side chain, or in the cross-linker. This disulfide bond is known to be stable under normal physiological conditions, but is cleaved under reductive conditions through thiol–disulfide exchange reactions.

Other “smart chemistries” can be used to control the drug release.^{237,238} External stimuli, such as light or application of heat for instance, can also be used to trigger the release.

Nowadays, significant activity is being focused on the development of “smarter” and multifunctional DDS, to achieve higher efficacy with less toxicity and better targeting. By manipulating the surface chemistry of the nanocarriers, or by attaching specific ligands to their surface, nanocarriers could become responsive to environmental conditions and could also be actively targeted.^{215,239,240} One has to be aware that despite the increasing number of papers published on DDS, less than 10 nanocarriers have been so far approved by the FDA, to deliver drugs to solid tumors, proving how challenging the development of a DDS is.²⁴¹

IV.2. POLY(2-OXAZOLINE) CONJUGATION TO BIOLOGICAL MOLECULES

Polymers can be conjugated to drugs, peptides or proteins. Because the biological molecule is covalently attached to the polymer, it undergoes some modifications. The main challenge is to preserve the biological activity of the active (bio)molecule while its stability, pharmacokinetics and solubility are improved.

Drug-polymer conjugates are the oldest drug delivery nano-systems and have been developed in the 1950's.²²² The first study on the conjugation of POx to biological molecules was conducted in 1992, with PMeOx and PEtOx that were conjugated to a synthetic peptide.²⁴² The peptide used, called HCPC[6-17] corresponded to residues 6-17 of the heavy chain of human protein C. Both PMeOx-

and PEtOx-peptide adducts retained avidity for the antibody directed against human protein C (HPC4-MAb) relatively to the underivatized parent peptide or the human protein C. Furthermore, the avidity of the adducts was not appreciably affected by the size of the polymer employed over the 1 to 10 KDa molecular weight range. This study served as a proof that POx-peptide conjugates could be a suitable polymer-drug conjugate, and numerous studies followed on the conjugation of POx to different proteins.

In 2011, Viegas *et al.* conjugated PEtOx to different enzymes including catalase, urinase and ribonuclease, but also to insulin and BSA proteins.¹⁴ From the POx-enzyme conjugates, they showed that the *in vivo* enzyme activity was dependent on the extent of their modifications: the less the enzyme was modified, the higher was its activity. The glucose-lowering activity of the PEtOx-insulin adduct was studied *in vivo*, by injection into rats (Figure 10-A). The polymer-insulin conjugate was more efficient than insulin alone, or even than one of the actual commercial products (Glargine-insulin conjugate), as it lowered the glucose activity for a longer time period after injection. PEtOx was also conjugated to bovine serum albumin (BSA, a serum albumin protein often used as protein standard) and injected into rabbits to test their immune response. The results showed that the conjugation to PEtOx decreased the immunogenic properties of BSA, which meant that it was no longer detected by the body as a “foreign guest”, representing another way to take advantage of the POx stealth behavior (Figure 10-B).

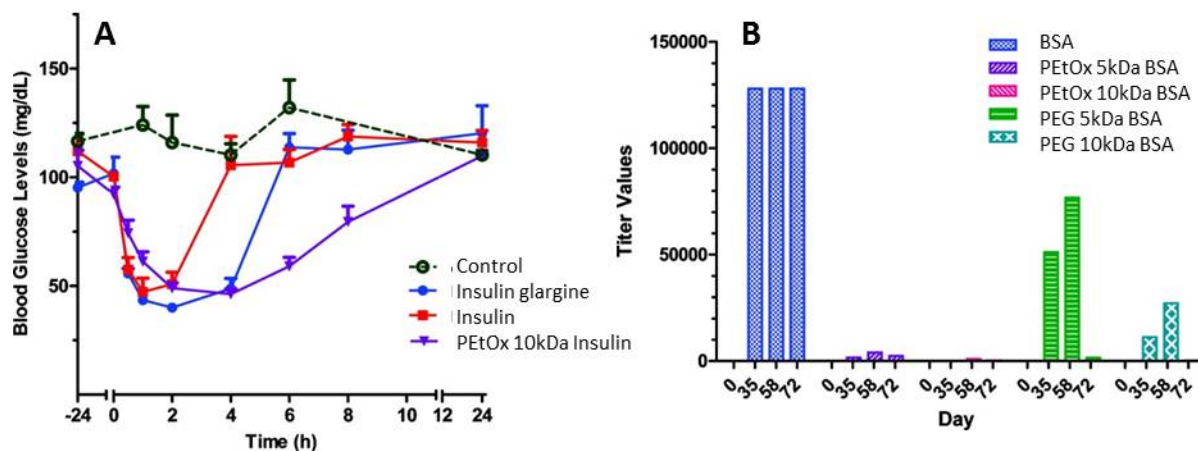


Figure 10 A) Effect of the subcutaneous injection of insulin, insulin glargine, and poly(2-ethyl-2-oxazoline)-insulin on the blood glucose levels in male rats. **B)** Relative immunogenicity of BSA, PEG-BSA, Poly(2-ethyl-2-oxazoline)-BSA in rabbits treated as measured by anti-BSA antibody levels. Treated on days 1, 14, 28 and 42. Adapted from ref. 14

PEtOx was also conjugated to the granulocyte colony stimulating factor (G-CSF). Protein activity was retained *in vitro* and *in vivo*, while the conjugation improved its stability toward aggregation at 37 °C, as compared to the protein alone, and prevented its premature degradation.¹³⁹ Almost the same conclusions were drawn for a POx conjugated to the protein superoxide dismutase I (SODI),

involved in some antioxidant therapies: the conjugate was highly stable in serum, while retaining 30 to 50% of its activity and enhancing the cellular uptake as compared to the native protein or even the PEG-SODI conjugate.²⁴³

POx copolymers were also used for protein conjugation, and the influence of POx composition and architecture on the protein activity was reported. Several homo-, random and block POx (co)polymers (MeOx, EtOx or 2-butyl-2-oxazoline (BuOx)) were conjugated with the horseradish peroxidase enzyme (HRP).²⁴⁴ Conjugation with P(MeOx-*b*-BuOx) led to the highest cellular uptake, in comparison to other conjugates. The inability of the conjugates produced from PMeOx or the copolymers P(EtOx-*co*-BuOx) in increasing the cellular uptake was attributed to the lack of a structurally ordered hydrophobic block, which could assist the hydrophilic enzyme in entering the cells. This was in agreement with results reported by Luxenhofer *et al.*¹¹ The data showed that modification by amphiphilic POx block copolymers was a promising strategy to enhance cellular delivery and protein drug transport.

PEtOx was also conjugated to a drug molecule employed for the treatment of acute and chronic human leukaemia, namely, cytosine arabinose, 1-(β -D-arabinofuranosyl)cytosine (Ara-C).³² Accelerated stability tests to hydrolysis of Ara-C conjugates showed stability towards the degrading enzyme (cytidine deaminase), while the drug was released under physiological conditions. Finally, conjugation induced a decrease in the *in vitro* drug cytotoxicity (30 times less toxic than the drug alone).

So far, all the systems presented were coupled by one polymer chain end, but an example of conjugate formed between a POx polymer with alkene functionalities on the side chain and an aptamer (a synthetic single strand nucleotide sequence with molecular recognition properties) has been recently reported.¹⁰² The aptamer was used against an allergy biomarker and the conjugate did not show any loss in activity.

All these systems established that conjugating POx to a (bio)molecule with biological interest represents a viable strategy: it improves the protein/drug stability, while both maintaining its biological activity and taking advantage of the POx properties such as biocompatibility and stealth behavior.

IV.3. SELF-ASSEMBLY OF POLY(2-OXAZOLINE)S AND THEIR USE IN BIOMEDICAL APPLICATIONS

As emphasized in the previous section, polymer-conjugates are one of the many possibilities for transporting a drug to a target site while using the stealth properties of POx. Most common DDS are self-assemblies issued from amphiphilic graft or block copolymers, and different structures can be obtained depending on the polymer characteristics: micelles, polymersomes (polymer vesicles) or aggregates. In these self-assembled structures, the drug is usually physically entrapped and not covalently linked to the polymer as in drug-polymer conjugates.

In this section, a brief overview of some of the smart self-assembled systems derived from POx is presented; they are also all listed in Table 7 (see further). Some systems are derived from POx copolymers, while others are “mixed systems” containing POx as one block and another polymer as the other block. It has to be highlighted that these selected examples are at different stages in their evaluation as drug delivery systems.

A statistical copolymer made of 2-decenyl-2-oxazoline (DecOx) (monomer 11, Table 2) and EtOx monomer units formed nanoparticles with a size between 240 and 660 nm by nanoprecipitation in water.²⁴⁵ *In vitro* studies showed that, after 24 h of incubation with mice fibroblast cells, the cellular uptake was efficient, with a uniform distribution into the cytosol. No toxic effect was observed during incubation. DecOx not only introduces hydrophobicity, but it can also be used as functional sites. As a consequence, the next step with this system would be not only to examine the drug loading and release profiles but also to functionalize the particles.

Milonzki *et al.* synthesized gradient copolymers from MeOx and PhOx and showed that different nanostructures (polymersomes, micelles and aggregates) were obtained depending on the monomer ratio, polymer chain length and solvent used.²⁴⁶ The encapsulation of a hydrophobic anti-inflammatory drug, namely, indomethacin, led to an increase of the system size by almost 50% (from 9 to 16 nm) compared to the unloaded structures.

Hruby *et al.* designed thermoresponsive micelles from ABA triblock copolymers, PMeOx-*b*-(PiPrOx-co-PButylOx)-*b*-PMeOx, with hydrophilic A blocks and a central thermoresponsive B block.²⁴⁷ Above the LCST of the copolymer, micelles were formed. The copolymer was radio-labelled with different iodine isotopes and these systems showed no cytotoxicity *in vitro* up to a concentration of 1 mg/mL. Depending on which isotope was attached, these micellar systems could be used for radio-diagnostic (¹²³I or ¹²⁴I, which are beta-emitting isotopes) or radiotherapy (¹³¹I, gamma-emitting isotope).

A complete study on another micellar system prepared from di- and triblock POx and used as drug delivery system was conducted by Luxenhofer *et al.* as depicted in Figure 11.^{248,249}

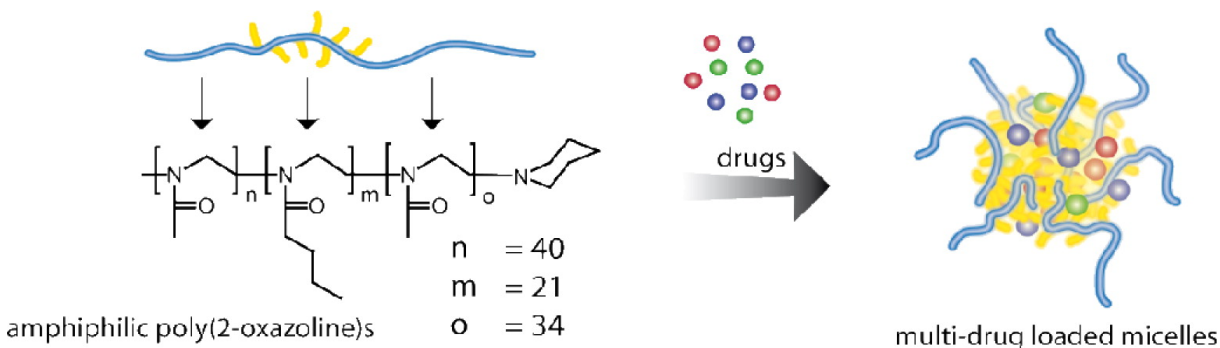


Figure 11 Structure of the triblock copolymers used to form micelles. Reprinted from ref. 249

In vitro toxicity studies conducted on different cell lines showed that, after 2 hours of incubation, the polymer itself was not cytotoxic up to a concentration of 20 mg/mL.²⁴⁸ These micelles were tested for single- and multi-drug cancer therapy. First, Paclitaxel (PTX), an anti-cancer drug which has a low solubility in water of 1 $\mu\text{g/mL}$, was encapsulated within the micelles. With the single-drug loaded micelles, a high loading was achieved (8.2 mg/mL of PTX, corresponding to 45 wt.%) combined with promising *in vitro* and *in vivo* tests.²⁴⁸ When micelles were loaded with hydrophobic binary or ternary drug combinations, loading capacities were slightly improved as compared to the single-drug loaded micelles (up to 50 wt.%), but more importantly, the stability was enhanced.²⁴⁹ The *in vivo* antitumor effect of the PTX-loaded micelles was studied on mice with subcutaneous lung tumors. A reduction in tumor growth was visible even after only one injection. Between 11 days and 25 days after injection, tumors in animals treated with PTX-micelles became even smaller than in animals treated with a commercial product (Cremophor EL *i.e.* Taxol®). Interestingly, the drug loading of such self-assembled structures could induce morphology changes. The drug loading of a micellar system made of a triblock polymer P(MeOx-*b*-BuOx-*b*-MeOx) changed, from worm-like micelles to spherical micelles, with also a raspberry-like micellar core when drug loading was increased.²⁵⁰

Dual stimuli responsive self-assembled systems were prepared from PiPrOx coupled to fluorenylmethoxycarbonyl-tyrosine phosphate (Fmoc-pY).¹²² The polymer, Fmoc-pY-PiPrOx, is thermoresponsive and has an LCST around body temperature, whereas the Fmoc-pY function is enzyme-responsive. Dephosphorylation occurred in the presence of phosphatase, leading to the self-assembly of Fmoc-Y. By tuning the temperature and the phosphatase concentration, different nanostructures were obtained, such as micelles and mesoglobules (Figure 12).

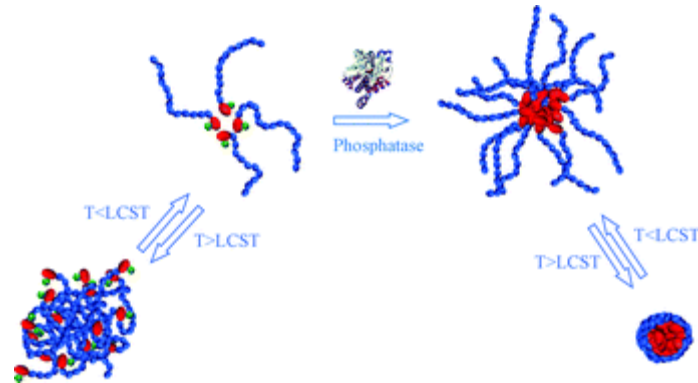


Figure 12 Schematic representation of enzyme- and temperature-induced self-assembly behavior of the polymer bio-conjugate. Reprinted from ref. 122

Knowing that phosphatase is present at the cell surface, one can expect to use such a system to release bioactive payloads, in response to cell surface phosphatase, but such tests have not yet been reported.

Polymersomes produced from di- or triblock copolymers made of PMeOx and PDMS, and used as a DDS, have been extensively studied by Meier *et al.*²⁵¹ Functionalities were introduced at the polymer chain-ends, which led to surface-functionalized polymersomes once self-assembled. Biotin-functionalized polymersomes (Figure 13)²⁵² were targeted against the scavenger receptor AI from macrophages. Receptor-specific binding of these generic carriers was followed by vesicular uptake in human and transgenic cell lines, while low non-specific binding supported the stealth properties of the carrier with no toxicity being noted.²⁵²

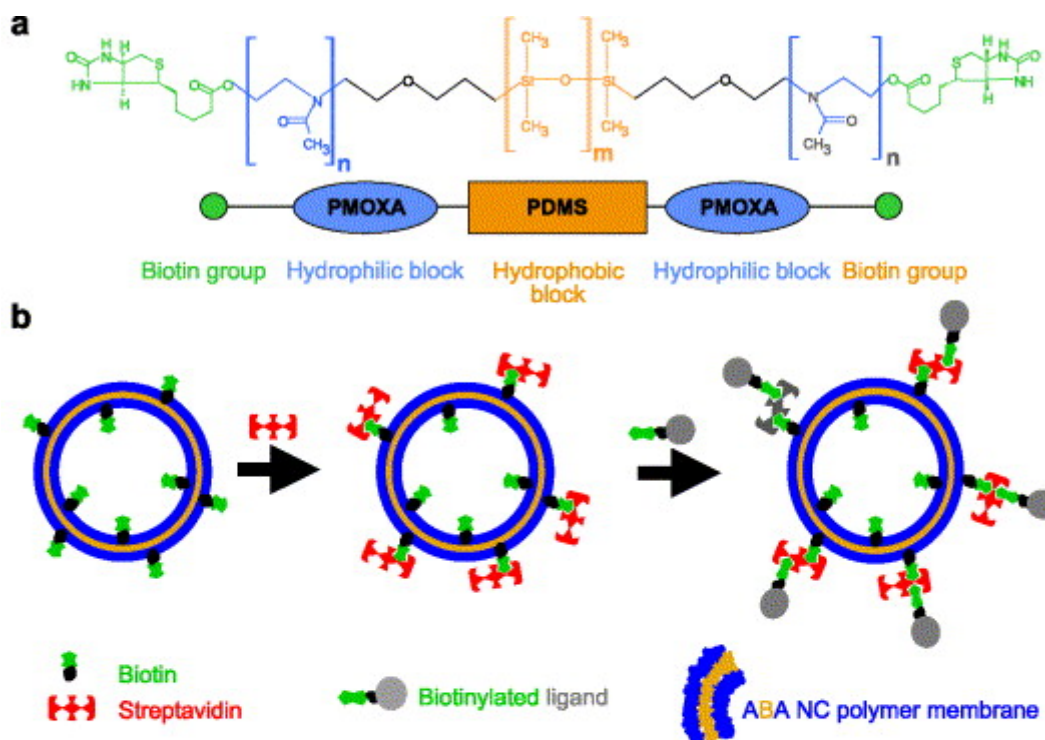


Figure 13 A) Biotinylated poly(2-methyl-2-oxazoline)-b-PDMS-b-poly(2-methyl-2-oxazoline) B) Functionalized polymersomes by streptavidin bridging. Reprinted from ref. 252

The same polymersomes were prepared from PDMS-*b*-PMeOx diblock copolymers functionalized with a secondary amine at the chain end.²⁵³ These amino-functional groups were then used to attach different antibodies to the surface of the polymersomes. Antibiotin IgG, which targets biotin surfaces, was first attached and specific attachment of these polymersomes to biotin patented surfaces was demonstrated. Functionalized polymersomes with Trastuzumab, an antibody known to target specifically HER2-positive breast cancer cells, were also prepared.²⁵³ Cellular uptake experiments with cells expressing the HER2 receptors on their surface were performed and, as expected, the uptake of polymersome-trastuzumab conjugates was significantly faster than for polymersomes without Trastuzumab. The *in vitro* cell proliferation inhibition activity was also studied and showed that after 24h, the conjugates were able to inhibit cell proliferation by a factor of 2. These studies showed how easy it could be to actively target a drug carrier by functionalizing the POx chain-ends to then functionalize the polymersome surface, providing a platform for targeting experiments. These polymersomes were also used as nanoreactors and as models to study the internalization of nanoparticles, thanks to polymersome properties that are similar to the one of phospholipids from cell membrane (fluidity and mechanical stability).^{254,255}

The self-assembly of PMeOx-*grad*-PPhOx in presence of phospholipids, namely, dipalmitoylphosphatidylcholine (DPPC), led to the formation of chimeric vesicle-like nanostructures.²⁵⁶ Indomethacin was successfully incorporated into these chimeric nanocarriers.

Micellar systems prepared from POx conjugated with other biocompatible polymers were also reported. Micelles formed from PEOx coupled to a hydrophobic glycopolymer, namely, peracetylated maltoheptaose, were used to encapsulate Indomethacin.²⁵⁷ The micelles were thermoresponsive with an LCST around 45 °C. *In vitro* drug release studies showed that the higher the temperature, the faster the release. For temperatures close to the LCST or higher, burst release was observed because of a change in the morphology (micelle deformation due to the fact that PEOx became hydrophobic). Micelles were also prepared by the self-assembly of the block copolymer PEOx-*b*-poly(4-methyl- ϵ -caprolactone).²⁵⁸ They were loaded with a hydrophobic drug used in cancer chemotherapy, namely, Doxorubicin (DOX). Thanks to the DOX entrapment, the cellular uptake was faster as compared to the free drug and it could reach the intracellular compartment and enter the nucleus.

Grafted copolymers can also serve to form micelle-like nanostructures. Star-shaped poly(ϵ -caprolactone) (PCL) with PEOx brush-like shell formed spherical nano-aggregates of 20 nm in diameter.²¹ No short term cytotoxicity was noted, nor adverse reaction with human blood in general. DOX was encapsulated successfully in these nano-aggregates.

The self-assembly of a grafted copolymer consisting of a PCL backbone and PMeOx coupled via click-chemistry was also reported.³⁴ As both PCL and PMeOx moieties are non-cytotoxic and biocompatible, one can assume that the resulting copolymers may show a similar behavior, but no *in vitro* nor *in vivo* studies have been reported.

Polyplexes are another kind of drug delivery carriers reported in the literature which can be prepared by the self-assembly of POx. As POx are neutral polymers, they have to be coupled to another charged polymer, to be able to form polyplexes. For example, block copolymers made from PEOx attached to hyaluronan, a natural anionic polysaccharide, formed polyplexes with cationic drug like diminazene, an anti-infective drug for animals.¹¹³ Stable colloidal particles with a hydrodynamic radius (R_H) around 130 nm were obtained.

Most commonly, polyplexes are made from branched or linear PEI as a transfection vector for gene delivery. It turns out that linear PEI is obtained from hydrolysis of PMeOx or PEOx as discussed earlier (section III.3.3). Diblock copolymers prepared from partially hydrolyzed PEOx coupled to non-hydrolyzed PEOx were also self-assembled in presence of DNA.^{24,259} A core-shell structure was obtained where the core was formed by the PEI-plasmid DNA complex. The core was sparingly soluble due to charge neutralization, but the shell containing the hydrophilic PEOx improved the overall solubility of the complex. *In vitro* trials showed that the block copolymer was less toxic than linear PEI because PEOx decreased the charge density, while the transfection was as high as for the linear PEI.

Table 7 Self-assembled nanostructures made from poly(2-oxazoline)s

POx/Polymer	NP morphology	Size – d (nm)	Drug loaded	Biological test	Ref.
P(DecOx- <i>stat</i> -EtOx)	Aggregates	240 to 660	-	<i>In vitro</i>	245
P(MeOx- <i>grad</i> -PhOx)	Micelles, polymersomes aggregates	18 to 32 82 -	Indomethacin	-	246
PMeOx- <i>b</i> -(PiPrOx- <i>co</i> -PButylOx)- <i>b</i> -PMeOx	Micelles	200	-	<i>In vitro</i>	247
P(MeOx- <i>b</i> -BuOx- <i>b</i> -MeOx)	Micelles	24 to 44	Paclitaxel	<i>In vitro</i> ; <i>In vivo</i>	248– 250
P(MeOx- <i>b</i> -BuOx- <i>b</i> -MeOx)	Micelles	28 to 43	Drugs combinations	<i>In vitro</i>	5
Fmoc- <i>pY</i> -PiPrOx	Micelles, mesoglobules	Varies with pH	-	-	122
PMeOx-PDMS-PMeOx	Polymersomes	50 to 500	-	<i>In vitro</i>	251– 255
P(MeOx- <i>grad</i> -PhOx) + DPPC	Vesicle-like structures	Varies with the ratio	Indomethacin	-	256
PEtOx- <i>b</i> -peracetylated maltoheptaose	Micelles	120 to 180	Indomethacin	-	257
PEtOx- <i>b</i> -poly(4-methyl- ϵ -caprolactone)	Micelles	127 to 318	Doxorubicin	<i>In vitro</i>	258
PCL- <i>b</i> -(PEtOx brush)	Micelles	20	Doxorubicin	<i>In vitro</i>	21
PCL- <i>b</i> -PMeOx	Micelles	70 to 80	-	-	34
PEtOx-hyaluronan	Polyplexes	260	Diminazene	-	113
PEtOx- <i>b</i> -PEI	Polyplexes	380	DNA	<i>In vitro</i>	24
P(EtOx- <i>stat</i> -Et)- <i>b</i> -PEtOx	Polyplexes	100 to 200	DNA	<i>In vitro</i>	259

All these self-assembled DDS have major advantages, such as the possibility to functionalize the surface or to design multi-compartment systems, e.g. polymersomes. However, they have one major

drawback which is their low stability toward dilution or changes in the environmental conditions. To prevent the drug delivery vehicle from disintegrating in the blood stream, there is a great need to produce structures with enhanced stability or robustness against environmental stimuli.

Chemically cross-linked structures, like nanogels (nanosize hydrogels¹⁵⁴), could be appropriate candidates for this purpose. The aim of the last section of this literature review is to present the few POx-based nanogel structures reported in the literature. This is also one important direction that we took in this PhD work (see chapter 2 and 5).

IV.4. POLY(2-OXAZOLINE)S CROSS-LINKED NANOSTRUCTURES

As discussed in section III.3, different processes can be used to form POx hydrogels. Nanogels are defined as soluble polymer networks with a dimension lower than 100 nm.¹⁵⁴ Hydrophilic nanogels possess the ability to swell in water or aqueous solution as they are soluble.²⁶⁰ The polymer network could be hydrophilic or amphiphilic, and the resulting nanogels may be composed entirely of a polymeric network or a core-shell structure with a hydrogel core or shell.²⁶¹ A general overview on nanogels will be given below, but several reviews have been published on the use of microgels and nanogels as DDS and the reader is invited to refer to them for more details.^{221,262–265}

IV.4.1. BRIEF OVERVIEW OF NANOGELES

As compared to other DDS, nanogels present some unique advantages. First, they are highly stable due to the fact that they are internally cross-linked. They can be highly hydrophilic and in biological environment, they will swell and contain a high level of water/body fluids making them generally biocompatible.²⁶⁰ In principle, higher drug-loading capacities can be expected for nanogels as compared to other drug nanocarriers, because in their swollen state, a larger inner space is available for the incorporation of drugs or macromolecules.²⁶⁶

The soft structure of nanogels is another distinctive quality. Hendrickson *et al.* showed that if a pressure close to the renal filtration pressure is applied to nanogels, they can pass through pores more than ten times smaller than their size.²⁶⁷ Nanogels softness has a direct influence on their biodistribution and circulation time in the body: nanogels can bypass some organs more easily and by decreasing the modulus of nanogels by eight times, the circulation time in the body was increased by 30 times.²⁶⁸

Nanogels are thus versatile systems: by manipulating the polymer or cross-linker structure, nanogels with radically different properties can be produced.²⁶⁹ They can be responsive to environmental

factors, like changes in pH, temperature or redox conditions depending on their chemical composition. For example, by introducing disulfide bridges in their structure (most often using a disulfide-containing cross-linker), nanogels will break apart in reductive environment leading to the release of their payload. The release rates can also be controlled by manipulating the cross-linking density. The position of the cross-linking group in the nanogel structure (*i.e.* the homogeneity of the nanogels) also affects the degradation rate of the carrier: when the cross-linking groups are individually and evenly spaced in the nanogels structure, varying the percentage of cross-linking has negligible influence on the degradation rate.²⁷⁰ However, when cross-linker groups are placed in pairs, the degradation rate decreases as the percentage of cross-linker increases. Moreover, the release is up to eight times slower as compared to nanogels produced with individually spaced cross-linking groups.

Due to their high surface area, there is also the possibility to functionalize effectively their surface with ligands that could be particularly useful for targeting.

IV.4.2. SYNTHETIC METHODS TO NANOGELS

Nanogels can be synthesized by different methods that have already been reviewed in the literature.^{266,271–273} Some techniques like microfluidic, photolithography or even spray drying involved some special piece of equipment and, hence are not the focus of this section. The two main approaches to synthesize nanogels involve cross-linking of preformed polymers and polymerization in heterogeneous media.^{266,271–273}

IV.4.2.1. Nanogel synthesis by cross-linking preformed polymers

This technique could either be used for natural or synthetic polymers that are water soluble. If there is no reactive group on the polymer backbone, the polymer has first to be functionalized (chemical or physical treatments). If the polymer is fully hydrophilic, the cross-linking reaction can be achieved either in dilute aqueous solution, or in an inverse emulsion. If the polymer exhibits amphiphilic character, it has to be self-assembled first in aqueous media, and the cross-linking reaction will then secure the self-assembled structure.

IV.4.2.2. Nanogel synthesis by polymerization in heterogeneous media

The advantage of this technique is that it is a one-pot process where the polymerization and the formulation of the nanogels are performed simultaneously. In this process, nanogels are commonly prepared by free-radical cross-linking copolymerization (RCC) directly in water. Recently, nanogels have also been prepared by atom-transfer radical-polymerization (ATRP)²⁷⁴ and reversible addition-

fragmentation chain-transfer (RAFT)^{260,275}, and in each case, a bifunctional monomer acting as the cross-linker and a controlling agent that delays macrogel formation were introduced.

If both the monomer and the polymer are hydrophilic, the polymerization can take place in inverse emulsion. Monomer(s) and initiator are introduced in the aqueous dispersed phase and surfactant(s) are added to stabilize the emulsion. Polymerization occurs in the water droplets and the nanogels thus obtained have the size of the initial droplets. If the monomer and initiator are soluble in water but the polymer is not, it can be polymerized by so-called precipitation polymerization. To do so, the monomer and initiator are placed in an aqueous solution, and as the polymerization takes place, the polymer precipitates out of the water, forming nanogels.

IV.4.3. POLY(2-OXAZOLINE)S CROSS-LINKED NANOSTRUCTURES/NANOGELES

Cross-linked nanostructures prepared from POx were first reported by Nardin *et al.*²⁵¹ Polymersomes were produced from a PMeOx-*b*-PDMS-*b*-PMeOx triblock copolymer, with methacrylate groups at both chain ends. This copolymer formed vesicular structures in dilute aqueous solution with a size that could be tuned between 50 and 500 nm. Once the polymersomes were formed, the methacrylate end-groups could be polymerized by UV-induced RCC. The cross-linking reaction did not lead to any morphological change, and the size and molecular weight were conserved. Thanks to this cross-linking reaction the vesicles maintained their integrity even after their isolation from the aqueous solution.

The only fully POx cross-linked nanostructures that can be found in the literature are core cross-linked micelles. First, a nanostructure was made from an amphiphilic P(EtOx-*b*-SoyOx) block copolymer (SoyOx corresponds to monomer 12 in Table 2).²⁷⁶ In aqueous solution, spherical micelles consisting of a PEtOx corona and a PSoyOx core were formed. The micellar core could then be stabilized by core-cross-linking under UV irradiation, as in the case of the hydrogel syntheses described above (see section III.3.2).² The UV dose applied to the system had to be adjusted carefully, because if it was too low, the cross-linking density was insufficient, and if it was too high, inter-micellar cross-linking occurred. The morphology of such core-cross-linked micelles could be reversibly transformed, from spheres to small rods (rice grains), whenever the micelles were transferred from water into a non-selective solvent for the constituent blocks (e.g. acetone). This morphological transition was attributed to swelling of the slightly cross-linked core.

The second example of core-cross-linked micelles made from POx was reported in 2011 by Brummelhuis *et al.*²⁷⁷ Amphiphilic poly(2-(3-butynyl)-2-oxazoline)-*b*-PEtOx formed micelles in water, which could be core-cross-linked by thiol-yne “click chemistry”. To do so, two different mercaptans were used: methyl 3-mercaptopropionate and 2-mercaptoethylaminehydrochloride. Micelles cross-

linked with methyl 3-mercaptopropionate bore carboxylate groups in their core, whereas micelles cross-linked with 2-mercaptoethylaminehydrochloride bore amino-group in their core. These micelles with core-confined ionic groups exhibited stimuli-responsive properties and were sensitive to changes in temperature, pH, ionic strength, and salt types.²⁷⁸ These systems are currently being evaluated as “smart drug carrier” and nanoreactors for catalysis.²⁷⁷

Graft copolymers with thermo-sensitive PNIPAAm backbone and hydrophilic PEtOx graft chains demonstrated a typical amphiphilic behavior.²⁷⁹ Above the LCST of PNIPAAm chain, stable micelles with R_H of 30-40 nm were obtained. They could be core cross-linked by electron-beam irradiation, and when the temperature was then lowered below the LCST of PNIPAAm, the core became hydrophilic and core/shell type nanogels were thus obtained. By substituting poly(2-carboxyethyl-2-oxazoline) (monomer 8, Table 2) for PEtOx, the core/shell nanogels obtained were not only thermosensitive, but also pH sensitive, due to the carboxylic groups.²⁸⁰ As a consequence, the core size could be varied by manipulating the temperature, whereas the thickness of the poly(2-carboxyethyl-2-oxazoline) corona could be tuned by changing the pH (Figure I4).

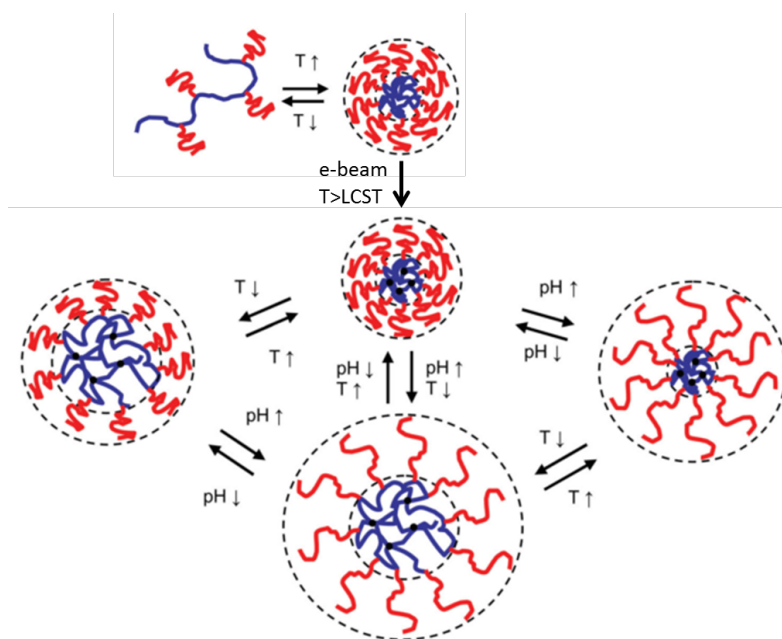


Figure I4 Strategy for the production of bisensitive nanogels and their supposed reaction to changes in stimuli like pH value and temperature. Red: side chains of poly(2-carboxyethyl-2-oxazoline); Blue: main chains of poly(N-isopropylacrylamide). Adapted from ref. 280

The other example of nanogels containing POx as one block was prepared from a triblock copolymer: PNIPAAm-*b*-POx-*b*-poly(2-hydroxyethyl methacrylate), where the POx segment corresponded to PMeOx or PEtOx.²⁸¹ Telechelic POx was first synthesized, which was followed by nanogel preparation by precipitation free radical copolymerization of NIPAAm, 2-hydroxyethyl methacrylate (HEMA) with the POx multifunctional macromonomers. The swelling-deswelling

behavior was directly related to the chemical composition (hydrophilic/hydrophobic balance) and the length of the inserted POx sequence, which could be controlled by synthesis. To study the ability of these nanogels as drug delivery carrier, BSA was encapsulated as model protein. The release of BSA was investigated with respect to variation in the cross-linking density. The higher the cross-linking density, the lower the swelling ability and the slower the release.

Even though these nanogels are promising candidates as DDS, none was studied for drug encapsulation or even for cytotoxicity studies. Such investigations, on specifically designed POx nanogels, were conducted in this PhD work and will be part of chapter 5.

Furthermore, no shell cross-linked nanostructures or nanogels prepared in inverse emulsion have been reported.

V. CONCLUSIONS

POx represent a special class of synthetic polymers that are regarded as analogues of polypeptides. They can be obtained by “controlled/living” cationic ring opening polymerization of 2-alkyl-2-oxazolines (CROP), under specific experimental conditions. CROP often requires long reaction times and can be complicated by the occurrence of some side reactions (transfer, coupling), when the polymerization is settled under conventional heating. Yet, these issues can be overcome when the reaction is performed in microwave reactors.

POx engineering has been already intensively studied and researchers have now at their disposal a substantial POx chemical toolbox. Both chain termini can be modified independently with specific functional groups, including hydroxyls, amines or carboxylic acid, and so on. A number of 2-oxazoline monomers are also commercially available and functional side chains (-OH, -COOH, -ene or -yne functions, etc.) can be introduced in the monomer, in a straightforward manner. In this context, clickable functionalities have first been considered, but some other chemical handles (e.g. aldehyde) may be further exploited.

By taking advantage of all these synthetic tools, it is now relatively easy to design POx with various architectures and compositions (copolymers, graft, star, hydrogels), and thus to tune their physico-chemical properties, such as thermal transitions (LCST and T_g), solubility and physical state (amorphous or semi-crystalline).

In many cases, POx show properties equivalent to or even outperform polymers that are commonly used in biomedical applications.²⁸² For instance, POx, and especially PMeOx and PEtOx, proved non-

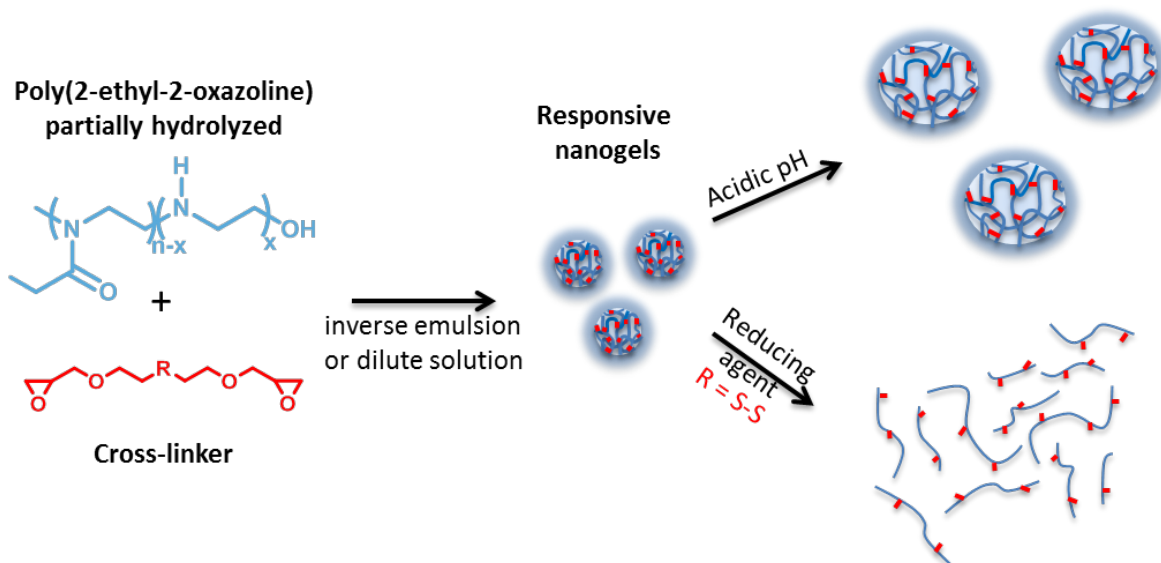
toxic to cells, hemocompatible and were internalized by cells. They also exhibit the same stealth behavior *in vivo* as PEG, and can be used as protein repellent. POx possess several advantages over PEG: they are less prone to oxidative degradation and side products are less cytotoxic than PEG ones and they offers much more possibilities for functionalization.

Consequently, there is a tremendous opportunity to develop engineered POx as key building blocks of drug delivery carriers. The background literature has shown that POx can be conjugated to proteins or drugs, can be grafted onto liposome surface and formulated as part of self-assembled systems. Numerous papers have also been published on the design of stimuli-responsive hydrogels that are mainly prepared from partially hydrolyzed POx. However, so far, not so many studies have been reported on POx nanogels and the use of such nanogels as drug delivery carriers.

On the basis of this literature overview on engineered POx, different orientations to this PhD work have been taken, as discussed in the following chapters. In chapter 2, the design of dual-responsive hydrogels and nanogels is presented. Chapter 3 focuses on the crystallization-driven self-assembly of POx block copolymers. The POx chemical toolbox is expended in chapter 4 by the development of post-polymerization reactions with a 2-oxazoline monomer bearing a protected aldehyde handle. Finally, in chapter 5, some biological properties of POx nanogels are evaluated.

CHAPTER 2

REDOX AND pH RESPONSIVE HYDROGELS AND NANOGELS MADE FROM POLY(2-ETHYL-2-OXAZOLINE)



Keywords: poly(2-oxazoline)s, hydrogels, nanogels, responsive, inverse emulsion, dilute media

Overview: This chapter describes the synthesis of hydrogels and nanogels made from partially hydrolyzed poly(2-ethyl-2-oxazoline) (PEtOx). Firstly, different cross-linkers (diglycidyl ethers, diacrylates, N-hydroxysuccinimide ester) were tested to achieve responsive and/or degradable PEtOx-based hydrogels. Secondly, nanogels were designed either in dilute aqueous media in the presence of 1,6-hexanediol diglycidyl ether (1) as the cross-linker or following an inverse w/o emulsion cross-linking process. In the latter case, in addition to cross-linker (1), a cleavable cross-linker homologue (2), namely 1,6-hydroxyethyl disulfide-bis-diglycidyl ether was used so as to produce cleavable nanogels. The pH-responsiveness of all the cross-linked PEtOx nanogels was demonstrated in acidic environment, owing to the protonation of residual ethylene imine groups and/or tertiary amines formed during the cross-linking reaction. As expected, nanogels derived from cross-linker (2) could readily be cleaved in a reducing environment, due to the presence of disulfide linkages at the cross-linking points.

Part of the work presented in this chapter has been published in *Polymer Chemistry* in 2013.¹

¹ Legros, C.; De Pauw-Gillet, M.-C.; Tam, K. C.; Lecommandoux, S.; Taton, D. *Polym. Chem.* **2013**, 4, 4801-4808

CHAPTER 2

PH AND REDOX RESPONSIVE HYDROGELS AND NANO GELS MADE FROM POLY(2-ETHYL-2-OXAZOLINE)

INTRODUCTION	67
I. SYNTHESIS AND PARTIAL HYDROLYSIS OF PETOX	69
II. HYDROGEL FORMATION AND CLEAVAGE.....	71
II.1. CROSS-LINKER SCREENING FOR THE HYDROGEL FORMATION	72
II.2. HYDROGEL FORMATION AND CLEAVAGE WITH DIGLYCIDYL ETHER CROSS-LINKERS.....	75
III. SYNTHESIS OF PETOX NANO GELS	77
III.1. IN DILUTE MEDIA	77
III.2. IN INVERSE EMULSION	78
CONCLUSIONS	80
EXPERIMENTAL SECTION	82
SUPPORTING INFORMATION	87

INTRODUCTION

Hydrogels are 3D-cross-linked polymeric networks capable of swelling in water while maintaining their overall structure. Cross-linking can be permanent (*via* chemical bonds) or temporary (*via* weak reversible interactions, such as hydrogen bonds, van der Waals or ionic interactions).¹ By selecting the polymer building block and the type of cross-linker, hydrogels can be made biocompatible and/or responsive to specific environmental conditions, two key attributes for a smart delivery system with a potential use in biomedical applications.²⁻⁴

As for nanogels, they are defined as soluble polymer networks with a dimension smaller than 100 nm.^{a5} Hydrophilic nanogels display the same structural features as hydrogels, as a result of their intra- and inter-molecular cross-linking points. They have emerged as a new class of nanocarriers for drug delivery applications.⁶⁻¹⁰ Formulation of nanogels can be achieved by different methods.^{6,8,11,12} Specific processes like microfluidics, photolithography or spray drying require specific processing equipment; hence they are not widely employed. Some of the more common synthetic approaches are radical cross-linking copolymerization (RCC) in heterogeneous media, or cross-linking of pre-formed linear polymers, e.g. by chemical post-modification or radiation with a high energy source. In the former case, nanogels can be generated in a one-pot process, where both polymerization and formulation are performed simultaneously.¹³ Cross-linking of a pre-formed polymer requires a polymer backbone with pendent reactive groups, which is referred to as a post-polymerization modification method.¹⁴⁻¹⁷ With hydrophilic precursors, however, the cross-linking reaction can be achieved either in dilute aqueous solution, or in an inverse water-in-oil (w/o) emulsion.^{7,10,11} With amphiphilic copolymers, self-assembly in aqueous media can take place first, which is followed by the cross-linking reaction aimed at stabilizing the self-assembled structure.^{7,10,11}

Poly(2-oxazoline)s are a particularly interesting class of hydrophilic polymers, as they can be regarded as amino-acid analogues.¹⁸ They are potential candidates for biomedical applications, in particular as drug carriers. More particularly, poly(2-ethyl-2-oxazoline) (PEtOx) is a biocompatible polymer that can be internalized by cells and that is characterized by stealth behavior, a feature that is commonly associated with poly(ethylene glycol) (PEG).¹⁹⁻²² As a consequence, PEtOx can act as protein repellent²³⁻²⁵ and enhance antimicrobial properties.²⁶ Previous studies demonstrated that PEtOx can be conjugated to

^a Nanogels are defined by IUPAC as a particle of gel of any shape with an equivalent diameter of approximately 1 to 100 nm. There is indeed a misperception in the current literature between nanogels and microgels. As a consequence, in the following text, we will qualify some of our compounds as nanogels, although their size is greater than 100 nm.

proteins or drugs, or be grafted onto the surfaces of liposomes, and be formulated as part of self-assembled systems, such as polymeric micelles or polymersomes, and used as drug delivery carriers.²⁷

Designing responsive hydrogels made from poly(2-oxazoline)s is relatively well documented,²⁸ one of the major challenges being the introduction of a 2-oxazoline monomer bearing a reactive functionality.²⁹ As presented in Chapter 1 (section 1.1.3.1), such materials can be prepared by copolymerization of 2-ethyl-2-oxazoline (EtOx) with a *bis*-2-oxazoline comonomer.^{30,31} Another strategy consists in the introduction of a 2-oxazoline co-monomer bearing a reactive functionality followed by post-polymerization modification.^{32,33} Hydrogels were also prepared from poly(2-oxazoline)s functionalized at both chain ends; for example, methacrylate end-functionalized PEtOx can also be crosslinked to achieve hydrogels by reaction with a 3-arm polylactide analogue.²⁶ Other examples of hydrogels formed with end-functionalized poly(2-oxazoline)s were reported.^{34–36} More recently, hydrogels were prepared by the copolymerization of a 2-oxazoline monomer bearing a *Boc*-protected amino group on the side chain (*BocOx*) with EtOx and further treatment with epichlorohydrin.³⁷ Hydrogels were also prepared by the copolymerization of 2-(dec-9-enyl)-2-oxazoline with either 2-methyl-2-oxazoline or EtOx and further cross-linking with dithiol molecules.³⁸ Lastly, amine functionalities can be statistically introduced by partial hydrolysis of pre-formed poly(2-alkyl-2-oxazoline) (alkyl = methyl or ethyl). The latter method was developed by Saegusa and coworkers who prepared redox-, light-, or temperature-responsive hydrogels depending on the cross-linkers used (e.g. diisocyanate, dicarboxylic acid, etc.).^{39–43} (Chap 1, section 1.1.3.3, scheme 10)

In contrast, true soluble nanogels made of poly(2-oxazoline)s and their use as drug delivery carriers have rarely been investigated. For instance, core-cross-linked micelles based on an amphiphilic poly(EtOx-*b*-2-“soy alkyl”-2-oxazoline) copolymer, where the 2-“soy alkyl”-2-oxazoline block was derived from a long fatty acid side chain bearing alkene functionalities, have been described by Huang *et al.*⁴⁴ The cross-linking process was achieved by UV irradiation. Another recent example was reported by Brummelhuis *et al.*⁴⁵ who cross-linked micelle-like nanostructures formed by self-assembly of an amphiphilic poly(2-(3-butynyl)-2-oxazoline)-*b*-PEtOx, using thiol-yne “click chemistry”. These core-cross-linked micelles exhibited stimuli-responsive properties and were sensitive to changes in temperature or pH or ionic strength.

The aim of the present work is to propose different synthetic methodologies to hydrophilic hydrogels and nanogels based on PEtOx. Secondary amine functionalities were first introduced into the polymer backbone by partial hydrolysis. The as-obtained statistical copolymers were then reacted with different cross-linkers (diglycidyl ethers, diacrylates, *N*-hydroxysuccinimide ester) (Scheme 1). Copolymer

materials issued from the reaction with the bis-glycidyl ether cross-linker were studied more thoroughly. For instance, the redox-sensitive cross-linker containing a disulfide functionality was used to produce degradable poly(2-oxazoline) hydrogels and nanogels. Nanogel synthesis was achieved following two distinct processes: in dilute aqueous media and in an inverse w/o emulsion. The redox and/or pH-responsive properties of nanogels obtained in this manner are demonstrated.

I. SYNTHESIS AND PARTIAL HYDROLYSIS OF PEtOx

The cationic ring-opening polymerization (CROP) of 2-ethyl-2-oxazoline was performed in acetonitrile at 85 °C, using methyl trifluoromethanesulfonate as the initiator, following a well-established procedure (see Scheme 1, further).^{46,47} A methanolic KOH solution was employed upon completion of CROP to quench the living polymer chain ends. The experimental degree of polymerization (DP) was 94 and a dispersity (\bar{D}) of 1.28 was obtained (Figure 1). The absolute molecular weight of PEtOx was then determined by SEC equipped with a laser light scattering detector (Figure 2).

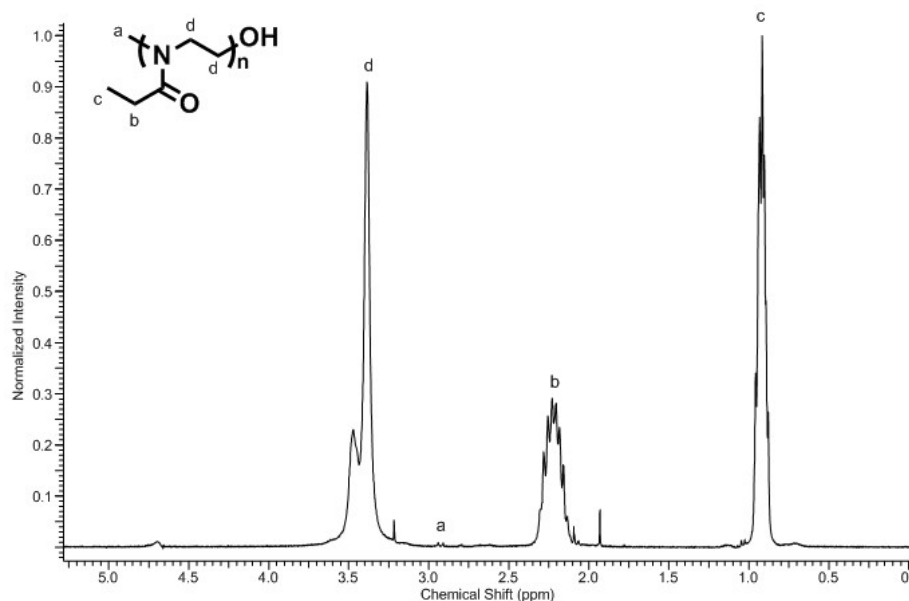


Figure 1 ¹H NMR spectra (400 MHz, D₂O) of poly(2-ethyl-2-oxazoline)₉₄

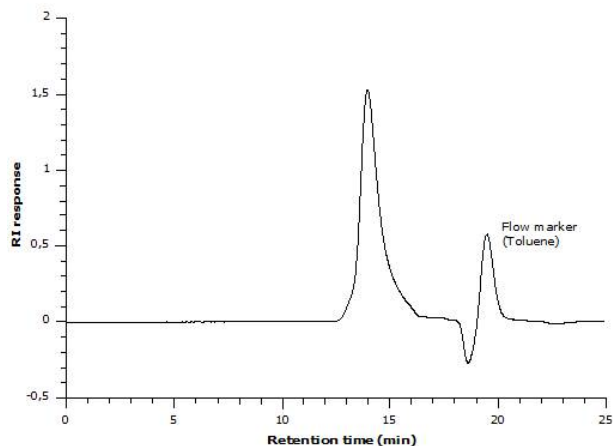


Figure 2 SEC trace of poly(2-ethyl-2-oxazoline)₉₄ in DMF obtained with a laser light scattering detector

This PEtOx precursor was next partially hydrolyzed to introduce secondary amine functionalities along the polymer backbone (see Scheme 1). Such a hydrolysis procedure has previously been studied in both acidic and basic media,^{48–50} where the hydrolysis rate was found to depend both on the amount of acid or base added and on the reaction time. Upon performing the hydrolysis under basic conditions, a decrease in both the polymer solubility and the reaction rate was noted. The reduction in solubility can be explained by the crystallization of linear poly(ethylene imine) (PEI) domains. In contrast, the polymer solubility was retained by performing hydrolysis in acidic media, which resulted in better control over the hydrolysis rate. This can be explained by the fact that the pH of the reaction medium was lower than the pKa of PEI (pKa = 8.5), the ethylene imine functionalities being protonated.

The hydrolysis kinetics were studied next with P(EtOx)₉₄ at 50 g/L in a HCl solution at 18.5 %, under reflux. Aliquots were withdrawn periodically (0.5, 1, 2, 3, 4 and 6.5 h), and after 6.5 hours a significant tail at higher retention time was observed in the SEC trace (Supporting information - SI†, Figures SI and S2). This could be due to polymer degradation or interactions of the polymer chains with the SEC columns, even in DMF, as previously described for similar polyamines.⁴⁸ Hence, the PEtOx chains were hydrolyzed within a 4 hour time window. The degree of hydrolysis was evaluated both by ¹H NMR spectroscopy and titration of the secondary amines (Figure 3 and Table I).

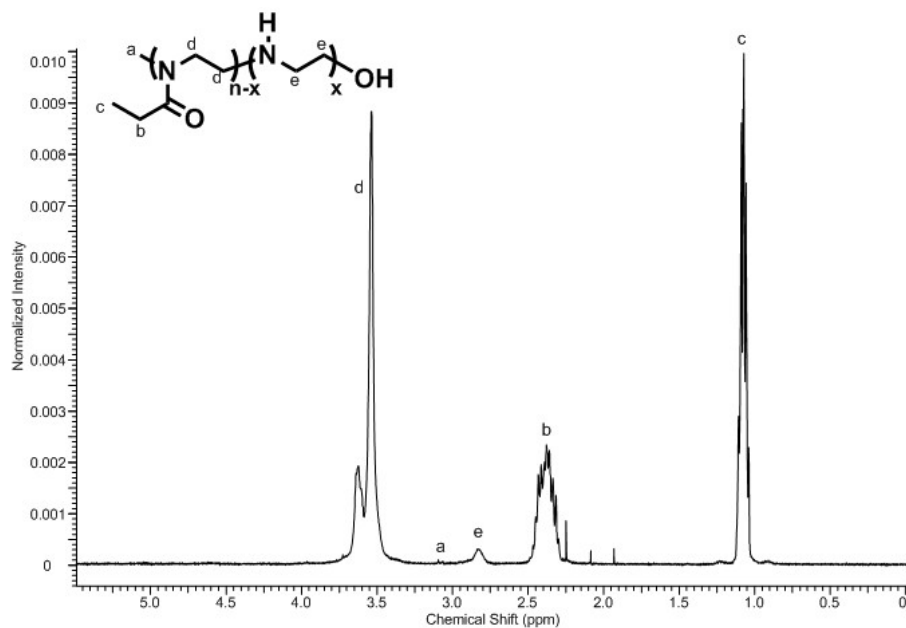


Figure 3 ^1H NMR spectra (400 MHz, D_2O) of poly((2-ethyl-2-oxazoline) $_{88}$ -stat-(ethylene imine) $_6$)

Table I Evolution of the degree of hydrolysis of poly(2-ethyl-2-oxazoline) $_{94}$ with time

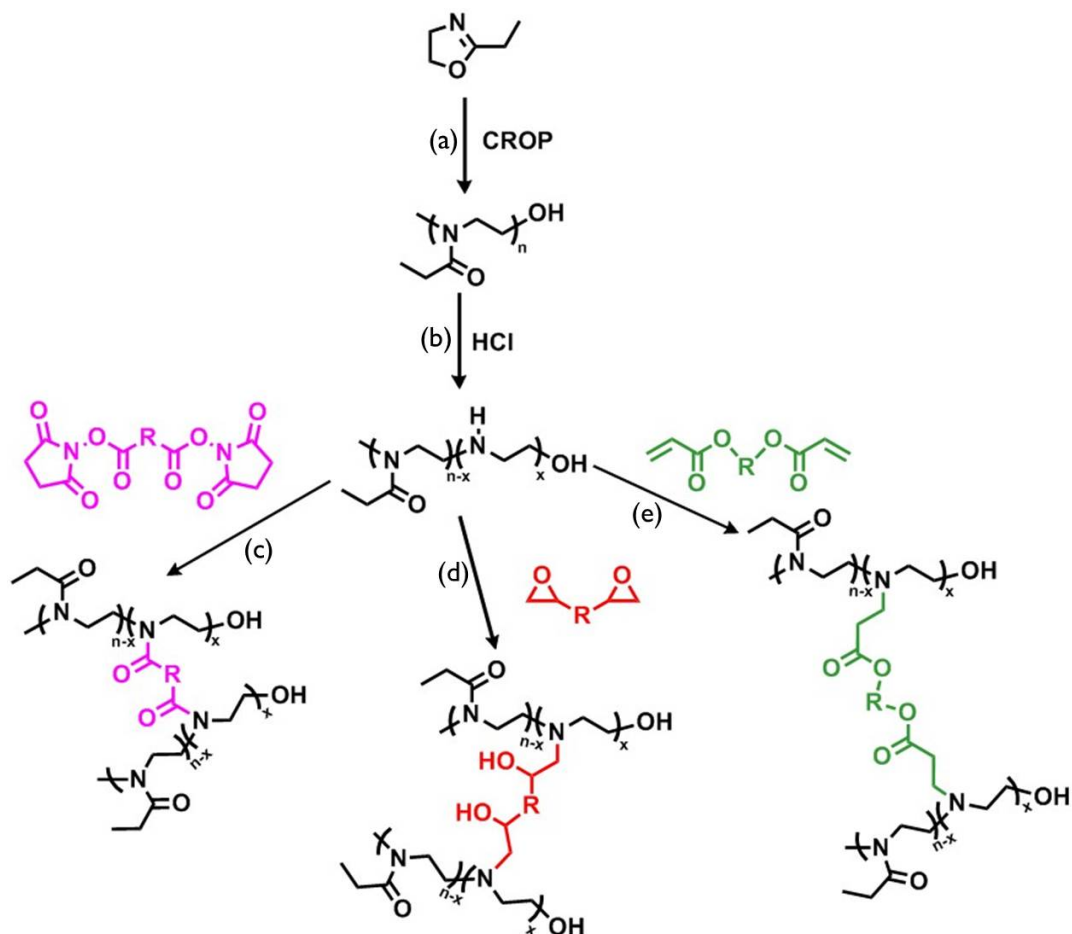
Hydrolysis reaction time (h)	Hydrolysis % (^1H NMR)	Hydrolysis % (Titration)
0.5	3.4	-
1	4.3	-
2	6.7	5.3
3	8.9	9.6
4	11.3	12

II. HYDROGEL FORMATION AND CLEAVAGE

The critical concentration for gelation of $\text{P}(\text{EtOx})_{94}$ was determined by measuring the intrinsic viscosity ($[\eta]$, Figure S3) and the radius of gyration (R_g). A R_g value of 3.65 nm was obtained corresponding to a critical concentration of 56 mg/mL.

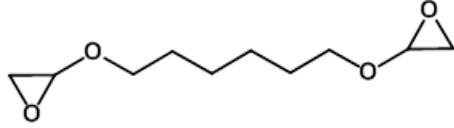
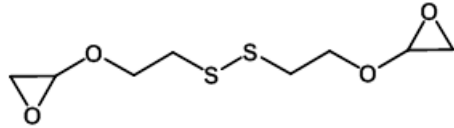
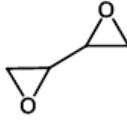
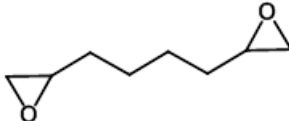
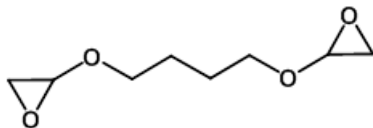
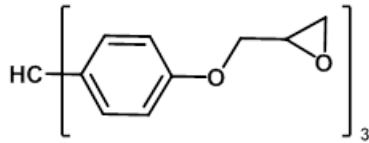
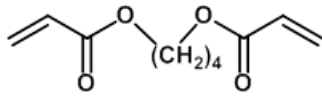
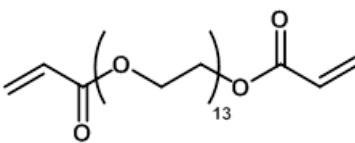
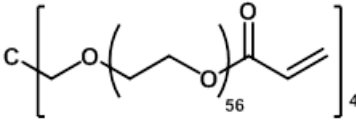
II.1. CROSS-LINKER SCREENING FOR THE HYDROGEL FORMATION

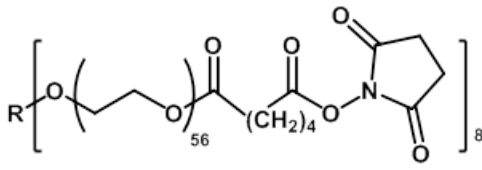
Hydrogels were then prepared from a range of cross-linkers, as illustrated in Scheme 1 (see also Table 2).



Scheme 1 Synthesis of hydrogels made from poly(2-ethyl-2-oxazoline): (a) Cationic ring-opening polymerization (CROP) of 2-ethyl-2-oxazoline. (b) Partial hydrolysis of the poly(2-ethyl-2-oxazoline). (c)-(e) Formation of hydrogels by reaction with cross-linker (c) *N*-hydroxysuccinimide ester (d) diepoxide/diglycidyl ether (e) diacrylate.

Table 2 Cross-linkers used to form hydrogel with partially hydrolyzed poly(2-ethyl-2-oxazoline) and conditions used for the hydrogel formation

			Solvent	T (°C)	Reaction time
EPOXIDE/ GLYCIDIL ETHER	1		H ₂ O	80 60	Overnight 3 days
	2		H ₂ O	80 60	Overnight 3 days
	3		H ₂ O	80	1 day
	4		H ₂ O	80	Overnight
	5		H ₂ O	80 60	Overnight 3 days
	6		THF: H ₂ O 2:3	80	2 h
ACRYLATE	7		H ₂ O	60 40 30	2h30 3 h 3h30
	8		Phosphate buffer 0.04M pH = 8	80 30	1h30 Overnight
	9		Phosphate buffer 0.04M pH = 8	30	Overnight

NHS ESTER	10	 <p>R = hexaglycerol core structure</p>	H ₂ O	RT	20 min
-----------	----	--	------------------	----	--------

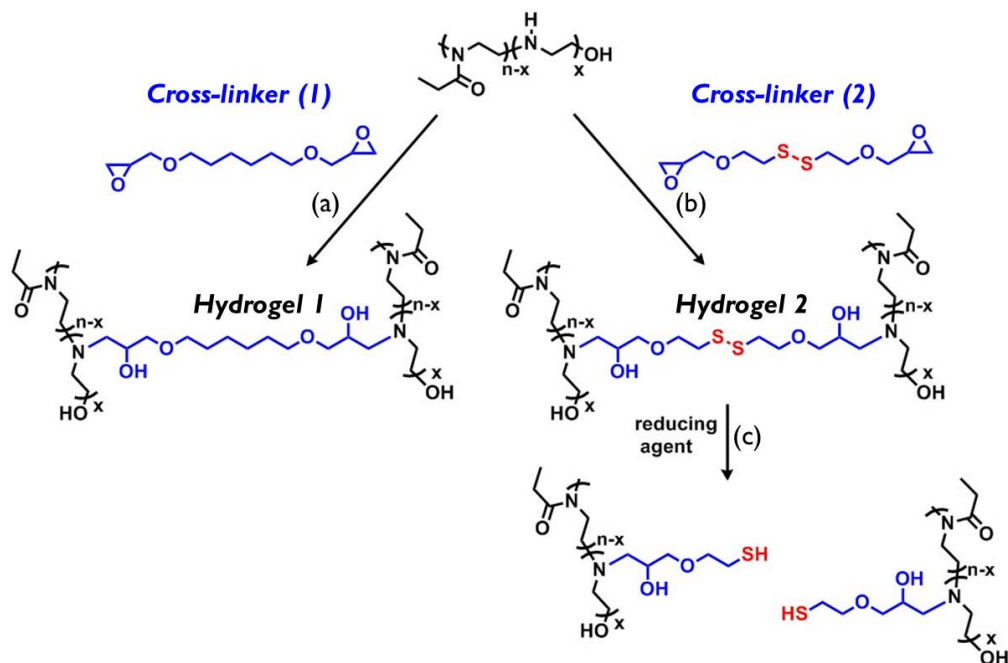
Three main families of cross-linkers were tested to react with secondary amines of the polyoxazoline backbone. Bis-epoxides (cross-linkers 1 to 8, Table 2) reacted *via* ring-opening of the epoxides with secondary amines. Diacrylates (cross-linkers 7 to 9) and secondary amines reacted *via* a Michael-type addition reaction under slightly basic conditions.⁵¹ The reaction of amines with *N*-hydroxysuccinimide ester compound (NHS ester, cross-linker 10) is used to cross-link or label peptides and proteins under physiological or slightly alkaline conditions (pH 7.2 to 9), yielding stable amide bonds. The reaction releases *N*-hydroxysuccinimide (NHS) as a by-product.⁵² However, hydrolysis of the NHS ester can compete with the amine reaction. The rate of hydrolysis increases with the buffer pH and contributes to less-efficient cross-linking in less-concentrated solutions.

All the reactions were conducted at a constant ratio of reactive functionalities in aqueous solution, except for tris(4-hydroxyphenyl)methane triglycidyl ether (cross-linker 6) that was not soluble in pure water. Hydrogels were obtained with all of the cross-linkers shown in Table 2, except 1,3-butadiene diepoxide (cross-linker 3). The flexibility of the cross-linker was found to be of great importance in order for the cross-linking reaction to proceed. A trial was carried out using cross-linker 3, but no hydrogel was obtained due to the tight/constrained structure of this cross-linker. On the other hand, increasing the alkyl chain length between the two epoxide rings decreases the water solubility of the cross-linker. Nevertheless, a gel was formed with 1,2,7,8-diepoxyoctane (cross-linker 4) despite the relatively poor water solubility of this cross-linker. This was confirmed by the formation of a white insoluble compound. In contrast, the use of diglycidyl ether cross-linker (cross-linkers 1, 2, 5 and 6) led to transparent gels exhibiting a greater affinity for water (di-epoxides are less soluble in water than the equivalent diglycidyl ether molecules). Diacrylate cross-linkers are more reactive than the diglycidyl ones, forming gels even at temperatures as low as 30 °C, which is a major advantage in the design of drug delivery devices. However, hydrogels formed with diacrylate cross-linkers in aqueous solution could be completely cleaved within two weeks by ester hydrolysis. As expected, the most efficient cross-linker tested in this series was the 8-arm NHS-containing PEG. This is due to the higher functionality of this commercially available cross-linker. NHS ester-amine coupling is one of the most popular coupling reactions for bio-systems as a result of the ease of the reaction and the mild conditions required.⁵² Further hydrolysis was still possible with these hydrogels also, as a result of the ester functionalities

present in the structure. Through modifications of the cross-linker R-group, some of the resulting hydrogels could be responsive to specific stimuli.

II.2. HYDROGEL FORMATION AND CLEAVAGE WITH DIGLYCIDYL ETHER CROSS-LINKERS

As the aim of the present study was to prepare hydrogels made of a polyoxazoline backbone that could be stimuli-responsive, only the compounds made from diglycidyl cross-linkers 1 and 2 (Table 2) were further studied. Hydrogels were formed using a non-cleavable cross-linker, namely 1,6-hexanediol diglycidyl ether (1) (Scheme 2). The cross-linking reaction was optimized *via* a kinetic study, withdrawing aliquots of various hydrolysis degrees (shown in Table 1) at a polymer concentration of 100 mg/mL. These precursors were first dissolved in deionized (DI) water and the cross-linker (1) was added to obtain a concentration of 40 mg/mL. The solutions were stirred at 80 °C overnight. The results suggest that a degree of hydrolysis of at least 6.7 % was required to observe gel formation. Thus, a new batch of P(EtOx)₉₄ hydrolyzed to 6.7 % (P(EtOx₈₈-stat-El₆)) was specifically synthesized and used for the rest of the study. Titrations were performed both before and after hydrolysis, as shown in Figure 4.



Scheme 2 Synthesis of hydrogels made from poly(2-ethyl-2-oxazoline): (a) Formation of non-cleavable hydrogels by reaction with 1,6-hexanediol diglycidyl ether (1). (b) Formation of cleavable hydrogels by reaction with hydroxyethyl disulfide-bis-diglycidyl ether (2). (c) Hydrogel cleavage under reducing environment.

The dry gel was analyzed by FTIR and compared to the spectrum of the parent PEOx. The appearance of a peak at 1109 cm^{-1} characteristic of an ether C-O stretch confirmed the incorporation of the cross-linker (SI†, Figures S4 and S5).

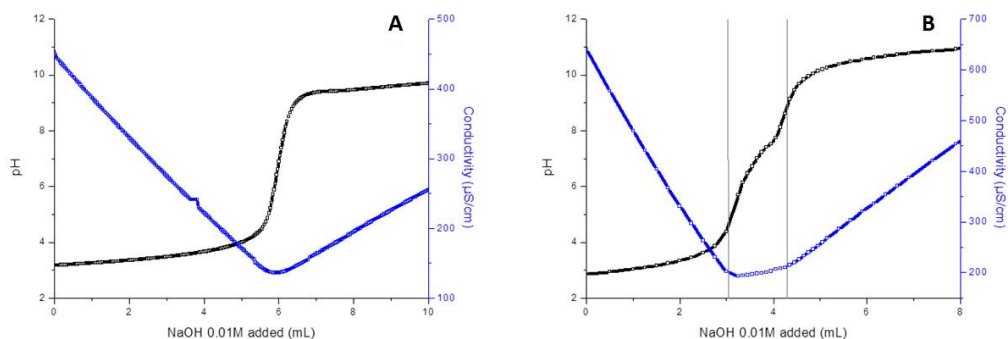


Figure 4 Titration of the secondary amine by pH-metry and conductivity measurements **A)** of parent poly(2-ethyl-2-oxazoline)₉₄ and **B)** of poly((2-ethyl-2-oxazoline)₈₈-stat-(ethylene imine)₆) copolymer

Hydrogels that could be chemically cleaved in a reducing environment were also prepared, using the same partially hydrolyzed polymer precursor, P(EtOx₈₈-stat-EI₆), and hydroxyethyl disulfide-bis-diglycidyl ether (2) as the cross-linker. The latter compound was synthesized following a procedure reported in the literature (SI†, Figures S7 and S8).⁵³ The appearance of a peak at 1104 cm^{-1} in the FTIR spectrum of the dry gel, again confirmed incorporation of the cross-linker (2) (SI†, Figure S6). Cross-linking points with a central disulfide bridge in related PEOx hydrogels could be cleaved in reducing environment. The cleavage reaction was implemented using 1 mL of a dithiothreitol (DTT) solution under nitrogen atmosphere. Within approximately 5 minutes, the central disulfide bridges were indeed cleaved and the gel transformed into a clear solution, as illustrated in Figure 5.

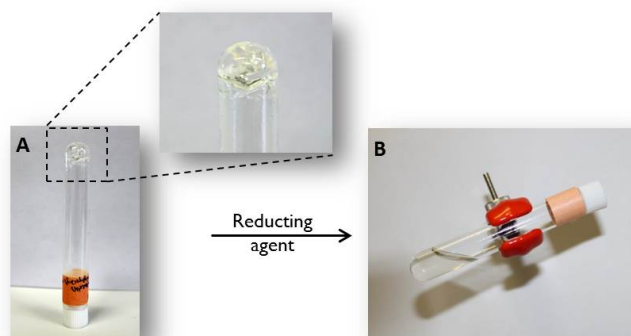


Figure 5 **A)** Hydrogel formed by the reaction of ethylene imine groups on the polymer backbone with hydroxyethyl disulfide-bis-diglycidyl ether (2). **B)** Clear solution obtained after addition of DTT to the hydrogel.

III. SYNTHESIS OF PEOX NANOGELS

III.1. IN DILUTE MEDIA

By drastically decreasing the concentration of both the partially hydrolyzed PEOx precursor to 10 mg/mL (instead of 100 mg/mL used in the previous section) and that of the cross-linker (1) to 2.2 mg/mL, nanogels could be formed in dilute media. The polymer and cross-linker were thus dissolved in a mixture of water (97 %) and ethanol (3 %) to improve the solubility of the cross-linker and the nanogel formation was monitored by dynamic light scattering (DLS). At the initial stage, all the species were soluble in the solvent mixture and the low scattered intensity attested to the presence of unimers in solution. Upon nanogel formation, the scattered intensity increased and both the size and size distribution of the as-formed compounds were directly determined.

Non-cleavable nanogels were formed within 3 hours, using cross-linker (1). The variation of decay rate versus the squared scattering vector is shown in Figure 6A. The slope of the linear fit corresponds to the translational coefficient and the hydrodynamic radius can be calculated using the Stokes-Einstein equation. A hydrodynamic radius of 205 nm was thus obtained. The formation of spherical nanostructures was also evidenced by transmission electron microscopy (TEM), a size in agreement with the DLS results was achieved (Figure 6C).

Attempts to derive cleavable nanogels using cross-linker (2) under the same conditions were less successful. Indeed, reduced solubility of cross-linker (2) was observed in the solvent mixture at the initial stage as compared to its non-cleavable analogue (1). Hence, no nanogels were successfully formed using this protocol; instead, macroscopic hydrogels were obtained after approximately 3 hours. Tries to optimize the conditions, including changes in solvents ratio, solvent mixture (H₂O/EtOH, H₂O/DMSO), polymer concentration, cross-linker concentration and ratio of reactive functionalities, did not allow us to achieve nanogels from cross-linker (2) in dilute media.

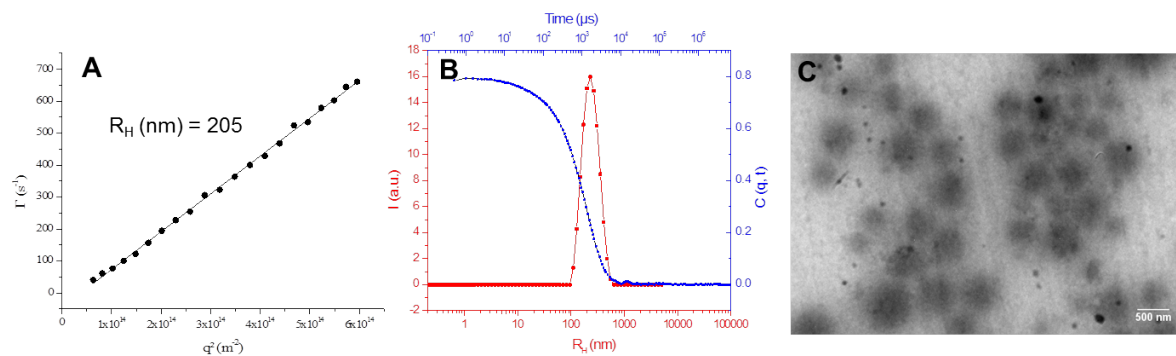


Figure 6 DLS analysis and TEM of permanently cross-linked nanogels prepared in dilute media, using cross-linker (1). A) Variations of decay rate versus squared scattering vector with a linear fit. B) Relaxation time plot obtained at 90°. C) TEM micrograph (scale bar = 500 nm)

III.2. IN INVERSE EMULSION

An inverse emulsion process was also implemented to access the targeted nanogels. The aqueous phase was composed of P(EtOx₈₈-El₆) and the diglycidyl ether cross-linker (1) or (2) in 100 μ L of DI water. The aqueous phase was added to 0.8 g of cyclohexane with 5% Span 80, a non-ionic surfactant. The emulsification was triggered by an ultrasonic probe and the reaction mixture was stirred at 80 °C overnight. The resulting compounds were then thoroughly washed, first with cyclohexane and THF, then by dialysis against water. The successful transfer of the materials into DI water confirmed the efficient removal of the surfactants.

Non-cleavable nanogels were first prepared using cross-linker (1). The variation of nanogel size with pH was investigated, as summarized in Figure 7. At neutral pH, a hydrodynamic radius of 126 nm was obtained. Upon addition of diluted HCl, yielding a solution pH of 3-4, an increase in nanogel size to 156 nm was noted, indicative of nanogel swelling. This can be explained by the protonation, in acidic environment, of residual ethylene imine groups and/or tertiary amines formed during the cross-linking reaction. This protonation increases the hydrophilicity of the compounds and charge repulsion within the nanogels. Average sizes determined by TEM were smaller than those obtained by DLS. This effect was attributed to the shrinking of the nanostructures on the TEM grid, during the preparation process. The main difference between the two techniques is the state of the nanogel compounds during analysis (hydrated state in DLS and dried state in TEM).

Nanogels were then successfully prepared with the cleavable cross-linker (2) *via* the inverse emulsion w/o process, and the influence of pH on nanogel size was studied (Figure 7). An increase in size, from

154 to 179 nm, was noted upon addition of HCl solution (pH = 3-4), demonstrating the pH-sensitivity of the compounds. The morphology was confirmed by TEM, the sizes being smaller as compared to those obtained by DLS, which again may be explained by solvent evaporation (the large diffuse areas correspond to residue of surfactants or artefact due to solvent drying).

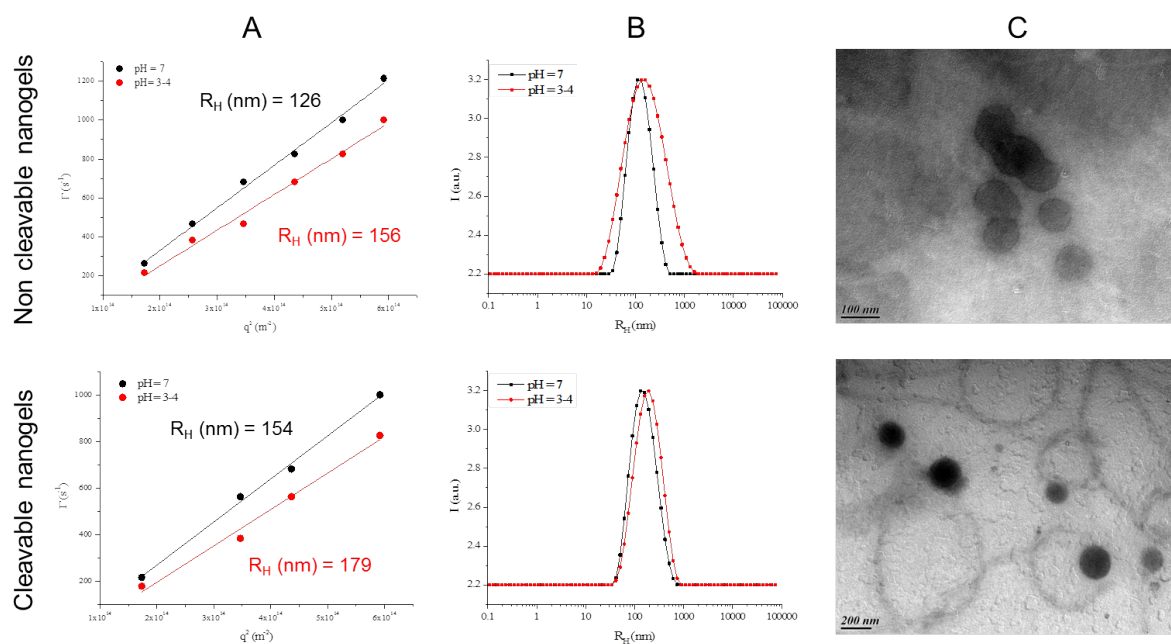


Figure 7 DLS and TEM analysis of the cleavable and non-cleavable nanogels. **Panel A:** Variations of decay rate versus squared DLS scattering vector with linear fits at different pHs. **Panel B:** Relaxation time plot obtained at 90° at different pHs. **Panel C:** TEM micrographs at neutral pH

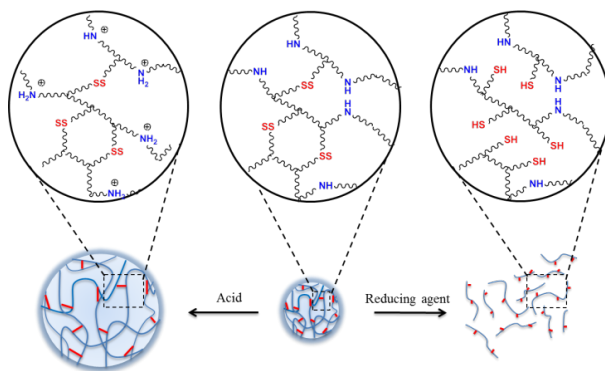
The influence of a second stimulus was then studied by the addition of a reducing agent. In the presence of DTT, indeed, the count rate decreased dramatically confirming the disruption of the nanogel structure (SI†, Figure S9). To confirm that this behavior was not linked to a dilution effect, the same volume of DI water (as DTT) was added to a second sample, also analyzed by DLS. In the latter case, the count rate decreased slightly but not as significant as in the case of DTT. Thus, the use of a cleavable cross-linker (2) enabled the synthesis of stimuli-responsive nanogels, responding to both a reducing environment and a pH change, as illustrated in Scheme 3.

CONCLUSIONS

We have demonstrated that partially hydrolyzed poly(2-ethyl-2-oxazoline) (PEtOx) can react with different of cross-linkers including bis-epoxides, bis-acrylates and bis-*N*-hydroxysuccinimide ester, in water to form cross-linked derivatives. Dual stimuli-responsive hydrogels and nanogels can be readily prepared from partially hydrolyzed PEtOx and hydroxyethyl disulfide-*bis*-diglycidyl ether.

Hoogenboom *et al.* recently reported that partially hydrolyzed PEtOx with up to 10 % of ethylene imine functions did not show any cytotoxicity *in vitro*.⁵⁴ The extent of hydrolysis of the PEtOx used in our study (6.7 %) is below this *in vitro* cytotoxicity limit. Additional cell viability experiments are addressed in Chapter 5.

Nanogel formation by cross-linking of the secondary amino groups can be triggered either in inverse w/o emulsion or in dilute aqueous media, using diglycidyl ethers as cross-linkers. The dilute medium process offers some noticeable advantages as nanogels were formed within a few hours in water, without the need of any surfactants or catalysts. However, this method is limited by the solubility of the reagents. For instance, no nanogels were obtained in the presence of the cleavable cross-linker, most likely due to its poor solubility in aqueous media. In contrast, non-cleavable and cleavable nanogels were synthesized using an inverse w/o emulsion process. Their sizes can potentially be tuned by adjusting the diameter of the emulsion droplet. The synthesized nanogels exhibited stimuli-responsive behavior, swelling in acidic environment was observed for all nanogels. This was a result of the protonation of residual ethylene imine groups and/or tertiary amines formed during the cross-linking reaction. In addition, nanogels made from the cleavable cross-linker could be readily disrupted in reducing environment due to the presence of disulfide bridges (Scheme 3).



Scheme 3 Schematic illustration of the dual-responsiveness of PEtOx-based nanogels: swelling in acidic environment and chemical cleavage in reducing environment.

These nanogels may potentially be used to encapsulate hydrophilic bio-macromolecules such as proteins which can be released specifically in tissues of low pH (acidic environment, i.e. inflamed tissues) and/or where reducing agents are present such as glutathione, a reducing peptide mainly found in tumor tissues.

EXPERIMENTAL SECTION

Materials and reagents

2-Ethyl-2-oxazoline (99%), methyl trifluoromethanesulfonate (96%) (MeOTf), and acetonitrile (99%) were purchased from Sigma-Aldrich, stored over calcium hydride and purified by vacuum distillation prior to use. Methanol purchased from Sigma-Aldrich was refluxed with sodium and distilled prior to use. Diethyl ether, ethanol, potassium hydroxide (KOH), sodium hydroxide (NaOH), hydrochloric acid solution (37%) (HCl), dithiothreitol (DTT), cyclohexane (99%), 1,4-butanediol diacrylate (90%) PEG diacrylate ($M_n = 700$ g/mol), tris(4-hydroxyphenyl)methane triglycidyl ether and sorbitan monooleate (Span 80) were used as received from Sigma-Aldrich. 1,6-Hexanediol diglycidyl ether (98%) was purchased from BOC sciences. 1,2,7,8-Diepoxyoctane (97%), 4-butanediol diglycidyl ether (>90%) were purchased from TCI. 4-arm PEG acrylate (pentaerythritol), M_w 10000 g/mol (99.8%) and 8-arm PEG succinimidyl adipate (hexaglycerol) $M_w = 15000$ g/mol (94.7%) were purchased from Jenkem technology. Hydroxyethyl disulfide-*bis*-diglycidyl ether was synthesized following a procedure reported in the literature (see Experimental procedure).⁵³

Instrumentation

NMR spectroscopy. ¹H NMR measurements were carried out at room temperature, on a Bruker Avance I spectrometer operating at 400 MHz. The D₂O signal was used as the reference signal ($\delta = 4.79$ ppm), and the relaxation time was fixed to 7.5 sec for all measurements.

Size-exclusion chromatography. Size-exclusion chromatography (SEC) using dimethylformamide (DMF) with LiBr (1 g/L) as the eluent was performed at 80 °C at a flow rate of 0.8 mL/min. The column set consisted of two 7.5 mm x 300 mm PLgel, 5 μ m Mixed-D columns (Polymer laboratories) coupled to a guard column, 7.5 mm x 50 mm, PLgel, 5 μ m model (Polymer laboratories). Injections were carried out in a 20 μ L loop and calibrated using polystyrene standards. Differential refractive index (RI) and UV detectors were used. To determine the absolute polymer molecular weight, analytical SEC measurements were performed on a system with a Waters 510 HPLC pump, a 50 μ L injection loop, and a Waters 410 differential refractometer (DRI) detector. A Wyatt MiniDAWN laser light scattering detector operating at a wavelength of 690 nm served to determine the absolute molecular weight of the polymers (measured at an angle of 90°). The column used was a 250 mm x 10 mm JORDI X-tream column Mixed bed model with a linear polystyrene molecular weight range of 102–107. This column is coupled with a guard column, a 50 mm x 10 mm JORDI X-tream Mixed Bed model. DMF with LiCl (1

g/L, added to minimize adsorption of the polymer on the column) at a flow rate of 1.0 mL/min served as the mobile phase, at room temperature.

Titration. Titration was performed with a Metrohm 809 Titando autotitrator for simultaneous measurement of conductivity and pH. The titrator is equipped with Tiamo software, which doses μL quantities of titrants. All measurements were performed in a jacketed vessel at 25 °C while stirring at a medium speed. 50 mL of solutions of the samples at 0.8 g/L were prepared in DI water. The pH of the solutions was adjusted to ~ 3 by adding 0.5 M HCl. The solutions were titrated using 0.01 M NaOH under nitrogen blanket and stirring. Conductivity and pH of the solutions were measured simultaneously until the pH of the samples approached 11. Finally, the pH and conductivity values were plotted against the volume of NaOH (in mL).

Intrinsic viscosity measurement. The intrinsic viscosities of partially hydrolyzed polymers were measured with an automated kinematic viscometer, MiniPV model, from the Cannon Instrument Company, at 25 °C. To do so, samples at different concentrations were prepared (1, 2, 4, 6, 8 mg/mL). For a known volume of a sample, the time taken for the level of the liquid to pass between two marks was measured twice. The relative, specific and reduced viscosities are directly calculated from these time values. The intrinsic viscosity corresponds to the value of the reduced viscosity when the concentration approaches zero.

Polymers dn/dc measurements. The refractive index increment (dn/dc) measurements were conducted on a Brookhaven instrument, BI DNDC, at a wavelength of 620 nm. Polymer solutions were prepared in DMF with LiCl (1 g/L, the same solvent used for SEC measurements) at the following concentrations: 0.5, 1, 2, 3 and 4 mg/mL. Analyses were carried out with the preparatory software supplied with the instrument.

Infrared spectroscopy. Infrared spectra were obtained on a Thermoscientific Nicolet IS10 spectrometer using the attenuated total reflection (ATR) mode. The spectra were acquired using 16 scans at a resolution of 4 wavenumbers.

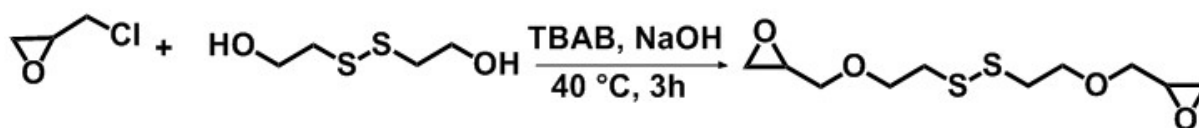
Dynamic light scattering. Dynamic light scattering (DLS) experiments of the nanogels prepared in dilute media were performed using an ALV CGS-3 Compact Goniometer System, equipped with a 35 mW HeNe linear polarized laser with a wavelength of 632.8 nm and an ALV/LSE-5004 light scattering electronic and Multiple Tau Digital correlator. The accessible scattering angles ranged from 30° to 150°. Samples (2 mL in 2 cm diameter cylindrical glass cells) were immersed into a filtered toluene bath. Three independent 20 s measurements were carried out to obtain the dynamic data. Mean hydrodynamic

diameters and size distributions were determined using a cumulant analysis method. Samples were first filtered with 0.8 μm nitrocellulose membrane. DLS measurements of nanogels prepared in inverse emulsion were performed using a Brookhaven BI-200SM instrument equipped with a He-Ne laser operating at $\lambda = 636 \text{ nm}$, at $20 \text{ }^\circ\text{C}$. Measurements were performed at different angles and data analyses were carried out using the Gendist software. The samples were first filtered with 0.8 μm nitrocellulose membranes.

Transmission electron microscopy. Transmission Electron Microscopy (TEM) images were recorded at Bordeaux Imaging center (BIC) on a Hitachi H7650 microscope working at 80 kV. Samples of nanogels synthesized in dilute media were prepared by drop depositing 0.7 μL of the nanogels solution in water onto a copper grid (200 mesh coated with carbon) and removing the excess after 5 min. Samples of the nanogels synthesized in inverse emulsion were prepared by drop depositing 0.7 μL of the solution of nanogels in THF onto a copper grid and left to dry. The grids were prepared in THF as it is miscible with both cyclohexane and water (the two emulsion phases), and if there is any surfactant left, it is also soluble in THF. As a matter of fact, only nanogels were observed. In both cases, they were subsequently stained with osmium tetroxide vapour for 45 min.

Experimental procedures

Synthesis of hydroxyethyl disulfide-bis-diglycidyl ether (2). Cross-linker (2) was synthesized following an established synthetic protocol.⁵³ In short, in a round bottom flask, 4.93 g of 2-hydroxyethyl disulfide (32 mmol), 3.98 g of sodium hydroxide (100 mmol) and 72 mg of tetrabutylammonium bromide (TBAB) (223 mmol) were mixed and heated to $40 \text{ }^\circ\text{C}$. 8.3 mL of epichlorohydrin (105.9 mmol) was added dropwise and the reaction was stirred for 3 h. The final product was purified by column chromatography (alumina column, cyclohexane/ethyl acetate 1:4) to obtain a yellow liquid (973 mg, 11%). ^1H NMR (400 MHz, CDCl_3): δ (ppm) 3.77 (m, 6H, $\text{CHCH}_2\text{OCH}_2\text{CH}_2\text{S}$), 3.35 (m, 2H, $\text{CHCH}_2\text{OCH}_2\text{CH}_2\text{S}$), 3.08 (m, 2H, $\text{CHCH}_2\text{OCH}_2\text{CH}_2\text{S}$), 2.86 (t, 4H, $\text{CHCH}_2\text{OCH}_2\text{CH}_2\text{S}$), 2.74 (m, 2H, $\text{CH}_2\text{OCHCH}_2\text{OCH}_2\text{CH}_2\text{S}$), 2.54 (m, 2H, $\text{CH}_2\text{OCHCH}_2\text{OCH}_2\text{CH}_2\text{S}$). ^{13}C NMR (400 MHz, CDCl_3): δ (ppm) 71.8, 69.7, 50.8, 44.1, 38.6



Scheme 4 Synthesis of cross-linker (2), hydroxyethyl disulfide-bis-diglycidyl ether

Synthesis of poly(2-ethyl-2-oxazoline) (PEtOx). A typical procedure is as follows. In a flame dried Schlenk flask, 13 mL of acetonitrile was introduced under vacuum. 56 μ L of MeOTf (0.5 mmol) was added. The flask was then placed in an ice bath at 0 °C and 5.7 mL of 2-ethyl-2-oxazoline (56.6 mmol) was added. The flask was then heated to 85 °C where it remained for 3 days. The reaction was quenched via the addition of 2.7 equivalents of a 0.3 N KOH solution in methanol. The solution was left to stir at room temperature overnight and the polymer was precipitated twice into diethyl ether and dried under vacuum. Yield = 4.95 g (89%). ¹H NMR (400 MHz, D₂O): δ (ppm) 3.6-3.3 (d, NCH₂CH₂), 2.8 (d, CH₃-NCH₂CH₂), 2.4-2.1 (m, NCOCH₂CH₃), 1.0-0.8 (q, NCOCH₂CH₃). dn/dc = 0.0789 (in DMF + 0.1% LiCl). M_n (SEC) = 9259 g/mol, \bar{D} = 1.28. DP = 94.

Partial hydrolysis of PEtOx in acidic media. 1.14 g of P(EtOx)₉₄ (1.22×10^{-4} mol) was dissolved in 10 mL of DI water and heated under reflux (at 100 °C). Subsequently, 10 mL of 37% HCl solution was added to the polymer solution yielding a final polymer concentration of 50 g/L. After 2 h, the solution was left to equilibrate to room temperature. A solution of 2.5 M NaOH was added to achieve a solution pH of 8. The polymer was purified by dialysis against DI water for 3 days and collected by lyophilization. Yield = 0.59 g (52%). ¹H NMR (400 MHz, D₂O): δ (ppm) 3.6-3.3 (d, NCOCH₂CH₂), 2.8 (d, CH₃-NCH₂CH₂), 2.9-2.7 (s, NHCH₂CH₂), 2.4-2.1 (m, NCOCH₂CH₃), 1.0-0.8 (q, NCOCH₂CH₃). \bar{D} = 1.20. IR: 3484 (m), 2977 (s), 2939 (s), 2880 (m), 1621 (s), 1470 (m), 1420 (s), 1374 (s), 1320 (w), 1236 (m), 1194 (s), 1078 (w), 1061 (m), 969 (w), 915 (w), 877 (w), 813 (m), 761 (w). %Hydrolysis: ¹H NMR spectroscopy = 6.7%, titration = 5.3%.

Hydrogel formation. To prepare the hydrogel, 10 mg of partially hydrolyzed poly(2-ethyl-2-oxazoline), denoted as P(EtOx₈₈-EI₆) where EI stands for ethylene imine, was dissolved in 100 μ L of DI water and 4 mg of 1,6-hexanediol diglycidyl ether (cross-linker 1) was added. The solution was stirred and heated at 80 °C overnight. The mixture was then left to equilibrate to room temperature and a hydrogel was obtained. The gel was purified by dialysis against DI water for 2 days and collected by lyophilization. IR (hydrogel 1, Scheme 2): 3431 (m), 2976 (m), 2938 (s), 2875 (m), 1621 (s), 1470(w), 1420 (s), 1374 (m), 1321 (w), 1238 (w), 1194 (s), 1109 (w), 1079 (w), 1061 (m), 914 (w), 814 (m), 761 (w). IR (hydrogel 2, Scheme 2): 3447 (m), 2976 (m), 2938 (s), 2875 (m), 1625 (s), 1470 (w), 1420 (s), 1375 (m), 1321 (w), 1237 (w), 1194 (s), 1105 (w), 1079 (w), 1061 (m), 912 (w), 814 (m), 759 (w).

Hydrogels made from the additional cross-linkers were prepared following the same procedure, keeping the molar ratio of reactive functionalities constant. Only the temperature and solvent were varied according to Table 2.

Chemical cleavage of hydrogels. Gels made with hydroxyethyl disulfide-*bis*-diglycidyl ether (cross-linker 2) may be cleaved in a reducing environment. To do so, the hydrogel was purged with nitrogen for 30 min and a solution of 30 mg (1.95×10^{-4} mol) of dithiothreitol (DTT) in 1 mL of degassed DI water was then added. The gel was stirred under nitrogen until complete dissolution of the gel was observed (within 5 minutes).

Nanogel synthesis in dilute media. 10 mg of the partially hydrolyzed polymer P(EtOx₈₈-EI₆) was dissolved in 1000 μ L of DI water. In another flask, a solution of 1,6-hexanediol diglycidyl ether (cross-linker 1) at 80 mg/mL was prepared in ethanol. Both solutions were filtered through a 0.2 μ m polypropylene filter and subsequently 28 μ L of the cross-linker solution in ethanol was added to the polymer solution. The mixture was stirred at 800 rpm at 80 °C for 3 hours. The cross-linking reaction and nanogels formation was followed by DLS at an angle of 90° on a Malvern ZetaSizer NanoZS instrument. Once the nanogels were formed, they were purified by dialysis for 2 days against DI water.

Nanogel synthesis in w/o emulsion. Nanogels were prepared in an inverse emulsion (W/O) process using ultrasonication. An aqueous solution containing 100 μ L DI water, 10 mg of the partially hydrolyzed polymer P(EtOx₈₈-EI₆), and 4 mg of cross-linker was prepared. In another flask, 0.25 g of Span 80 in 5 g of cyclohexane were mixed together to form the organic phase. 0.8 g of the organic phase was transferred into an Eppendorf tube and the aqueous phase was added. The mixture was ultrasonicated with an ultrasonic probe Q sonica, LLC from Misonix sonicators (XL-2000 series), for 2 min, at 6 W output. The emulsion was then transferred to a glass tube and placed in an oil bath to stir, at 80 °C, overnight. The product was then centrifuged and the supernatant (cyclohexane and surfactant) removed. The residue was then mixed with new cyclohexane, and the solution vortexed. This process was repeated 3 times. Subsequently, THF was added and the same process was repeated twice. Finally water was added and the resulting nanogel solution purified by dialysis for 3 days prior to any DLS measurements. The size of the nanogels was measured in DI water (0.5 mL). To study the influence of pH on the size of the nanogels, 24 μ L of a 0.5 N HCl solution was added to 0.5 mL of the initial nanogels. When nanogels were prepared with the cleavable cross-linker (2), the nanogel sizes were measured after addition of DTT (16 μ L of a DTT solution at 10 mg/mL was added to 0.5 mL of nanogel solution).

SUPPORTING INFORMATION

The ^1H NMR spectrum of PEOx₉₄ shows protons of the α -end of the polymer chain (CH_3 -) appearing as a double peak (peak a in Figure 1). The splitting of this peak was attributed to its attachment to the amide backbone, which has two resonance states.⁵⁵ The rotation around the C-N bond of the amide is not completely free which leads to delocalization of the nitrogen to give a partial “double-bond character” to the C-N bond.

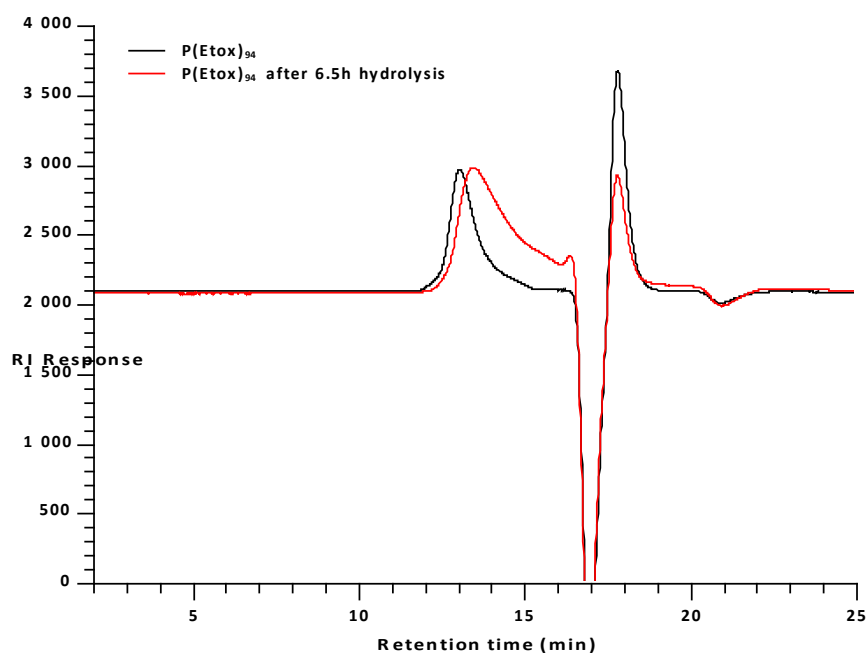


Figure S1 SEC traces of poly(2-ethyl-2-oxazoline)₉₄ and poly((2-ethyl-2-oxazoline)-*stat*-(ethylene imine)) copolymer obtained after 6.5 h of hydrolysis in DMF

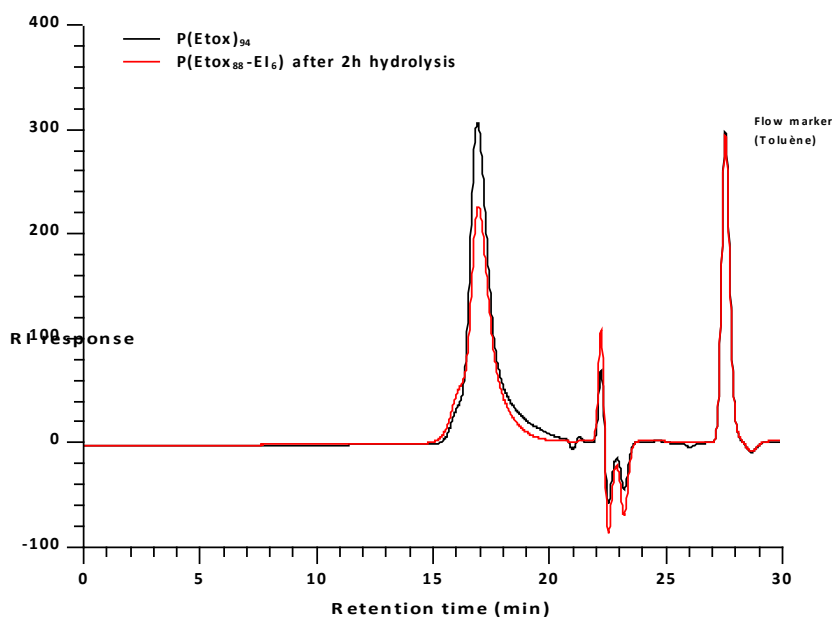


Figure S2 SEC traces of poly(2-ethyl-2-oxazoline)₉₄ and poly((2-ethyl-2-oxazoline)₈₈-stat-(ethylene imine)₆) statistic copolymer after 2 h of hydrolysis in DMF

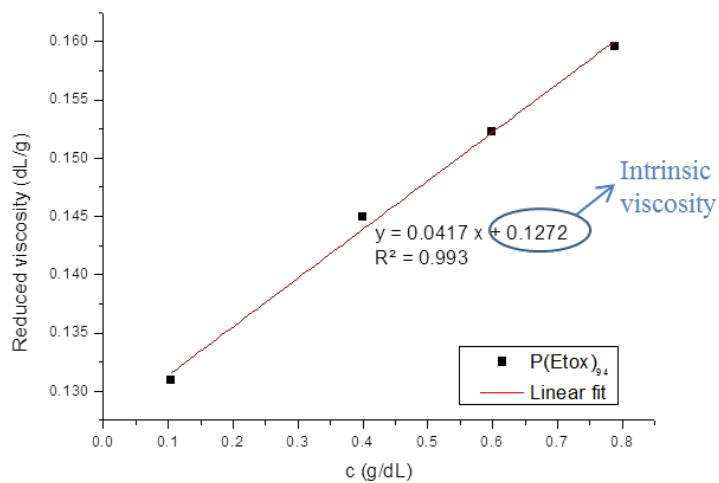


Figure S3 Determination of the intrinsic viscosity of poly(2-ethyl-2-oxazoline)₉₄ by plotting the reduced viscosity as a function of the concentration.

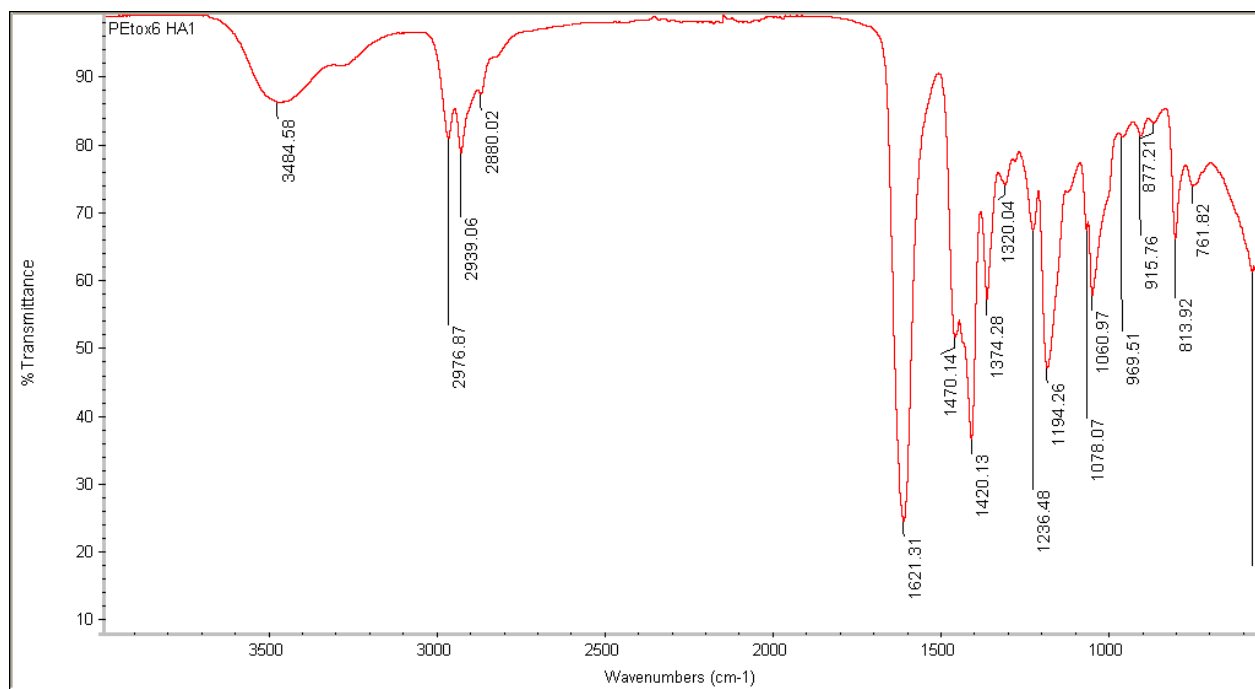


Figure S4 FT-IR spectrum of poly((2-ethyl-2-oxazoline)₈₈-stat-(ethylene imine)₆)

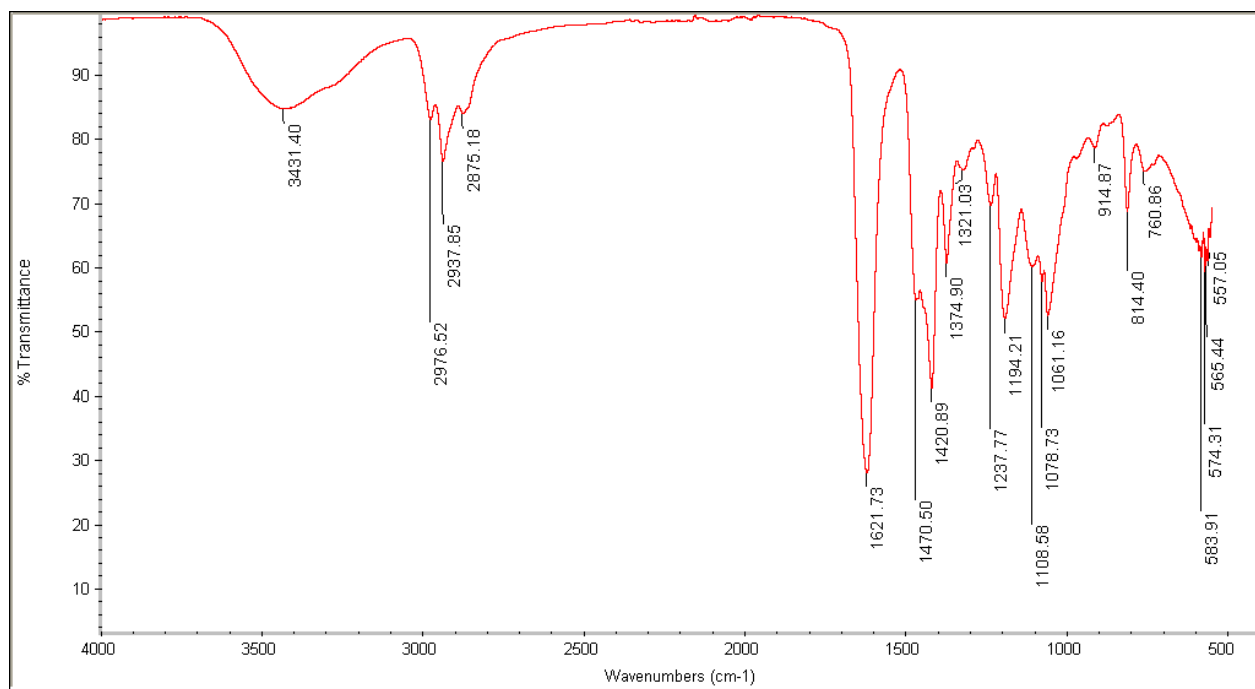


Figure S5 FT-IR spectrum of the dry hydrogel made with poly((2-ethyl-2-oxazoline)₈₈-stat-(ethylene imine)₆) and 1,6-hexanediol-diglycidyl ether

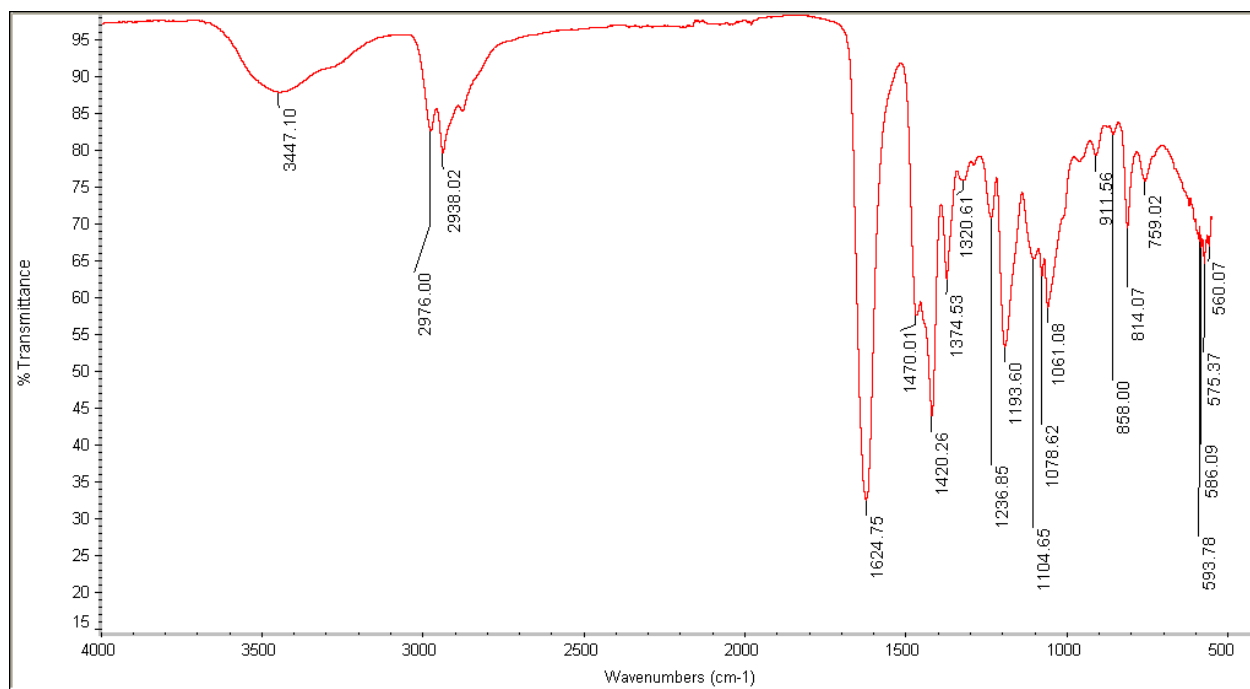


Figure S6 FT-IR spectrum of the dry hydrogel made up of poly((2-ethyl-2-oxazoline)₈₈-stat-(ethylene imine)₆) and hydroxyethyl disulfide-*bis*-diglycidyl ether (2)

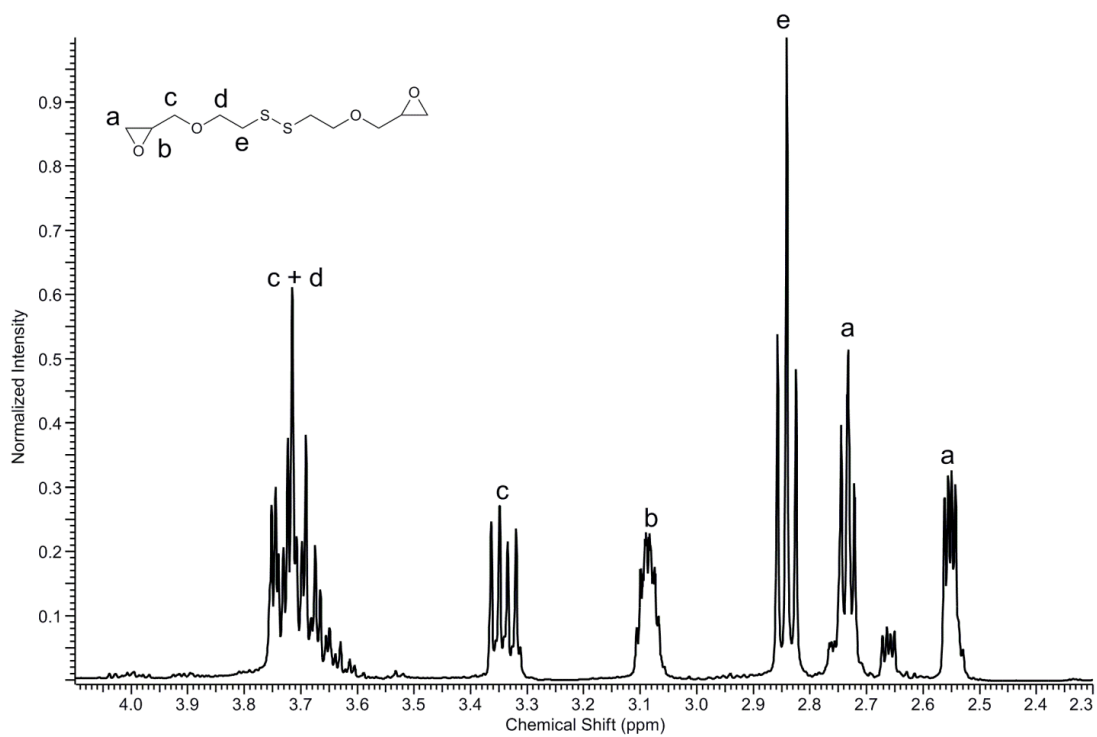


Figure S7 ¹H NMR spectrum (400 MHz, CDCl₃) of hydroxyethyl disulfide-*bis*-diglycidyl ether (cross-linker 2)

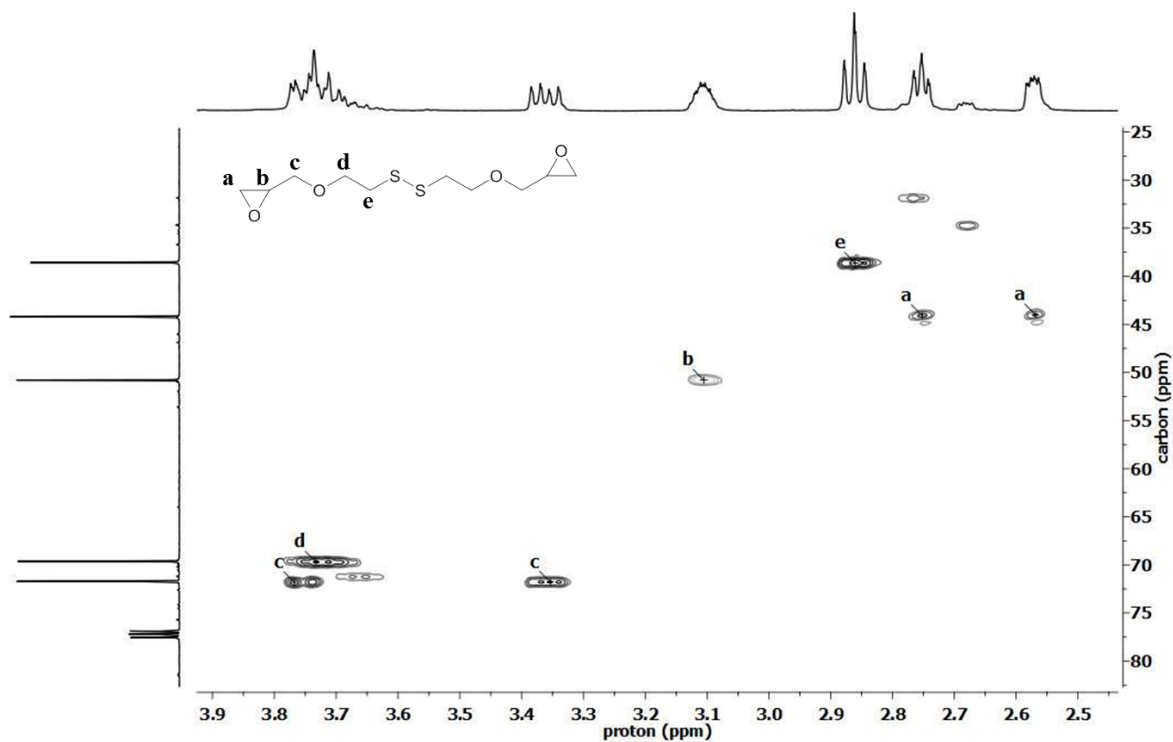


Figure S8 HSQC NMR spectrum (400 MHz, CDCl₃) of hydroxyethyl disulfide-bis-diglycidyl ether (cross-linker 2)

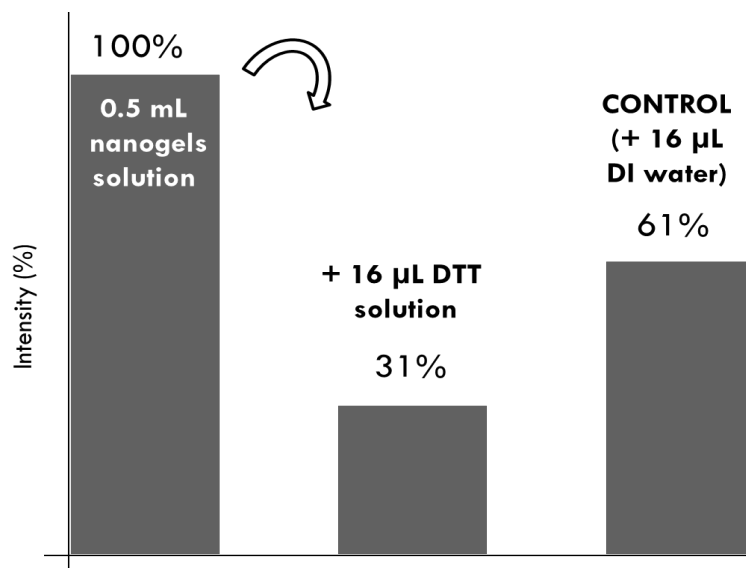


Figure S9 Decrease in relative count rate (%) measured by DLS at 90°, after addition of DTT or DI water.

Appendix S1 – Determination of the critical concentration for gelation

Once the intrinsic viscosity is known, the radius of gyration (R_g) of the polymer can be calculated using the Fox-Flory equation (1)⁵⁶:

$$R_g^3 = \frac{M [\eta]}{\varphi'} \quad (1)$$

where M is the polymer molecular weight, $[\eta]$ its intrinsic viscosity and $\varphi' = 3.1 \cdot 10^{24}$ (with $[\eta]$ in cm^3/g).

The critical concentration corresponds to the concentration where the polymer chains start to entangle. Assuming polymer as hard spheres, the critical concentration can be written as follow:

$$c^* = \frac{\phi^* M_n}{N_a V_{chain}} \text{ where } \phi^* = \frac{V_{chain}}{V_{total}} = 0.74$$

$$V_{chain} = \frac{4}{3} \pi R_g^3$$

Diluted regime $c < c^*$ $c = c^*$ and

Table S1 Determination of the critical concentration c^* of poly(2-ethyl-2-oxazoline)₉₄

Polymer	M_n (g/mol)	PDI	M_w (g/mol)	$[\eta]$ (dL/g)	R_g (nm)	V (m^3)	c^* (g/L)
P(Etox) ₉₄	9259	1.28	11851	0.1272	3.65	$2.04 \cdot 10^{-25}$	55.9

Appendix S2 – DLS measurements/equations

In DLS, a sample of particles in solution is placed in a laser beam. When the laser beam hits small particles, the light is scattered in all directions. DLS measurements rely on the fact that particles in solution undergo Brownian motions which lead to time-dependent fluctuations in the scattering intensity. The fluctuation rate is directly correlated to the size of the particles: the smaller the particle, the quicker they will move.

The dynamic information on the particles is derived from an autocorrelation of the intensity trace recorded during the experiment (i.e. the cross-correlation of the intensity signal with itself, where the x

axis corresponds to the delay time, τ). From the inverse Laplace transformation of the intensity correlation function, a distribution plot of the relaxation times can be obtained.

Then from equation (1), where n_0 corresponds to the refractive index of the solvent, λ the wavelength of the laser and θ the angle at which the measurement is done, one can plot the decay rate (Γ) as a function of q^2 , small spherical particles show no angular dependence, hence no anisotropy, resulting in a horizontal line. The translational diffusion coefficient D_T corresponds to the slope of this line.

$$q = \frac{4\pi n_0 \sin\left(\frac{\theta}{2}\right)}{\lambda} \quad (1)$$

$$D_T = \frac{\Gamma}{q^2} \text{ where } \Gamma = \frac{1}{\tau}$$

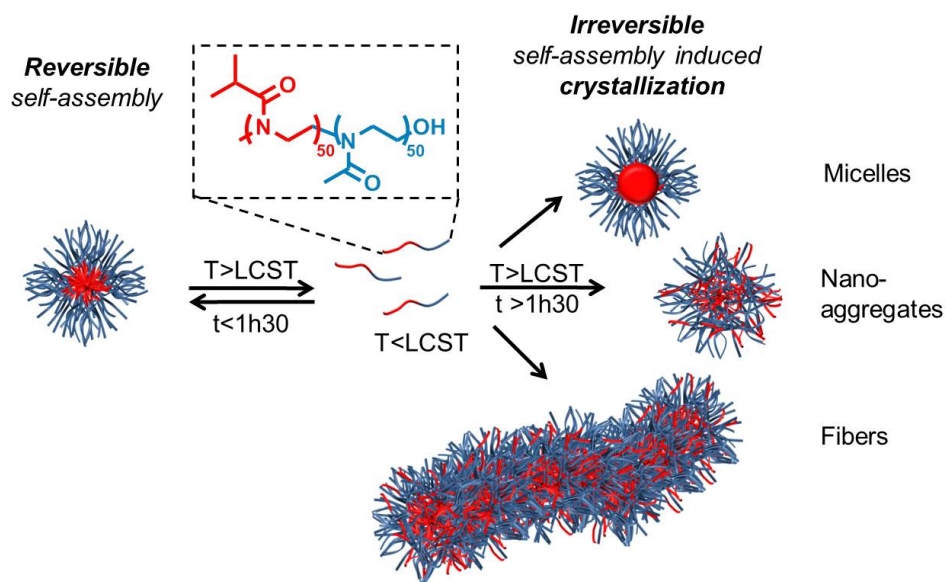
The hydrodynamic radius can be calculated thanks to the Stokes-Einstein equation (2):

$$R_H = \frac{k_B T}{6\pi\eta D_T} \quad (2)$$

Where T is the temperature, k_B the Boltzmann constant ($1.38 \cdot 10^{-23}$ J/K), η is the viscosity of the solvent.

CHAPTER 3

CRYSTALLIZATION-DRIVEN SELF-ASSEMBLY OF POLY(2-ISOPROPYL-2-OXAZOLINE)- BLOCK-POLY(2-METHYL-2-OXAZOLINE) ABOVE THE LCST



Keywords: poly(2-oxazoline), block copolymer, crystallization, self-assembly, LCST

Overview: A poly(2-isopropyl-2-oxazoline)-block-poly(2-methyl-2-oxazoline) copolymer, denoted as P(iPrOx-b-MeOx), was synthesized by sequential cationic ring opening polymerization of the corresponding 2-alkyl oxazoline monomers. This copolymer exhibited a lower critical solution temperature (LCST) around 56 °C, due to the presence of the PiPrOx block. The ability of this polymer to crystallize in water above its LCST was further exploited to induce the self-assembly of the P(iPrOx-b-MeOx) block copolymer in aqueous solution. The influence of the hydrophilic stabilizing PMeOx block on the crystallization process and on the crystalline structures was then investigated in detail. Thus, spherical micelles of 32 nm diameter were observed by transmission electron microscopy (TEM) from an aqueous solution of the block copolymer solution above the LCST of PiPrOx. These micelles could be disassembled in a reversible manner when kept for a short period of time (i.e. $t < 1\text{h}30$) above the LCST and cooled down to room temperature. Annealing the copolymer solution for more than 1h30 at 65 °C induced the crystallization of PiPrOx, as evidenced by wide angle X-ray scattering (WAXS) experiments. This crystallization-driven self-assembly phenomenon resulted in a number of different morphologies, including core-crystallized spherical micelles, non-spherical micelle-like nanostructures (nano-aggregates) and micron-size fibers, depending on annealing time, as observed both by dynamic light scattering (DLS) experiments and TEM imaging. The three morphologies were found to coexist, their relative proportion varying with the annealing time. Formation of micron-size range fiber-like structures might be explained by a re-organization of both core-crystallized micelles and nano-aggregates. The crystal structure, as determined by WAXS, indeed appeared to be identical to that of the PiPrOx homopolymer. Lastly, the influence of both the polymer concentration and the heating rate on the morphological behavior was also studied: while concentration was varied, the same crystalline structures were obtained but they were not predominant at the same annealing time, whereas when the heating rate was slower, the crystalline objects seemed to evolve towards better defined micron-size structures.

CHAPTER 3

CRYSTALLIZATION-DRIVEN SELF-ASSEMBLY OF POLY(2-ISOPROPYL-2-OXAZOLINE)-*BLOCK*-POLY(2- METHYL-2-OXAZOLINE) ABOVE THE LCST

INTRODUCTION	101
I. SYNTHESIS OF P(IPROX ₅₀ - <i>B</i> -MEOX ₅₀) COPOLYMERS BY CATIONIC RING OPENING POLYMERIZATION ..	103
II. REVERSIBLE SELF-ASSEMBLY OF P(IPROX ₅₀ - <i>B</i> -MEOX ₅₀) ABOVE THE LCST	104
III. MORPHOLOGY EVOLUTION BY CRYSTALLIZATION OF P(IPROX ₅₀ - <i>B</i> -MEOX ₅₀)	105
IV. INFLUENCE OF EXTERNAL PARAMETERS ON THE CRYSTALLIZATION PROCESS.....	112
IV.1. POLYMER CONCENTRATION	112
IV.2. HEATING RATE.....	114
CONCLUSIONS	115
EXPERIMENTAL SECTION	117
SUPPORTING INFORMATION	119

INTRODUCTION

Block copolymers (BCPs) are formed by two or more homogeneous polymer fragments joined together by a covalent bond.¹ Recent advances in precision macromolecular synthesis have allowed designing BCPs with engineered properties that can meet specific needs.² As a result of the incompatibility between the two blocks, BCPs can self-assemble in solution^{3,4} into well defined nanostructures, including micelles of different shapes (spheres, cylinders or toroids)^{5,6} or polymeric vesicles (also referred to as polymersomes).⁷⁻⁹ In many cases, the self-assembly is driven by hydrophobic interactions. Some examples can also be found in the literature where the self-assembly is driven by electrostatic interactions between a pair of oppositely-charged BCPs,¹⁰ or BCPs with complementary chirality.¹¹ However, when multiple forces are involved, more complex nanostructures can be achieved.

Interestingly, Manners and coworkers have reported that crystallization of one block can induce the self-assembly of specific BCPs based on polyferrocenylsilane (PFS) that was used as the hydrophobic and crystallizable block. When PFS was arranged with a synthetic polypeptide block, namely, poly(γ -benzyl-L-glutamate), self-assembly occurred in dimethylformamide (DMF). However, annealing the same solution induced crystal growth of PFS, which resulted into well-defined truncated elliptical micelles from the less ordered original structures.¹² When PFS was associated to poly(2-vinylpyridine), the morphology of the self-assembled structures (spheres, cylinders, platelets) could be tuned, depending on the solvent selectivity, which was correlated to the different levels of crystallinity (amorphous, single core-crystal and polycrystalline, respectively).¹³ Cylindrical micelles of controlled length¹⁴ and fiber-like micelles¹⁵ were also obtained with other copolymer systems. O'Reilly and coworkers also described some crystallization-driven self-assembly systems made from diblock poly(L-lactide)-*block*-poly(acrylic acid) (PLA-*b*-PAA), where the morphology was tuned from spherical to controlled-length rod-like micelles upon annealing. Interestingly, no core-crystallization occurred when amorphous atactic poly(lactide) was used.¹⁶⁻¹⁹

In the present chapter, we report on the self-assembly and further crystallization of a particular polyoxazoline-based block copolymer, towards the formation of physically cross-linked structures at the nano- or the microsize range.

As highlighted in the literature overview (chapter 1), the cationic ring-opening polymerization (CROP) of 2-alkyl-2-oxazolines has been adapted for the synthesis of well-defined copolymers, which allows the tuning of their physico-chemical properties.²⁰⁻²² For example, the hydrophobicity of the polymer is controlled by the length of the alkyl substituent, 2-methyl-, 2-ethyl-, and 2-isopropyl-2-oxazolines

resulting in water-soluble polymers at room temperature.²³ Thermal properties of poly(2-oxazoline)s (POx) are also tunable over a broad range of temperature and are dependent on both their molar masses and their polymer architecture.²⁴ The versatility of POx, associated with their interesting biological properties (structural similarities with polypeptides,²⁵ biocompatible character and stealth behavior of some POx^{26–28}) has led to their recent revival.

Among the different 2-alkyl oxazoline monomers, the commercially available 2-isopropyl-2-oxazoline (iPrOx) is of particular interest. Its corresponding polymer, PiPrOx, is indeed a structural isomer of poly(N-isopropylacrylamide) (PNIPAAm). Like PNIPAAm, PiPrOx thus possesses a lower critical solution temperature (LCST) around 36 °C,^{29–31} which makes it a good candidate for the design of thermo-responsive polyoxazoline-based compounds.³² In addition, and in contrast to PNIPAAm, PiPrOx is capable of crystallizing above its LCST.³³

Advantage of such a behavior has been taken by Schlaad *et al.* who observed hierarchical structures, such as micron-size assemblies of fibrils from the homopolymer.^{34,35} The morphology was eventually found to evolve with time for a 1 wt% PiPrOx aqueous solution that was heated to 65 °C; network-like structures developed into micron-size assemblies.³⁶ A statistical copolymer made of iPrOx and 2-(3-butenyl)-2-oxazoline units was also synthesized and found to self-assemble and crystallize above its LCST into spherical micron-size structures, which was further used for carbohydrate protein recognition.³⁷ Self-assembly and crystallization of a PiPrOx-*graft*-pullulan copolymer were also reported.³⁸ Micron-sized ring-like structures with short fibrils emanating from the ring circumference, or a “sea urchin”-like morphology were obtained but other morphologies were observed, depending on the experimental conditions (addition of salts, with/without stirring). It is worth pointing out that PiPrOx is not the only POx that can undergo crystallization. Chiral POx,³⁹ PEtOx⁴⁰ and a series of homopolymers with linear side chains of different alkyl length⁴¹ were also demonstrated to crystallize upon annealing.

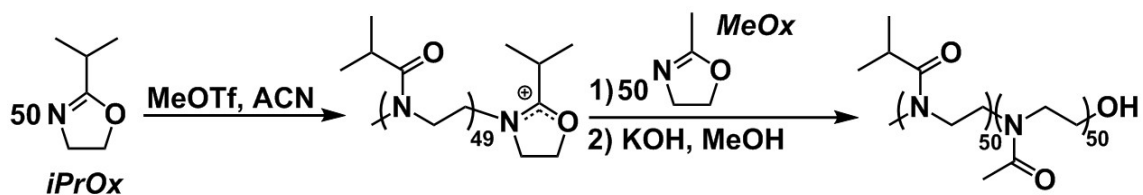
In this chapter, we investigate the aqueous solution behavior of poly[(2-isopropyl-2-oxazoline)-*block*-poly(2-methyl-2-oxazoline)] BCP, denoted as P(iPrOx-*b*-MeOx), above the LCST of PiPrOx. The synthesis, self-assembly and crystallization of P(iPrOx-*b*-MeOx) are investigated in details. To the best of our knowledge, this is the first study describing the self-assembly properties of POx-based BCPs induced by a crystallization phenomenon. The self-assembly into spherical micelles, above the LCST of PiPrOx, is evidenced by dynamic light scattering (DLS), whereas the change in morphology due to crystallization is monitored by DLS and transmission electron microscopy (TEM). The crystallization is analyzed by differential scanning calorimetry (DSC) and wide-angle x-ray scattering (WAXS). Lastly, the influence of

external parameters such as polymer concentration and heating rate on the morphologies formed is also discussed.

I. SYNTHESIS OF P(iPrOx₅₀-*b*-MeOx₅₀) COPOLYMERS BY CATIONIC RING OPENING POLYMERIZATION

The P(iPrOx-*b*-MeOx) BCPs were obtained by sequential CROP of corresponding 2-oxazoline monomers, as depicted in Scheme 1.^{42,43} In order to achieve a well-defined BCP, iPrOx has to be polymerized first as its corresponding macro-cation is more prone to initiate the polymerization of MeOx for the growth of the second block, than if one starts by the polymerization of MeOx first.^{44,45} Indeed, SEC traces showed some homopolymer PMeOx left over for the copolymer obtained by starting by the CROP of MeOx first (SI†, Figure S3). In contrast, a complete shift to the higher molecular weight region was noted when iPrOx was polymerized first, suggesting that all macro-PiPrOx chains could initiate the CROP of MeOx. Due to prolonged reaction times required for the synthesis of these BCPs (several days), some side reactions (chain transfer) also likely occurred to some extent, as a small tailing effect can be observed in the SEC traces (SI†, Figure S3). One possible way to obtain better defined copolymers would be to perform the sequential CROP in a microwave reactor, so as to dramatically shorten the reaction times.⁴⁶

The P(iPrOx-*b*-MeOx) block copolymer used in the rest of the study was obtained with a dispersity of 1.19 and a degree of polymerization of 50 for each block (SI†, Figures S2 and S3).



Scheme 1 Synthesis of P(iPrOx₅₀-*b*-MeOx₅₀) BCP by sequential cationic ring-opening polymerization

II. REVERSIBLE SELF-ASSEMBLY OF P(IPrOX₅₀-*b*-MeOX₅₀) ABOVE THE LCST

The cloud point, *i.e.* the temperature where turbidity first appeared,⁴⁷ of a 10 mg/mL solution of P(iPrOx-*b*-MeOx) was evaluated by DLS measurements, and was determined to be approximately 57 °C (SI†, Figure S4). Due to the presence of the hydrophilic PMeOx block, the LCST was thus found to be higher than that reported for the P*i*PrOx homopolymer (around the body temperature).^{29,48–50} Below the LCST, the copolymer proved to be fully soluble in water. By increasing the temperature above the LCST, *i.e.* at 65 °C, the formation of well-defined micelles was noted, as shown in Figure 1. Sizes ($d = 32$ nm), as determined by DLS and TEM image statistical analysis, were in good agreement.

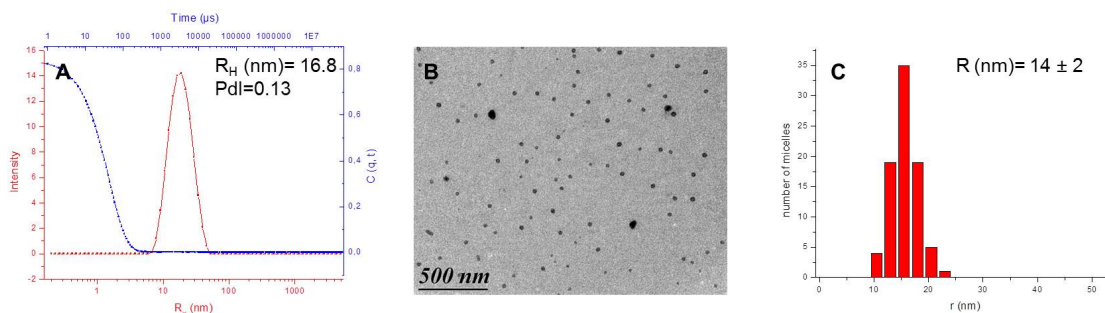


Figure 1 P(iPrOX₅₀-*b*-MeOX₅₀) micelle characterization at 65 °C **A)** DLS analysis with correlogram and size distribution obtained at 90°, **B)** TEM micrograph **C)** distribution of micelle size by TEM, determined by Image J.

Micelle formation above the LCST of the BCP was found to be a reversible process, but only if the corresponding aqueous solution was kept above the LCST for a short period of time (< 1h30). Thus, unimers were observed when the solution was cooled down to 25 °C, after heating at 65 °C, as summarized in Figure 2.

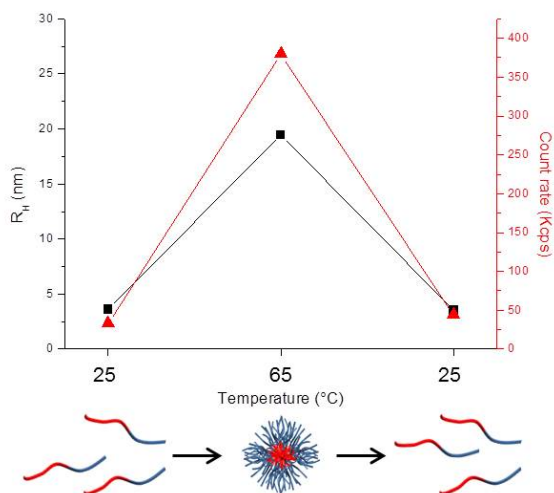


Figure 2 P(iPrOx₅₀-*b*-MeOx₅₀) micelles size evolution with temperature measured by DLS

III. MORPHOLOGY EVOLUTION BY CRYSTALLIZATION OF P(IPROX₅₀-*b*-MEOX₅₀)

As mentioned above, PiPrOx has been reported to crystallize when kept for 2 hours or more above its LCST.³⁴ In the present work, we studied the influence of the presence of the hydrophilic stabilizing PMeOx block on the crystallization process and on the as-formed crystalline structures.

To monitor the morphology evolution with time, *in situ* DLS measurements were performed on a 10 mg/mL copolymer sample of P(iPrOx₅₀-*b*-MeOx₅₀) in water, at 65 °C. We noted that the initially well-defined and nearly monodisperse micelles progressively became unstable (Figure 3). Increase in polydispersity, count rate and size was indeed observed with time, indicating that micelles evolved into larger and increasingly less defined structures. Nevertheless, after about 4 hours, the system seemed to reach a steady state.

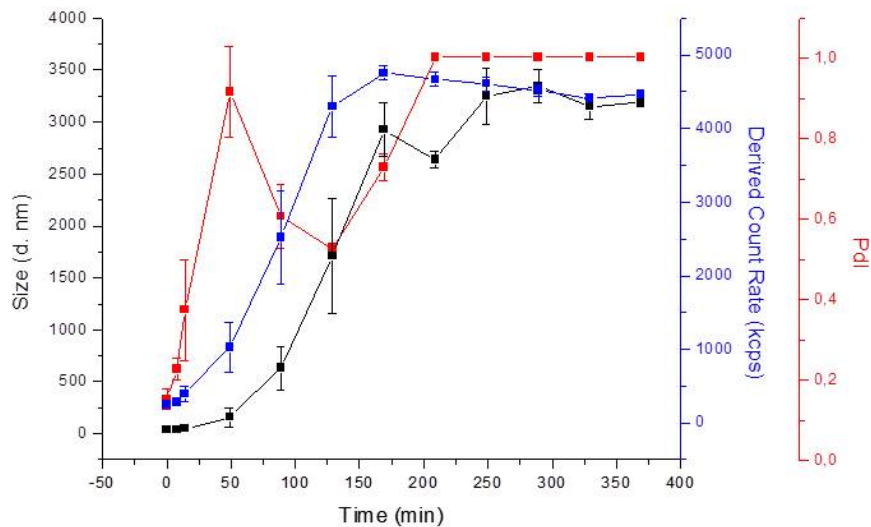


Figure 3 *in situ* DLS measurements of P(iPrOx₅₀-b-MeOx₅₀) in water at 10 mg/mL and 65 °C

The change in morphology also resulted in a change of the solution turbidity. Crystal formation could also be macroscopically detected. This morphology evolution was found to be irreversible. In order to get a better understanding on the assembly behavior, aliquots were taken at different annealing times (1h30, 3h, 4h30, 7h and 24h) and were allowed to cool back to room temperature. No significant change in the scattered intensity was observed by DLS, compared to the sample measured *in situ* at 65 °C (SI†, Table S1), suggesting that the previously formed nano/micro-objects remained stable. Structures obtained at the different annealing times were further characterized by TEM (Figure 4). Withdrawn samples were deposited onto the TEM grid after cooling to room temperature, the nanostructures being supposedly 'locked', as suggested by DLS.

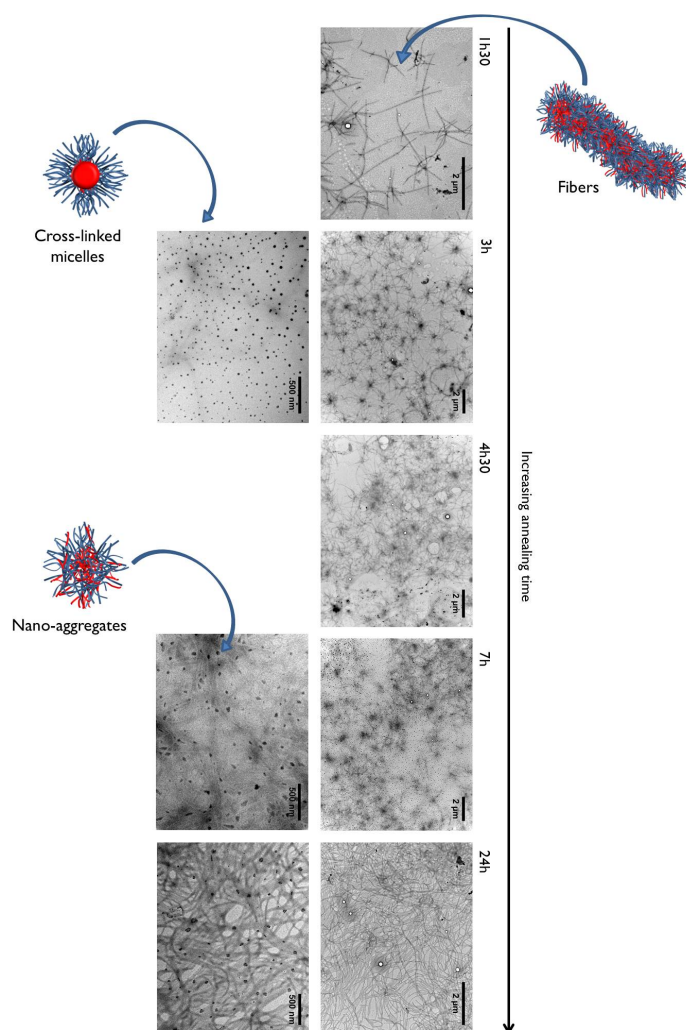


Figure 4 TEM micrographs of 10 mg/mL of P(iPrOx₅₀-*b*-MeOx₅₀) solution in water heated at 65 °C for 1h30, 3h, 4h30, 7h and 24h

At first glance, one can note that the P(iPrOx-*b*-MeOx) BCP did crystallize and that the morphologies obtained evolved with the annealing time. After 1h30, indeed, some anisotropic fiber-like structures were observed, with a polydispersity (Pdl) of 0.28 as determined by DLS. After 3h, the proportion of fiber-like structures increased and appeared to arrange into denser “fiber-nods”. Nevertheless, some micellar nanostructures still remained present, suggesting that these micelles experienced a core-cross-linking phenomenon due to the crystallization process. At longer annealing times, the proportion of

fibers further increased until network-like structures were achieved. Yet, small non-spherical micelle-like nanostructures (nano-aggregates), around 30 nm in diameter, could still be detected. We assumed that the aforementioned structures could coexist at each annealing time, but differed only in their proportion. Due to the length scale difference, however, all of these structures could not be imaged. Our hypothesis is supported by the fact that small-sized nano-structures (core-cross-linked micelles or nano-aggregates) were still detected even after 24 h, as part of the fiber-like structures. It is thus highly likely that these primary crystalline nanostructures took part of the fiber formation.

It is worth mentioning that crystallization only occurred above the LCST of P(iPrOx₅₀-*b*-MeOx₅₀) in aqueous solution. As the copolymer concentration was kept constant, progressive increase in the amount of crystalline materials, as determined by TEM, suggested that the extent of reversible micelles decreased proportionally. Thus, the self-assembled micelles might act as crystallization seeds and the spatial restriction caused by the crystallization of the PiPrOx block could result in the formation of the

observed nano-aggregates and fibers. A similar mechanism was described by O'Reilly *et al.* regarding the crystallization-driven self-assembly of PLA-*b*-PPA, where spherical micelles underwent crystallization that nucleated the growth of cylindrical structures.¹⁸

The arrangement of the fibers seemed to evolve following specific steps. Firstly, individual growth was observed after which some fibers-nods were found. With increasing proportion of the fibers, inter-connection between fibers occurred leading, ultimately, to a more uniform fiber-network.

TEM observations were in agreement with results delivered by DLS (Figure 3). Initially (in the first hour), an increase in polydispersity was noted, as individual anisotropic fibers were formed, which coexisted with a large number of reversible micelles (not observable by TEM prepared at room temperature). Subsequently, a drop in polydispersity was noted, corresponding to the formation of larger and more isotropic fiber-nods shielding the smaller nanostructures. In a final step, upon formation of the fiber network, an increase in polydispersity was again observed

Morphologies observed herein with the P(iPrOx₅₀-*b*-MeOx₅₀) BCP differed from those observed with the PiPrOx homopolymer, for which fibers initially formed and further assembled into micron-size spherical structures.³⁶ This difference can obviously be explained by the presence of the PMeOx block, forming a hydrophilic stabilizing shell. Both core-cross-linked micelles and nano-aggregates were directly issued from the self-assembly of the BCP above its LCST, and the formation of a network -rather than a micro-spherical aggregated structure as observed by Schlaad *et al.*^{34,36}- can be ascribed to the likely core-shell structure of the block copolymer fibers.

Crystal formation was also evidenced by DSC experiments. Thermograms of the P(iPrOx₅₀-*b*-MeOx₅₀) BCP obtained without any further post-treatment (dry polymer, at room temperature) and after 24 h of annealing at 65 °C are compared in Figure 5.

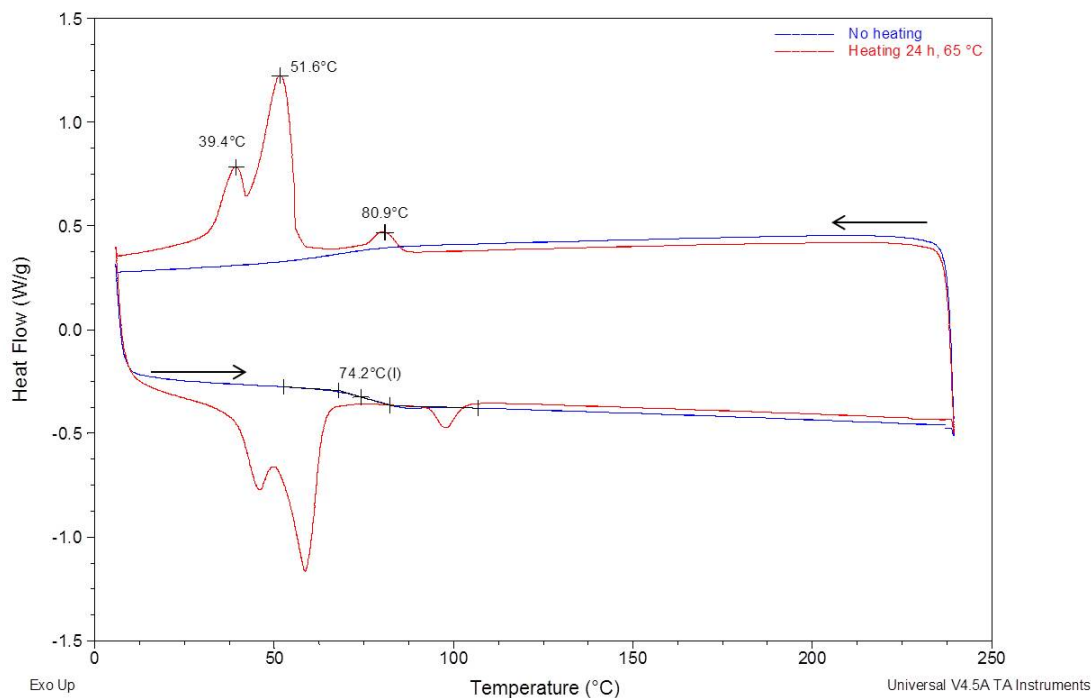


Figure 5 DSC thermograms of P(iPrOx₅₀-*b*-MeOx₅₀) without any further post-treatment and after 24 h heating in aqueous solution at 65 °C

The glass transition temperature (T_g) was clearly detected at 74 °C for the non-treated BCP, highlighting its amorphous character. After 24 h of annealing at 65 °C (10 mg/mL), however, no T_g could be detected (DSC trace is flat in this region). In addition, three endothermic and exothermic peaks appeared, respectively, upon heating and cooling the latter sample. These peaks could be attributed to the melting and crystallization of the PiPrOx block, respectively (peaks areas matching very well each other). Multiple melting peaks during the heating scan is a known phenomenon for semi-crystalline polymers, such as poly(ethylene),⁵¹ poly(ether ether ketone)^{52,53} or poly(ether terephthalate).⁵⁴ More recently, crystal main-chain of enantiopure and racemic poly(2-butyl-4-ethyl-2-oxazoline)s also showed a similar behavior.³⁹ Multiple melting transitions can be explained by the following major mechanisms: partial melting-recrystallization of original crystals and subsequent re-melting during heating scan, namely, melt-recrystallization, or melting of coexistent lamellar stack populations with different lamellar thicknesses and/or different degree of ordering or perfection, namely, dual lamellae population or finally melting and/or phase transformation between the different crystal structures.^{39,55}

It is interesting to note that, on the first heating curve of each copolymer (SI†, Figure S6), a melting peak was also detected around 200 °C, but that was not reversible in the time scale of the DSC experiment. This temperature corresponds to the melting temperature of the PiPrOx homopolymer.³⁵ As the polymer was kept for over 2 years before DSC analyses, this peak might correspond to slow

crystallization occurring under storage conditions. PMeOx and PiPrOx are both known to be hygroscopic polymers;^{35,56,57} thus, even small amounts of water uptake under storage conditions can induce crystallization, by increasing the polymer chain mobility, and favoring chain alignment.³⁵

In addition, the melting temperatures observed for the block copolymers on the DSC thermograms are lower than the melting temperature of the PiPrOx homopolymer, indicating that the crystals formed with the block copolymer are less perfect.

In order to monitor the crystal structure with time, the same aliquots were dried and analyzed by wide angle X-ray scattering (WAXS; Figure 6).

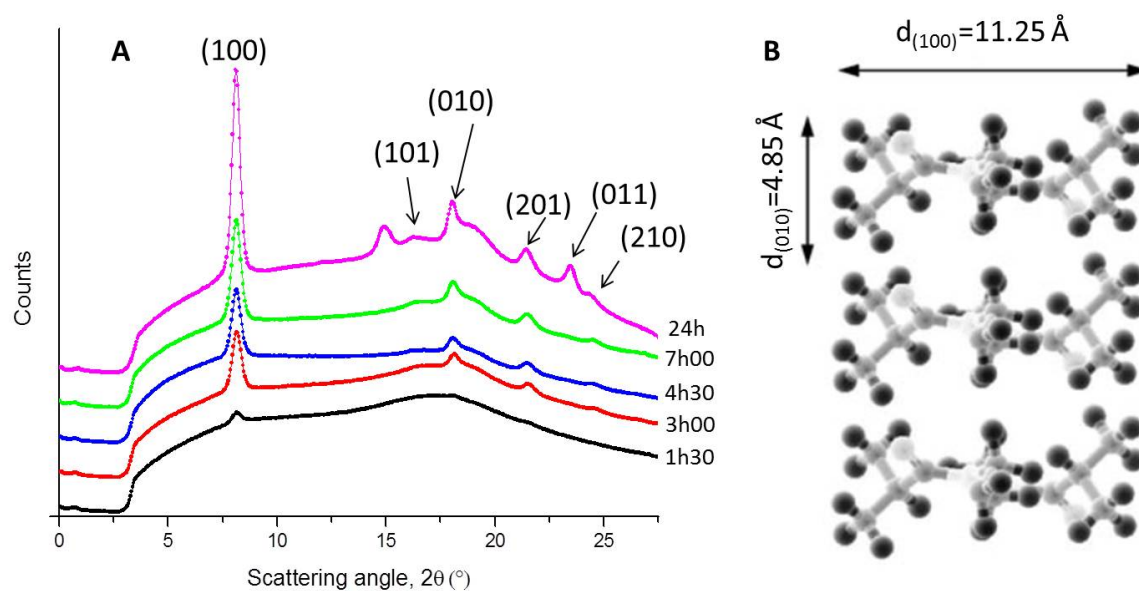


Figure 6 A) WAXS patterns of P(iPrOx₅₀-b-MeOx₅₀) after 1h40, 3h, 4h30, 7h and 24h of annealing at 65 °C. Peaks assignment according to ref. 35 B) Crystal structure adapted from ref. 35

As in the case of the crystallization of the PiPrOx homopolymer, an amorphous halo was observed, and both the intensity and the sharpness of the crystalline peaks increased with time,³⁶ confirming that the BCP exhibited semi-crystalline character. The majority of X-ray peaks could be assigned, matching those reported in literature (SI†, Figure S5 and Table S2).^{35,58} Thus, the two main peaks were observed at the same scattering angle as that of the homopolymer ($2\theta = 8^\circ$ and 18.25° corresponding to $d = 11.25$ and 4.85 \AA , respectively). The first crystalline structure was thus identical to PiPrOx, with the polymer backbone being aligned along the [001] direction while the isopropyl side groups were alternately aligned along the [100] direction to either side of the backbone, and the amide dipoles oriented along the [010] direction, also alternating in direction (Figure 6 B).³⁵

To gain a better insight into the types of crystallites, the nature of the interactions into the crystal structure was evaluated. Hydrophobic interactions⁵⁹ are expected to play a crucial role in the crystallization phenomenon of our POx-based BCP, the crystallization occurring above the LCST, when the copolymer becomes amphiphilic. However, and as reported earlier, dipolar interactions could also be involved in the crystallization process.^{20,33,35} Solubility tests were carried out to investigate that point. BCPs were first annealed for 24h at 65 °C, dried and dispersed in pure water or in a mixture of water and trifluoroacetic acid (TFA) (SI†, Figure S7). In the former case, a turbid suspension was obtained, confirming that nanostructures remained intact, while in the water/TFA mixture, a clear solution was observed, suggesting that crystalline structures were disrupted by TFA. TFA is often used as additive to minimize aggregation phenomena due to hydrogen bondings³⁴ in naturally occurring or synthetic polypeptides. However, hydrogen bonding interactions are not expected to develop neither in PMeOx nor in PiPrOx, although Schlaad *et al.* have suggested the existence of such interactions in PiPrOx in his first report.³⁴ In our case, it is highly likely that TFA could minimize strong dipolar Van der Waals interactions in water solution of our BCP, and prevent crystallization from developing. In absence of TFA, the crystallization mechanism might be similar to that proposed by Winnick *et al.*,³³ where hydrophobic interactions initially enable to arrange PiPrOx blocks close to each other, while the polymer chain shifts from trans and gauche conformation to an all trans conformation, leading to the alignment of dipolar amide groups³⁵ and the development of inter-chain dipolar interactions, which favors main chain crystallinity (Figure 7).⁵⁶

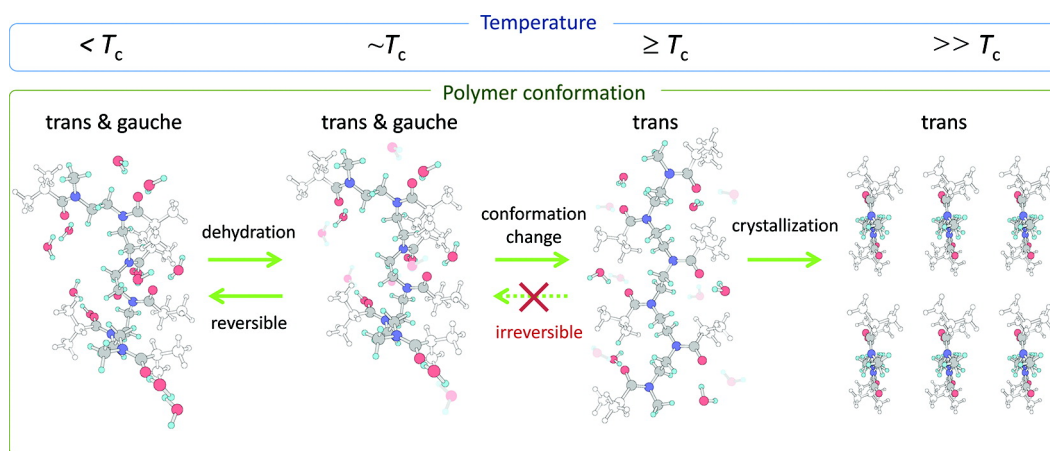


Figure 7 Schematic representation of the changes in the conformation of PiPrOx in water as a function of temperature. Reprinted from ref. 33

IV. INFLUENCE OF EXTERNAL PARAMETERS ON THE CRYSTALLIZATION PROCESS

It was previously demonstrated that the annealing time significantly not only influenced the crystal structures (core-crystallized micelles, nano-aggregates or fibers), but also their relative proportion. Other parameters, such as the heating rate and the polymer concentration, were varied in order to elucidate their respective influence on the crystalline structures.

IV.1. POLYMER CONCENTRATION

Firstly, the influence of BCP concentration on the crystallization process was investigated. To do so, a solution of 1 mg/mL was annealed at 65 °C and compared to the results previously obtained at 10 mg/mL. The crystallization and morphology evolution were monitored both by DLS (Figure 8) and TEM (Figure 9).

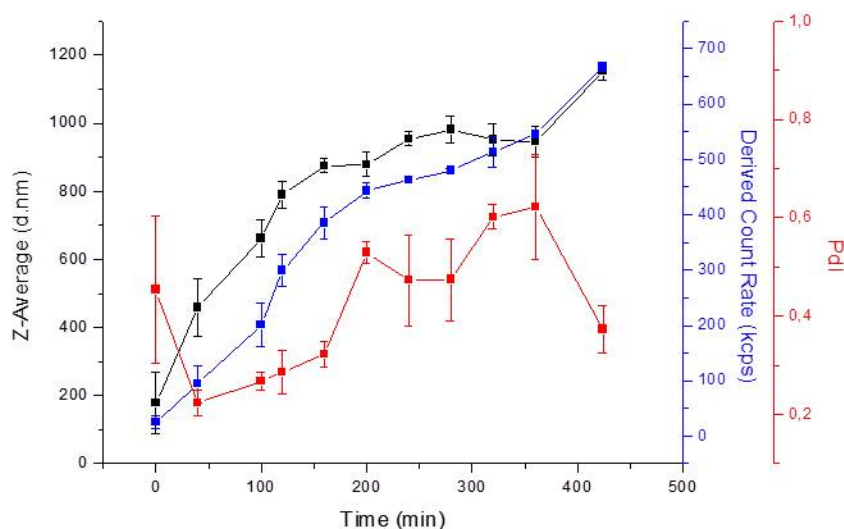


Figure 8 *In situ* DLS measurements of P(iPrOx₅₀-b-MeOx₅₀) in water at 1 mg/mL and 65 °C

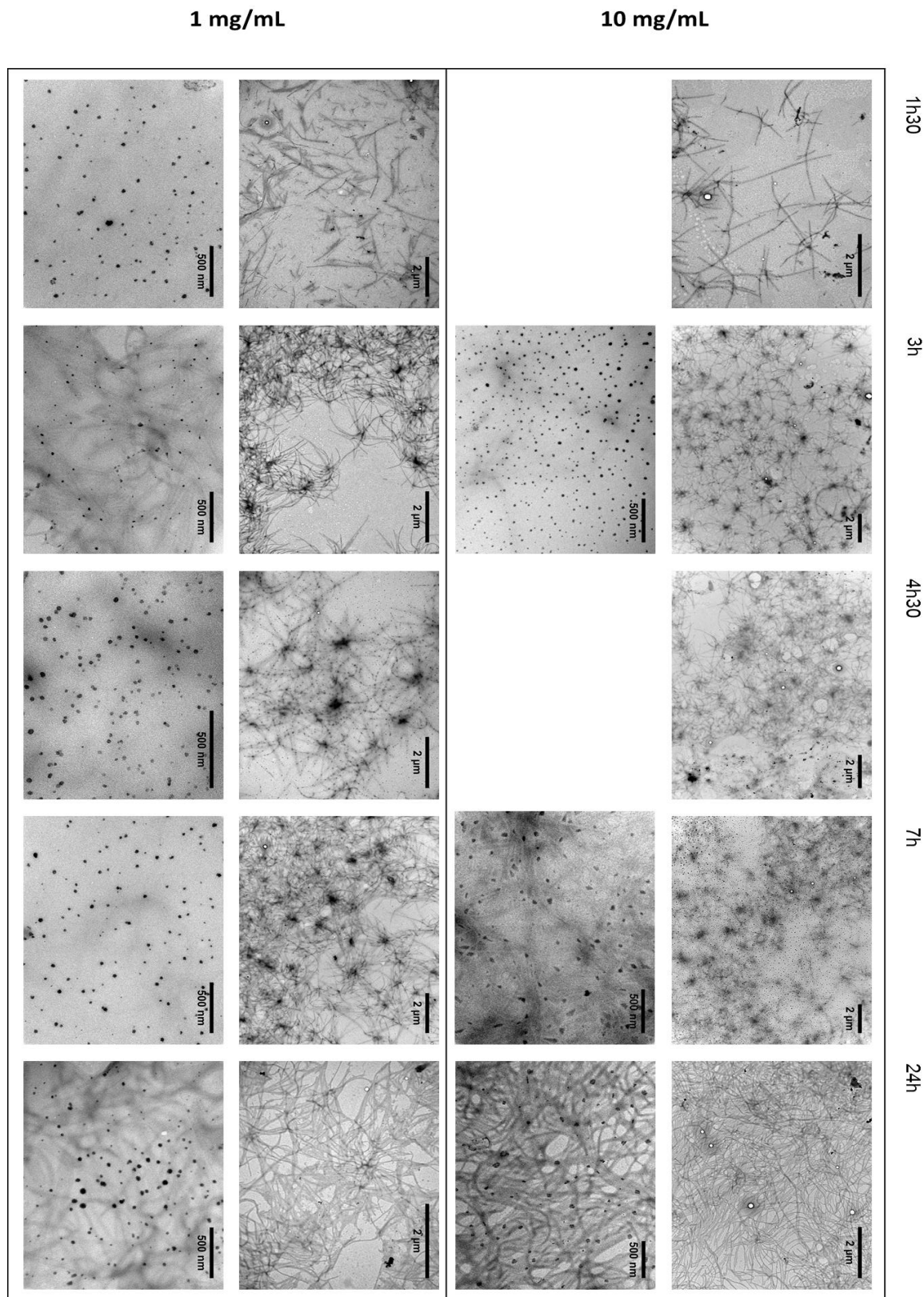


Figure 9 TEM micrographs of 10 mg/mL of P(iPrOx₅₀-*b*-MeOx₅₀) solution in water heated at 65 °C for 1h30, 3h, 4h30, 7h and 24h

At this lower concentration, the three morphologies previously observed at 10 mg/mL, *i.e.* fibers, nano-aggregates and core-cross-linked micelles, were again evidenced. In this case, as the concentration was lower, smaller morphologies (nano-aggregates and core-cross-linked micelles) could be more easily detected. The polymer concentration was also found to have an influence on the kinetic of crystallization: at 10 mg/mL, core-cross-linked micelles were mainly observed after 7h of annealing at 65 °C, whereas at 1 mg/mL the same structures were predominant already after 4h30. In addition, an increase in the count rate and size was again noted after 7h, by *in situ* DLS measurements whereas a plateau was already reached after 3h30 at a concentration of 10 mg/mL.

IV.2. HEATING RATE

The influence of the temperature was then studied by monitoring the morphology evolution with temperature. The BCP concentration was maintained at 10 mg/mL, and the solution was gradually heated, from 25 to 65 °C, at a rate of 0.1 °C/min (Figure 10).

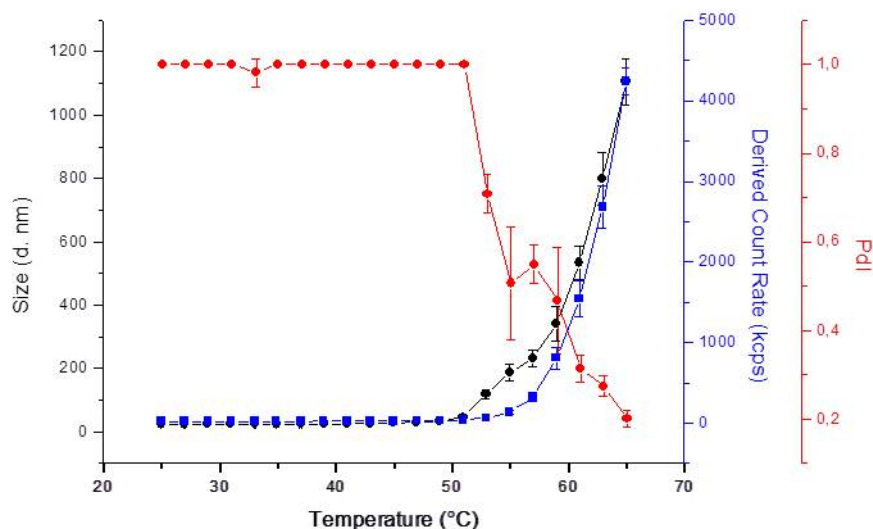


Figure 10 *In situ* DLS measurements of a 10 mg/mL P(iPrOx₅₀-b-MeOx₅₀) solution in water heated at 0.1 °C/min from 25 °C up to 65 °C.

As long as the temperature was maintained below the LCST of the BCP, the count rate was close to the detection limit of the DLS, indicating that the BCP was well dispersed in water. Above the LCST, however, an increase in the count rate and size was observed, along with a decrease in polydispersity. A final size of 1100 nm (polydispersity of 0.20) was determined at 65 °C. In addition, when the solution was allowed to cool to 25 °C, a particle size of 1500 nm (polydispersity of 0.12) was found, with a count

rate comparable to that obtained at 65 °C (4007 kcps). This was attributed to the crystallization of the micron-size aggregates. The increase in particle size upon cooling might be explained by re-swelling of the aggregates as the BCP chains became more hydrophilic: the PMeOx blocks became more hydrated when the temperature was decreased to room temperature, and if all the PiPrOx blocks were not involved yet in the crystallization, the non-crystallized ones could swell.

The heating rate had also a major influence on the nature of nanostructures:⁶⁰ from micelle-like structures (16 nm of radius) to micron-size particles. The slower the BCP solution was heated, the longer the time was needed to reach and pass the LCST for all copolymer chains (LCST is molecular weight dependent).²⁹ As a consequence, there is a temperature range where copolymer chains are partly amphiphilic, with other chains being still hydrophilic. Their organization being slower, self-assembly competes with the crystallization process, leading to the formation of larger structures. However, when the copolymer solution is heated rapidly above its LCST, all the chains become amphiphilic more or less simultaneously, self-assembling into micelles. To get more insight into the micron-size structure formed, it would be worth trying to image them and study their crystalline morphologies (micelle-like structure or micron-size aggregates made of fibers, etc.).

CONCLUSIONS

In this chapter, the aqueous solution behavior of a particular block copolymer, P(iPrOx₅₀-*b*-MeOx₅₀), synthesized by sequential CROP, was investigated at temperatures above the cloud point (56°C) of the PiPrOx. When heated to 65 °C for a short period of time, well-defined and reversible micelle-like nanostructures were evidenced by DLS and TEM imaging, with a hydrodynamic diameter of 32 nm.

Annealing this BCP above its LCST for a period of time higher than 1h30, induced the crystallization of PiPrOx, as attested by combined techniques, including WAXS, DSC, and TEM. The longer the annealing time, the higher the extent of crystallinity. Monitoring the crystallization process by DLS and TEM showed that three different morphologies, namely, core-crystallized micelles, nano-aggregates and fibers were achieved, as illustrates in Scheme 2.

EXPERIMENTAL SECTION

Materials and reagents

2-Methyl-2-oxazoline (99%) (EtOx), methyl trifluoromethanesulfonate (96%) (MeOTf), and acetonitrile (99%) were purchased from Sigma-Aldrich, stored over calcium hydride and purified by vacuum distillation prior to use. Methanol purchased from Aldrich was refluxed with sodium and distilled prior to use. Diethyl ether, potassium hydroxide (KOH), isobutyronitrile (99.6%) and cadmium acetate dehydrate (98%) were purchased from Sigma-Aldrich and used as received. 2-Aminoethanol was purchased from Fisher Scientific. 2-Isopropyl-2-oxazoline (iPrOx) was synthesized as described elsewhere (see Experimental procedures).⁶¹

Instrumentation and measurements

NMR spectroscopy. ¹H NMR measurements were carried out at 298K on a Bruker Avance I spectrometer operating at 400 MHz. CDCl₃ or D₂O were used as an internal reference ($\delta = 7.26$ and 4.79 ppm respectively), and the relaxation time was fixed to 5 sec for all measurements.

Size-exclusion chromatography. Size-exclusion chromatography (SEC) using dimethylformamide (DMF) with LiBr (1 g/L) as the eluent was performed at 80 °C at a flow rate of 0.8 mL/min. The column set consisted of two 7.5 mm × 300 mm PLgel, 5 μ m Mixed-D columns (Polymer laboratories) coupled to a 7.5 mm × 50 mm, PLgel, 5 μ m guard column (Polymer laboratories). A 20 μ L injection loop was used and calibration was performed with polystyrene standard. Differential refractive index (RI) and UV detectors were used.

Dynamic light scattering. Dynamic light scattering measurements (DLS) were run in triplicate on a Malvern Zetasizer apparatus (Nano-ZS90 model), at a back scattering angle of 90 °.

Transmission electron microscopy. Transmission Electron Microscopy (TEM) images were recorded at Bordeaux Imaging center (BIC) on a Hitachi H7650 microscope working at 80 kV. Samples were prepared by drop depositing 0.7 μ L of a 0.05 wt% of the desired copolymer solution onto a copper grid (200 mesh coated with carbon) and removing the excess after 5 minutes. In order to image the reversible micelles observed only above the LCST of the copolymer, the grid was left to dry at 65 °C (*i.e.* above the LCST). Statistical size analyses of particles observed by TEM were carried out using Image J.

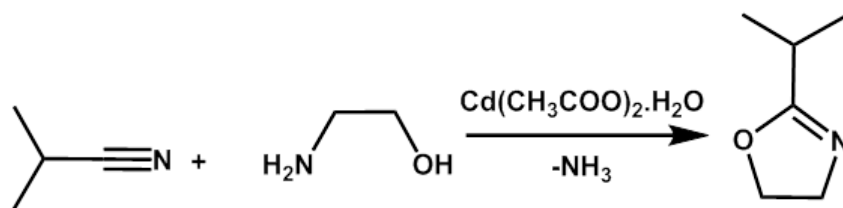
Differential scanning calorimetry. Differential scanning calorimetry (DSC) measurements were carried out on a Q1000 apparatus from TA Instruments. DSC experiments were performed in

aluminium sealed pans, at a constant heating/cooling rate of 10 °C/min and gas purging (N₂) at a flow rate of 100 mL/min.

Wide angle X-ray scattering. Wide angle X-ray scattering experiments (WAXS) were carried out at the Centre de Recherche Paul Pascal (CRPP, Pessac, France). Measurements were carried out on a Rigaku Nanoviewer (XRF microsource generator, MicroMax 007HF) with a rotating copper anode coupled to a confocal Osmic Max-Flux mirror (Applied Rigaku Technologies, Austin, USA), producing a beam with a wavelength of 1.5418 Å with an energy of 8 keV. Data were collected with a Mar345 detector (Marresearch, Norderstedt, Germany). Polymer solutions were freeze-dried and put into a 1.5 mm diameter glass capillary, placed at a distance of 150 mm away from the detector (diameter of 345 mm), providing access to 2θ angles in the range of 0.9° to 49°.

Experimental procedures

Synthesis of 2-isopropyl-2-oxazoline (iPrOx). 2-Isopropyl-2-oxazoline (iPrOx) was synthesized as described elsewhere: ⁶¹



Scheme 3 Synthesis of 2-isopropyl-2-oxazoline

2-Amino-ethanol (51 g, 0.83 mol) was added drop-wise to a suspension of isobutyronitrile (54.5 g, 0.79 mol) and cadmium acetate dihydrate (10.65 g, 0.04 mol) at 130 °C. The solution was stirred for 24 h at 130 °C and then fractionated by vacuum distillation. Yield: 64 g (0.57 mol, 72%). ¹H NMR (400 MHz, D₂O, δ): 1.1 (d, 6H, CCH(CH₃)₂), 2.35 (m, 1H, CCH(CH₃)₂), 3.7 (t, 2H, OCH₂CH₂N), 3.96 (t, 2H, OCH₂CH₂N). NMR Spectrum: Figure S1.

Synthesis of poly[(2-isopropyl-2-oxazoline)₅₀-block-poly(2-methyl-2-oxazoline)₅₀] (P(iPrOx₅₀-b-MeOx₅₀)). A typical procedure was as follows: in a flame dried Schlenk flask, 6.6 mL of acetonitrile was introduced under vacuum. 28.3 μL (0.25 mmol) of MeOTf was added. The flask was then placed in an ice bath at 0 °C and 1.48 mL (12.5 mmol) of 2-isopropyl-2-oxazoline was added. The flask was then maintained at 85 °C for 3 days, until complete consumption of the monomer (monitored by ¹H NMR spectroscopy). 1 mL of 2-methyl-2-oxazoline (11.7 mmol) was added and the reaction was quenched by adding 2.7 equivalents of a 0.3N KOH solution in methanol at 95% conversion (determined

by ^1H NMR spectroscopy). The solution was left to stir at room temperature overnight and the polymer was precipitated twice into diethyl ether and dried under vacuum. Yield = 2.08 g (89 %). ^1H NMR (400 MHz, D_2O , δ): 3.7-3.3 (s, NCH_2CH_2), 3.1 (s, $\text{CH}_3\text{-NCH}_2\text{CH}_2$), 3.0-2.55 (d, $\text{COCH}(\text{CH}_3)_2$), 2.2-2.0 (m, NCOCH_3), 1.15-1 (s, $\text{NCOCH}(\text{CH}_3)_2$). $\delta = 1.19$.

Synthesis of poly[(2-methyl-2-oxazoline) $_{50}$ -block-poly(2-sopropyl-2-oxazoline) $_{50}$] (P(MeOx $_{50}$ -*b*-iPrOx $_{50}$)). The same procedure, as described above for P(iPrOx $_{50}$ -*b*-MeOx $_{50}$) was also used to synthesize P(MeOx $_{50}$ -*b*-iPrOx $_{50}$), except the monomers were added in the reverse order. Yield = 1.15 g (47 %). ^1H NMR (400 MHz, D_2O , δ): 3.7-3.3 (s, NCH_2CH_2), 3.1 (s, $\text{CH}_3\text{-NCH}_2\text{CH}_2$), 3.0-2.55 (d, $\text{COCH}(\text{CH}_3)_2$), 2.2-2.0 (m, NCOCH_3), 1.15-1 (s, $\text{NCOCH}(\text{CH}_3)_2$). $\delta = 1.33$. $\text{DP}(\text{MeOx}) = 52$, $\text{DP}(\text{iPrOx}) = 50$.

SUPPORTING INFORMATION

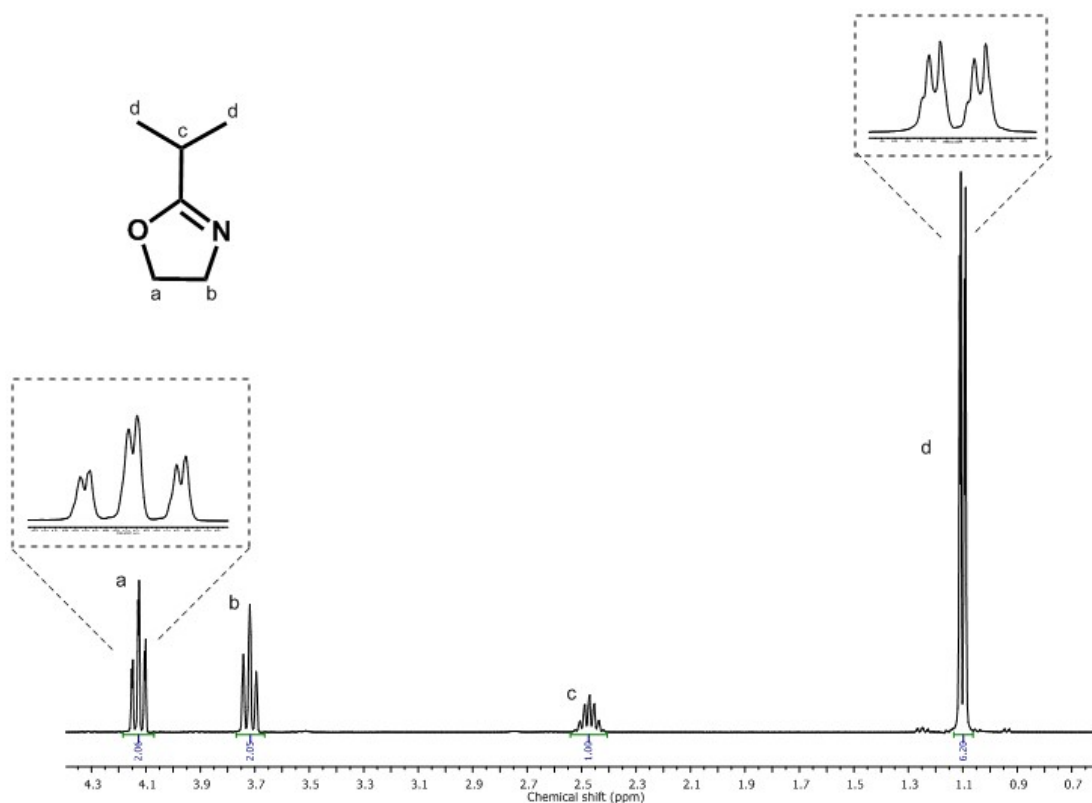


Figure S1 ^1H NMR spectrum (400 MHz, CDCl_3) of 2-isopropyl-2-oxazoline (iPrOx)

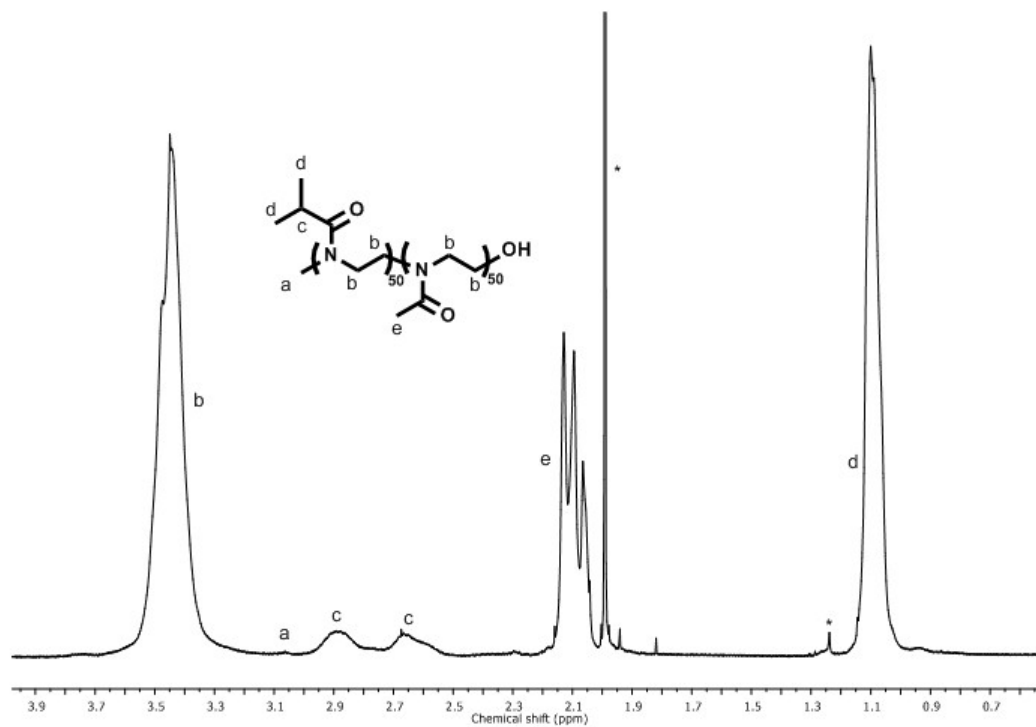


Figure S2 ¹H NMR spectrum (400 MHz, CDCl₃) of poly[(2-isopropyl-2-oxazoline)-b-(2-methyl-2-oxazoline)] (P(iPrOx-b-MeOx))

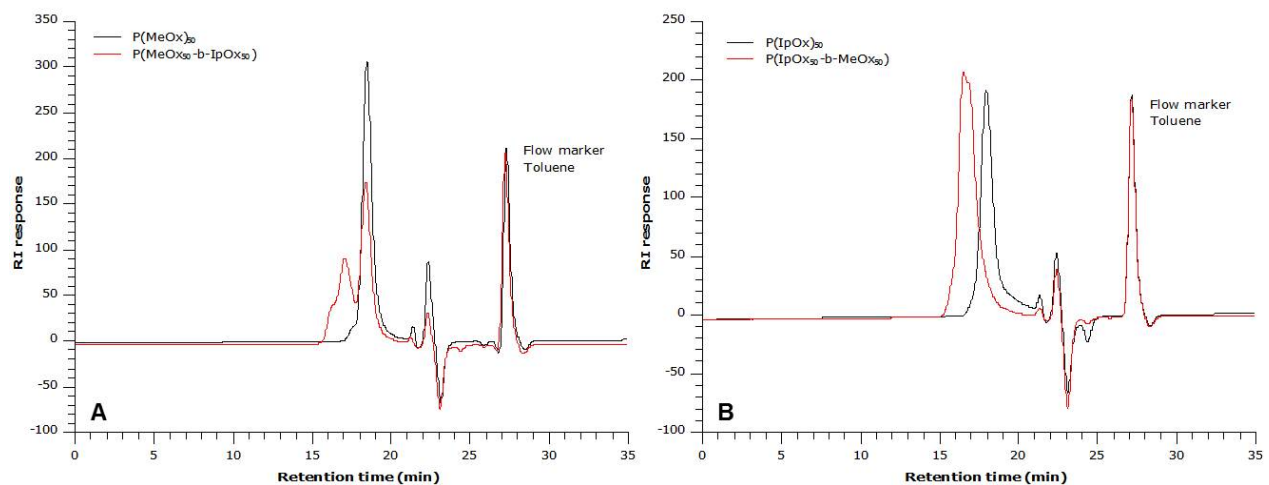


Figure S3 SEC trace of **A**) poly[(2-methyl-2-oxazoline)-b-(2-isopropyl-2-oxazoline)] and **B**) poly[(2-isopropyl-2-oxazoline)-b-(2-methyl-2-oxazoline)] in DMF

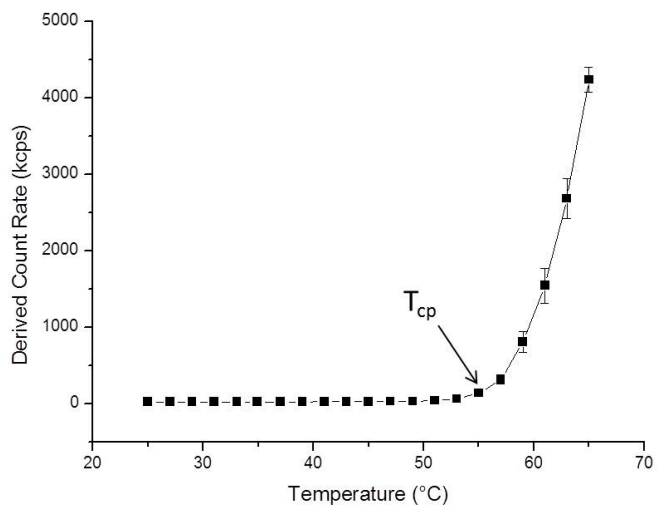


Figure S4 DLS measurements determining the cloud point of P(iPrOx-*b*-MeOx) (cloud point = 57 °C)

Table S1 DLS measurements determined at 65 and 25 °C of aliquots taken at a various annealing times after annealing at 65 °C

Annealing time	65 °C			25 °C		
	Size d (nm)	PdI	Count rate (kcps)	Size d (nm)	PdI	Count rate (kcps)
1h30	423	0.69	1898	796	0.28	1947
3 h	2666	0.71	4810	2712	0.62	9879
4h30	2956	1	4580	3793	0.85	9546
7 h	3140	1	4510	2725	1	4676

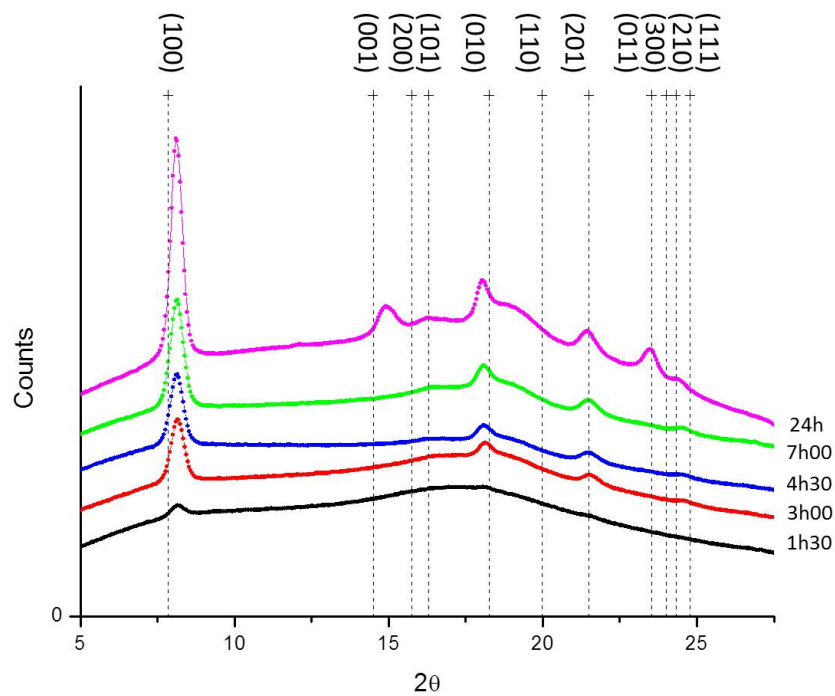


Figure S5 WAXS patterns of P(iPrOx₅₀-b-MeOx₅₀) after 1h40, 3 h, 4h30, 7 h and 24 h of annealing at 65°C. Peak assignment according to ref. 35

Table S2 WAXS scattering angles and corresponding spacing between the crystallographic planes obtained from Bragg's law

Crystallographic planes	2θ (°)	d (Å)
(100)	7.89	11.21
?	15.05	5.89
(101)	16.56	5.35
(010)	18.28	4.86
?	19.22	4.62
(201)	21.72	4.09
(011)	23.59	3.77
(210)	24.38	3.65

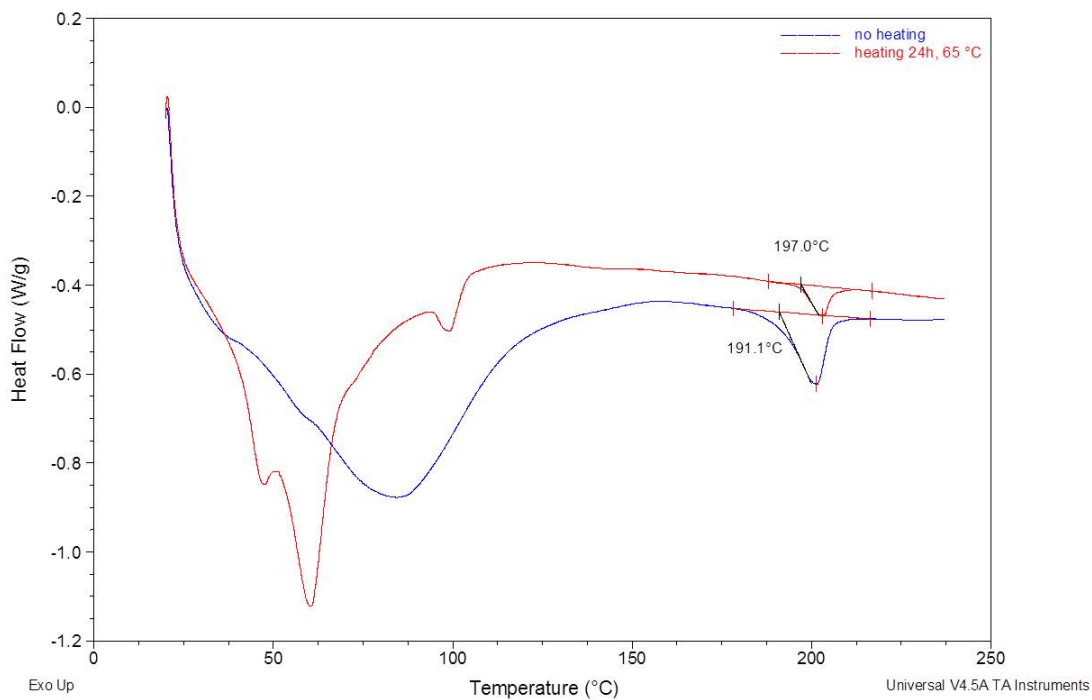


Figure S6 DSC thermograms of the first heat ramp of P(iPrOx₅₀-b-MeOx₅₀), non-treated and kept under storage condition (blue) and after 24 h of heating in aqueous solution at 65 °C (red)

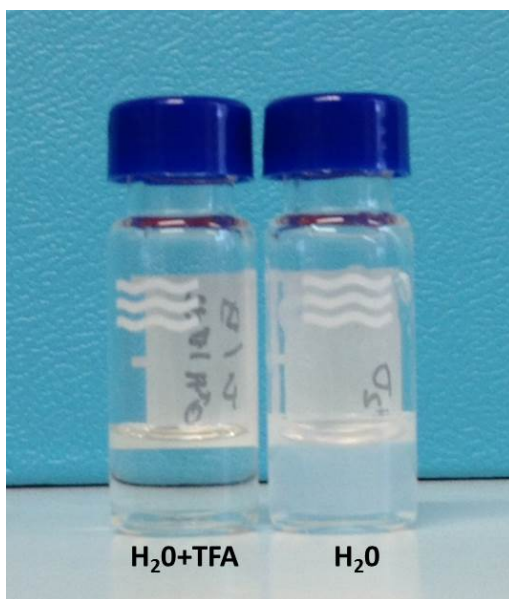


Figure S7 Appearance of P(iPrOx₅₀-b-MeOx₅₀) in water/trifluoroacetic acid mixture (1/5 v/v) and in pure water

Appendix S1 - WAXS measurement principle and determination of the crystal structure

Wide-angle X-ray scattering (WAXS) is a non-destructive characterization technique which probes matter ordering on the angstrom-scale. It is often used to determine the crystalline structure of polymers. It consists of the observation of the scattered intensity of an X-ray beam hitting a sample as a function of the incident and scattered angles. As the angles for coherent and incoherent scattering from a crystal lattice are obtained (Figure S8), by using Bragg's law (equation 1), the spacing between the crystal planes can be calculated, and a crystal structure can be proposed.

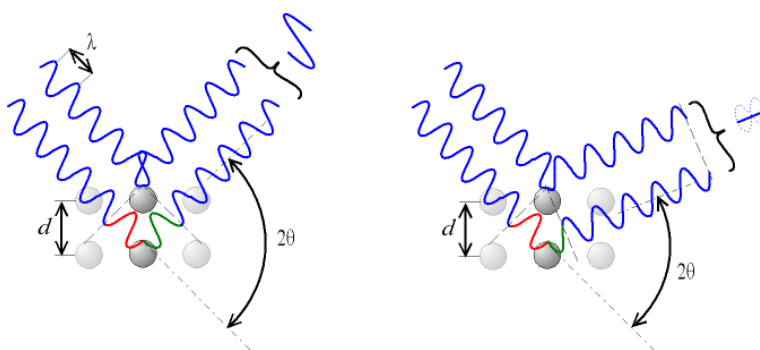


Figure S8 Illustration of constructive and destructive interferences. Adapted from ref. 62

Bragg's law:
$$\lambda = 2d\sin(\theta) \quad (1)$$

Where λ is the wavelength of the incident wave

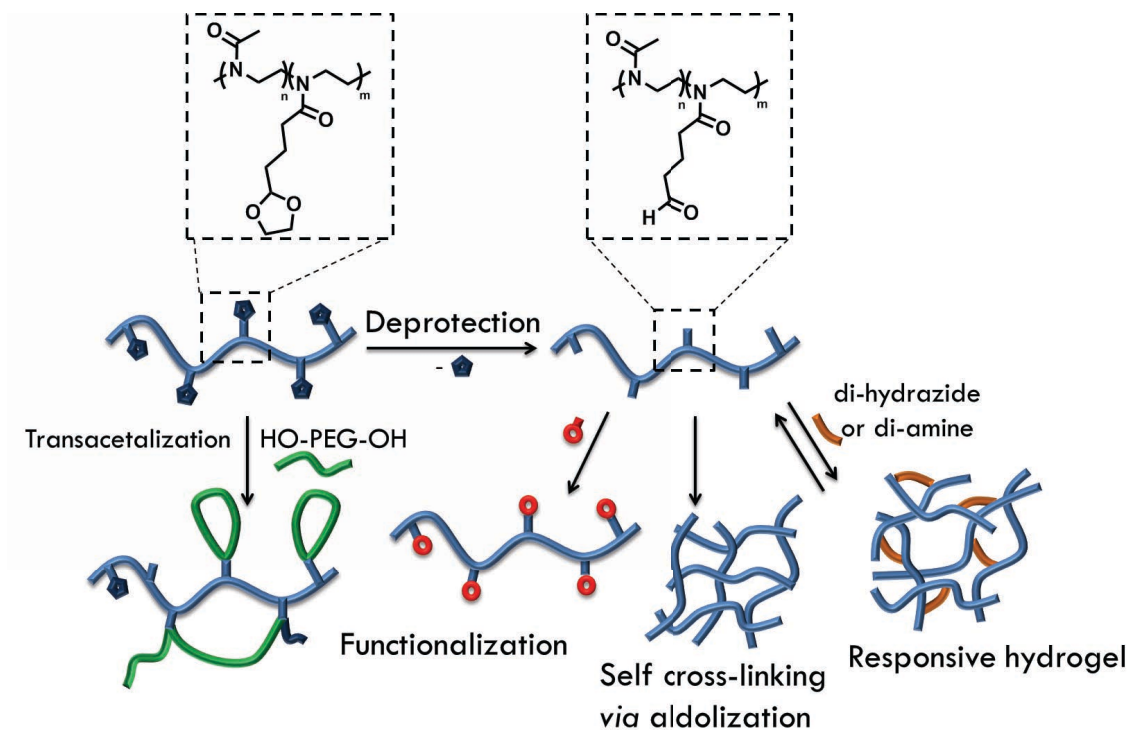
d is the spacing between the crystalline planes

θ is the angle between the incident ray and the scattering planes

Demirel *et al.*⁴⁰ reported the structural model of the homopolymer PiPrOx crystal, based on WAXS and scanning force microscopy (SFM) data of the nanofibers, collected using Cerius 2 software. A periodicity of $d = 11.25 \text{ \AA}$ (corresponding to WAXS peak at $2\theta = 7.85^\circ$) could only be achieved when the side chains of neighboring polymers formed a bilayer. Steric constraints prevent the orientation of the neighboring side chains in the same direction, thus alternation of side chains on either side of the backbone was determined. This starting structure was then refined by rotations of the isopropyl groups and the carbonyl groups separately such that the calculated WAXS peaks by Cerius 2 software reproduced the experimental WAXS data.

CHAPTER 4

KETAL- AND ALDEHYDE-FUNCTIONAL COPOLYMERS BASED ON POLY(2-OXAZOLINE) FOR POST-POLYMERIZATION MODIFICATION



Keywords: Aldehyde, hydrogel, poly(2-oxazoline), post-polymerization modification, aldolization, transacetalization.

Overview: Protected and non-protected homopolymers and related statistical copolymers based on poly(2-oxazoline) were synthesized by cationic ring-opening (co)polymerization, using a protected aldehyde 2-oxazoline monomer, namely, 2-[3-(1,3-dioxolan-2-yl)propyl]-2-oxazoline (DPOx). The (co)polymer precursors were subsequently used as reactive platforms enabling the synthesis of miscellaneous derivatives, including graft and cross-linked copoly(2-oxazoline)s. Aldehyde-functional (co)polymers were first reacted with mono- or bi-functional amino- and hydrazido-containing reagents, forming grafted copolymers or chemically cross-linked networks, respectively. The latter compound consisting of hydrazone-type linkages formed hydrogels that could be slowly degraded at physiological pH over 3 days, but readily cleaved in a more acidic environment (pH = 3). Aldehyde-containing (co)polymers were also found to be subject to an intermolecular self-aldolization reaction under acidic conditions, leading to branching and ultimately to the formation of dense 3D-networks. As for (co)polymer precursors possessing protected aldehyde functions in the form of ketal rings, they could be directly reacted with a large excess of poly(ethylene glycol) (PEG), via transacetalization, forming PEG-grafted poly(2-oxazoline)s.

Part of this chapter has been published in *European Polymer Journal* in 2014.¹

¹ Legros, C.; Pauw-Gillet, M.-C. De; Tam, K. C.; Lecommandoux, S.; Taton, D. *Eur. Polym. J.* **2014**, DOI: 10.1016/j.eurpolymj.2014.08.026.

CHAPTER 4

KETAL- AND ALDEHYDE-FUNCTIONAL COPOLYMERS BASED ON POLY(2-OXAZOLINE) FOR POST- POLYMERIZATION MODIFICATION

INTRODUCTION	131
I. SYNTHESIS OF PDPOX ₂₁ BY CATIONIC RING-OPENING POLYMERIZATION	132
II. CONJUGATION OF POBOX WITH AMINO-CONTAINING REAGENTS	133
III. COPOLYMER SYNTHESIS AND DEPROTECTION OF P(MEOX ₄₁ -STAT-DPOX ₉)OH	135
IV. HYDROGEL FORMATION BETWEEN P(MEOX ₉₃ -STAT-OBOX ₁₁)PIP AND ADIPIC ACID DIHYDRAZIDE ..	138
V. TRANSACETALIZATION REACTION FROM P(MEOX ₄₁ -STAT-DPOX ₉)OH WITH AN EXCESS OF PEG ₃₀₀	139
CONCLUSIONS	142
EXPERIMENTAL SECTION	143
SUPPORTING INFORMATION	149

INTRODUCTION

Post-polymerization modification, also called polymer-analogous modification, is a powerful synthetic tool in polymer chemistry. It consists in accessing new polymers by modification of a preformed polymer carrying functional handles that are chemically or physically transformed. Interestingly enough, diverse polymer derivatives with different structures and properties can be achieved from one single reactive polymer precursor.¹⁻³ For example, post-polymerization modification allows for chemical transformation of commodity polyolefins into value-added materials,⁴ or to tailor poly(carbonate)s for specific biomedical applications.⁵⁻⁷ A wide variety of chemoselective and/or orthogonal reactions, including thiol-ene addition,⁸ thiol exchange, Diels-Alder cycloaddition,⁹ Michael addition or reactions with active esters,¹⁰ epoxides, anhydrides, isocyanates, ketones and aldehydes, have been applied to modify functional polymer precursors.^{11,12}

Aldehyde functional groups are of special interest owing to the diversity of reactions that can be implemented with antagonist functional groups, such as alcohols, amines and hydrazines, forming reversible acetal, imine, and hydrazone linkages, respectively. Moreover, aldehydes can also be reduced to hydrocarbons *via* the so-called Wolff-Kishner reaction.¹³ They are also involved in key reactions in molecular chemistry, such as Grignard, Wittig and aldolization reactions.^{14,15} Surprisingly, the number of reports describing polymers with pendant aldehydes is somewhat limited. The synthesis of polymers with aldehyde handles can be achieved by anionic¹⁶ and cationic polymerization,¹⁷ ring opening metathesis polymerization,¹⁸ reversible addition-fragmentation chain transfer¹⁹⁻²² or by the modification of biopolymers.²³ Related (co)polymers have been further employed to engineer polymer materials for specific applications: injectable hydrogels,²⁴⁻²⁷ microgels *via* a microfluidic device,²⁸ or shell cross-linked micelles²⁹ obtained with dihydrazide cross-linkers. Nanoparticles were also formed using a copolymer based on vinylbenzaldehyde units; further cross-linking or conjugation with chemotherapy compounds *via* Schiff base or imine formation was achieved.³⁰ Lastly, poly(4-vinyl benzaldehyde) has also been successfully functionalized with desired compounds using the Kabachnik-Fields post-polymerization reaction.³¹

Here, we investigate the potential of poly(2-oxazoline)s (POx) possessing pendant aldehyde functions for polymer-analogous modification. POx represent a special class of polymers that have (re)gained an increasing interest in the last decade. This is due, in particular, to their structural similarities with polypeptides,³² the biocompatible character and the stealth behaviour of some POx.³³⁻³⁵ In addition, the relatively easy access to POx by cationic ring opening polymerization^{36,37} allows the tuning of their

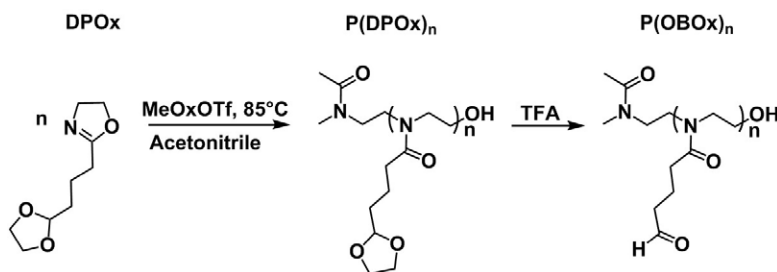
physico-chemical properties, such as hydrophilicity and thermo-responsiveness.^{38–40} The synthesis of POx with functional handles can also be achieved by resorting to specific functional 2-oxazoline monomers, which most often requires protection of the functional group prior to its (co)polymerization, in order to avoid side reactions. Synthetic strategies to functionalize POx have been recently reviewed.^{41,42} Alkene- or alkyne-functionalized monomers can remain unprotected,^{43–45} but monomers containing an amine⁴⁶ or alcohol⁴⁷ require protection in the form of *tert*-butyloxycarbonyl (BOC) or ester groups, respectively. To the best of our knowledge, there is only one report about the synthesis and post-polymerization modification of aldehyde-functional POx, as described by Taubmann *et al.*,¹⁷ who employed a protected aldehyde oxazoline monomer in the form of a ketal ring. POx with pendant aldehyde functions was readily obtained after deprotection, and subsequent modification with amino-oxy-containing reagents yielding the oxime was reported.

In this chapter, we wish to further exploit the reactivity of such POx-based (co)polymers bearing pendant protected and non-protected aldehyde functions. We demonstrate that aldehyde-containing POx can readily react with mono- and bi-functional amines and hydrazines, enabling the synthesis of both grafted POx and POx-based hydrogels that can be chemically cleaved off under acidic conditions. We also evidence that aldehyde-containing POx chains can undergo intermolecular aldolization under acidic conditions. Lastly, the functionalization of POx through transacetalization of ketal-containing POx (protected form) is also presented.

I. SYNTHESIS OF PDPOX₂₁ BY CATIONIC RING-OPENING POLYMERIZATION

Following a similar protocol to the one employed for non-functional polymers, the aldehyde protected polyoxazoline, PDPOx, was obtained *via* cationic ring opening polymerization of 2-[3-(1,3)-dioxolan-2-ylpropyl]-2-oxazoline (DPOx), in the presence of *N*-methyl-2-methyl-2-oxazolinium triflate (MeOxOTf) as initiator, and acetonitrile as solvent (see Scheme 1). Taubmann *et al.* showed that MeOxTf and methyl trifluoromethanesulfonate (MeOTf) were both efficient to initiate this polymerization,¹⁷ but an oxazolinium salt was used as initiator for the polymerization as a proof of concept for further synthesis of an end-functionalized PDPOx.³⁶ PDPOx was obtained with a degree of polymerization (DP) close to the target based on the initial $[DPOx]_0/[MeOxOTf]_0$ molar ratio, with a narrow dispersity ($\mathcal{D} = 1.17$) (SI†, Figure S3). Both ¹H and ¹³C NMR spectra confirmed that the aldehyde functionality remained protected in the form of the ketal ring after polymerization (SI†, Figure S3). The deprotection step of PDPOx₂₁ was next accomplished by hydrolysis, using a 5% TFA solution. As discussed by Taubmann *et*

al.,¹⁷ this ketal hydrolysis is equilibrated, hence the reaction was carried out in a dialysis setup to achieve full conversion (see Scheme 1). Analysis by ¹H NMR spectroscopy of the resulting compound attested to complete deprotection, as the characteristic signals due to the protons of the cyclic ketal rings vanished after hydrolysis; instead, the signal of the aldehyde proton appeared at 9.7 ppm (SI†, Figure S4). In addition, two peaks appeared at 2731 cm⁻¹ and 1715 cm⁻¹ in the FTIR spectrum, which could be assigned to the C-H and C=O stretches of the aldehyde group, respectively (SI†, Figures S5 and S6).



Scheme 1 Cationic ring opening polymerization of 2-[3-(1,3)-dioxolan-2-ylpropyl]-2-oxazoline and subsequent deprotection (inspired from ref. 17)

II. CONJUGATION OF POBOX WITH AMINO-CONTAINING REAGENTS

Taubmann *et al.* have already reported the post-polymerization modification of POBOx through the reaction of aldehyde groups with amino-oxy compounds in methanol, at 50 °C.¹⁷ Our aim here was to further expand the reactivity of this polymer precursor with respect to a range of either mono- or bi-functional commercial amines and dihydrazines, under mild conditions. Both modifications involve a first step that is reversible, forming an imine and a hydrazone, respectively.^{48,49} The second step consists in the irreversible reduction of the functional polymer intermediate into a secondary amino-functional polymer derivative. POBOx₂₁ was thus treated with an excess of benzylamine in a sodium acetate solution at pH = 5.4,⁵⁰ which was followed by a reduction using sodium cyanohydroborate (see Figure 1). Note that benzylamine is sparingly soluble in water, favoring precipitation of the imino-containing reaction product.⁴⁸ The poor solubility of the polymer in aqueous solution and in common organic solvents, even after purification, suggested the formation of an amphiphilic compound due to efficient grafting of benzylamine onto POBOx₂₁. This was verified by FTIR showing the disappearance of the two signals of the aldehyde (2731 cm⁻¹ and 1715 cm⁻¹), while signals characteristic of aromatic C-H and C=C bendings appeared at 736 cm⁻¹ and 700 cm⁻¹ and at 1570 cm⁻¹, respectively (SI†, Figure S7).

Reductive amination was also carried out using Jeffamine D400 and adipic acid dihydrazide in sodium acetate solution. As both reagents are bi-functional, both could act as cross-linkers, giving rise to gels, as illustrated in Figure 1. FTIR of compounds purified by dialysis was again used to confirm the successful ligation, with complete disappearance of the aldehyde peaks along with the appearance of a characteristic ether C-O stretch at 1090 cm^{-1} for the polymer derived from Jeffamine D400, and of the amine N-H stretch at 3248 cm^{-1} from that issued from adipic acid dihydrazide (SI†, Figures S8 and S9). In contrast, the same reaction performed with POBOx-based statistical copolymers did not lead to gel formation in aqueous solution (see further).

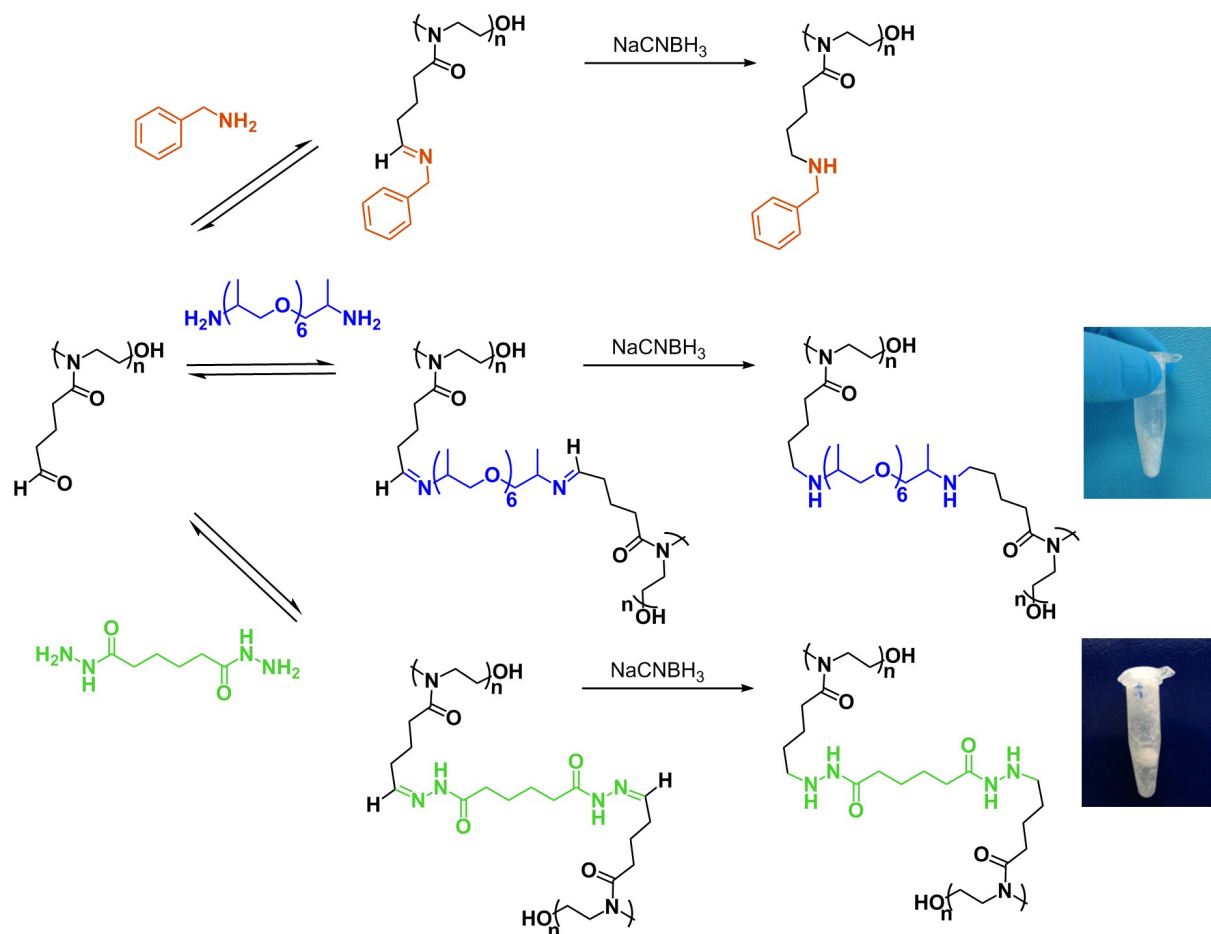


Figure 1 Post-polymerization modification of POBOx₂₁ with benzylamine, Jeffamine D400 and adipic acid dihydrazide

Thus, the successful reaction of POBOx₂₁ with several amine or hydrazine compounds confirmed the accessibility of the aldehyde functionalities, enabling the access to grafted or cross-linked polymer derivatives. In all cases, post-polymerization modification was effective under mild conditions, *i.e.* at room temperature in aqueous solution.¹⁷ The ligation with adipic acid dihydrazide can be considered as chemoselective as the amino-oxi “click” ligation reaction.⁵¹

III. COPOLYMER SYNTHESIS AND DEPROTECTION OF P(MEOx₄₁-STAT-DPOx₉)OH

A statistical copolymer based on 2-methyl-2-oxazoline (MeOx) and DPOx was synthesized in order to tune the density of pendant reactive groups. In their report, Taubmann *et al.* established that both monomers are consumed at the same rate during copolymerization, providing statistical copolyoxazolines.¹⁷ A statistical copolymer with 20% of DPOx was thus prepared. The copolymer was obtained with a DP for each monomer unit close to targeted values, and a dispersity of 1.14 (SI†, Figures S10, S11 and S12). Deprotection of the copolymer led to a derivative that was hardly soluble in DMF, hence SEC was performed in Tris buffer as the elution solvent. Broadening of the SEC trace and appearance of a shoulder in the high molecular weight region was noted after deprotection (Figure 2). Analysis by SEC of another copolymer sample, 10 days after deprotection, showed an even more noticeable molecular weight shoulder. This suggested the occurrence of subsequent intermolecular reactions involving the deprotected aldehyde functions in the dry state.

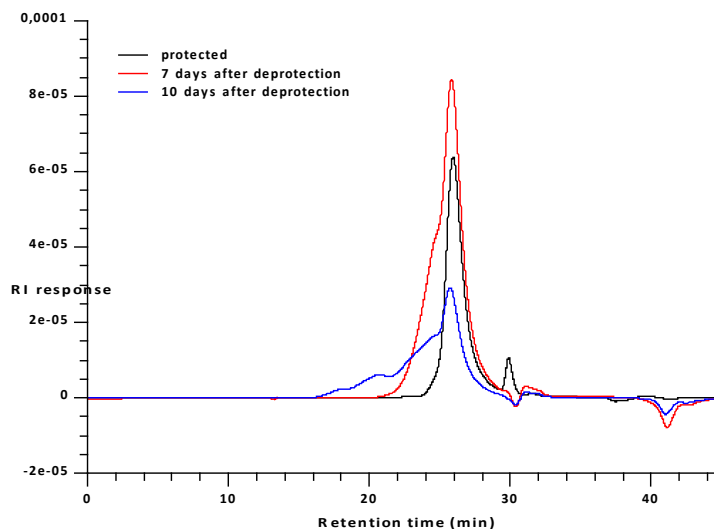
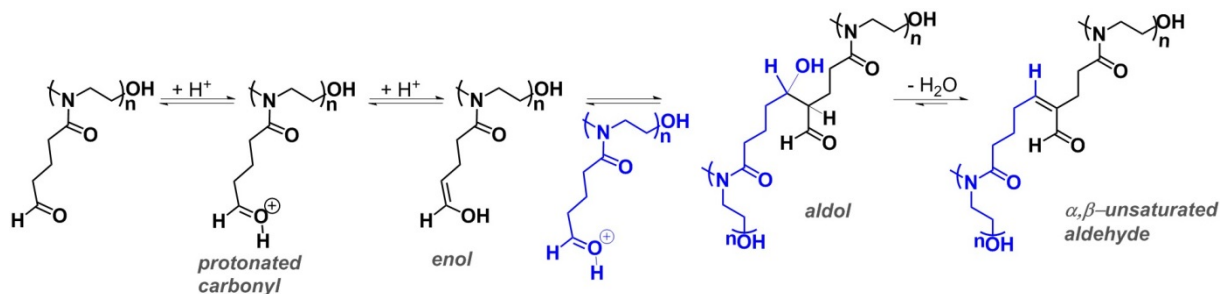


Figure 2 SEC traces in Tris buffer of P(MEOx₄₁-stat-DPOx₉)OH before and after deprotection

In the case of the P(OBOx)₂₁ homopolymer discussed above, such intermolecular reactions were not studied in details; this sample was readily dissolved in acetate buffer after deprotection and the work-up procedure was slightly different from the copolymeric samples. Nevertheless, P(OBOx)₂₁ was less soluble in the acetate solution during the post-polymerization reaction, indicating that some intermolecular branching/cross-linking may have also occurred in this case.

To explain these observations, we hypothesized that pendant aldehyde functions could be subjected to an aldolization reaction in the presence of catalytic acid traces. In a second step, the as-generated aldol units could undergo a dehydration step (referred to as the crotonization reaction¹⁵), leading to α,β -unsaturated groups (see Scheme 2). It should be noted that the alcohol terminal functionality of the copolymer chain could also be involved in aldol formation.



Scheme 2 Aldol condensation and subsequent dehydration resulting in α,β -unsaturated aldehydes

To test our hypothesis the deprotected polymer, $\text{P}(\text{MeOx}_{41}\text{-stat-OBOx}_9)\text{OH}$, was analyzed by solid state ^{13}C NMR at two rotation speeds (changing the rotation speed allows determining the presence of rotation peaks; S1†, Figure S15). Only one rotation peak was found (indicated by a star in Figure 3), and the observation of diagnostic peaks due to alkene groups clearly confirmed the occurrence of aldol formation, followed by dehydration.

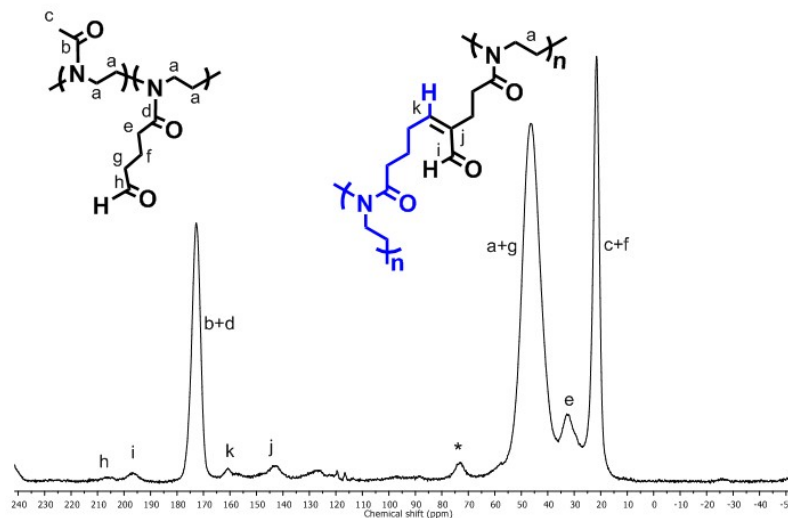


Figure 3 Solid state ^{13}C NMR of the self-cross-linked $\text{P}(\text{MeOx}_{41}\text{-stat-OBOx}_9)\text{OH}$, rotation speed = 10000 Hz, ns = 16000

A series of statistical copolymers based on DPOx were then synthesized (P(MeOx₆₃-stat-DPOx₁₄)pip, P(MeOx₁₂₄-stat-POx₁₂)OH and P(MeOx₉₃-stat-DPOx₁₁)pip; see Table I in the experimental procedure section and SI†, Figures S13 and S14), in order to study the influence of aldehyde density on the occurrence of the aldol reaction. SEC traces show a bimodal distribution in some cases. For instance, a shoulder can be noted in the low molecular weight region of the SEC traces of both P(MeOx₁₂₄-stat-POx₁₂)OH and P(MeOx₉₃-stat-DPOx₁₁)pip (SI†, Figures S16 and S17). This minor population can be ascribed to chains grown by chain transfer reaction to the monomer. As for SEC traces of P(MeOx₆₃-stat-DPOx₁₄)pip (SI†, Figure S18), the side population appearing in the high molecular weight region is presumably due to the occurrence of irreversible coupling of a small proportion of growing chains at the completion of the polymerization. Both side reactions have indeed been described, and related mechanisms are well established.^{52–54} The three different polymerization reactions were run in parallel and only stopped after three days, *i.e.*, once all the monomer was consumed. Total consumption of the monomer was confirmed only in one case, for P(MeOx₉₃-stat-DPOx₁₁)pip, and all the polymerizations were quenched at the same time. One can thus assume that the synthesis of the P(MeOx₆₃-stat-DPOx₁₄)pip sample, that is of a lower DP, was completed, in contrast to the two other polymers of higher DP. As a consequence, the occurrence of chain coupling was more likely for the former copolymer. Furthermore, the probability for chain transfer increases with the polymer molecular weight. Herein, the P(MeOx₄₁-stat-DPOx₉)OH sample had a lower molecular weight as compared to the three other copolymers, which can explain why no such side reaction was evidenced for the former copolymer. However, despite the existence of these side populations, it was decided to carry on the study with these samples, as they should not be detrimental to the reactivity of aldehyde functionalities.

A P(MeOx₉₀-stat-DPOx₁₀)pip copolymer was also prepared in a stainless steel reactor following the procedure reported by Hoogenboom *et al.* (*i.e.* 140 °C at a monomer concentration of 4M).^{55,56} Under these conditions, the polymerization was completed within 1h, as compared to 3 days when conducting the copolymerization at 85 °C in a Schlenk flask. However, the copolymer had a higher dispersity, $\bar{D} = 1.61$ at 140 °C, as compared to 1.34 at 85 °C, hence this sample was not used further in this study. This increase in polydispersity is likely due to the increased reaction temperature (140 °C), monomer concentration and viscosity (the reaction was carried out above the boiling point of the solvent but the pressure was not monitored), leading altogether to a loss of control.

Characterization by SEC in Tris buffer of the deprotected copolymers did not indicate any intermolecular aldolization in the investigated time scale (1, 3, 7 and 10 days after deprotection; see SI†), in contrast to the P(MeOx₄₁-stat-DPOx₉)OH sample showing significant tailing at high molecular weight, seven days after deprotection (see Figure 2). Four and a half months later, the deprotected copolymers

were no longer soluble in Tris buffer, presumably owing to intermolecular self-cross-linking of the samples under storage conditions.

The influence of the aldehyde functionality content on the aldolization is illustrated in Figure 4 when comparing vials A and C (20% and 10% aldehyde, respectively). The influence of the end group functionality can be observed for copolymers with the same aldehyde content (vials B and C corresponding to samples with OH and piperidine end groups, respectively; see Figure 4). It can be seen that the copolymer with the alcohol terminus is more prone to self-cross-linking as compared to the sample with the piperidine end group. The sample combining a high content in aldehyde functions and an alcohol terminal group, P(MeOx₄₁-stat-DPOx₉)OH, led to rapid intermolecular self-cross-linking (see Figure 4).

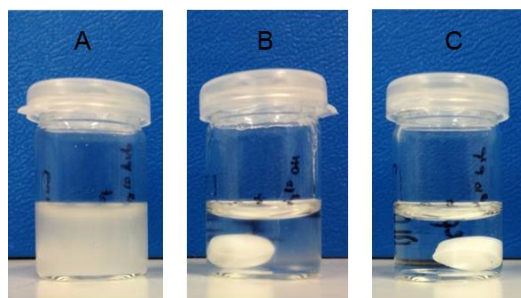


Figure 4 Solubility in Tris buffer, after 4 ½ months, of A) P(MeOx₆₃-stat-DPOx₁₄) pip B) P(MeOx₁₂₄-stat-DPOx₁₂)OH C) P(MeOx₉₃-stat-DPOx₁₁)pip

In conclusion, deprotected PDPOx-based copolymers can undergo branching by aldolization, the rate of which reaction depends on both the aldehyde and alcohol content. Prolonged reactions can lead to cross-linked networks. However, aldehyde-functional copolymers can be manipulated in solution and be used for further post-polymerization reactions even ten days after the deprotection step, without the occurrence of aldolization, in particular using the P(MeOx₉₃-stat-DPOx₁₁)pip sample.

IV. HYDROGEL FORMATION BETWEEN P(MeOx₉₃-STAT-OBOX₁₁)PIP AND ADIPIC ACID DIHYDRAZIDE

The synthesis of hydrogels was also achieved from the P(MeOx₉₃-stat-OBOX₁₁)pip copolymer precursor that was reacted with adipic acid dihydrazide as cross-linker. The first attempt was carried out in a 2% acetate solution, under the same aforementioned conditions employed for the reaction between

POBO_{x21} and adipic acid dihydrazide. Hydrogel formation was instantaneous, though subsequent cleavage of the hydrazone linkages constituting the cross-linking points was also immediate under slightly acidic aqueous conditions (pH = 5.4).⁴⁹ This rapid cleavage was not observed when the reaction was carried out with POBO_{x21}, within a time scale of investigation of one hour, most likely because of the higher percentage of aldehyde functionalities. Keeping these observations in mind, hydrogel formation successfully occurred in dry DMSO, in the presence of sodium acetate and molecular sieves (3Å) at room temperature, such conditions favoring the formation of hydrazone linkages. The as-obtained gel was found to be stable over several weeks and was shown to swell when soaked in DMSO (Figure 5). This gel could be readily cleaved, however, by hydrolysis when immersed in an aqueous solution, and the reaction rate could be tuned by adjusting the pH. As shown in Figure 5, in 10 mM phosphate buffer (pH = 7.4), the hydrogel was completely cleaved after 3 days, whereas it was readily cleaved within 3 minutes in acidic conditions (0.01 M HCl, pH = 3).

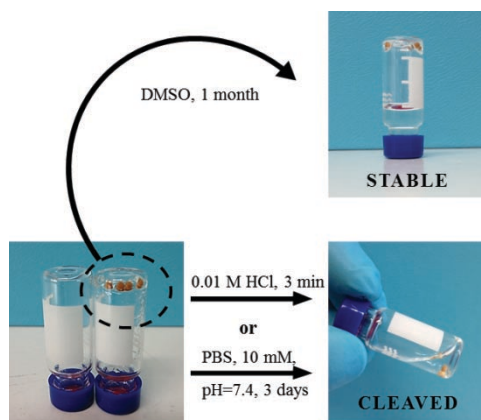
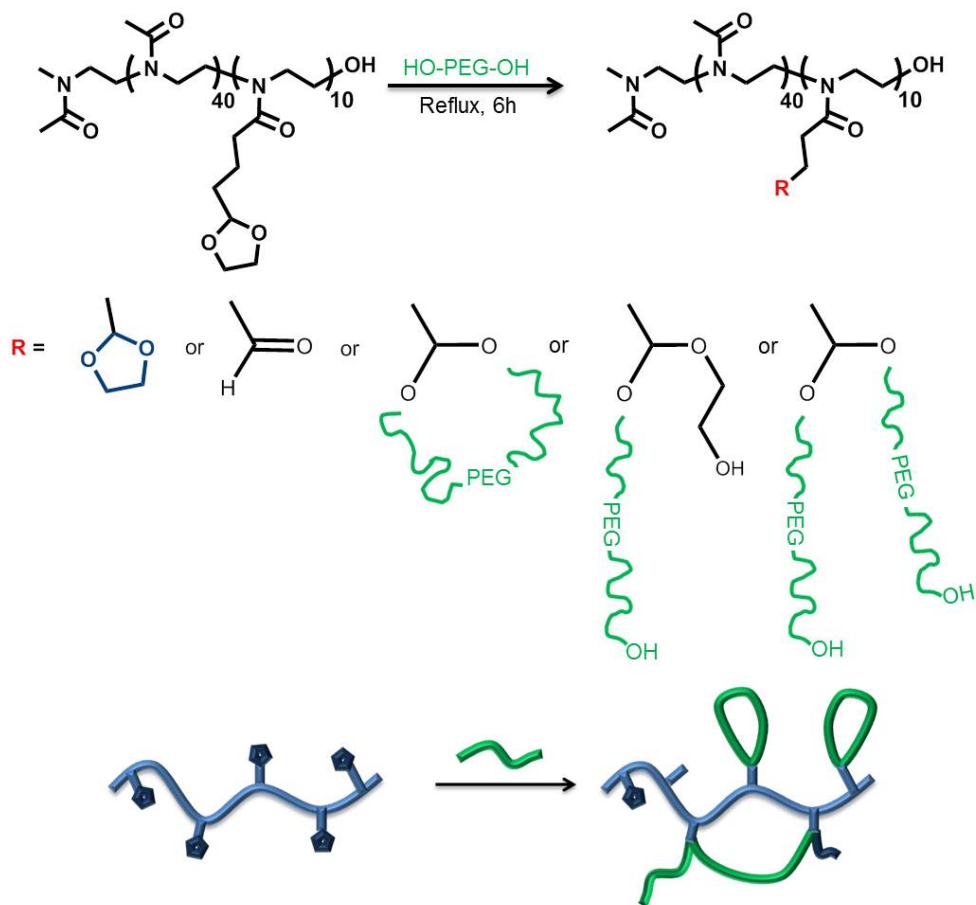


Figure 5 Gel formation and cleavage between P(MeOx₉₃-stat-OBOx₁₁)pip and adipic acid dihydrazide

V. TRANSACETALIZATION REACTION FROM P(MEOX₄₁-STAT-DPOX₉)OH WITH AN EXCESS OF PEG₃₀₀

Lastly, we investigated the possibility to directly modify the protected ketal-functional P(MeOx₄₁-stat-DPOX₉)OH by an acid-catalyzed transacetalization reaction, using a large excess of PEG₃₀₀ (see Scheme 3). It is important to note that, under such conditions, PEG₃₀₀ plays both the role of reactant and solvent.



Scheme 3 Transacetalization reaction from $P(\text{MeOx}_{41}\text{-stat-DPOx}_9)\text{OH}$ with an excess of PEG_{300} and its schematic representation

In order to shift the equilibrium towards the PEG-functionalized derivative, ethylene glycol supposedly generated as by-product was removed by distillation (boiling point = 197 °C). The $P(\text{MeOx}_{41}\text{-stat-DPOx}_9)\text{OH}$ sample was directly dissolved in an excess of PEG_{300} , in presence of *p*-toluene sulfonic acid (PTSA) as catalyst. The polymer was subsequently purified by dialysis to remove the excess of PEG_{300} .

Analysis of the resulting compound by DOSY-NMR confirmed the successful grafting of PEG chains onto the poly(2-oxazoline) backbone (SI†, Figure S19). These data also suggested that transacetalization seemingly occurred by an intramolecular reaction rather than by intermolecular reaction pathway, as only one diffusion coefficient was observed.

The ^1H NMR spectrum (Figure 6) not only showed that characteristic peaks of ethylene glycol decreased significantly while the peak due to the protons of PEG appeared, but a small proportion of free (deprotected) aldehyde was also present. From the peak integration, the number of PEG grafted chains and of protected DPOx units left over was estimated to be 10 PEG chains per poly(2-oxazoline)s chain,

with 1.3 DPOx and 0.2 deprotected aldehyde. Since the initial $P(\text{MeOx}_{41}\text{-stat-DPOx}_9)\text{OH}$ contained 9 ethylene glycol protecting groups per chain, which could theoretically lead to 18 PEG grafted chains for a complete modification, these results suggested that cyclic PEG-type grafts were likely formed by transacetalization (see Scheme 3). This might be due to the fact that cyclic acetals are thermodynamically more stable than non-cyclic ones, mainly for entropic reasons.

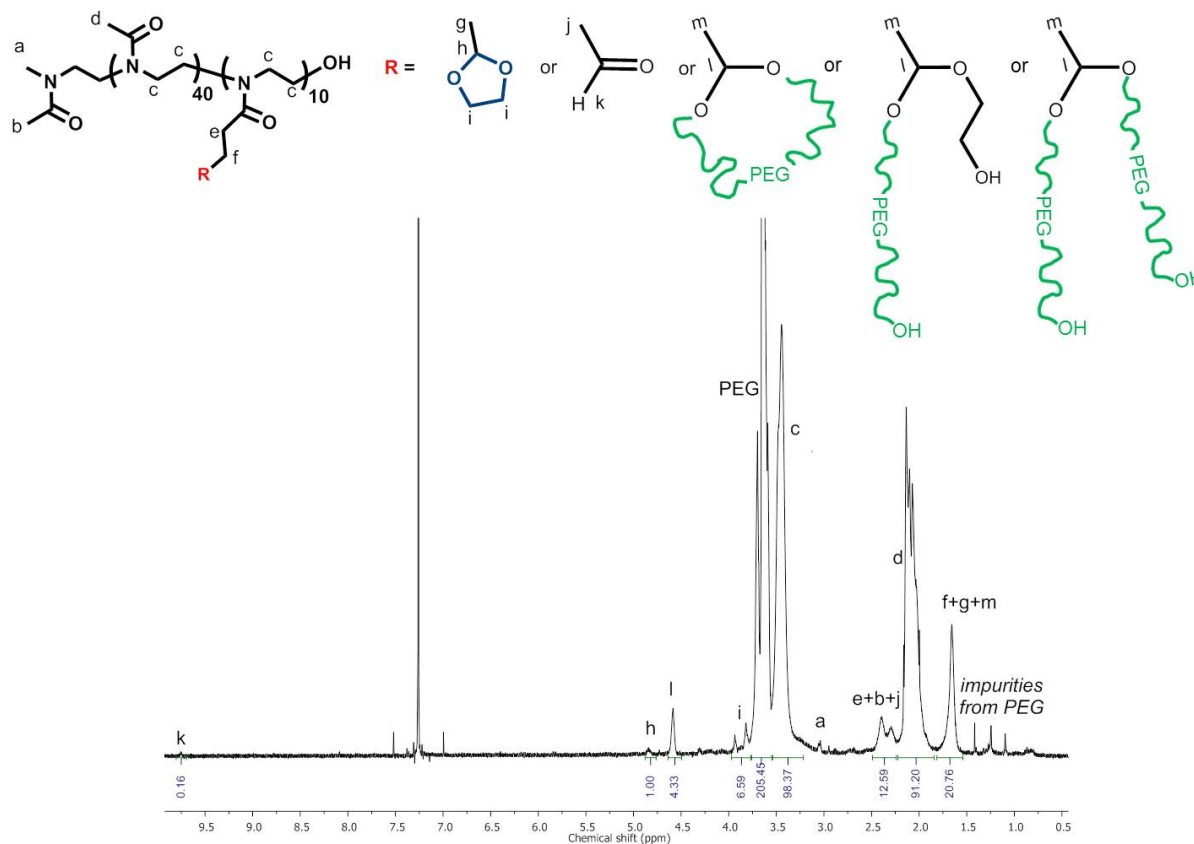


Figure 6 ^1H NMR spectrum after transacetalization between $P(\text{MeOx}_{41}\text{-stat-DPOx}_9)\text{OH}$ and PEG_{300}

Unfortunately, attempts to access hydrogels by intermolecular transacetalization reaction using substoichiometric amounts of PEG_{300} relatively to DPOx units were not successful. In contrast to the previous case, indeed, a co-solvent with a high boiling point was required because of the high solid content, in order to remove ethylene glycol as by-product. Use of a low molecular weight PEG dimethylether as co-solvent was unsuccessful due to solubility issues. Designing alternative monomers from protecting groups with lower boiling temperatures (e.g. dimethylacetal) might enable to achieve polyoxazoline-based hydrogels with PEG cross-linkers.

CONCLUSIONS

This study illustrates the versatility of protected and non-protected aldehyde-functional (co)poly(2-oxazoline)s for post-polymerization modification under mild conditions. A library of statistical copolymers derived from 2-methyl and 2-[3-(1,3)-dioxolan-2-ylpropyl]-2-oxazoline could be synthesized to this aim, with different contents of protected aldehyde and different polymer chain ends. Aldehyde handles along the polyoxazoline chains were shown to readily react with antagonistic groups, including amines and hydrazines, the functionality of which can be varied to generate grafted or 3D-cross-linked polymer derivatives. For instance, chemoselective ligation of adipic acid dihydrazide onto a statistical copolymer containing 10% of aldehyde enabled the synthesis of pH-responsive hydrogels. As the chemistry used for cross-linking is selective, it could allow for the simultaneous encapsulation or entrapment of molecules, such as drugs and proteins during the cross-linking process. Moreover, one could expect that the release of the encapsulated molecules could be controlled by the pH.

The aldehyde functional copolyoxazolines were also found to undergo an acid-catalyzed intermolecular self-aldolization, leading to branched structures and ultimately to cross-linked networks under forced conditions. The cross-linking process could be time controlled by adjusting the copolymer composition (*i.e.* the aldehyde function density and polymer end group).

Last but not least, copolymers with pendant aldehydes protected in the form of ketal rings could be directly modified by transacetalization using a large excess of a PEG precursor, generating preferentially cyclic pendant loops rather than PEG brushes.

The versatility of post-polymerization modification of aldehyde-based reactive platforms developed in this work, combined with the known properties of poly(2-oxazoline)s, thus expand the range of possibilities of this special class of polymeric materials.

EXPERIMENTAL SECTION

Materials and reagents

2-Methyl-2-oxazoline (99%), methyl trifluoromethanesulfonate (96%) (MeOTf), and acetonitrile (99%) were purchased from Sigma-Aldrich, stored over calcium hydride and purified by vacuum distillation prior to use. Methanol (Sigma-Aldrich) was refluxed with sodium and distilled prior to use. Dimethylsulfoxide (DMSO, from Sigma-Aldrich), dichloromethane (CH₂Cl₂, from Sigma-Aldrich) and tetrahydrofuran (THF,) were cryo-distilled prior to use. 2-(2-Bromoethyl)-1,3-dioxolane (Sigma-Aldrich) and piperidine (99%, from Acros) were distilled prior to use. Trifluoroacetic acid (99%) (TFA), diethyl ether, ethanol, potassium hydroxide (KOH), sodium hydroxide (NaOH), hydrochloric acid solution (37%) (HCl), cyclohexane (99%), *p*-toluene sulfonic acid (PTSA), sodium acetate and Jeffamine D400 were used as received from Sigma-Aldrich. Butyl lithium solutions in hexane (1.6 M), chloroform, magnesium sulfate (MgSO₄), sodium hydrogenocarbonate (NaHCO₃), ethyl acetate, cyclohexane and triethylamine were used as received. Tetramethylethylene diamine (TMEDA, from Sigma-Aldrich) was stirred with KOH pellets for 2 h before distillation. PEG₃₀₀ was purchased from Fluka and used as received. Benzylamine (98%), adipic acid dihydrazide (98%), PEG₃₅₀ monomethyl ether, molecular sieves 3Å (0.4-0.8 mm) and sodium cyanohydroborate (NaBH₃CN) were used as received from Alfa Aesar.

Instrumentation and measurements

NMR spectroscopy. ¹H NMR, ¹³C NMR and HSQC measurements were carried out at 298K on a Bruker Avance spectrometer operating at 400 MHz. CDCl₃ was used as an internal reference ($\delta = 7.26$ ppm), and the relaxation time was fixed to 2 sec for all measurements.

DOSY (Diffusion Ordered Spectroscopy) measurements were performed at 298K on a Bruker Avance III HD 400 spectrometer operating at 400.33 MHz and equipped with a 5 mm Bruker multinuclear z-gradient direct cryoprobe-head capable of producing gradients in the z-direction with strength 53.5 G/cm. The DOSY spectra were acquired with the *ledbpgp2s* pulse program from Bruker topspin software. The duration of the pulse gradients and the diffusion time were adjusted in order to obtain full attenuation of the signals at 95% of maximum gradient strength. The values were 2.5 ms for the duration of the gradient pulses and 150 ms for the diffusion time. The gradients strength was linearly incremented in 32 steps from 5% to 95% of the maximum gradient strength. A delay of 3 s between echoes was used. The data were processed using 8192 points in the F2 dimension and 64 points

in the F1 dimension with the Bruker topspin software. Field gradient calibration was accomplished at 25 °C using the self-diffusion coefficient of H₂O+D₂O at $19.0 \times 10^{-10} \text{ m}^2/\text{s}$.

¹³C CPMAS (cross polarization magic angle spinning) NMR measurements were carried out on a 9,4T spectrometer operating at 100.6 MHz and equipped with a CPMAS probe (impulsion at 90 °: 3.4 μs at 59.6 W, 2 ms contact time, 3 s relaxation time, 35 ms acquisition time).

Size-exclusion chromatography. Size-exclusion chromatography (SEC) using dimethylformamide (DMF) with LiBr (1 g/L) as the eluent was performed at 80 °C at a flow rate of 0.8 mL/min. The column set consisted of two 7.5 mm × 300 mm PLgel, 5 μm Mixed-D columns (Polymer laboratories) coupled to a 7.5 mm × 50 mm, PLgel, 5 μm guard column (Polymer laboratories). Injections were realized in a 20 μL loop and calibration was performed with polystyrene standard. Differential refractive index (RI) and UV detectors were used.

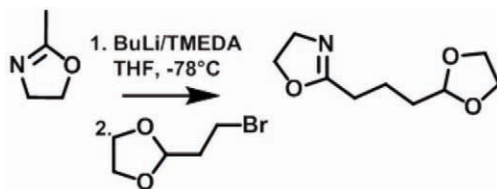
SEC was performed at 40 °C at a flow rate of 0.6 mL/min, using Tris buffer as the eluent. The column set consisted of two 8.0 mm × 300 mm columns, OHPak, 10 μm and 6 μm respectively (Shodex) coupled to a guard column, 6.0 mm × 500 mm, OHPak (Shodex). Injections were realized in a 20 μL loop and calibration was performed with PEG standards from Polymer Laboratories. Differential refractive index (RI) and UV detectors were used. Ethylene glycol was used as a flow marker.

Infrared spectroscopy. Infrared spectra were obtained from a Thermoscientific Nicolet IS10 spectrometer using the attenuated total reflection (ATR) mode. The spectra were acquired using 16 scans at a resolution of 4 wavenumbers.

Experimental procedures

Synthesis of 2-[3-(1,3)-dioxolan-2-ylpropyl]-2-oxazoline (DPOx)

2-[3-(1,3)-Dioxolan-2-ylpropyl]-2-oxazoline (DPOx) was synthesized following a procedure reported in the literature (Scheme 4).¹⁷

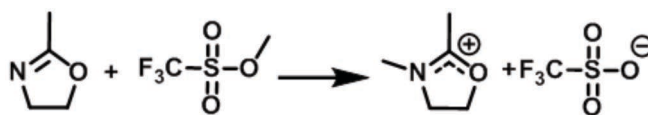


Scheme 4 Synthesis of 2-[3-(1,3)-dioxolan-2-ylpropyl]-2-oxazoline

In a flame-dried round bottom flask, under inert atmosphere, 8.2 mmol of TMEDA were dissolved in 37.5 mL of dry THF and cooled to $-78\text{ }^{\circ}\text{C}$. 7.8 mmol of a 1.6 M butyl lithium solution in hexane were added dropwise during 30 minutes, under strong stirring, with a syringe purged with nitrogen. The mixture turned yellow. The solution was stirred for 1 hour at $-78\text{ }^{\circ}\text{C}$. 8.2 mmol of MeOx in 3.75 mL of dry THF was then added dropwise to the reaction mixture. After 2 hours of stirring at $-78\text{ }^{\circ}\text{C}$, 6.9 mmol of 2-(2-bromoethyl)-1,3-dioxolane in 3.75 mL of dry THF was added slowly. The solution was allowed to re-equilibrate to room temperature under stirring overnight. 5 mL of methanol was added to quench the reaction by deactivating the butyl lithium. A color change from brownish to light yellow was observed at this point. The solvent was then removed under reduced pressure, and the oily yellow residue dissolved in a mixture of 25 mL of chloroform and 25 mL of a saturated NaHCO_3 solution. The aqueous phase was extracted twice with 12.5 mL of chloroform. The organic phases were combined, dried over MgSO_4 and concentrated under reduced pressure. The crude product was subsequently purified by column chromatography (silica, mobile phase: ethyl acetate/cyclohexane/triethylamine, ratio 10/5/1), and distillation. A colorless liquid is obtained, yield = 262 mg (49%). ^1H NMR (CDCl_3): δ (ppm) 4.8 (t, 1H, $\text{CH}_2\text{CH}(\text{OR}_2)$), 4.2 (t, 2H, $\text{NCH}_2\text{CH}_2\text{O}$), 4-3.75 (m, 6H, $\text{NCH}_2\text{CH}_2\text{O}/\text{OCH}_2\text{CH}_2\text{O}$), 2.35 (t, 2H, $\text{NOCCH}_2\text{CH}_2$), 1.75 (m, 4H, $\text{CH}_2\text{CH}_2\text{CH}_2\text{CH}$). ^{13}C NMR (CDCl_3): δ (ppm) 169 (NOCCH_2), 105 ($\text{CH}_2\text{CH}(\text{OR}_2)$), 67 ($\text{NCH}_2\text{CH}_2\text{O}$), 64 ($\text{OCH}_2\text{CH}_2\text{O}$), 54 ($\text{NCH}_2\text{CH}_2\text{O}$), 33 ($\text{NOCCH}_2\text{CH}_2$), 27 ($\text{CH}_2\text{CH}_2\text{CH}_2\text{CH}$), 19 ($\text{CH}_2\text{CH}_2\text{CH}_2\text{CH}$). NMR Spectrum given in Figure S1

Synthesis of N-methyl-2-methyl-2-oxazolinium triflate (MeOxOTf)

N-methyl-2-methyl-2-oxazolinium triflate (MeOxOTf) was synthesized following the procedure described by Kobayashi *et al* (Scheme 5).⁵⁷



Scheme 5 Synthesis of N-methyl-2-methyl-2-oxazolinium triflate

2 mmol of MeOx in 400 μL of CH_2Cl_2 was put into a flame dried Schlenk flask and cooled in ice. 4 mmol of MeOTf was added dropwise to the reaction mixture. The mixture was then stirred for 2 hours at room temperature and a color changed from clear to dark red was observed. The product was collected by precipitation into cold diethyl ether and dried under vacuum. Yield = 404 mg (81%). ^1H NMR (CDCl_3): δ (ppm) 5 (t, 2H, $\text{NCH}_2\text{CH}_2\text{O}$), 4.3 (t, 2H, $\text{NCH}_2\text{CH}_2\text{O}$), 3.45 (s, 3H, NCH_3), 2.5 (s, 3H, CNOCH_3). NMR Spectrum given in Figure S2

Synthesis of poly(2-[3-(1,3)-dioxolan-2-ylpropyl]-2-oxazoline) (PDPOx₂₁). A typical procedure is as follows. In a flame dried Schlenk flask, 4.4 mL of acetonitrile was introduced under vacuum. 10.8 mg (0.043 mmol) of MeOxOTf and 200 mg (1.07 mmol) of DPOx were added. The flask was maintained at 85 °C for 3 days, and the reaction was quenched by adding 2.7 equivalents of a 0.3N KOH solution in methanol. The solution was left to stir at room temperature overnight and the polymer was precipitated twice into diethyl ether and dried under vacuum. Yield = 95 mg (48 %). \bar{D} = 1.17. DP = 21. ¹H NMR (CDCl₃): δ (ppm) 4.86 (s, CH₂CH(OR)₂), 3.95-3.8 (m, OCH₂CH₂O), 3.6-3.3 (s, NCH₂CH₂), 2.8 (d, CH₃-NCH₂CH₂), 2.4-2.1 (m, NCOCH₂CH₂), 1.7-1.4 (s, NCOCH₂CH₂CH₂). ¹³C NMR (CDCl₃): δ (ppm) 174-172 (NCOCH₂), 104.4 (CH₂CH(OR)₂), 65 (OCH₂CH₂O), 48-41 (NCH₂CH₂N), 34-32 (NCOCH₂CH₂CH₂CH), 20 (NCOCH₂CH₂CH₂CH). IR: 3459 (w), 2947 (w), 2882 (w), 2767 (s), 1630 (m), 1566 (s), 1450 (w), 1366 (s), 1256 (s), 1224 (s), 1132 (m), 1029 (m), 939 (m) cm⁻¹.

Synthesis of poly[(2-methyl-2-oxazoline)-co-(2-[3-(1,3)-dioxolan-2-ylpropyl]-2-oxazoline)]: P(MeOx₄₀-stat-DPOx₁₀)OH, P(MeOx₄₀-stat-DPOx₁₀)pip, P(MeOx₉₀-stat-DPOx₁₀)OH, P(MeOx₉₀-stat-DPOx₁₀)pip. Synthesis of P(MeOx₄₀-stat-DPOx₁₀)OH: In a flame dried Schlenk flask, 22.5 mL of acetonitrile was introduced under vacuum. 55 mg (0.22 mmol) of MeOxOTf, 407 mg (2.2 mmol) of DPOx and 750 mg (8.8 mmol) of MeOx were added. The flask was heated at 85 °C for 3 days, and the reaction was quenched by adding 2.7 equivalents of a 0.3 N KOH solution in methanol. The solution was left to stir at room temperature overnight and the polymer was precipitated twice in diethyl ether and dried under vacuum. ¹H NMR (CDCl₃): δ (ppm) 4.86 (s, CH₂CH(OR)₂), 3.95-3.8 (m, OCH₂CH₂O), 3.6-3.3 (s, NCH₂CH₂), 2.8 (d, CH₃-NCH₂CH₂), 2.4-2.1 (m, NCOCH₂CH₂), 2.2-2 (m, NCOCH₃), 1.7-1.4 (s, NCOCH₂CH₂CH₂). ¹³C NMR (CDCl₃): δ (ppm) 174-173 (NCOCH₂), 172-170 (NCOCH₃), 104.4 (CH₂CH(OR)₂), 65 (OCH₂CH₂O), 48-41 (NCH₂CH₂N), 34-32 (NCOCH₂CH₂CH₂CH), 20 (NCOCH₂CH₂CH₂CH).

P(MeOx₄₀-stat-DPOx₁₀)pip, P(MeOx₉₀-stat-DPOx₁₀)OH and P(MeOx₉₀-stat-DPOx₁₀)pip were synthesized following a similar procedure to that described above, using the respective [MeOx]₀/[DPOx]₀ ratio and termination agent (St†).

P(MeOx₉₀-stat-DPOx₁₀)pip was synthesized as follows in a stainless steel reactor at 140 °C. 1.55 mL of acetonitrile, 0.766 mg (9 mmol) of MeOx, 185 mg (1 mmol) of DPOx and 25 mg (0.1 mmol) of MeOxOTf were added into the reactor, in the glovebox. The global monomer concentration was 4M. The reactor was then heated at 140 °C for 1 hour and cooled in an ice bath. 2.7 eq. of piperidine was added to quench the reaction. The solution was left to stir at room temperature overnight and the polymer was precipitated twice into diethyl ether and dried under vacuum.

Table 1 Characteristics of DPOx-based copolymers

$\frac{[\text{MeOx}]_0}{[\text{I}]_0}$ a)	D_{PMeOx} b)	$\frac{[\text{DPOx}]_0}{[\text{MeOTf}]_0}$ a)	DP_{DPOx} b)	Yield (%)	\bar{D} c)	T (°C)	Termination agent	Polymer
40	41	10	9	91	1.14	85	Methanol KOH (0.3 N)	P(MeOx ₄₁ -stat-DPOx ₉)OH
40	63	10	14		1.28	85	Piperidine	P(MeOx ₆₃ -stat-DPOx ₁₄)pip
90	124	10	12		1.13	85	Methanol KOH (0.3N)	P(MeOx ₁₂₄ -stat-DPOx ₁₂)OH
90	93	10	11	80	1.34	85	Piperidine	P(MeOx ₉₃ -stat-DPOx ₁₁)pip
90	101	10	10		1.61	140	Piperidine	P(MeOx ₁₀₁ -stat-DPOx ₁₀)pip

a) Initial monomer to initiator molar ratio

b) Experimental degree of polymerization as determined by ¹H NMR spectroscopy

c) Dispersity index as determined by SEC in Tris buffer

Deprotection of the aldehyde functionality: synthesis of poly[2-(4-oxobutyl)-2-oxazoline] (POBOx).

Deprotection of aldehyde functions of (co)polymers based on DPOx was carried out under acidic conditions, following a procedure described by Taubmann *et al.* ¹⁷. In a typical experiment, 150 mg of PDPOx₂₁ was dissolved in 4 mL of 5% aqueous TFA solution (v/v). The solution was transferred into a dialysis membrane (Cut-off 1000 g/mol) and dialyzed for 2–3 h against 400 mL of the same aqueous TFA solution. The polymer solution was then dialyzed twice against 2 L deionized water (2 h) until the pH returned to neutrality and lyophilised, yielding the following (co)polymers.

POBOx₂₁: Yield = 128 mg (86%). ¹H NMR (CDCl₃): δ (ppm) 9.7 (s, CH₂CHO), 3.6-3.3 (s, NCH₂CH₂), 2.8 (d, CH₃-NCH₂CH₂), 2.4-2.1 (m, NCOCH₂CH₂CH₂CHO), 1.7-1.4 (s, NCOCH₂CH₂CH₂). ¹³C NMR (CDCl₃): δ (ppm) 202 (CH₂CHO), 174-173 (NCOCH₂), 48-41 (NCH₂CH₂N/ NCOCH₂CH₂CH₂CHO), 34-32 (NCOCH₂CH₂CH₂CHO), 18-15 (NCOCH₂CH₂CH₂CHO). IR: 3400 (w), 2938 (m), 2731 (s), 1714 (m), 1617 (m), 1418 (m), 1245 (s), 1166 (s), 1123 (s), 1067 (s), 981 (s) cm⁻¹.

For P(MeOx₄₁-stat-OBOx₉)OH: ¹H NMR (CDCl₃): δ (ppm) 9.7 (s, CH₂CHO), 3.6-3.3 (s, NCH₂CH₂), 2.8 (d, CH₃-NCH₂CH₂), 2.5-2.1 (m, NCOCH₂CH₂CH₂CHO), 2.2-2 (m, NCOCH₃), 1.9-1.6 (s, NCOCH₂CH₂CH₂). ¹³C NMR (CDCl₃): δ (ppm) 202 (CH₂CHO), 174-173 (NCOCH₂), 172-170 (NCOCH₃), 48-41 (NCH₂CH₂N/ NCOCH₂CH₂CH₂CHO), 34-32 (NCOCH₂CH₂CH₂CHO), 20 (NCOCH₃), 18-15 (NCOCH₂CH₂CH₂CHO).

Conjugation of POBOx with amino-containing reagents. A typical procedure is as follows. 5 mg of POBO_{x21} was dissolved in 1 mL of a 2% sodium acetate solution (pH = 5.6) overnight. 3 μ L of benzylamine was added into the polymer solution, and the mixture was stirred for 1h at room temperature. 43 μ L of sodium cyanohydroborate (10 eq. of a 20 mg/mL solution) was added, and the solution was freeze-dried, re-dispersed in a mixture of chloroform and acetonitrile (1/1) and precipitated into diethyl ether. The polymer was dried under vacuum. IR: 3408 (w), 3000 (s), 2934 (s) 1580 (m), 1407 (m), 1248 (s), 1183 (s), 1043 (m), 1012 (m), 923 (m), 736 (s), 700 (s), 646 (m), 609 (m) cm⁻¹.

The same procedure was used for conjugation of adipic acid dihydrazide and Jeffamine D400 instead of benzylamine.

IR - Adipic acid dihydrazide: 3420 (w), 3248 (w), 2938 (m), 2865 (s), 1621 (m), 1556 (s), 1454 (m), 1421 (m), 1367 (s), 1246 (s), 1175 (m), 1123 (s), 1057 (s), 935 (s) cm⁻¹.

IR - Jeffamine D400: 3305 (w), 2968 (w), 2929 (w), 2666 (w), 2322 (s), 1636 (m), 1449 (m), 1421 (m), 1372 (m), 1344 (s), 1298 (s), 1246 (s), 1090 (w), 1017 (s), 923 (s) cm⁻¹.

Hydrogel formation from POBOx-based copolymers with the bis-hydrazido-containing cross-linker. 10 mg of P(MeOx₉₃-stat-OBOx₁₁)pip was dissolved in 50 μ L of dry DMSO in the presence of molecular sieves (3 \AA). In a separate Schlenk flask, 10 mg of adipic acid dihydrazide was dissolved in 100 μ L of dry DMSO. 5 μ L of a 50 mg/mL sodium acetate solution in dry methanol was added to the polymer solution. Adipic acid dihydrazide solution was added to the polymer solution, and formation of a hydrogel was immediately observed.

Transacetalization reaction from protected PDPOx with an excess of PEG₃₀₀. In a Schlenk flask, 20 mg of P(MeOx₄₁-stat-DPOx₉)OH, 300 mg of PEG₃₀₀ and 3.5 mg of *p*-toluene sulfonic acid (PTSA) were added. Once the mixture was homogeneous, it was heated to 100 °C over 6 hours, in a distillation setup. The mixture was dialyzed against water (3500 MW cut-off) for 3 days and lyophilized. ¹H NMR (CDCl₃): δ (ppm) 9.7 (s, CH₂CHO), 4.86 (s, CH₂CH(OR)₂), 3.95-3.8 (m, OCH₂CH₂O), 3.8-3.6 (m, PEG), 3.6-3.3 (s, NCH₂CH₂), 2.8 (d, CH₃-NCH₂CH₂), 2.4-2.1 (m, NCOCH₂CH₂, CH₂CHO), 2.2-2 (m, NCOCH₃), 1.7-1.4 (s, NCOCH₂CH₂CH₂, CH₂CH(PEG)₂).

SUPPORTING INFORMATION

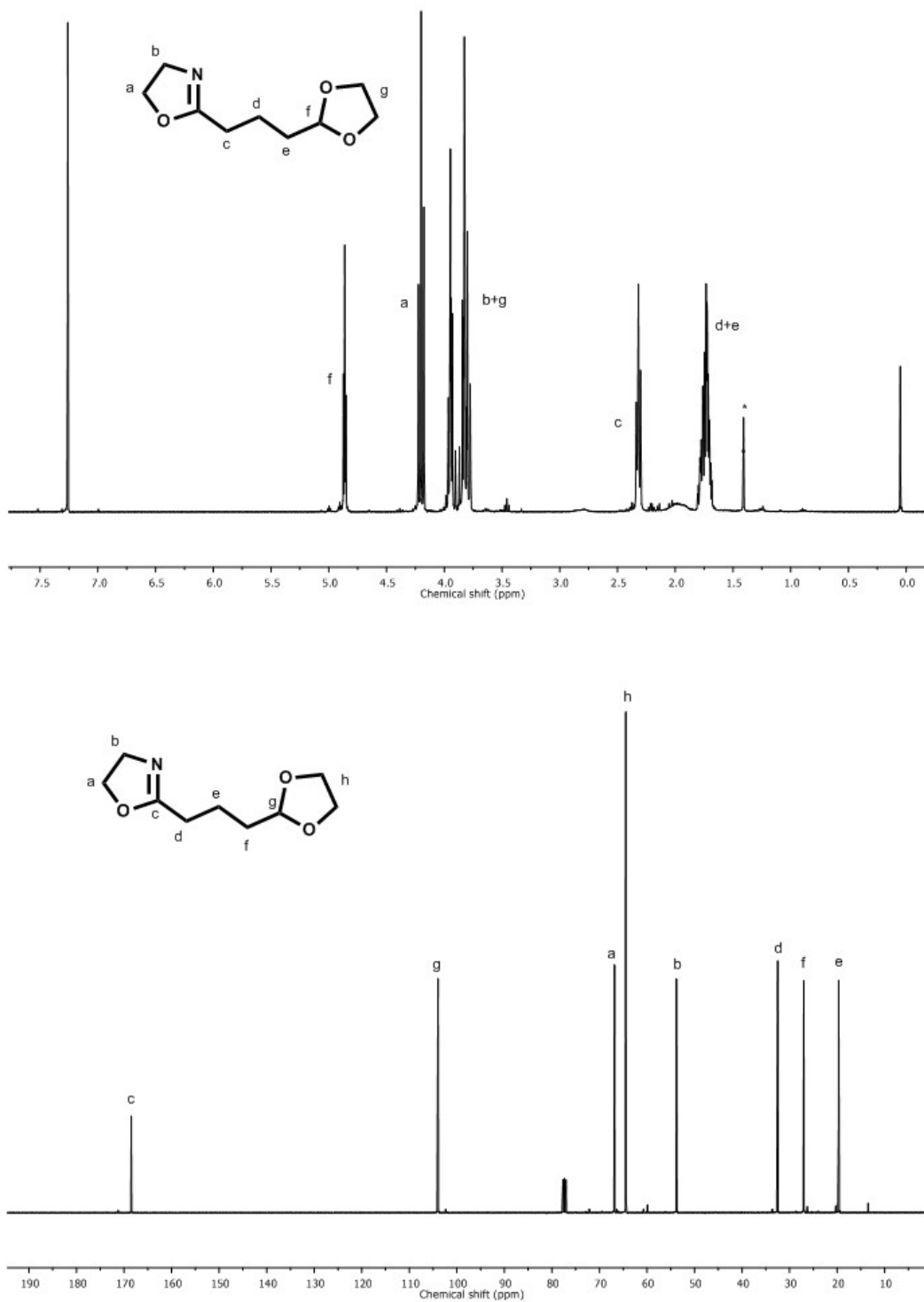


Figure S1 ¹H and ¹³C NMR spectra (400 MHz, CDCl₃) of 2-[3-(1,3)-dioxolan-2-ylpropyl]-2-oxazoline (DPOx)

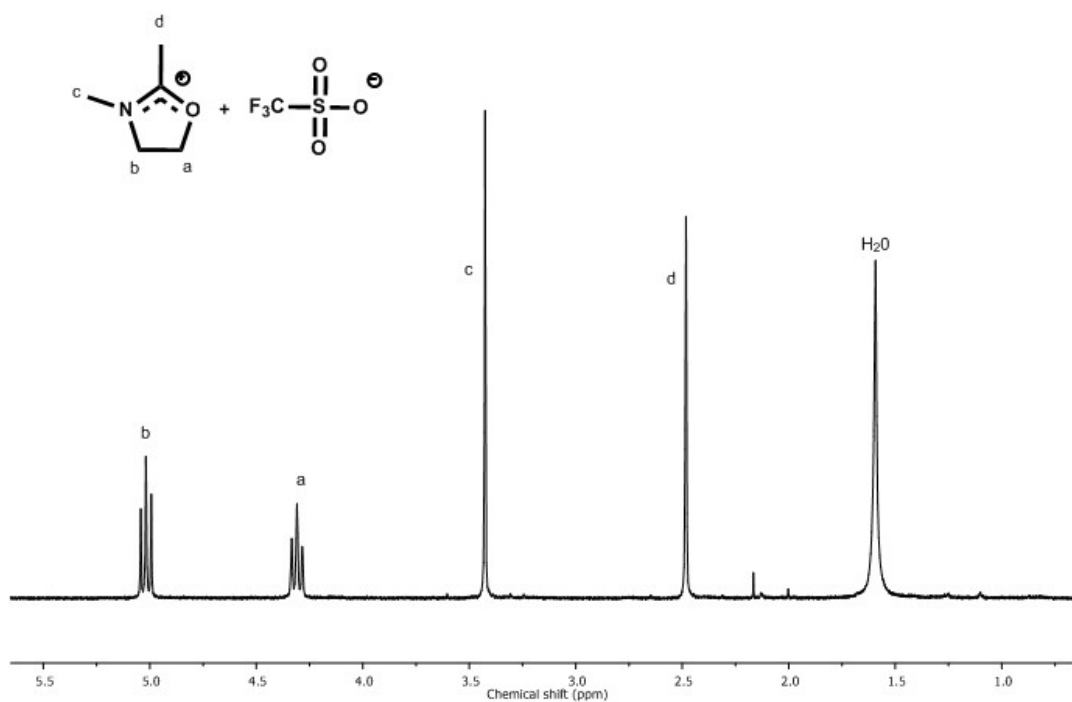


Figure S2 ¹H NMR spectrum (400 MHz, CDCl₃) of N-methyl-2-methyl-2-oxazolinium triflate

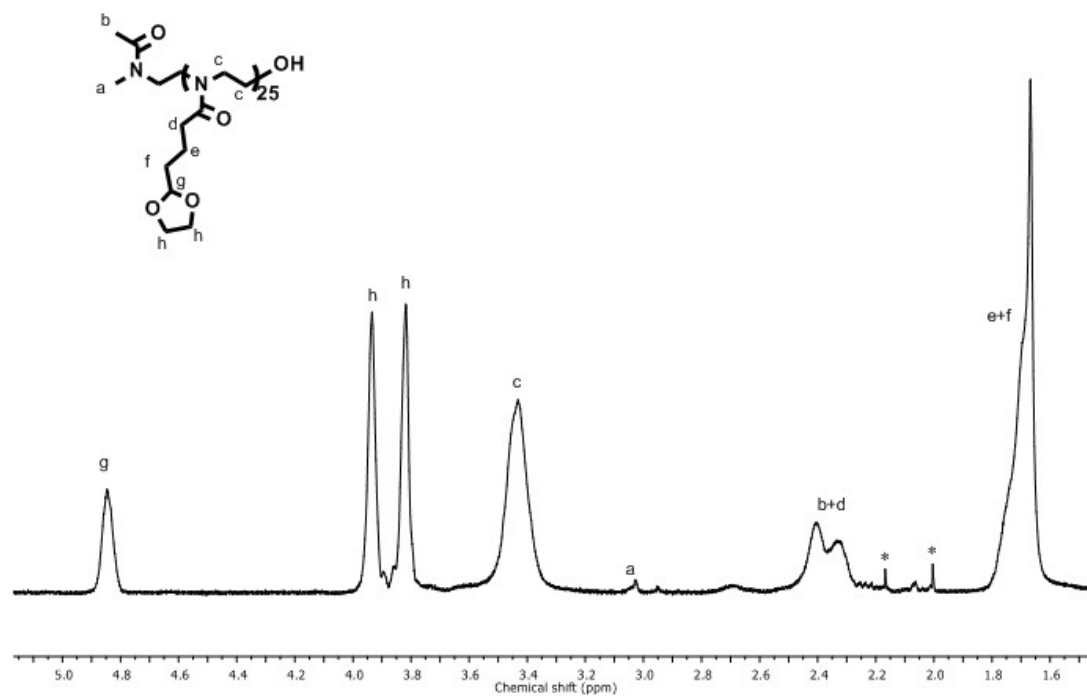


Figure S3 ¹H NMR spectrum (400 MHz, CDCl₃) of poly(2-[3-(1,3)-dioxolan-2-ylpropyl]-2-oxazoline)₂₁ (PDPOx₂₁)

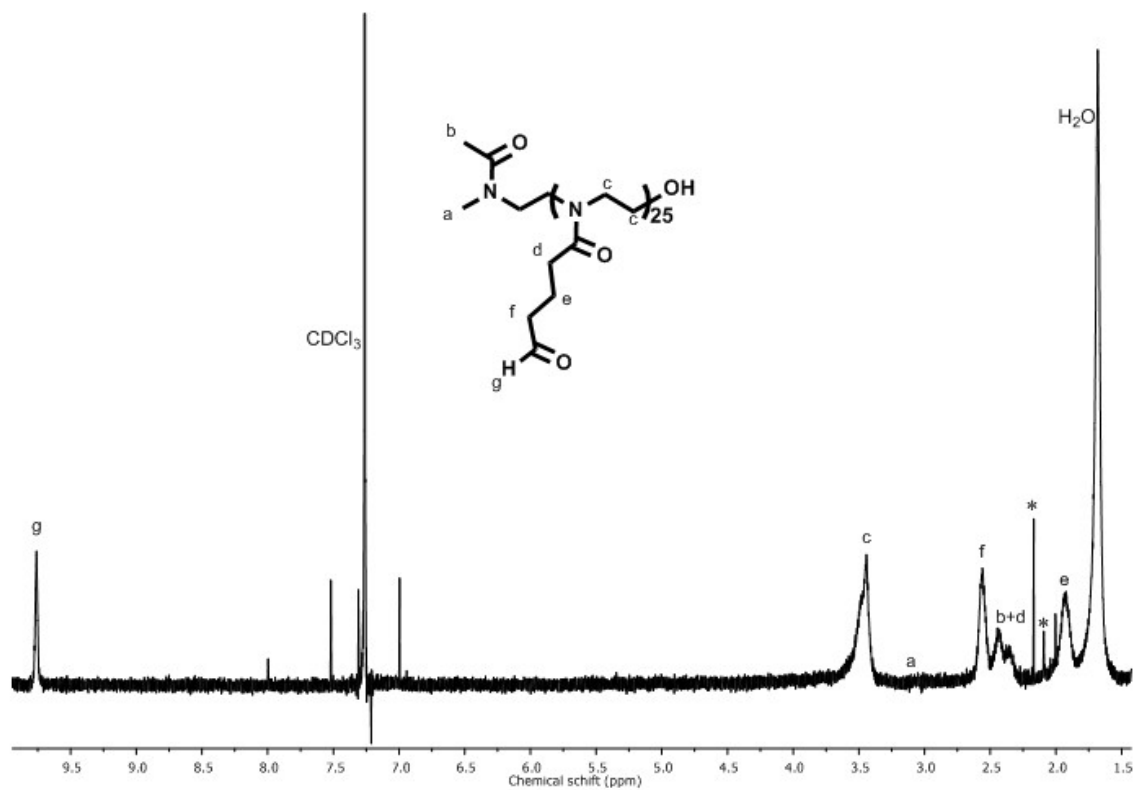


Figure S4 ^1H NMR spectrum (400 MHz, CDCl_3) of PDPOx_{21} after deprotection (POBOx_{21})

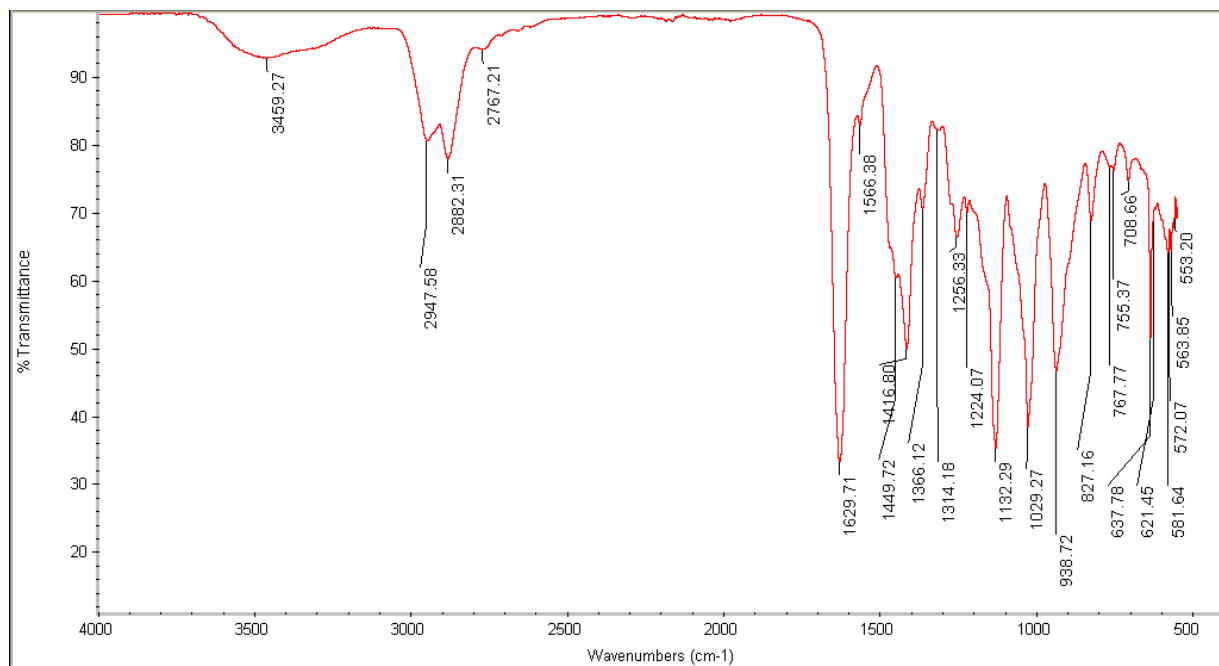


Figure S5 FTIR spectrum of PDPOx_{21}

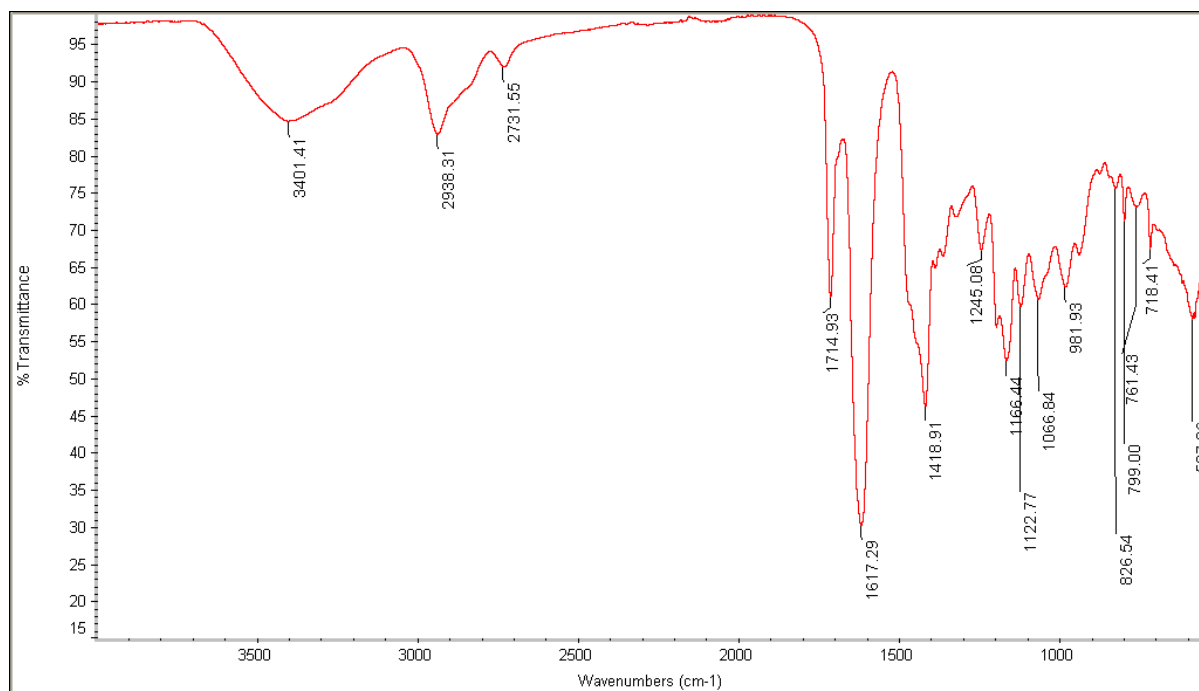


Figure S6 FTIR spectrum of POBO_{x21}

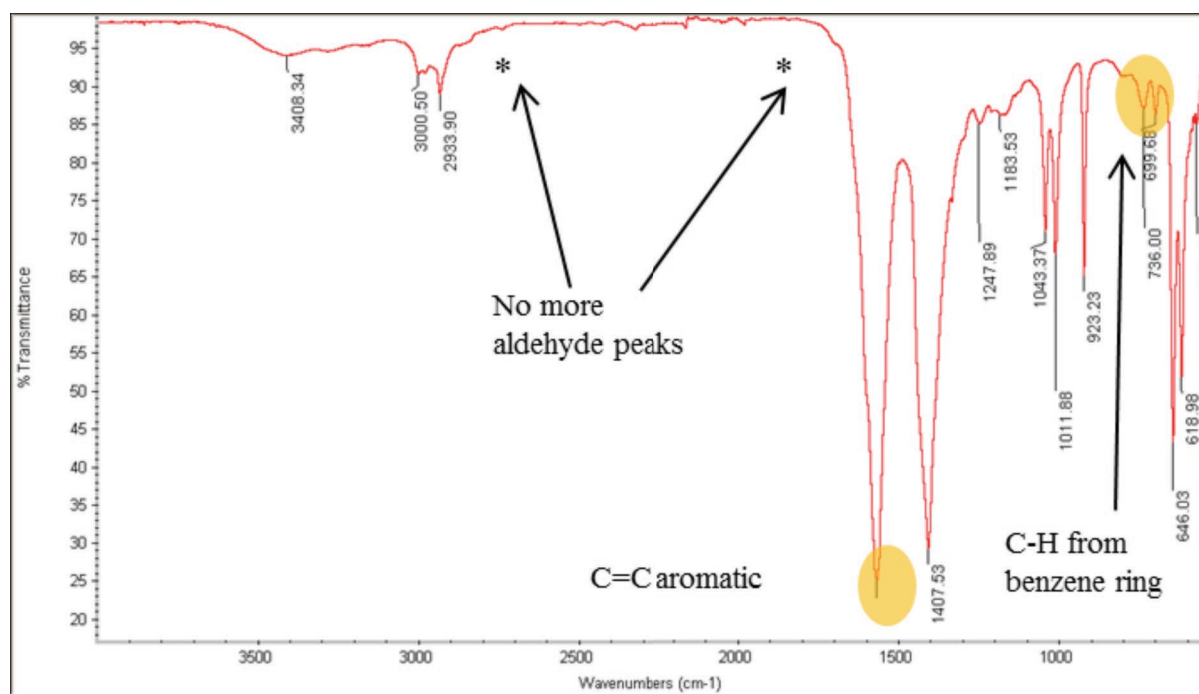


Figure S7 FTIR spectrum of POBO_{x21} after reaction with benzylamine

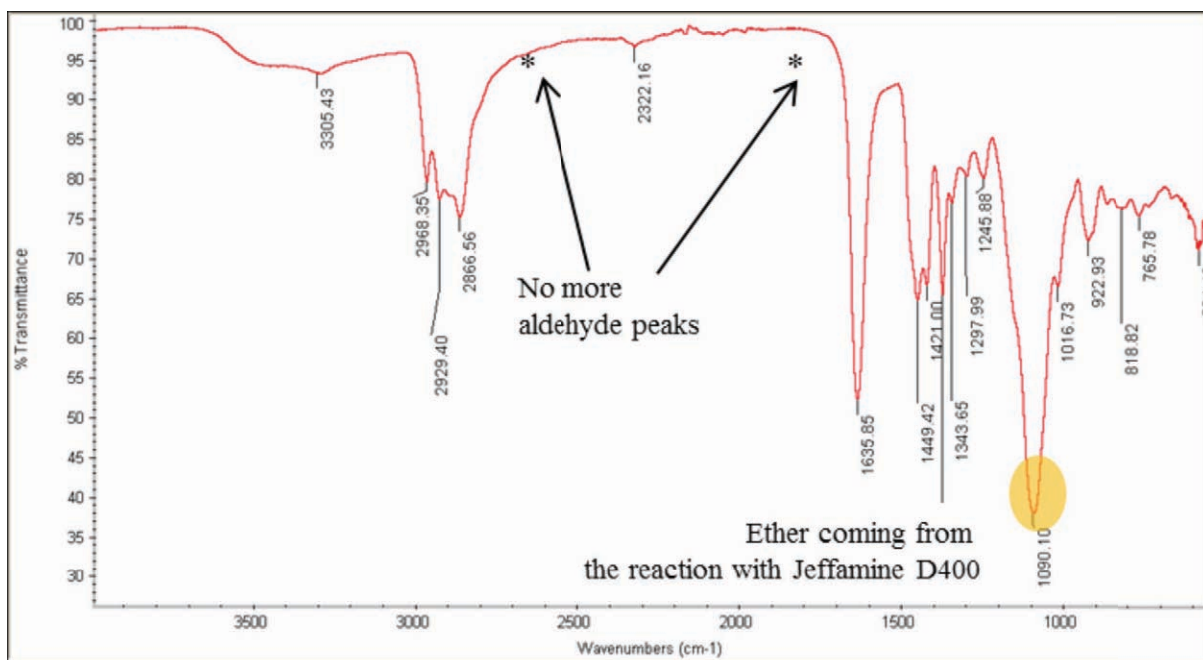


Figure S8 FTIR spectrum of POBO_{x21} after reaction with Jeffamine D400

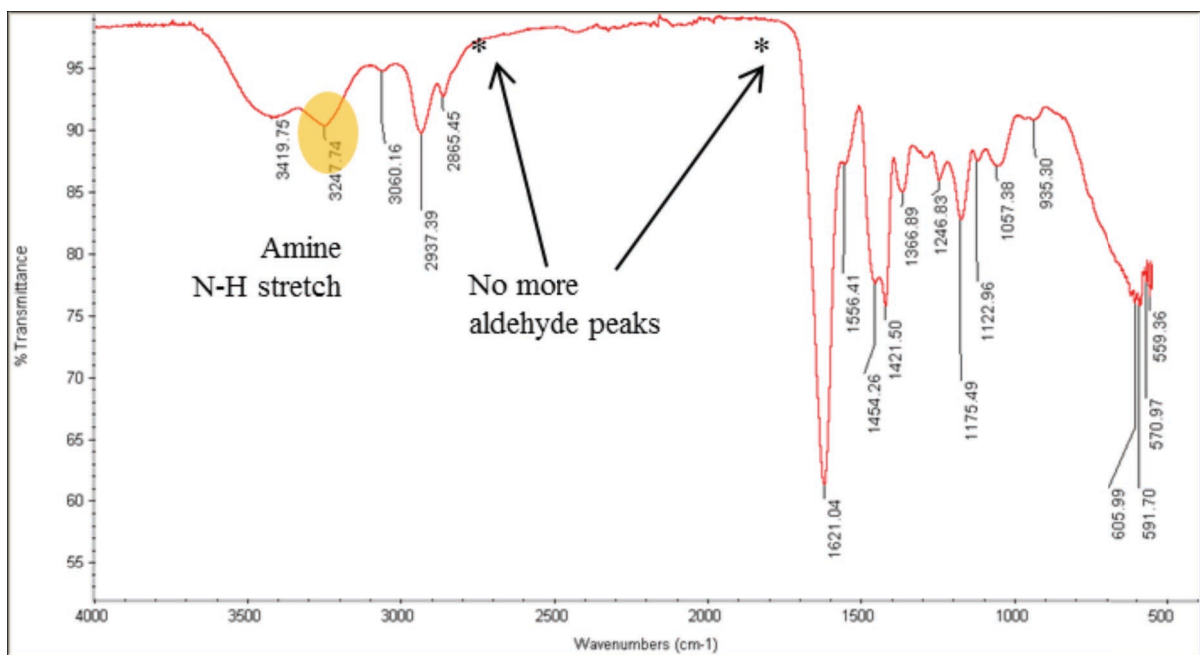


Figure S9 FTIR spectrum of POBO_{x21} after reaction with adipic acid dihydrazide

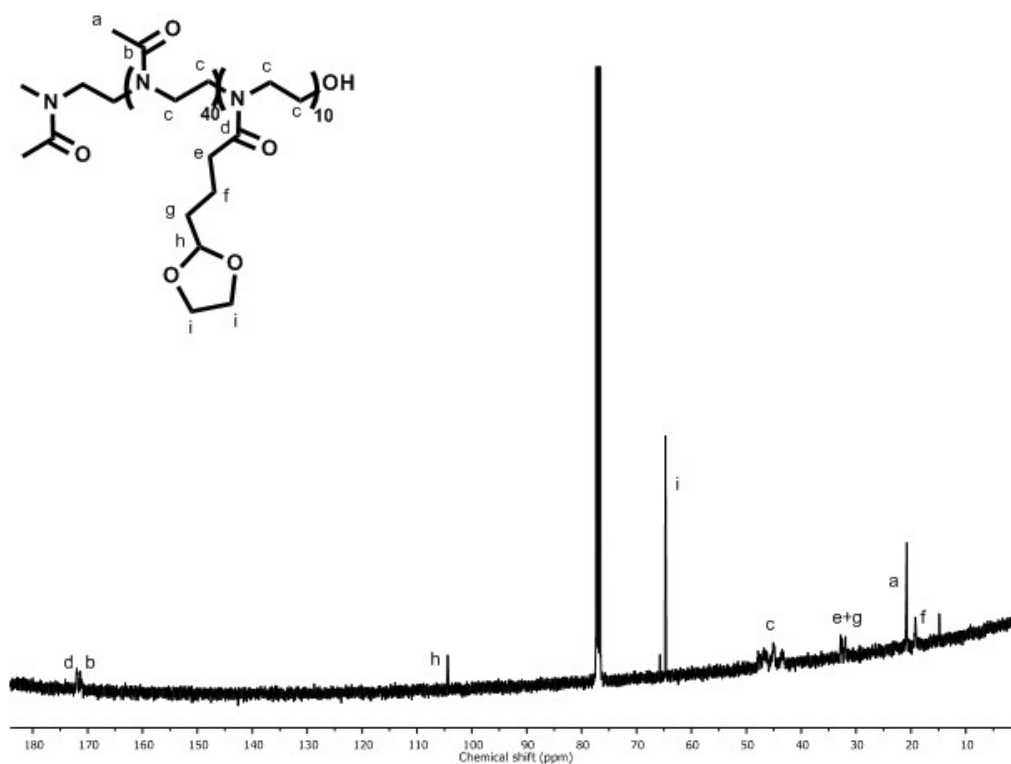
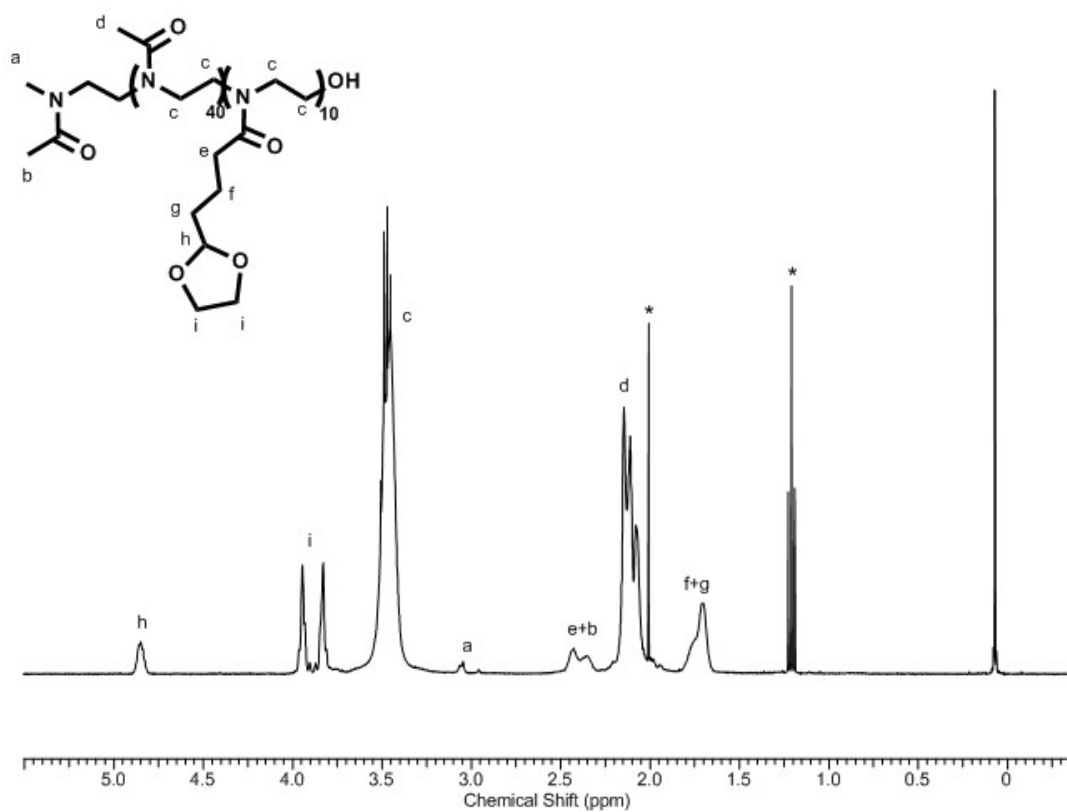


Figure S10 ¹H and ¹³C NMR spectra (400 MHz, CDCl₃) of P(MeO_{x41}-stat-DPO_{x9})OH

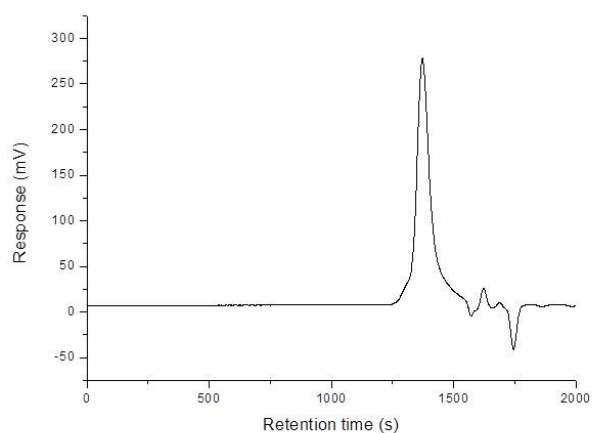


Figure S11 SEC trace of P(MeOx₄₁-stat-DPOx₉)OH in DMF

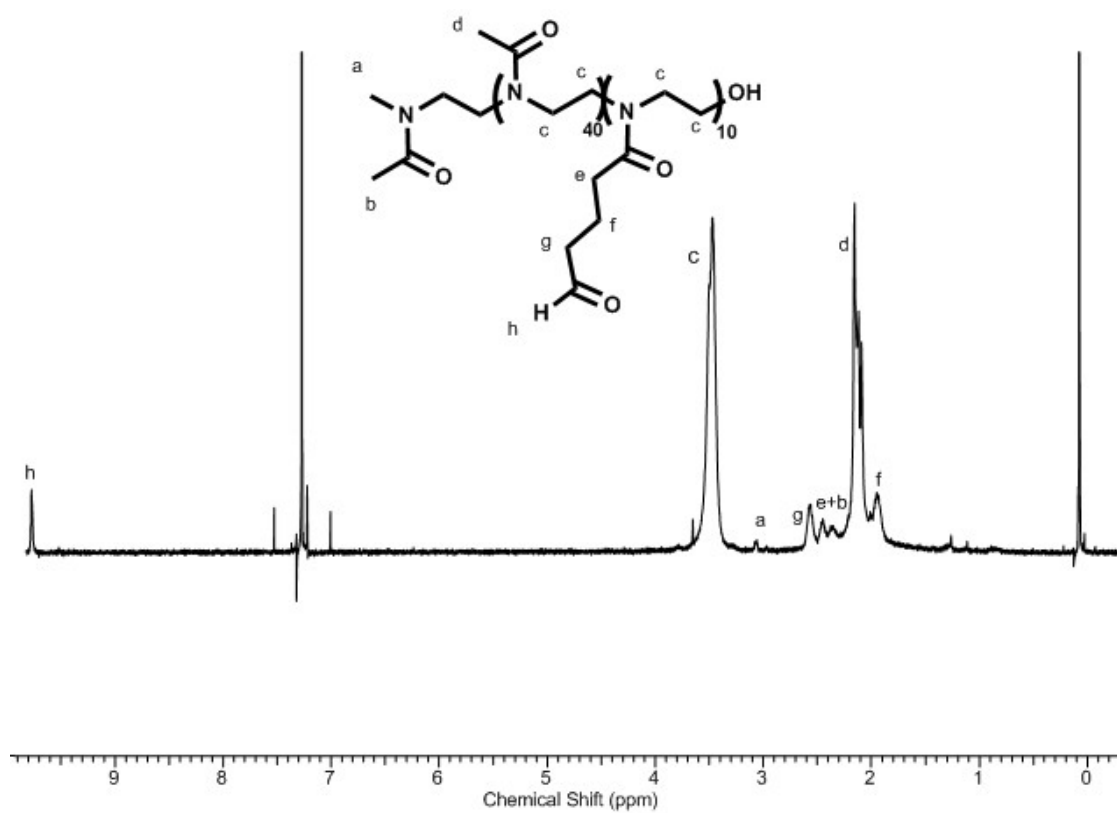


Figure S12 ¹H NMR spectrum (400 MHz, CDCl₃) of P(MeOx₄₁-stat-DPOx₉)OH after deprotection (P(MeOx₄₁-stat-OBOx₉)OH)

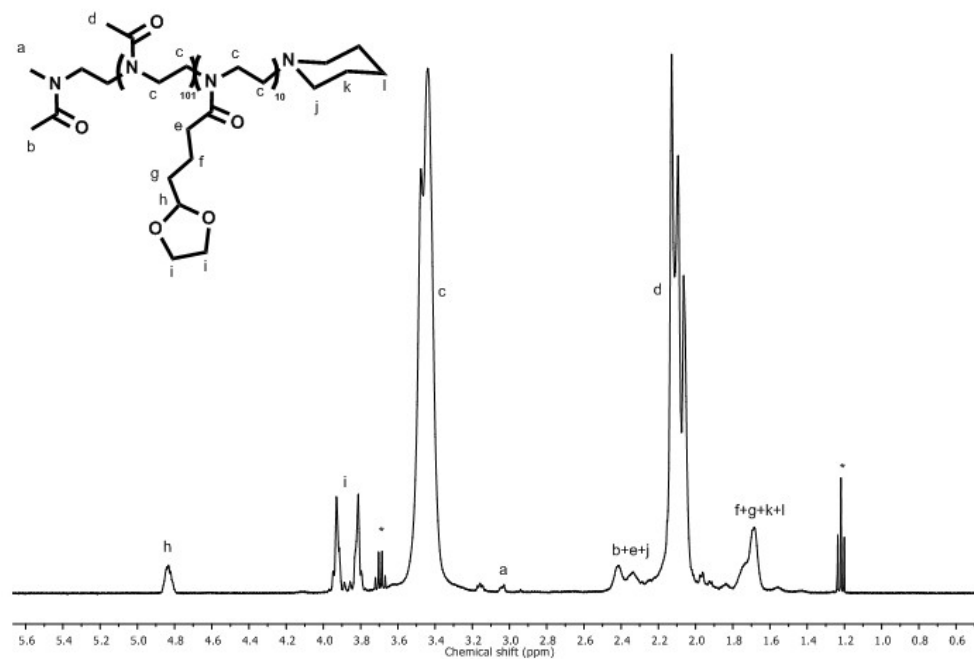


Figure S13 ¹H NMR spectrum (400 MHz, CDCl₃) of P(MeOx₁₀₁-stat-DPOx₁₀)pip

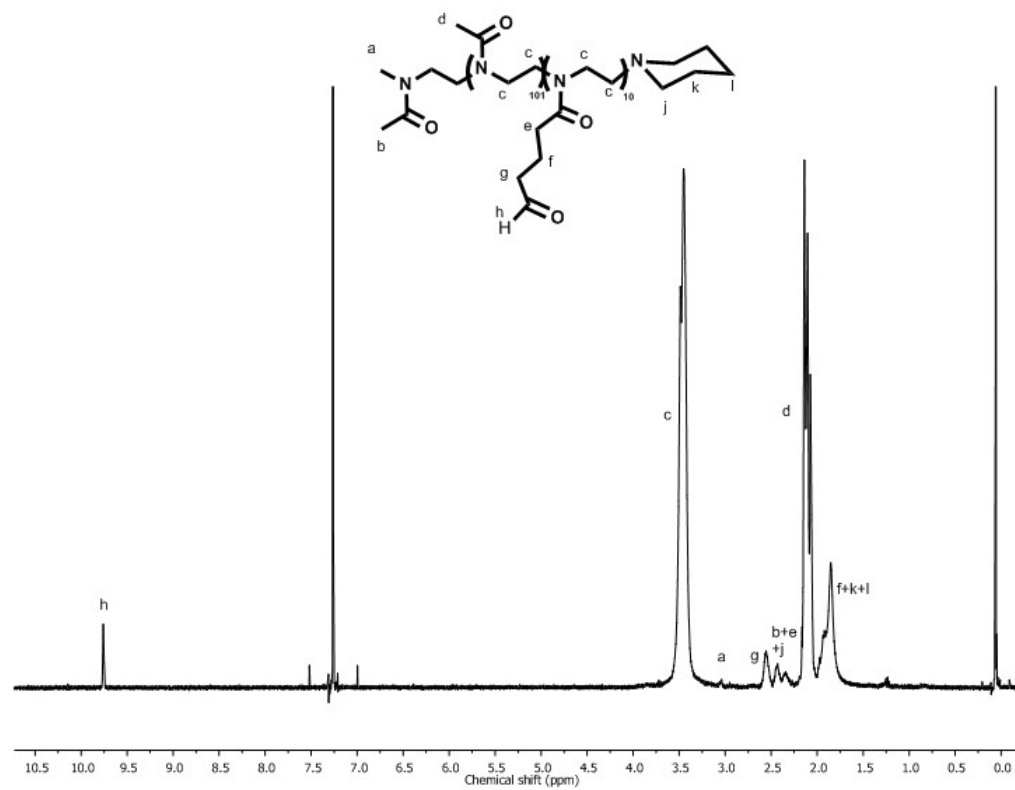


Figure S14 ¹H NMR spectrum (400 MHz, CDCl₃) of P(MeOx₁₀₁-stat-OBOx₁₀)pip

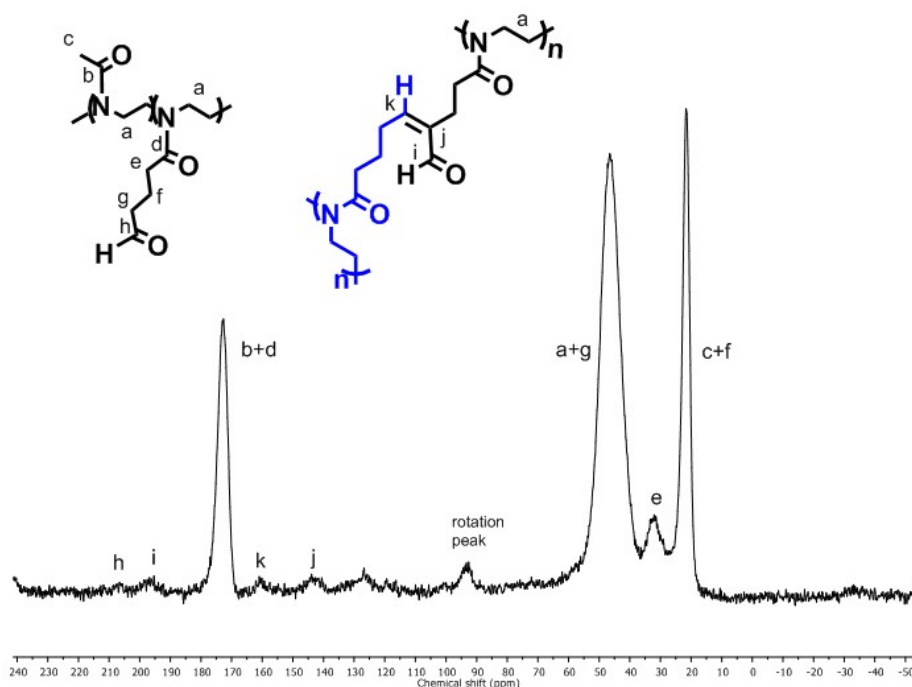


Figure S15 Solid ^{13}C NMR spectrum of the self cross-linked $\text{P}(\text{MeOx}_{40}\text{-stat-OBOx}_{10})\text{OH}$, rotation speed = 8000 Hz, ns = 7000

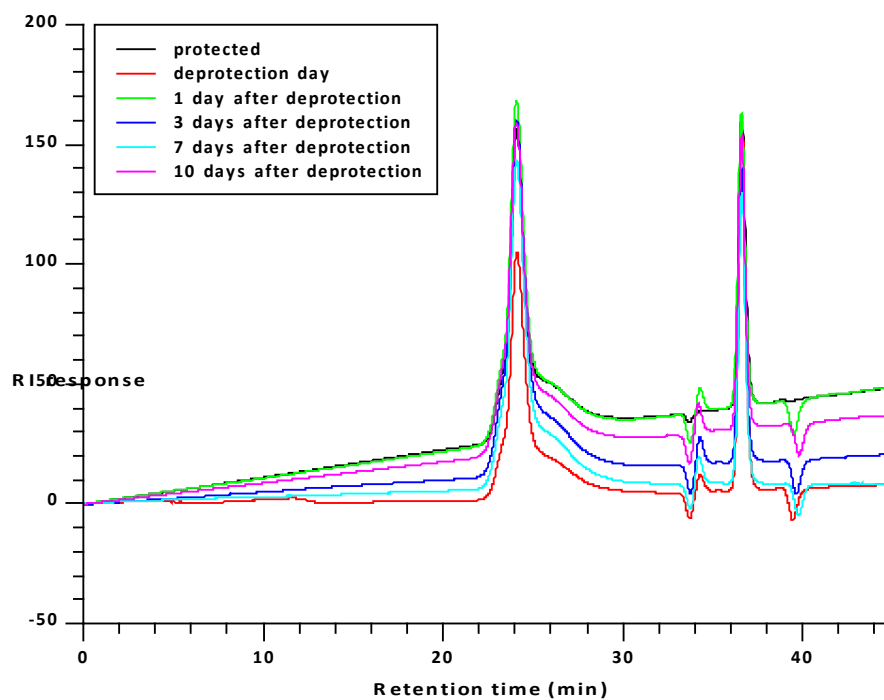


Figure S16 Evolution with time of the SEC traces in Tris buffer of $\text{P}(\text{MeOx}_{124}\text{-stat-OBOx}_{12})\text{OH}$

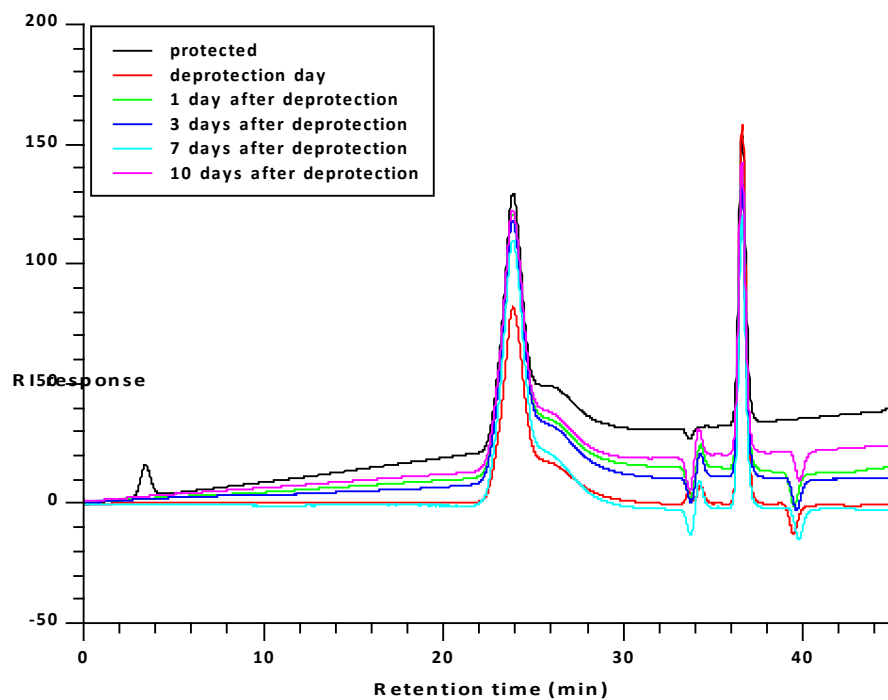


Figure S17 Evolution with time of the SEC traces in Tris buffer of P(MeOx₉₃-stat-OBOx₁₁)pip

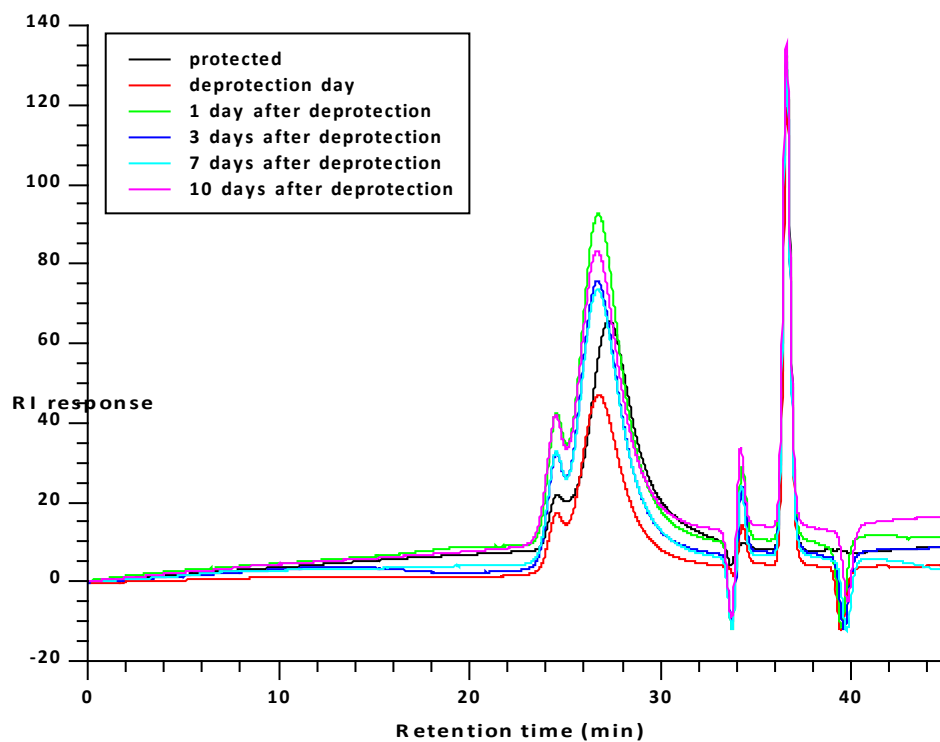


Figure S18 Evolution with time of the SEC traces in Tris buffer of P(MeOx₆₃-stat-OBOx₁₄)pip

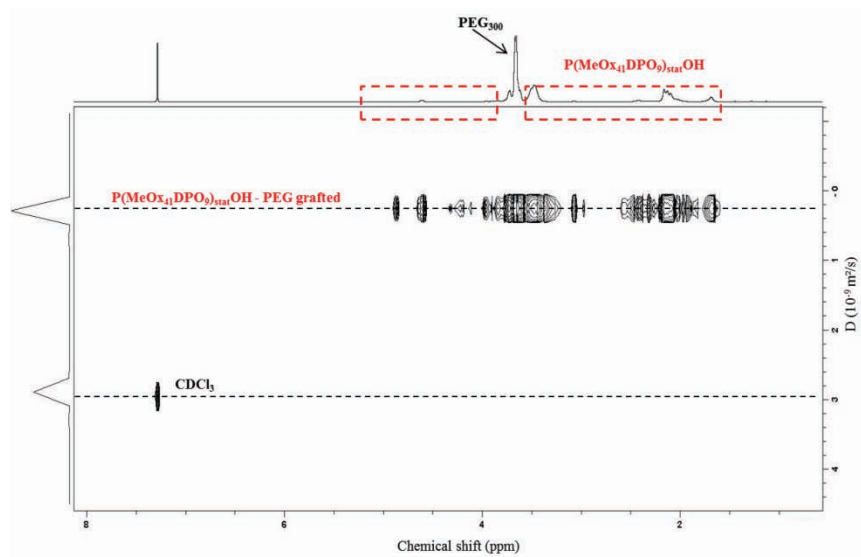
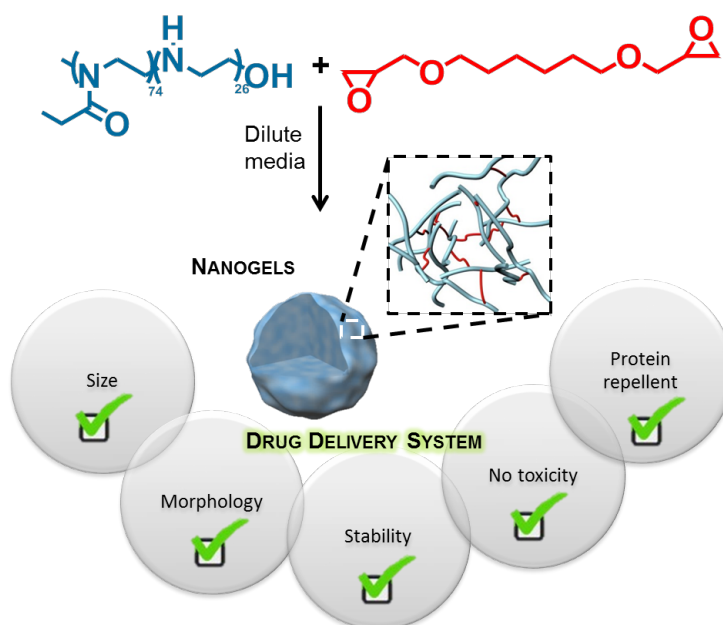


Figure S19 DOSY spectrum after transacetalization between $\text{P}(\text{MeOx}_{41}\text{-stat-DPO}_9)\text{OH}$ and PEG_{300}

CHAPTER 5

POLY(2-OXAZOLINE) BASED NANOGELS AS BIOCOMPATIBLE PSEUDO-POLYPEPTIDE DRUG DELIVERY SYSTEM



Keywords: nanogels, poly(2-oxazoline), cytotoxicity, protein repellent

Overview: Hydrophilic nanogels based on partially hydrolyzed poly(2-ethyl-2-oxazoline) were synthesized in dilute aqueous media in the presence of 1,6-hexanediol di-glycidyl ether as a cross-linker. Nanogel formation was monitored by DLS and HSQC NMR spectroscopy, and the final nano-objects were characterized by DLS, TEM, AFM and NanoSight analyses. Nanogels with a hydrodynamic radius of 78 nm exhibiting a slight positive surface charge were obtained. MTS assays (cell metabolic activity test) evidenced that the nanogels were non-toxic in the investigated concentration range (i.e. 0.1 to 400 $\mu\text{g/mL}$), and that no specific interaction with bovine serum albumin was observed. Altogether, such nanogels showed a great potential as drug delivery systems, as they combined some of the major properties required for this application, namely appropriate size and morphology, robustness and flexibility, slightly positively charged surface, no cytotoxicity and potential stealth behavior.

Part of this chapter has been published in *Biomacromolecules* in 2014.¹

¹ Legros, C.; Wirotius, A.; De Pauw-Gillet, M.-C.; Tam, K. C.; Taton, D.; Lecommandoux, S. *Biomacromolecules* **2014**, DOI: 10.1021/bm501393q.

CHAPTER 5

POLY(2-OXAZOLINE) BASED NANOGELS AS BIOCOMPATIBLE PSEUDO-POLYPEPTIDE DRUG DELIVERY SYSTEM

INTRODUCTION	167
I. PETOX SYNTHESIS AND PARTIAL HYDROLYSIS.....	168
II. NANOGEL FORMATION IN AQUEOUS DILUTE MEDIA.....	169
III. NANOGEL CHARACTERIZATION	172
IV. CYTOTOXICITY TEST AND EVALUATION OF NANOGEL-PROTEIN INTERACTIONS	174
V. COMPLEMENT SYSTEM ACTIVATION	177
V.1. MEASUREMENT PRINCIPLES	177
V.2. EIA AND LIA RESULTS.....	178
V.3. DISCUSSION.....	180
CONCLUSIONS	181
EXPERIMENTAL SECTION	183
SUPPORTING INFORMATION	190

INTRODUCTION

Drug delivery nanotechnologies have been studied for several decades¹ and only a few therapeutic nano-carriers have been approved for clinical use by the FDA.² These systems are currently commercialized, mainly for cancer therapy, most of them being based on liposomes³ or polymer-drug conjugates.⁴ Nevertheless, these systems are still far from ideal drug delivery systems (DDS) and one of the remaining challenges is to create DDS with increasing targeting efficiency while decreasing therapeutic side effects.² As a consequence, an array of alternative nano-carriers is currently being developed. They can be produced from a wide variety of materials including inorganic materials,⁵ lipids⁶ or polymers,^{7,8} and load different cargos such as drugs, proteins, DNA, siRNA, or magnetic nanoparticles, to address specific requirements. A rational design of a DDS requires taking into account specific parameters including morphology, size, stability, degradability, surface chemistry, charge, stealth properties and stimuli-responsive behavior.^{7,9} By controlling the aforementioned parameters, it may be possible to achieve less toxic DDS with improved pharmacokinetic and targeting properties.

Polymeric nanoparticles have a great potential in this area due to their versatility. A wide range of polymer-based nano-systems have thus been designed, such as self-assembled polymeric micelles and polymersomes,^{8,10,11} dendrimers,¹² microgels⁹ and nanogels,¹³ their properties being tuned by the nature, composition and architecture of the (co)polymer used. For all these nano-structures, the biocompatible character of the polymer is crucial to ensure the safety of patients which somewhat restricts the polymers that may be used in clinics. Poly(ethylene glycol) (PEG), poly(*N*-isopropylacrylamide), polysaccharides and poly(amino acid)s are the most commonly used polymer building blocks in this application. The group of S. Lecommandoux (LCPO, Bordeaux) has been, in particular, very interested over the last years in the development of polypeptide-based nanocarriers, taking advantage of the biocompatibility and responsiveness properties of poly(amino acid)s.¹⁴ In addition, poly(2-oxazoline)s (POx) represent a special class of polymers of particular interest for a use in biomedical applications, and especially as DDS. Indeed, POx are often viewed as pseudo-polypeptides,¹⁵ as the chemical composition of both families of polymers is very similar, and do not display any degradation issue. Moreover, biological studies carried out on poly(2-ethyl-2-oxazoline) (PEtOx) have established the biocompatibility of this polymer,¹⁶ and its non-toxicity for systems with molecular weights up to 15 000 g/mol.¹⁷ PEtOx can be internalized by cells¹⁸ and does not accumulate in the body.¹⁹ It also exhibits a stealth behavior similar to that of PEG.^{20–23} As part of a DDS, PEtOx has already been conjugated to proteins, drugs, or has been grafted onto the surface of liposomes and formulated as part of self-assembled systems, such as polymeric micelles and polymersomes.²⁴ Because of the intensive use of PEG, especially in the food

Polymerization went to completion, leading to a polymer with a degree of polymerization (DP) of 100 and a dispersity of 1.23 (SI†, Figures S1, S2 and S3). In order to introduce secondary amine functionalities along the polymer backbone, partial hydrolysis was conducted in acidic media.³² A percentage of hydrolysis of 26 % was achieved, as confirmed by ¹H NMR analysis (SI†, Figures S4 and S6). SEC trace of the as-hydrolyzed statistical copolymer, denoted as P(EtOx₇₄-stat-El₂₆), displayed a larger retention time compared to the non-hydrolyzed PEOx precursor, presumably due to polymer interactions with the SEC columns, as already reported (SI†, Figure S5).³³

II. NANOGEL FORMATION IN AQUEOUS DILUTE MEDIA

Nanogels were next obtained in aqueous dilute media, by reacting the secondary amines of the polymer backbone with 1,6-hexanediol di-glycidyl ether as a cross-linker, following a slightly modified procedure developed in our group (see Chapter 2).³² The number of reactive secondary amine functionalities available for cross-linking was indeed increased to 26 % (as compared to 7 % in our previous study), allowing the formation of denser nanogels. The molar ratio of reactive functionalities was kept constant, *i.e.* the amount of cross-linker was increased. Note that 3% of ethanol was added to the aqueous solution so as to improve the solubility of the cross-linker. Nanogel formation could be monitored by DLS, upon heating at 80 °C for 6 h. Higher concentrations in cross-linker led to a non-homogeneous reaction mixture, even in the presence of up to 6% of ethanol. Under such conditions, nanogel formation could not be monitored only by DLS because of the formation of nano-aggregates at the early stage of the reaction.

However, DLS measurements performed on the reaction mixture after heating and stirring it at 80 °C for 6 h followed by purification by dialysis against ethanol and water, evidenced the formation of nano-objects. It is worth mentioning that nanogels of small size do not scatter much light (small size and low compactness inherent to the nanogel structure itself), making their analysis challenging. In order to differentiate the small aggregates observed after mixing the reactants and the final nanogels, control experiments were monitored by DLS, changing one parameter at a time: in the absence of polymer, in the absence of cross-linker, and without heating (Table I).

Table I DLS measurements confirming nanogel formation

Reaction ^{a)}	Before reaction			After dialysis		
	Count rate [Kcps]	PDI	Size, d [nm]	Count rate [Kcps]	PDI	Size, d [nm]
Nanogels	963	0.08	288	43	0.31	172
No polymer	1151	0.08	139	3.5	0.47	-
No cross-linker	15.5	0.8	3	8.8	0.54	3
No heating	2296	0.09	377	10	0.39	156

a) Size given as the average of three measurements

These experiments showed that nano-aggregates were only observed at the early stage of the reaction when the cross-linker was introduced in the reaction medium. This confirmed that initial nano-objects corresponded to nano-aggregates arising from the presence of the cross-linker, due to its low solubility. In the absence of polymer and without heating, nano-aggregates were observed at the initial stage but not at the final stage of the reaction. In fact the final count rate was low, in the same range as that of the solvent. This suggested that 'cross-linker nano-aggregates' observed at the initial stage had a higher solubility at 80 °C than at room temperature and are no longer observed at the final stage. In the absence of cross-linker, no nano-objects were detected at the initial or final stage of the reaction, meaning that the polymer alone is fully soluble in the reaction mixture. Lastly, no nano-objects were observed when the polymer and cross-linker were mixed and left at room temperature, confirming that the final nano-objects observed when heated at 80 °C correspond to real cross-linking between the polymer and cross-linker.

The nanogel formation was also monitored by HSQC NMR experiments. These experiments were carried out in an NMR tube in the appropriate mixture of D₂O and deuterated ethanol (EtOD), at 80 °C. HSQC measurements were recorded every hour (Figure 1 and SI†, Figures S7 and S8).

Figure 1 shows the progressive disappearance of both signals of the NHCH₂CH₂ of the polymer backbone (signal e) and of the diglycidyl ether (signal f and g), along with the appearance of new signals that are characteristic of linkages formed between the P(EtOx₇₄-stat-El₂₆) and the cross-linker (signal g'). Moreover, broadening of peaks in the ¹H NMR spectra was observed with time, indicating an increase in sample inhomogeneities, which is consistent with nanogel formation.

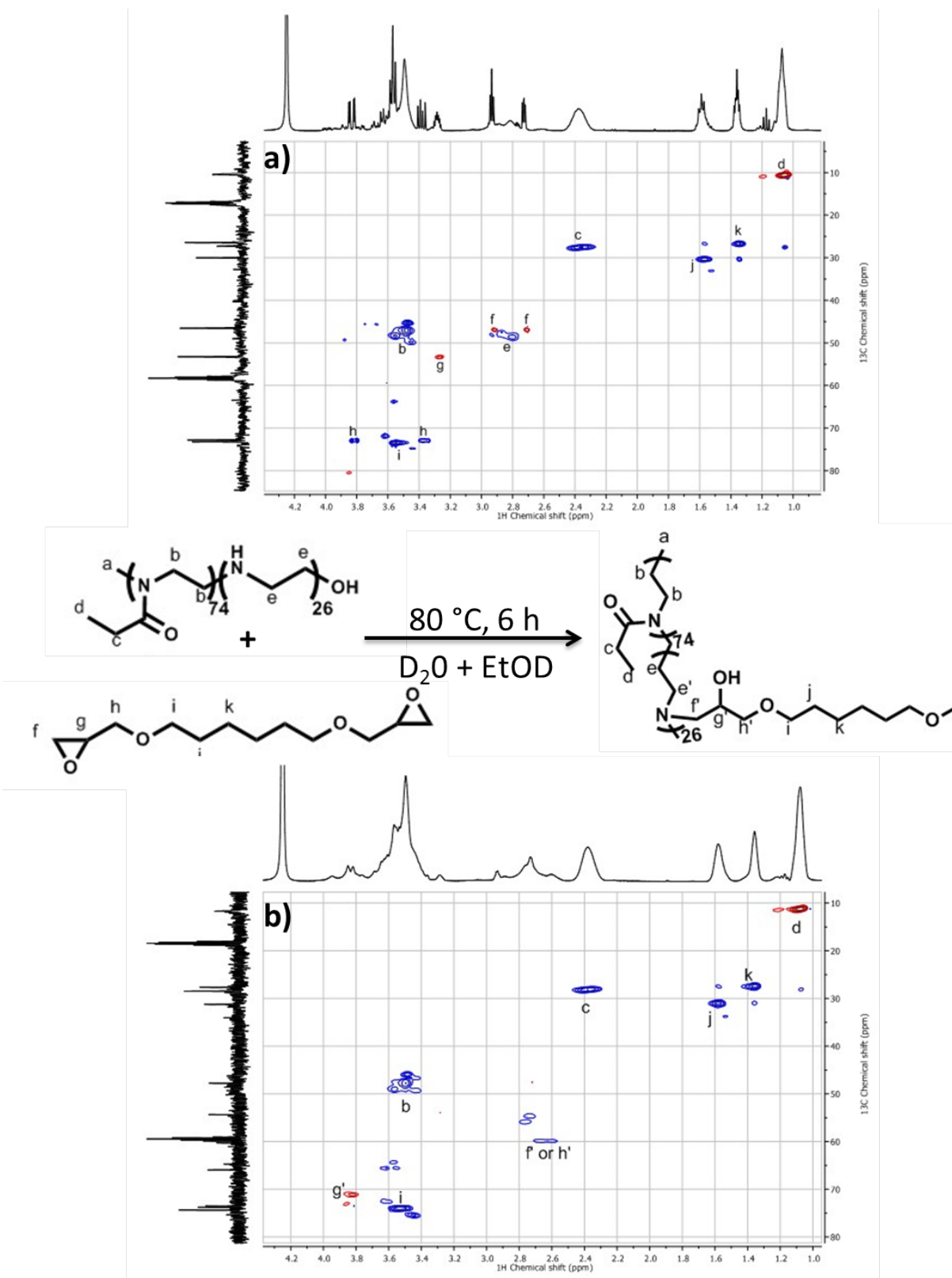


Figure 1 HSQC NMR spectra of the nanogel formation a) T_0 , b) T_{6h} at $80\text{ }^\circ\text{C}$

III. NANOGEL CHARACTERIZATION

Nanogels were first characterized by multi-angle laser light scattering (MALLS). The variation of decay rate *versus* the squared scattering vector is shown in Figure 2. From the Stokes-Einstein equation and the translational coefficient obtained from the slope of the linear fit, the hydrodynamic radius was directly calculated. A hydrodynamic radius (R_H) of 78 nm with a polydispersity of 0.3 was obtained. The formation of spherical nanostructures was also confirmed by TEM and AFM (Figure 2 and SI†, Figures S9 and S10).

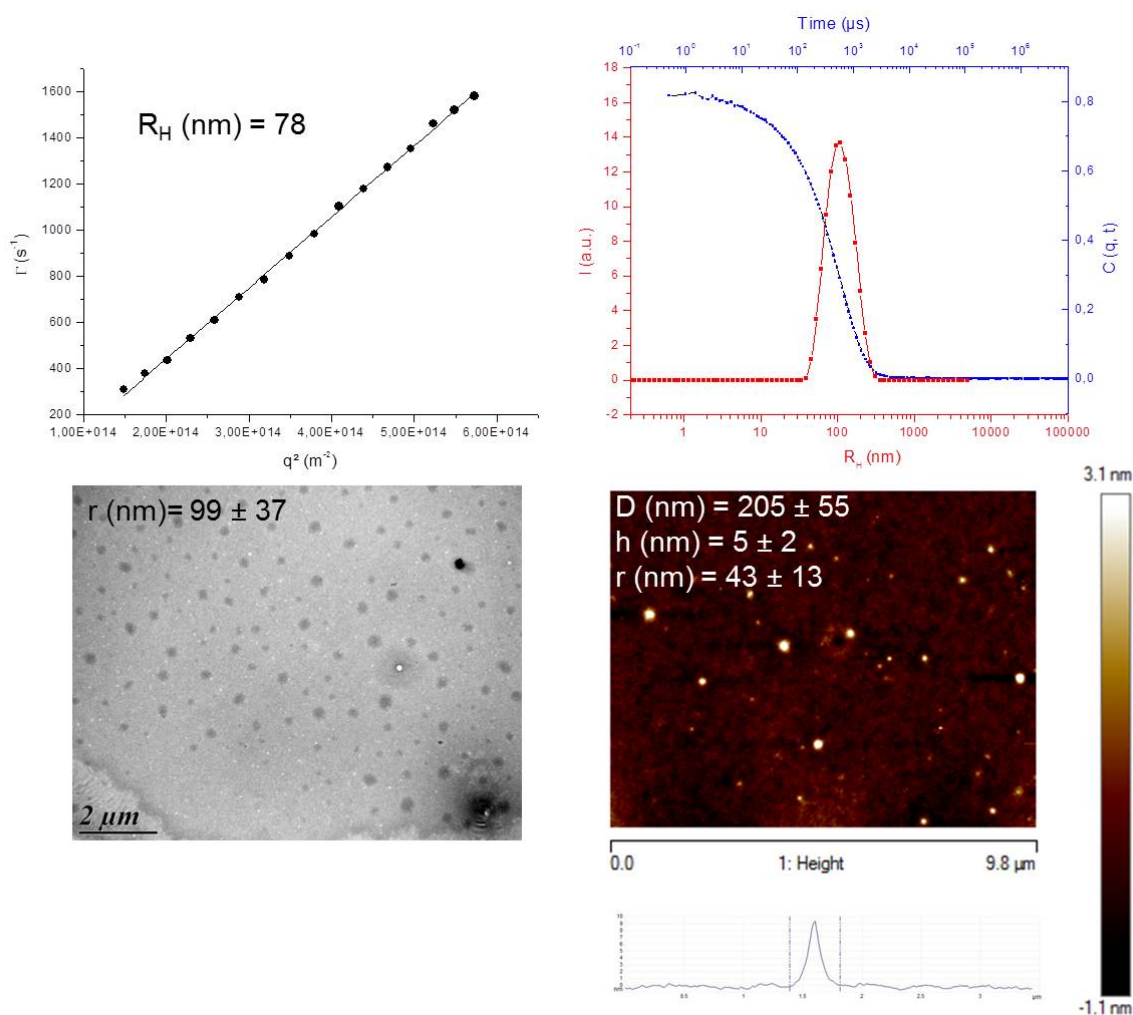


Figure 2 Nanogel characterization. Top: DLS analysis; left: variation of decay rate versus squared scattering vector with linear fits; right: relaxation time plot obtained at 90°. Bottom, left: TEM micrograph. Bottom, right: Tapping mode AFM image and section profile of the AFM imaging

By statistical analyses of the images, radii of 99 ± 37 nm and 43 ± 13 nm were obtained, respectively, by TEM and AFM. The size obtained by AFM analysis was significantly smaller than that obtained by MALLS and TEM. This is expected because, compared to TEM statistical analyses where more than 100 nanogels were taken into account, the number of nanogels present on the AFM mica surface was lower, leading to less reliable statistics. In addition, surface interactions and spreading/contractions of the nanogels strongly depend on the surface properties. Indeed, one can expect that the slightly positively charged nanogels (see further) interact significantly with the negatively charged mica surface, then resulting to a nanogel contraction.

Nanogels previously reported in the first chapter were made from P(EtOx-*stat*-EI) with a percentage of hydrolysis of 7% and exhibited a R_H of 205 nm by MALLS. By comparing these two systems, a decrease in nanogel size was noted with increasing number of reactive functionalities involved in the cross-linking process. In this contribution, denser and smaller nano-systems were formed.

In view of using these nanogels as DDS, an optimum size should be in the range from 20 to 200 nm. Below 20 nm, indeed, nano-systems would be cleared by renal filtration or extravasion, whereas above 200 nm clearance by opsonisation would occur.^{2,7} With a R_H of 78 nm, our nanogels are in the expected range, and would be able to circulate for longer in the blood stream. Pharmaceutical carriers with a long longevity in the blood, tend to accumulate in pathological sites with affected and leaky vasculature *via* the enhanced vascular permeability and retention effect (EPR), leading to passive targeting of the cargo.^{2,34} Such a behavior is aimed for our nanogels.

Conductivity titration also proved that not all the amine functionalities were involved in the cross-linking process, since 12.8 % remained in solution, 13.2 % being involved in the cross-linking reaction (SI†, Figure SI 1). The zeta potential of the nanogel solution was measured at different pH values, from 3 to 10.5, and was always positive, varying from +44 mV to +6 mV (SI†, Figure SI2). This could be linked to the protonation of the tertiary amines present in the structure and/or the free ethylene imine functions. If these extra ethylene imine functionalities were accessible, they could potentially be used to covalently attach a fluorescent dye molecule for further biological studies, such as cell internalization, or to functionalize the surface with a targeting ligand for active targeting, leading to the formation of “smart DDS”.^{35,36} They could also be used as a gene carrier, for DNA or siRNA binding, as already mentioned in the literature for cationic nanogels^{37,38} and for P(Ox-*stat*-EI) hydrogels.^{39,40}

Additional nanogel analyses were carried out with the NanoSight LM10 apparatus. This technique is based on an optical microscope allowing monitoring the particles movement in a cell of a known volume illuminated by a laser light source. Particles can thus be observed individually as they diffuse due to

Brownian motion. By tracking them, the number of particles present in the cell can be evaluated. Measurements were carried out at different concentrations within the linear range of the device. Above 1×10^9 particles/mL, the measured number of particles/mL no longer varied linearly with the mass concentration. If the concentration is too low, there are not enough particles for accurate statistical measurements. The final number of particles/mL obtained in a solution at 4.7 mg/mL was 4.3×10^{10} particles/mL. From these measurements, the approximate mass of a single nanogel and the number of polymer chains per nanogel could be evaluated (see Table 2).

Table 2 Nanogel characteristics calculated from NanoSight results

C_m^{a)} [mg/mL]	C_n^{b)} [particles/mL]	m^{c)} [g/nanogel]	N_{polymer} chains/nanogel^{c)}
4.7	4.3×10^{10}	1.09×10^{-13}	7.8×10^6

- a) Concentration measured by solvent evaporation
- b) Concentration measured by the NanoSight LM10 apparatus
- c) Calculated from C_m and C_n, considering M = 8420 g/mol for one polymer chain

Finally, no aggregation or increased polydispersity of particles was observed by DLS monitoring over 6 months, indicating that our nanogels were colloiddally stable when stored at 4 °C.

IV. CYTOTOXICITY TEST AND EVALUATION OF NANOGEL-PROTEIN INTERACTIONS

Nanogels produced from P(EtOx-*stat*-EI) contained remaining ethylene imine functionalities even after cross-linking with 1,6-hexanediol di-glycidyl ether, as determined by titration. Cytotoxicity of both PEtOx and poly(ethylene imine) (PEI) have already been reported in the literature: PEtOx is an amino-acid analogue (= pseudo-polypeptides),¹⁵ and is thus expected to be biocompatible. PEtOx is already approved by the FDA as an indirect food contact agent (which was also the case for polyethylene glycol (PEG) before being approved for biomedical applications), and can now rival with commonly hydrophilic polymers used for drug delivery applications,²³ especially PEG.^{20,22,41} Cytotoxicity of a library of poly(2-oxazoline)s with different pendant chains has been recently evaluated: no cytotoxicity has been observed even at high concentration.¹⁶ Another study has shown that PEtOx, even up to 15 000 g/mol, is non-cytotoxic.¹⁷ The potential cytotoxicity of PEtOx-drugs, proteins^{42,43} or enzyme conjugates⁴⁴ or of nano-

assembled systems, such as micelles^{45–47} or nanoparticles⁴⁸ with one block made of PEtOx, has also been assessed and no cytotoxicity has been evidenced.

The cytotoxicity of partially hydrolyzed PEtOx has been reported to increase with increasing percentage of hydrolysis, and PEI is also known to be cytotoxic,^{49–51} mainly because of its high positive charges. However, up to the percentage of hydrolysis of 9%, at a concentration up to 5 mg/mL, no cytotoxicity has been found.⁵² However, due to the positive zeta potential values at physiological pH ($\zeta = 15$ mV) (SI†, Figure S12), cellular toxicity and some interactions with the immune system can be suspected.

The cell proliferation and viability were assessed with our nanogels, using the MTS cell metabolic activity test. The fibroblast-like L929 cells were incubated for 72 hours (a time long enough to reveal any eventual toxicity exerted by the nanoparticles) with increasing nanogel concentration. Metabolic activity, directly related to cell viability, was measured by spectrophotometry *via* the reduction of MTS into the colored formazan product by active mitochondrial dehydrogenases. As can be seen on Figure 3, nanogels do not show any cytotoxicity to the L929 cells in the concentration range tested (from 0.1 to 400 $\mu\text{g/mL}$).

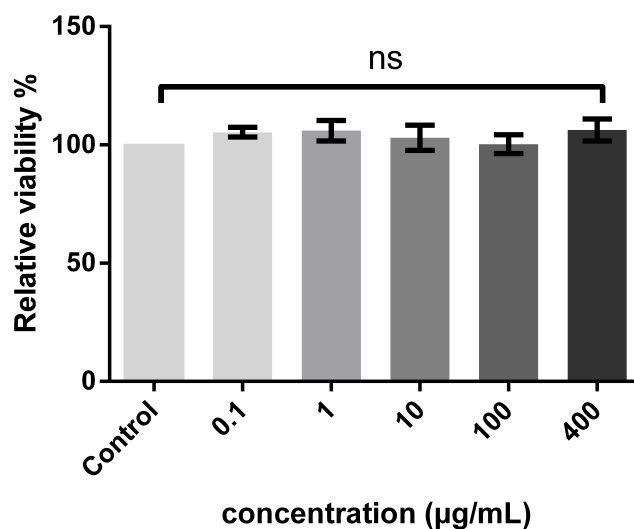


Figure 3 MTS assay conducted on mouse fibroblast-like L929 cells.

In addition, even after 72 hours of incubation, the cells were nicely spread in the wells, and some were still going through mitosis (SI†, Figure S13). Hence, our synthesized nanogels did not exhibit any cytotoxicity despite their positive surface charge. These characteristics are particularly interesting considering previous reports claiming that nanoparticles smaller than 200 nm and with slight positive charge are preferentially accumulated and remain within tumor sites compared to neutral or negatively charged nanoparticles.⁵³

When administered in the blood stream, nanogels could interact with plasma proteins. Nanogel-proteins interactions strongly depend on nanogel surface characteristics (e.g. functionalities,⁵⁴ hydrophobicity⁵⁵ or charges).⁵⁶ Herein, nanogels might interact with negatively charged serum proteins (such as albumin, the main protein of human blood plasma) or red blood cells, forming big aggregates. The aggregation behavior of cationic nanogels in serum has already been demonstrated elsewhere.⁵⁷ In our case, nanogel stability study in serum *via* DLS measurement was not feasible, as the count rate of the nanogels alone was already low. Bovine serum albumin (BSA) was chosen as a model protein to study the interactions between plasma proteins and nanogels. BSA was incubated with the nanogels overnight, at different incubation concentration (IC, corresponds to the mass ratio BSA over nanogels) (75%, 50%, 25%, 12.5%, 6.25% and 3.5%), and the potential interactions were assessed by gel retardation assay. BSA is negatively charged at physiological pH ($IP = 4.95$ mV, $SI \uparrow$, Figure S14) and could potentially create electrostatic interactions with nanogels. The gel electrophoresis was run for each IC and the intensities of the bands obtained were compared to the ones of BSA alone, at the same concentration. Nanogels being more than 10 times larger than the protein, they should remain in the well and not migrate on the gel, or in the worst case situation migrate more slowly than the free BSA. As can be seen in Figure 4, for each IC, the intensity of the bands for BSA and for nanogels incubated with BSA overnight was similar, suggesting there was no retardation in BSA mobility and that BSA did not significantly bind to the nanogels.

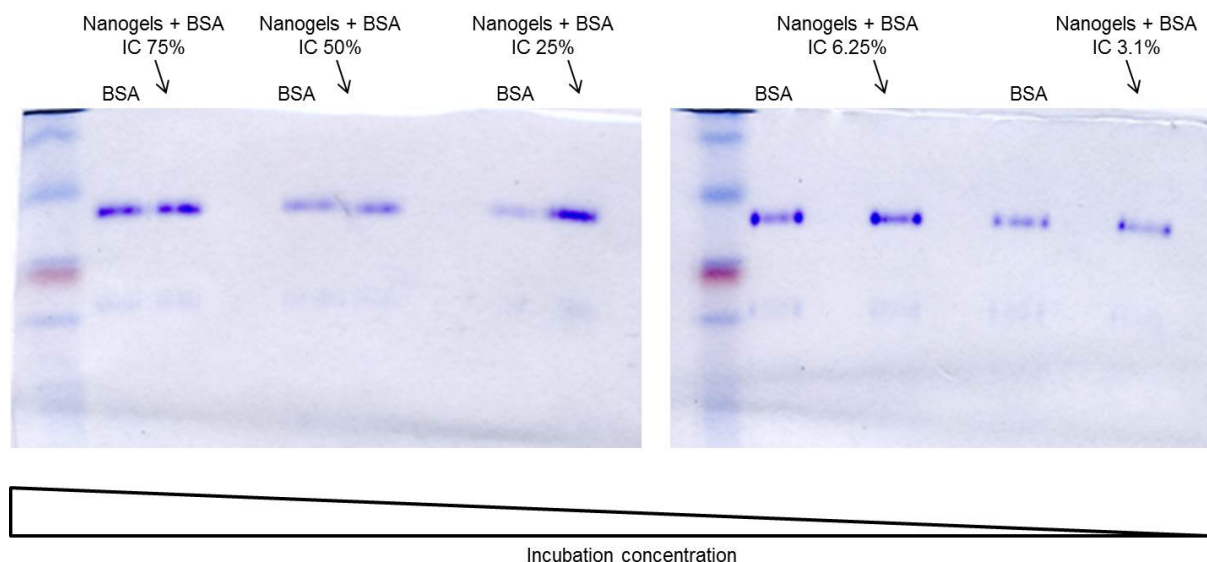


Figure 4 Native gels run for BSA and nanogels-BSA mixture at different incubation concentrations

This can be attributed to their stealth behavior, as reported in the literature for PEtOx,^{58,59} one of the gold parameters to achieve for a DDS. These results were corroborated with other POx involved

polymer brushes,⁶⁰ bottle-brush brushes,⁶¹ capsules,⁶² hydrogels,^{63,64} or simply amphiphilic POx block copolymers⁶⁵ which were reported as protein repellent systems.

V. COMPLEMENT SYSTEM ACTIVATION

V.1. MEASUREMENT PRINCIPLES

If administered intravenously, DDS could be rapidly cleared from the blood stream by different ways: renal and hepatic clearance, destabilization, aggregation, opsonization and clearance by the mononuclear phagocytic system (MPS).^{7,66} MPS is a part of the immune system that consists of phagocytic cells, such as blood monocytes and macrophages accumulated in lymph nodes, spleen and other tissues.^{67,68} The biochemical cascade that removes pathogens is known as the complement system: it consists of numerous plasma and membrane-bound proteins, numbered at more than 50 in 2010.⁶⁹⁻⁷¹ A number of complement proteins are proteases that are themselves activated by proteolytic cleavage and such enzymes are called zymogens. In the case of the complement system, the precursor zymogens are widely distributed throughout body fluids and tissues without adverse effect. At sites of infection, however, they are activated locally and trigger a series of potent inflammatory events. The complement system activates through a triggered-enzyme cascade. In such a cascade, an active complement enzyme generated by cleavage of its zymogen precursor then cleaves its substrate, another complement zymogen, to its active enzymatic form. This in turn cleaves and activates the next zymogen in the complement pathway. In this way, the activation of a small number of complement proteins at the start of the pathway is hugely amplified by each successive enzymatic reaction, resulting in the rapid generation of a disproportionately large complement response.⁷²

There are three pathways of complement activation: the classical pathway, which is initiated by antigen-antibody complexes or by direct binding of complement component C1q to the pathogen surface; the MB-lectin pathway, which is triggered by mannan-binding lectin, a normal serum constituent that binds some encapsulated bacteria; and the alternative pathway, which is triggered directly on pathogen surfaces. The three main consequences of complement activation are opsonization of pathogens, the recruitment of inflammatory cells, and direct killing of pathogens.⁷⁰⁻⁷²

The opsonization corresponds to the interaction/adsorption of plasma proteins (opsonins) onto the pathogen which signals it as a foreign material and will subsequently lead to its ingestion by macrophages

by phagocytosis. It is considered as the main barriers to nanoparticles stability and delivery *in vivo*, especially opsonization by the most abundant plasma proteins such as albumin, apolipoprotein, immunoglobulins, complement and fibrinogen.

It was previously demonstrated in this work that BSA did not adsorb to our nanogels, but protein binding to the surface of nanoparticles does not only depend on particle surface characteristics, such as hydrophilicity, charge and surface functional groups,^{54,55,73} but also on the protein properties. In order to evaluate in depth the potential stealth properties of the nanogels, complement activation assay, one of the standard hemo-compatibility assay,⁶⁹ was investigated. To do so, different methods could be used^{69,74,75} such as CH₅₀ and APH₅₀ hemolytic assays,^{76,77} 2D-immuno electrophoresis,⁷⁸ enzyme immunoassay (EIA) or liposome immunoassay (LIA).⁷⁶ A comparative study between CH₅₀, EIA and LIA showed good correlation between the three, but better sensitivity for EIA and LIA.⁷⁶

V.2. EIA AND LIA RESULTS

EIA and LIA assays were run at the same nanogel concentration as for the cytotoxicity assay, to ensure their biocompatibility. For both methods, negative and positive controls were used. Poly(methyl methacrylate) (PMMA) nanoparticles were suspended in sterile PBS and used as a positive control as previously reported in the literature.^{79,80} As poly(ethylene glycol) (PEG) is often used as the gold standard for stealth properties, poly(ethylene glycol)-*b*-poly(lactic acid) (PEG-PLA) micelles were used as a negative control.^{75,81} Lastly, hyaluronan-*b*-poly(γ -benzyl-L-glutamate) (Hya-PBLG) micelles and discs were also used as negative controls as hyaluronan is known to not activate the complement system.⁸²⁻⁸⁴ The efficacy of nanogels treatment was established by comparison with control levels.

Before evaluating the complement activation of our samples by the EIA method, a calibration was run using standards with known activity. The intensity measured evolved linearly with the activity up to 400 U/mL.

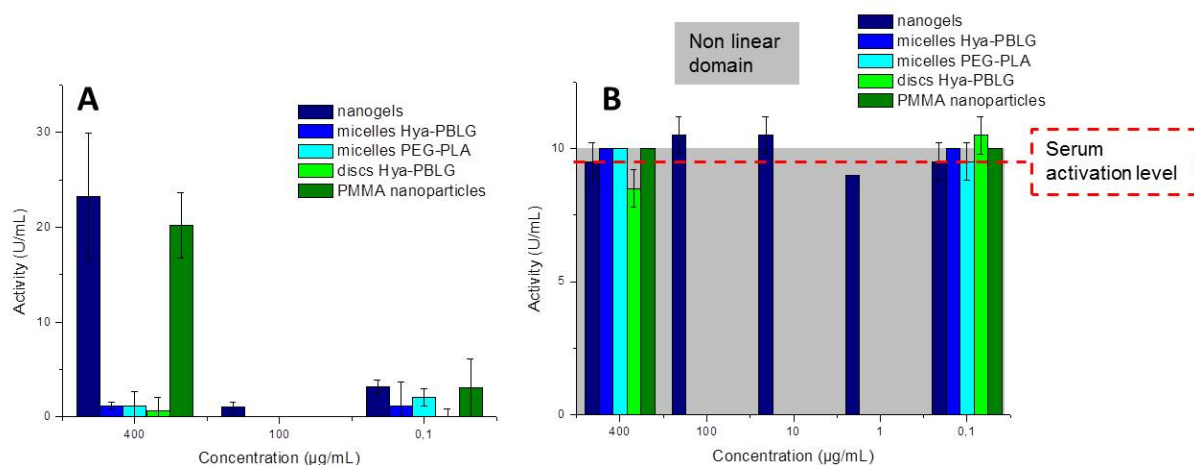


Figure 5 Results for complement activation by A) the EIA method, B) the LIA method

As shown in Figure 5, a nanoparticle concentration of 0.1 µg/mL is too little to lead to any complement activation as all the nano-particles tested (i.e. nanogels, positive and negative controls) presented really low complement activation. On the other hand, at 400 µg/mL, a clear difference in activity was noticed between the positive (PMMA nanoparticles) and negative controls. Surprisingly, the complement activity measured in the presence of nanogels appeared to be comparable to that of the positive control. A relatively low activity was measured at a concentration of 100 µg/mL for the nanogels, but unfortunately no control experiments were run at this concentration.

Concerning the LIA assay, regardless of which nanoparticle were tested and their concentration, the activation levels measured were close to the one of the serum alone and at the limit of the linear range (see Figure 5). Some measurements were run with another serum presenting a higher activity, but again the activities measured were equal to the activity of the serum tested without nanoparticles, which means that no complement activation was detected. The LIA technique is used routinely in hospitals to analyze patients' sera, but doesn't seem appropriate for our nanoparticles. The fact that liposomes are in the same size range as some of the nanoparticles tested could be part of the problem.

Finally, the experiments on complement activation are not conclusive and further analyses are needed to get clear information.

V.3. DISCUSSION

One of the most successful strategies to avoid interaction of nanoparticles with components of biological fluids is coating with a neutral hydrophilic flexible polymer to prevent adsorption of plasma proteins and avoid recognition by the MPS and subsequent clearance, PEG being the most commonly used polymer. The current increasing interest for poly(oxazoline)s, and especially for poly(2-methyl-2-oxazoline) and poly(2-ethyl-2-oxazoline), is mainly due to their reported stealth properties, similar to PEG.²⁰⁻²³

In the present work, BSA appeared not to interact with or adsorb on the nanogels. This is in good agreement with the literature where interactions between human serum albumin and micelles with the outside shell made of PEtOx was reported to be really low⁶⁵ and where PEtOx is even presented as a good candidate to design non-fouling surface coatings.⁶⁰ On the other hand, at a concentration of 400 µg/mL, nanogels seemed to activate the complement system from EIA method, even though no activation could be seen by the LIA method, in our hands. The fact that BSA did not adsorb on the nanogel surface but that nanogels activated the complement system could be perceived as contradictory. It is actually reported in the literature that when biomaterials enter in contact with body fluids such as serum, the serum proteins immediately adsorb and cover the surface of the biomaterial. The complement upon activation, first associate to the already adsorbed proteins on the surface of the biomaterial and the extent of covalent complement protein adsorbing directly to the biomaterials is minor.^{85,86} There is also competitive protein exchange on surfaces, in which proteins already adsorbed on a surface could be displaced by subsequently arriving proteins (also called the Vroman effect).⁸⁷ That is to say that the adsorption of the complement protein should takes place after that of serum albumin and biomaterials that adsorbed much larger amounts of serum proteins are being thus strong activators of the complement system.⁸⁸

Even though our nanogels had no specific affinity for BSA, other serum proteins such as globulin or fibrinogen for example could have been adsorbed, which could explain the complement activation.

On the other hand, we are also well aware that particle characteristics such as the size, surface charge, surface polarity and morphology influence their *in vitro* and *in vivo* fate.⁸⁹ Herein, we compared activation level of particles with different morphologies (nanogels, micelles, discs, plain nanoparticles) and different sizes (from 27 nm to 210 nm) which could definitely influence the complement activation.

One has to take into consideration that these results are preliminary: the BSA-nanogels interactions were evaluated by gel electrophoresis, which cannot be fully considered as a quantitative method. In addition, EIA complement activation assays were only run in duplicate at two different concentrations.

Complementary assays will have to be carried out before reaching final conclusions (additional concentrations run in triplicate). Moreover, there is substantial inter-individual variation in complement response to an activator. This necessitates the testing of multiple sera in order to evaluate the frequency of reactions and the extent of activation in reactive sera.⁶⁹

CONCLUSIONS

Hydrophilic nanogels based on partially hydrolyzed poly(2-ethyl-2-oxazoline) were synthesized in aqueous dilute media, in the presence of 1,6-hexanediol di-glycidyl ether as the cross-linker. The nanogel formation could be precisely monitored by DLS and HSQC NMR spectroscopy, where the disappearance of signals corresponding to the reactive functionalities of the polymer and cross-linker together with the appearance of new signals characteristic of the new linkages confirmed the successful nanogel formation.

The nanogels thus obtained exhibited a spherical structure with a hydrodynamic radius of 78 nm. Overall, the influence of the extent of hydrolysis on the final nanogel size was clearly demonstrated: the size decreased when increasing the extent of hydrolysis, that was, by increasing the percentage of reactive amino-functionalities reacting with the bis-epoxide cross-linker. The nanogel size was found to be within the optimal range for drug delivery system (DDS), with a view at taking advantage of the EPR effect in order to reach the targeted site. By further characterizing the nanogels using the NanoSight LM10 apparatus, it was possible to obtain the approximate mass of a single nanogel and the number of polymer chains per nanogel, which were found to be 1.09×10^{-13} g/mol and 7.8×10^6 , respectively.

In addition, the nanogel surface was positively charged, but did not induce any cytotoxicity, as attested by the MTS assay carried out on fibroblast-like L929 cells. Furthermore, no specific interactions with bovine serum albumin were observed. This was attributed to the stealth behavior of PEtOx. Last, the synthesized nanogels remained stable over at least a 6 months period, as monitored by DLS: the robustness of such systems will enhance their *in vitro* and *in vivo* stability.

These nanogels thus have great potential as DDS, as they combine some of the crucial properties required: appropriate size and morphology, robustness and flexibility, slight positive surfaces charge without any cytotoxicity and with potential stealth behavior. However, some additional assays should be conducted before drawing any conclusion on the complement activation ability of these nanogels. Last,

these nanogels were synthesized by a straightforward and surfactant free-method, which can be easily scalable and transferred to clinical trials.

EXPERIMENTAL SECTION

Materials and reagents

2-Ethyl-2-oxazoline (99%) (EtOx), methyl trifluoromethanesulfonate (96%) (MeOTf), and acetonitrile (99%) were purchased from Sigma-Aldrich, stored over calcium hydride and purified by vacuum distillation prior to use. Methanol (Sigma-Aldrich) was refluxed over sodium and distilled prior to use. Diethyl ether, ethanol, potassium hydroxide (KOH), sodium hydroxide (NaOH), hydrochloric acid solution (37%) (HCl), cyclohexane (99%), 1,4-butanediol di-acrylate, bovine serum albumin (fraction V, approximately 99 %) (BSA) were used as received from Sigma-Aldrich. 1,6-Hexanediol di-glycidyl ether (98%) was purchased from BOC sciences and used as received.

Instrumentation

NMR spectroscopy. ^1H NMR measurements were carried out, at room temperature, on a Bruker Avance I spectrometer operating at 400 MHz. The D_2O signal was used as reference ($\delta = 4.79$ ppm), and the relaxation time was fixed to 7.5 sec for all measurements.

Phase sensitive HSQC experiment was used to acquire the 2D spectra giving DEPT type information in addition to the ^1H - ^{13}C connectivity. This experiment was performed at 353 K on a Bruker Avance III HD NMR spectrometer operating at 400 MHz. The spectral widths were 4800 and 16000 Hz for the ^1H and ^{13}C dimensions, respectively. The number of collected complex points was 2048 for the ^1H dimension with a recycle delay of 2s. The number of transients was 4, and 256 time increments were always recorded in the ^{13}C dimension. The ^1JCH used was 145 Hz. Prior to Fourier transformation, the data matrices were zero filled to 1024 points in the ^{13}C dimension. The D_2O signal was used as the reference signal ($\delta = 4.25$ ppm). Data processing was performed using Mnova.

Size-exclusion chromatography. Size-exclusion chromatography (SEC) using dimethylformamide (DMF) with LiBr (1 g/L) as the eluent was performed at 80 °C at a flow rate of 0.8 mL/min. The column set consisted of two 7.5 mm \times 300 mm PLgel, 5 μm Mixed-D columns (Polymer laboratories) coupled to a guard column, 7.5 mm \times 50 mm, PLgel, 5 μm model (Polymer laboratories). Injections were done in a 20 μL loop and calibration was performed with polystyrene standard. Differential refractive index (RI) and UV detectors were used.

Infrared spectroscopy. Infrared spectra were obtained on a Thermoscientific Nicolet IS10 spectrometer using the attenuated total reflection (ATR) mode. The spectra were acquired using 16 scans at a resolution of 4 wavenumbers.

Dynamic light scattering. Dynamic light scattering experiments were performed using an ALV CGS-3 Compact Goniometer System, equipped with a 35 mW HeNe linear polarized laser with a wavelength of 632.8 nm and an ALV/LSE-5004 light scattering electronic and Multiple Tau Digital correlator. The accessible scattering angles ranged from 30° to 150°. Samples (2 mL in 2 cm diameter cylindrical glass cells) were immersed in a filtered toluene bath. Three independent 20s measurements were carried out to obtain dynamic data. Mean hydrodynamic diameters and size distributions were determined using a cumulant analysis method. The samples were first filtered with 0.8 µm nitrocellulose membranes.

NanoSight analyses. NanoSight analyses were conducted on a LM10 apparatus. This technique combines a conventional optical microscope with a laser light source to illuminate nano-scale particles within a 0.3 mL sample introduced to the viewing unit with a disposable syringe. Particles appear individually as point-scatters moving due to Brownian motion. Measurements were done in triplicate, at room temperature, over a period of 60s. The particles size and concentration were evaluated thanks to the Nanoparticle Tracking Analysis (NTA) software.

Transmission electron microscopy. Transmission Electron Microscopy (TEM) images were recorded at the Bordeaux Imaging Center (BIC) on a Hitachi H7650 microscope working at 80kV. Samples were prepared by spraying a 4.7 mg/mL aqueous solution of the nanogels onto a copper grid (200 mesh coated with carbon) using a homemade spray tool. They were subsequently stained with osmium tetroxide vapor for 45 minutes.

Atomic force microscopy. Atomic force microscopy (AFM) images were recorded in air using a Veeco Dimension Icon System equipped with a Nanoscope V controller and operating in tapping mode. The probes were commercially available silicon tips with a spring constant of 42 N/m, a resonance frequency of 285 kHz and a typical radius of curvature in the 8-10 nm range. Freshly cleaved Mica was used as sample substrate materials. For the observation of isolated nanogels, sample solutions in water at a concentration of 4.7 mg/mL were deposited on the substrate (20 µL) and immediately spin-coated (duration: 60 s; rate: 2000 rpm). Measurements of diameter were done using the section Particle Analysis tool provided by the AFM software (Nanoscope Analysis VI.20 from Bruker).

Titration. Titration was performed with a pH 730 pH-meter from inOLab (WTW series) and a conductivity meter K912 5.0 from Consort for simultaneous measurement of pH and conductivity. All

measurements were performed at 25 °C while stirring at a medium speed 30 mL of nanogels solutions at 0.8 g/L in DI water. The pH of the solutions was adjusted to ~2 by adding 0.5M HCl. The solution was titrated using 0.01M NaOH under stirring. Conductivity and pH of the solutions were measured simultaneously until the pH of the samples approached 11. Finally, the pH and conductivity values were plotted against the volume of NaOH added (in mL).

Electrophoretic mobility measurements. Zeta potential measurements were performed on a Malvern Nano ZS ZetaSizer at 25 °C. Laser Doppler electrophoresis in phase mode was conducted with sequential fast and slow field reversal applying a potential of ± 150 V. The so-measured electrophoretic mobility (μ) was then converted to zeta potential (ζ) using the Smoluchowski approximation. Samples were prepared at 4.7 mg/mL in DI water. 0.01M HCl or 0.01M KCl solutions were added respectively to adjust the pH.

Experimental procedures

Synthesis of poly(2-ethyl-2-oxazoline) (PEtOx). A typical procedure is as follows. In a flame dried Schlenk flask, 14 mL of acetonitrile was introduced under vacuum and 56 μ L (0.5 mmol) of MeOTf was added. The flask was placed in an ice bath at 0 °C and 5.05 mL (50 mmol) of 2-ethyl-2-oxazoline was added. The flask was then heated at 85 °C for 3 days, and the reaction was quenched by adding 2.7 equivalents of a 0.3N KOH solution in methanol. The solution was left to stir at room temperature overnight, and the polymer was precipitated twice into diethyl ether and dried under vacuum. Yield = 4.51 g (89 %). ^1H NMR (400 MHz, D_2O , δ): 3.7-3.45 (d, NCH_2CH_2), 3.1 (d, $\text{CH}_3\text{-NCH}_2\text{CH}_2$), 2.5-2.3 (m, $\text{NCOCH}_2\text{CH}_3$), 1.15-1 (q, $\text{NCOCH}_2\text{CH}_3$). $D = 1.23$. $dn/dc = 0.0789$ (in DMF + 0.1% LiCl). Degree of polymerization (DP) = 100. IR: $\nu = 3481$ (m), 2977(s), 2939 (s), 2880 (m), 1621 (s), 1470 (m), 1420 (s), 1374 (s), 1320 (w), 1238 (m), 1194 (s), 1078 (w), 1061 (m), 969 (w), 915 (w), 877 (w), 814 (m), 756 (w), 637 (s), 571 (s).

Partial hydrolysis of PEtOx in acidic media: synthesis of P(EtOx-stat-EI). The partial hydrolysis was adapted from our previously reported procedure.³² 3.54 g ($3.57 \cdot 10^{-4}$ mol) of $\text{P}(\text{EtOx})_{100}$ was dissolved in 35 mL of DI water and heated under reflux (oil-bath set at 100 °C). Subsequently, 35 mL of 37 % HCl solution was added to the polymer solution, yielding a polymer concentration of 50 g/L. Once the targeted percentage of hydrolysis was achieved, the solution was left to equilibrate to room temperature. A solution of 2.5M NaOH was added to reach pH = 8. Samples were then dialyzed against DI water for 3 days and freeze-dried. Yield = 1.84 g (52%). ^1H NMR (400 MHz, D_2O , δ): 3.6-3.3 (d, $\text{NCOCH}_2\text{CH}_2$), 3.1 (d, $\text{CH}_3\text{-NCH}_2\text{CH}_2$), 3.0-2.7 (s, NHCH_2CH_2), 2.5-2.3 (m, $\text{NCOCH}_2\text{CH}_3$), 1.15-1 (q,

NCOCH₂CH₃). \bar{D} = 1.201. IR: ν = 3484 (m), 2977(s), 2939 (s), 2880 (m), 1621 (s), 1470 (m), 1420 (s), 1374 (s), 1320 (w), 1236 (m), 1194 (s), 1078 (w), 1061 (m), 969 (w), 915 (w), 877 (w), 813 (m), 761 (w). Percentage hydrolysis: ¹H NMR = 26 %.

Nanogel synthesis in dilute media under sterile conditions. 1.35 g of the partially hydrolyzed polymer P(EtOx₇₄-stat-El₂₆) was dissolved in 135 mL of DI water. In another flask, a solution of 1,6-hexanediol di-glycidyl ether at 80 mg/mL was prepared in ethanol. Both solutions were filtered through a 0.2 μ m polypropylene filter and 8.37 mL of the cross-linker in ethanol was subsequently added to the polymer solution. The mixture was stirred at 800 rpm at 80 °C for 6 hours. The cross-linking reaction and nanogel formation were monitored by DLS at an angle of 90° on a Malvern ZetaSizer NanoZS instrument. Once the nanogels were formed, they were dialyzed for 2 days first against ethanol to sterilize the nanogel solution and to remove excess cross-linker, secondly against DI water to remove any unreacted polymer chains. 229 mL of the nanogel aqueous solution was obtained at a concentration of 4.7 mg/mL.

Cell culture and cell cytotoxicity assay against fibroblast-like L929 cells. The mouse fibroblast-like L929 cells were routinely cultured in Dulbecco's Modified Eagle's Medium (DMEM, Lonza) supplemented with 10% fetal bovine serum (FBS, Gibco, Grand Island, NY, United States), 1% of antibiotics (penicillin/streptomycin 10 000 U/ 10 000 μ g/ml, Lonza), 1% sodium pyruvate and 1% Glutamax (Gibco). Cells were maintained at 37 °C in a 5% CO₂ humidified incubator. After rinsing with PBS (Ca²⁺/Mg²⁺ free, Lonza) buffer solution to remove the serum, the cells were detached with 0.5% Trypsin-EDTA solution 10 \times (Gibco, Grand Island, NY, United States) diluted 10 fold in PBS (Ca²⁺/Mg²⁺ free) buffer solution.

For cytotoxicity measurements, the cells were first seeded in 96-well plates at a density of 2000 cells/well and grown in DMEM complete medium for 24 h prior to treatment. Cells were then exposed to the nanogels in a mixture of 10% PBS buffer solution (pH = 7.4, 154 mM NaCl, Ca²⁺/Mg²⁺ free) and 90% DMEM complete medium with different concentrations (100, 10, 1, 0.1, 0.01 μ g/mL) for 72 h. After 72 h, the cells were rinsed with PBS (with Ca²⁺/Mg²⁺, Lonza) buffer solution (100 μ L/well), and cell viability was evaluated via the MTS (3-(4,5-dimethylthiazol-2-yl)-5-(3-carboxymethoxyphenyl)-2-(4-sulfophenyl)-2H-tetrazolium) solution (Promega) assay. Specifically, 20 μ L of MTS and 100 μ L of PBS (with Ca²⁺/Mg²⁺) buffer solution were added to each well, and then the plates were incubated at 37 °C for 30 min. The absorbance at 490 nm was measured using a Power wave X (Biotek instrument Inc.) micro-plate UV-vis spectrometer. For the positive control, cells were incubated with the media alone.

Results were expressed as the percentage of metabolic activity of treated cells relative to untreated cells. Independent experiments were carried out 3 times with 8 replicates per condition.

Nanogel-protein interaction evaluation by gel retardation assay. The native polyacrylamide gel electrophoresis was performed according to the Laemmli procedure.⁹⁰ BSA proteins were left to incubate with a 4 mg/mL nanogel solution in phosphate buffer, 10 mM, pH = 7.4, at different incubation concentrations (IC), overnight. The incubation concentration corresponding to the mass ratio of BSA over nanogels. The next morning, the nanogel-BSA solutions were mixed with 6 μ L of loading buffer to achieve a final BSA content of 5 μ g in each well (for the IC of 3.5%, only 2.8 μ g were put in the well). The mixtures were loaded on a 7.5 % tris-acrylamide gel. Euromedex pre-stained protein ladder was used as reference. The gel run was performed in a Mini-Protean tetracell system from Bio-Rad. The run in the stacking gel was carried out with a constant voltage of 100 V. After the bromophenol blue band attained the resolving gel, the voltage was changed to 200 V. Staining was achieved by shaking the gel overnight in a solution of coomassie brilliant blue R-250. Destaining was performed in a solution of 40% ethanol and 10% glacial acetic acid.⁹¹

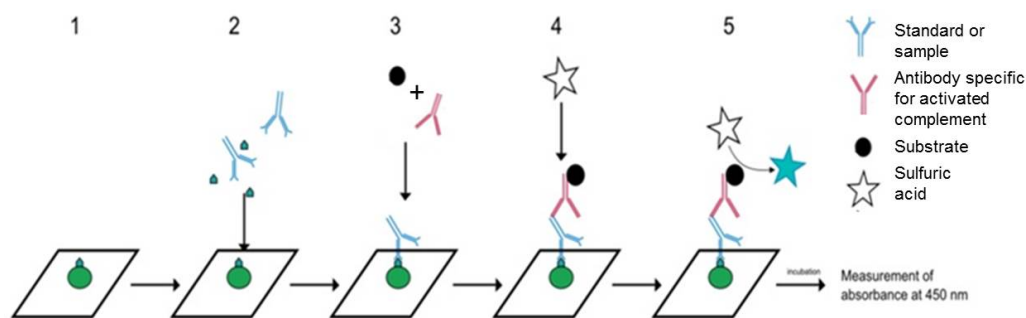
Complement system activation - Samples preparation. To measure complement activation *in vitro*, we determined nanogel-induced rise of human serum complement activation products using respective ELISA kits or LIA immunoassay. First, sterile nanogels aqueous solution was diluted with PBS 10 \times (purchased from Lonza) in order to obtain the desired concentrations (4000, 1000 and 1 μ g/mL). The reaction was initiated by diluting the previous nanogel solutions with undiluted fresh human serum (Serum from human male AB plasma, USA origin, sterile-filtered purchased from Sigma-Aldrich), at a typical nanoparticles/serum volume ratio of 1/9, in Eppendorf tubes (in duplicate). Solutions were incubated at 37 °C for 1 h.

Control nanoparticles were synthesized following procedures described in the literature, reported in Table I. Control serum incubations contained PBS (the same volume as the nanogels) for assessing background levels of complement activation products. The efficacy of nanogels treatment was established by comparison with control levels.

Table 3 Characteristics of the control nanoparticles used for the complement system activation assay

Control	Particles	Size (PDI) [nm]	Ref
+	PMMA	210 (0.12)	79
-	PEG-PLA micelles	27	92,93
-	Hya-PBLG micelles	40 (0.2)	94,95
-	Hya-PBLG discs	211 (0.13)	94,95

Enzyme immunoassay (EIA) principle. Measurements were carried out using the human total 50% complement hemolytic unit (CH50) ELISA kit from BlueGene. CH50 ELISA kit applies the quantitative sandwich enzyme immunoassay technique (see Figure 6). A microtiter plate had been pre-coated with a monoclonal antibody specific for complement activation (CA). Standards or samples were then added to the plate wells and complement if activated, would bind to the antibody pre-coated wells. In order to quantitatively determine the amount of CA present in the sample, a standardized preparation of horseradish peroxidase (HRP)-conjugated polyclonal antibody, specific for CA were added to each well to “sandwich” the complement immobilized on the plate. The microtiter plate was incubated, and then the wells were thoroughly washed to remove all unbound components. Next, substrate solutions were added to each well. The enzyme (HRP) and substrate were allowed to react over a short incubation period. Only the wells that contain complement activated and enzyme-conjugated antibody would exhibit a change in color. The enzyme-substrate reaction was terminated by addition of a sulphuric acid solution and the color change was measured spectrophotometrically at a wavelength of 450 nm. A standard curve was plotted relating the intensity of the color (O.D.) to the concentration of standards. The CA concentration in each sample was interpolated from this standard curve. The experimental data are the average of two independent experiments and measurement sensitivity is of 1 U/mL.

**Figure 6 Enzyme immunoassay (EIA) principle (adapted from ref. %)**

Liposome immunoassay (LIA) principle.⁹⁷ Measurements were made at the Hospital CHR Citadelle in Liège, Belgium, in the medical analysis laboratory Labo Cita, using a Wako AutoKit CH50. Dinitrophenyl (DNP)-coated liposomes that contain the enzyme glucose-6-phosphate dehydrogenase was used (see Figure 7). When a sample is mixed with the reagent, the complement in the sample is activated by the antigen-antibody complex on the liposomes. The activated complement breaks the membrane of the liposome. The enzyme glucose-6-phosphate dehydrogenase (G6PDH) contained in the liposome reacts with nicotinamide adenine dinucleotide (NAD) and glucose-6-phosphate (G6P) in the reagent. During this enzyme reaction the NAD is reduced to NADH and an increase in absorbance at 340 nm is observed. The absorbance increase is proportional to the total complement activity in the sample. The experimental data are the average of two independent experiments. The measurable range is from 10 to 60 U/mL and the sensitivity is 4 U/mL.

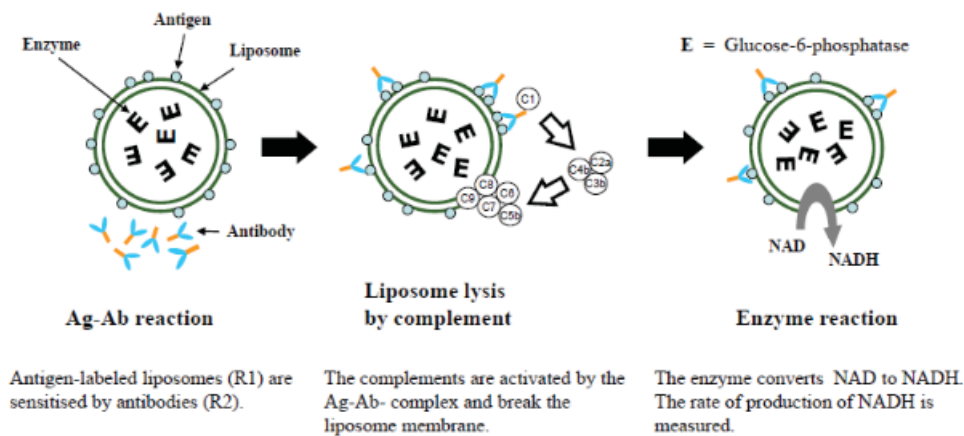


Figure 7 Principle of the LIA assay (adapted from ref. ⁹⁷)

SUPPORTING INFORMATION

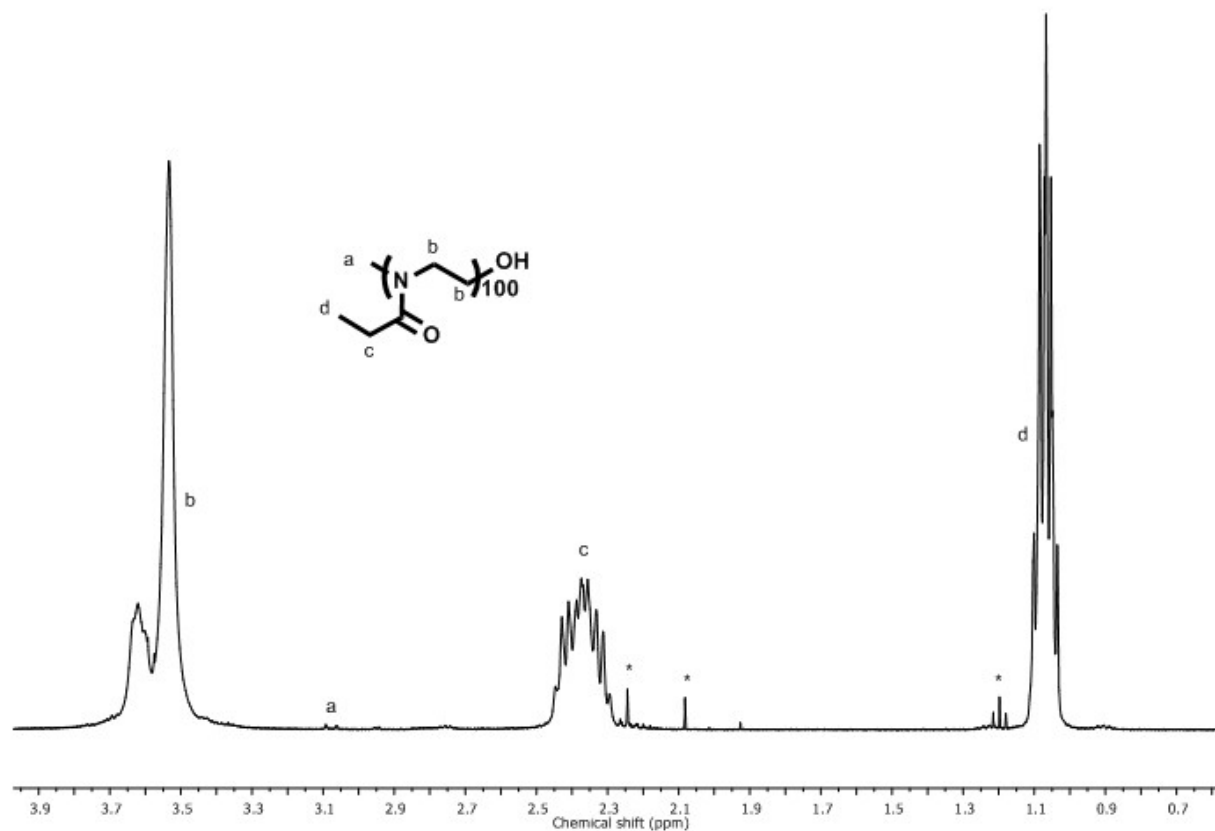


Figure S1 ¹H NMR spectrum (400 MHz, D₂O) of PEtOx₁₀₀

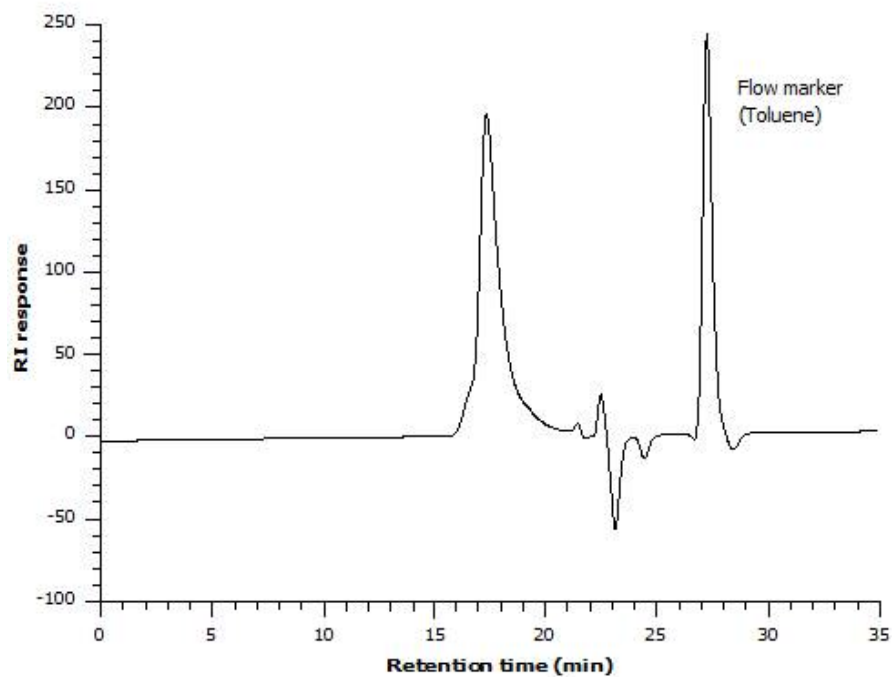


Figure S2 SEC trace of PEtOx₁₀₀ in DMF

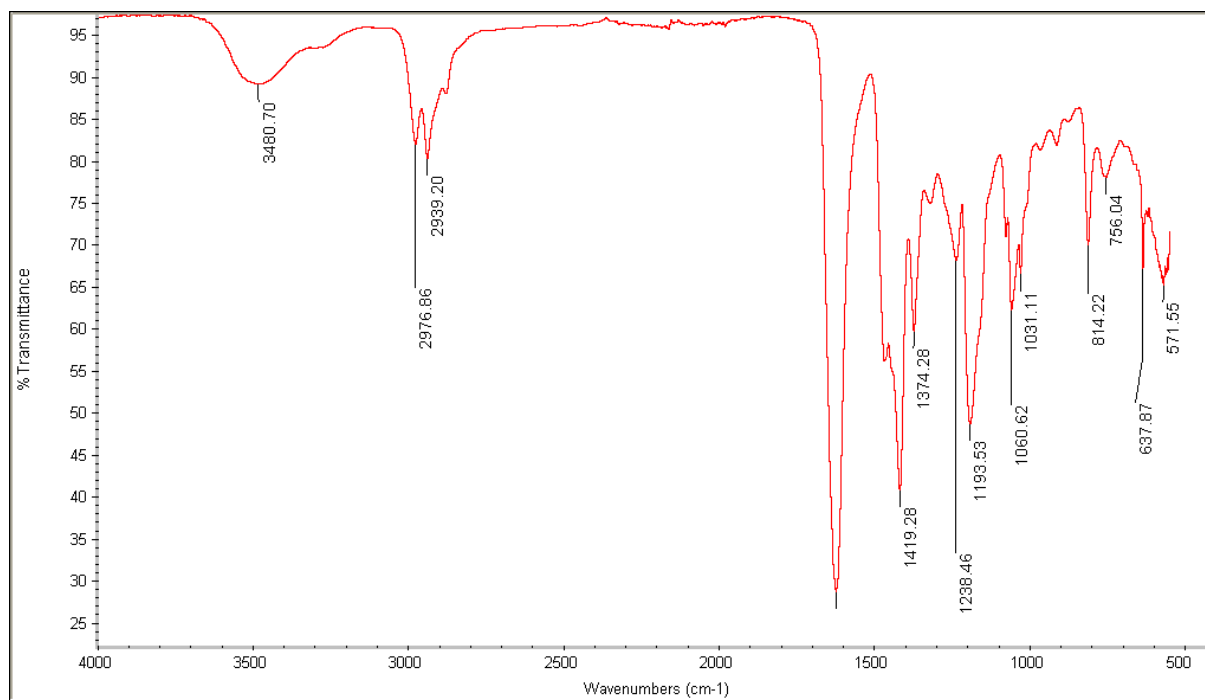


Figure S3 FT-IR spectrum of PEtOx₁₀₀

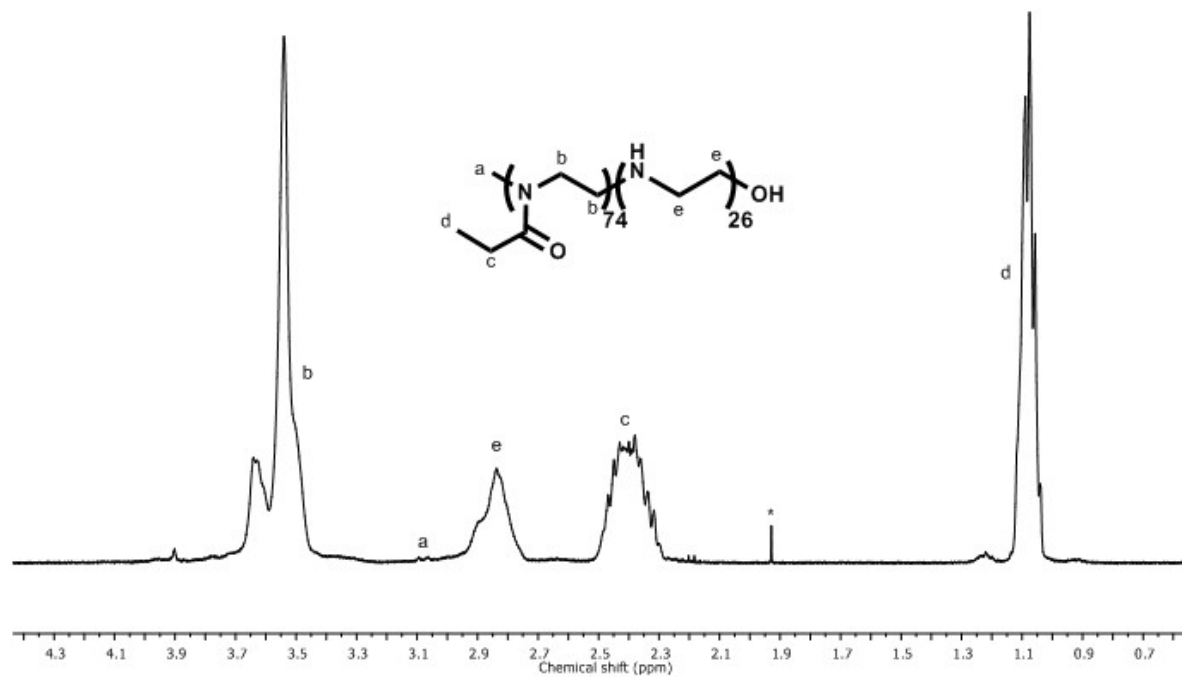


Figure S4 ^1H NMR spectrum (400 MHz, D_2O) of $\text{P}(\text{EtOx}_{74}\text{-stat-EI}_{26})$

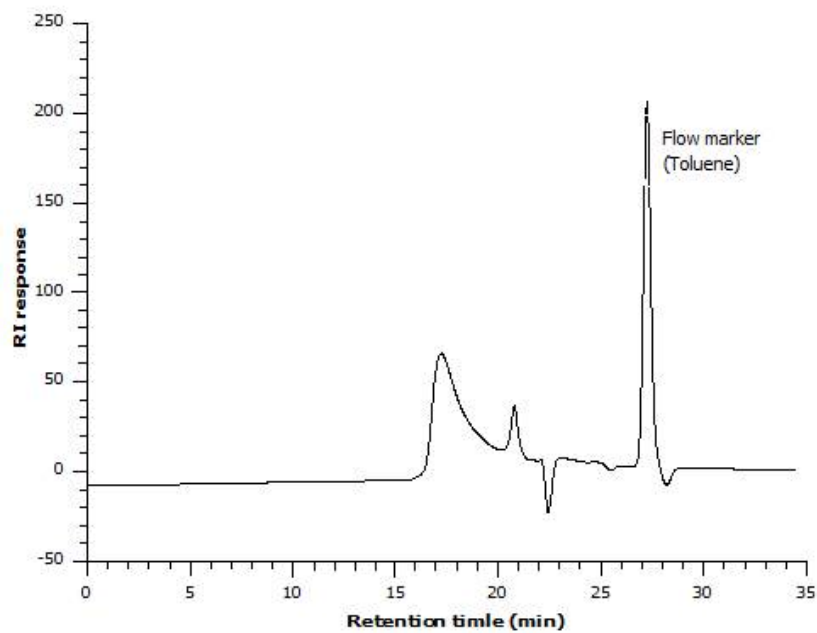


Figure S5 SEC trace of $\text{P}(\text{EtOx}_{74}\text{-stat-EI}_{26})$ in DMF

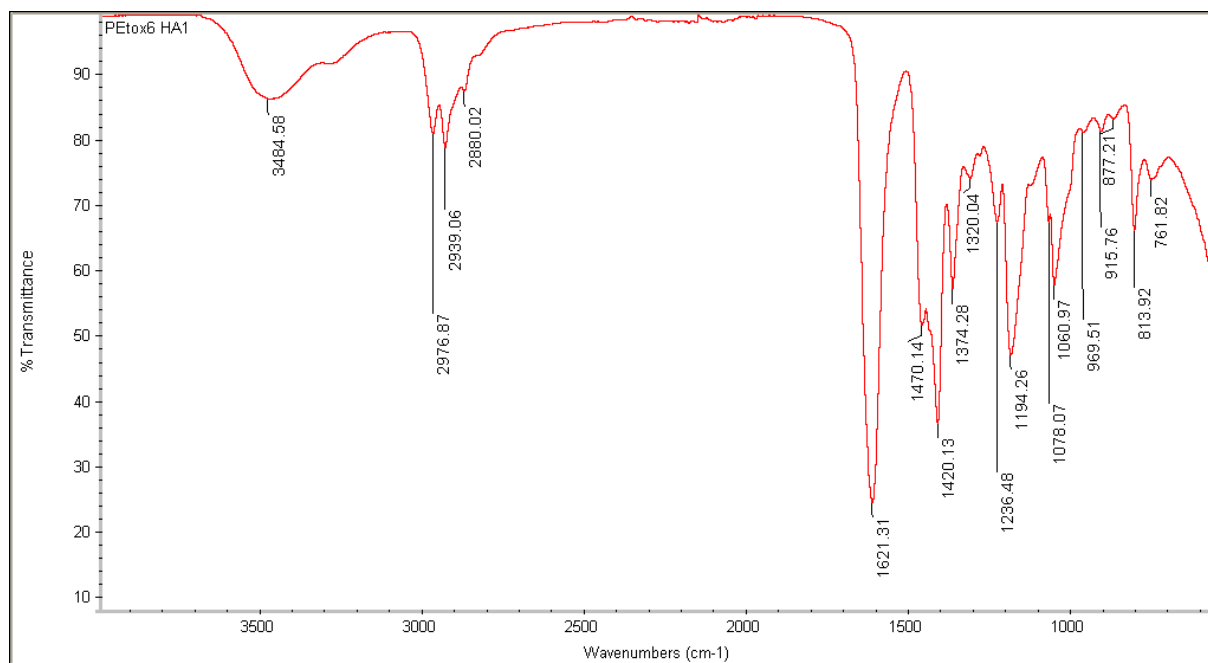


Figure S6 FT-IR spectrum of P(EtOx₇₄-stat-EI₂₆)

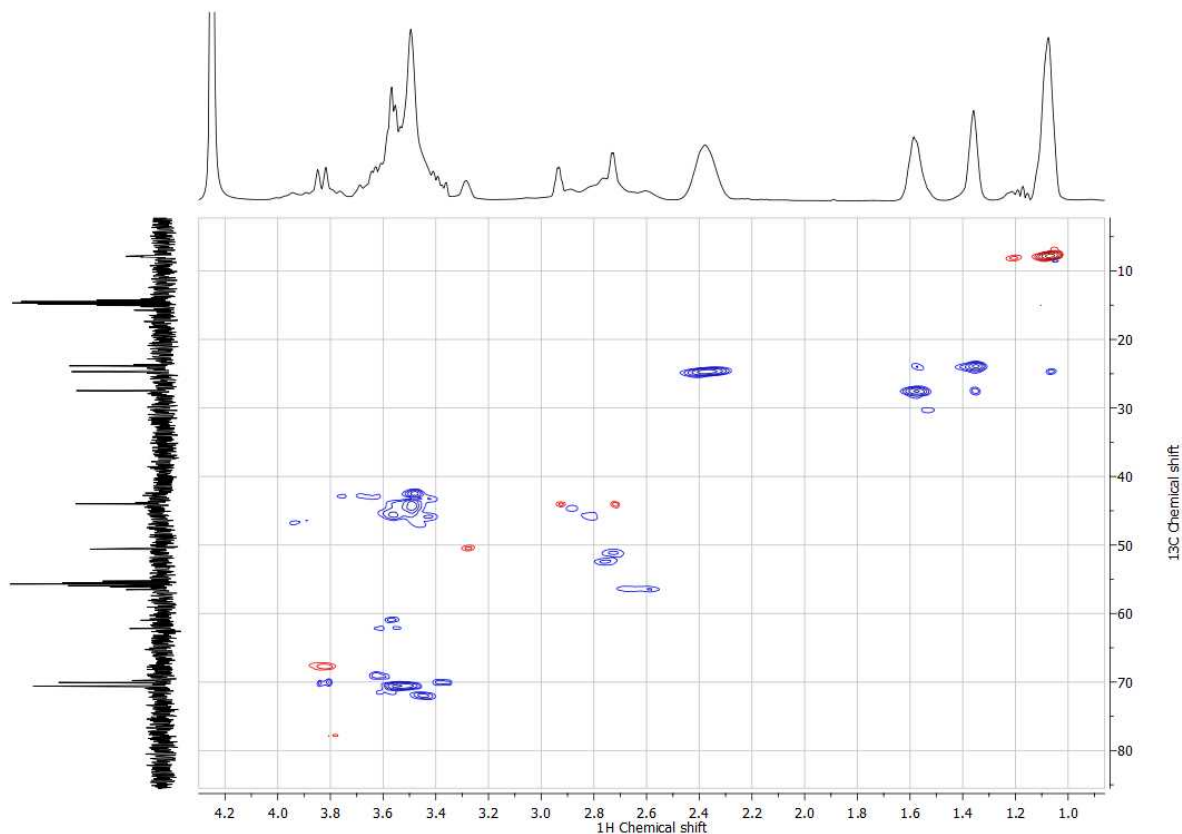


Figure S7 HSQC NMR spectrum of nanogel formation after 2 h at 80 °C

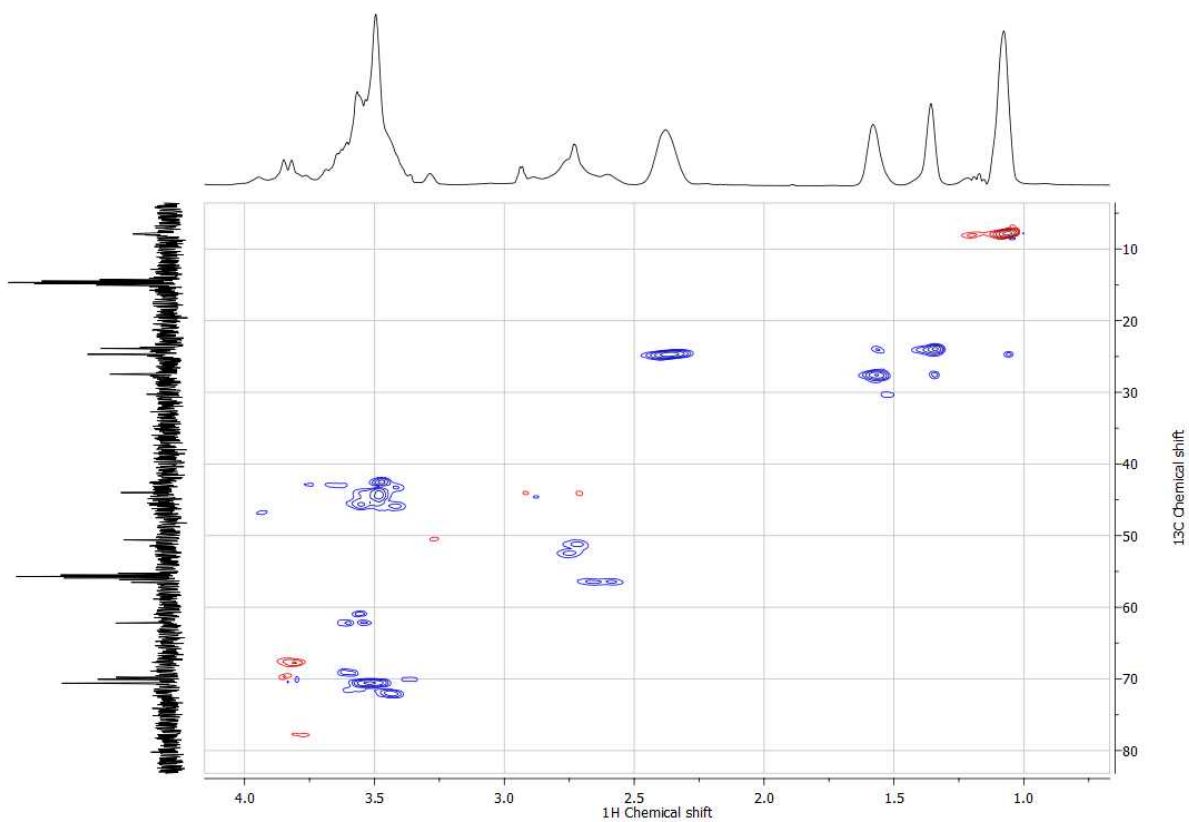


Figure S8 HSQC NMR spectrum of nanogel formation after 5 h at 80 °C

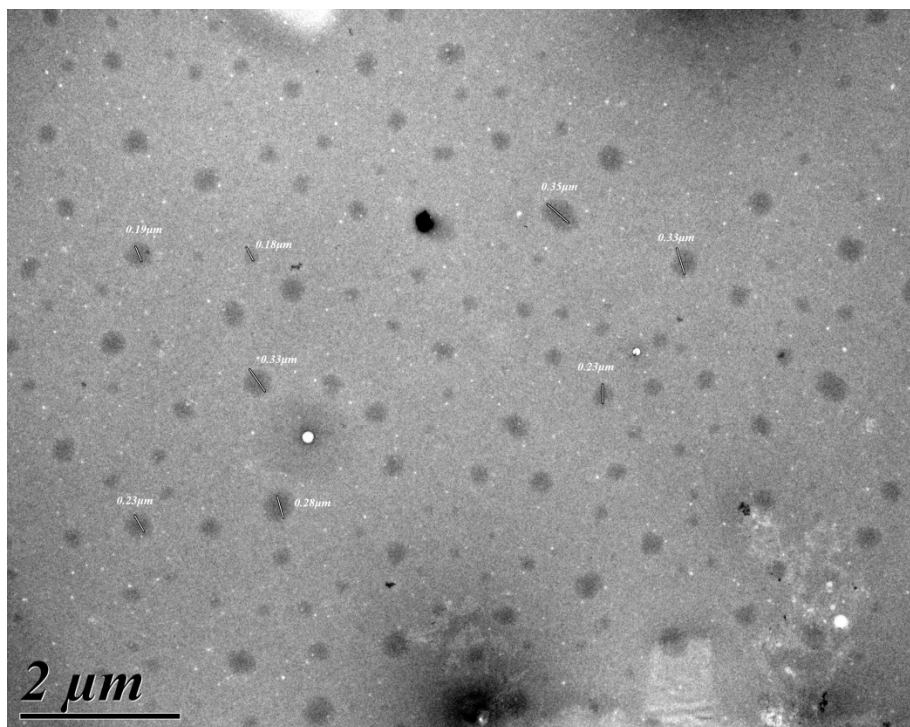


Figure S9 TEM micrograph of nanogels with size measurements

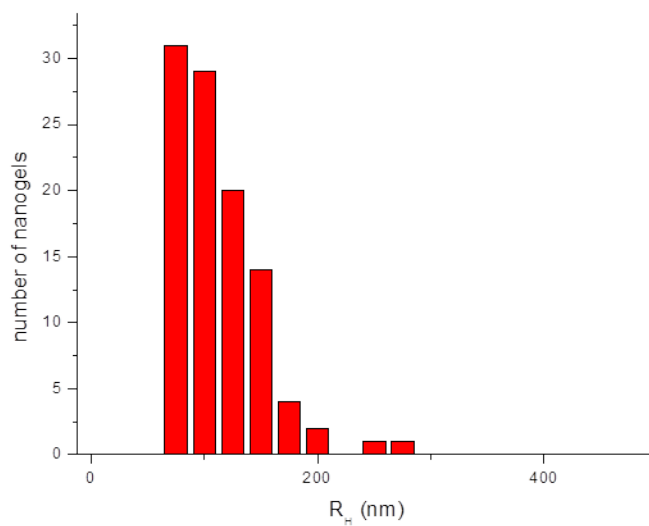


Figure S10 Statistical distributions of TEM particle hydrodynamic radii

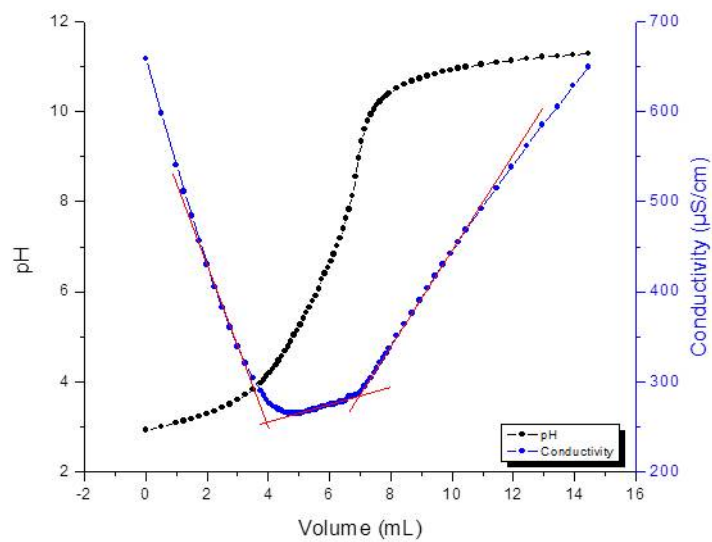


Figure S11 Titration of the secondary amine by pH-metry and conductivity measurements

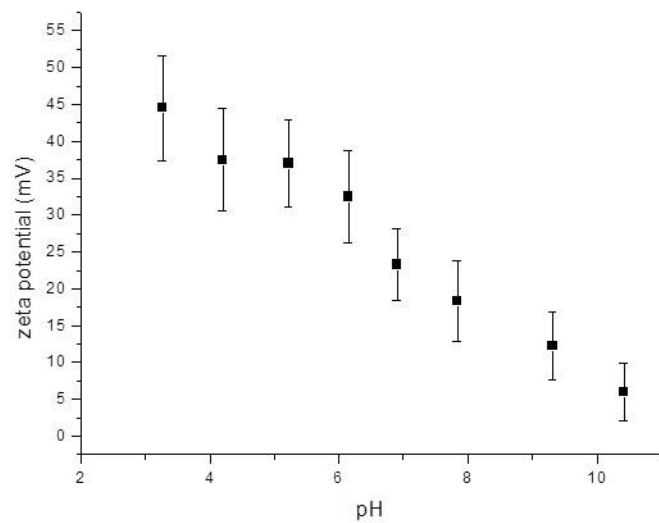


Figure S12 Variation of the zeta potential of nanogels with pH

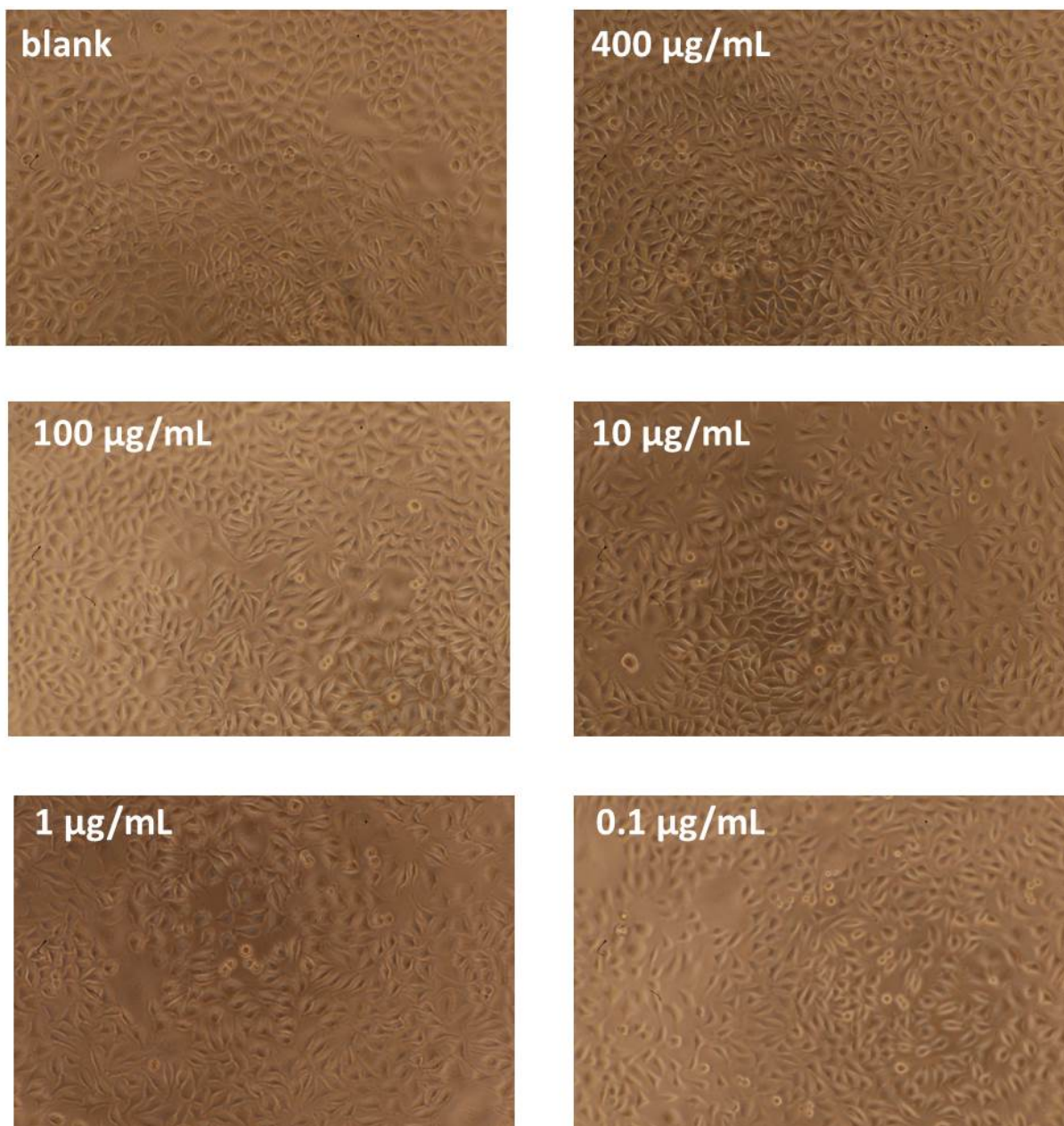


Figure S13 Images obtained on inverted IX81 microscope of fibroblast-like L929 cells after 72 h exposure to nanogel solutions

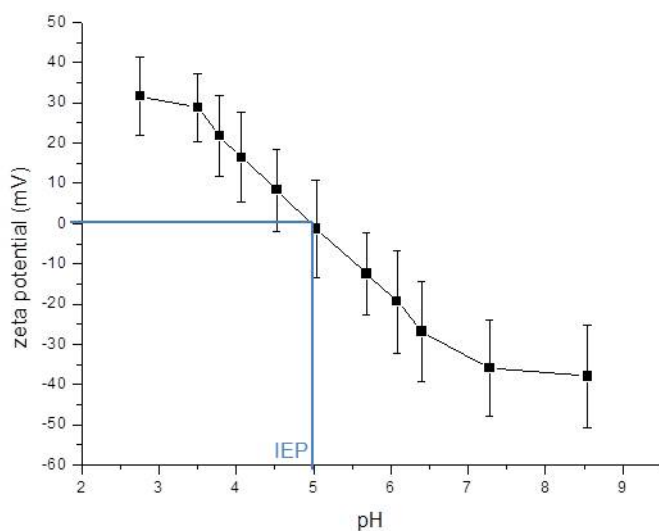


Figure S14 Measurement of isoelectric point of BSA by zetametry

Table S1 NanoSight measurements on the nanogel solution, c = 4.7 mg/mL

Dilution factor	Cn measured ^{a)} [particles/mL]	Cn calculated ^{b)} [particles/mL]	Measurement error min	Measurement error max	Comment
10	2.25E+09	2.25E+10	1.91E+10	2.59E+10	Over concentrated
50	6.23E+08	3.12E+10	2.65E+10	3.58E+10	Linear range
100	4.30E+08	4.30E+10	3.66E+10	4.95E+10	Linear range
1000	2.63E+08	2.63E+11	2.24E+11	3.03E+11	Not enough particles
10000	1.03E+08	1.03E+12	8.73E+11	1.18E+12	Not enough particles

a) Concentration measured by the NanoSight apparatus

b) Concentration in the initial nanogel solutions calculated from Cn measured and the dilution factor

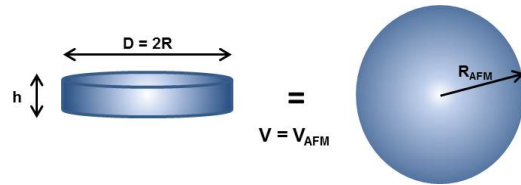
Appendix SI - AFM procedure

The distinct spread of particles onto the mica surface allowed the analysis of section dimensions. This spreading can be modelled as a disc-like structure. The radius of nanogels (R_{AFM}) can then be estimated from the dimensions of the observed discs (diameter D radius R and height h), assuming that the volume of the discs (V) is equal to the volume of spherical nanogels (V_{AFM}):

Volume of spherical nanogels: $V_{AFM} = \frac{4}{3} \pi R_{AFM}^3$

Volume of disc: $V = \pi R^2 h$

Assuming $V = V_{AFM}$, we obtained: $R_{AFM} = \left(\frac{3}{4} R^2 h\right)^{1/3}$



BIBLIOGRAPHY

INTRODUCTION

- (1) Kirschner, C. M.; Anseth, K. S. *Acta Mater.* 2013, 61, 931–944.
- (2) Wichterle, O.; Lim, D. *Nature* 1960, 185, 117–118.
- (3) Alemán, J.; Chadwick, a.; He, J.; Hess, M.; Horie, K.; Jones, R. G.; Kratochvíl, P.; Meisel, I.; Mita, I.; Moad, G.; Penczek, S.; Stepto, R. F. T. *Pure Appl. Chem.* 2007, 79, 1801–1829.
- (4) Sultana, F.; Arafat, M.; Sharmin, S. J. *Appl. Pharm. Sci.* 2013, 3, 95–105.
- (5) Qiu, Y.; Park, K. *Adv. Drug Deliv. Rev.* 2012, 64, 49–60.
- (6) Döring, A.; Birnbaum, W.; Kuckling, D. *Chem. Soc. Rev.* 2013, 42, 7391–7420.
- (7) Miyata, T.; Uragami, T.; Nakamae, K. *Adv. Drug Deliv. Rev.* 2002, 54, 79–98.
- (8) Kim, J. J.; Park, K. J. *Control. Release* 2001, 77, 39–47.
- (9) Lapeyre, V.; Gosse, I.; Chevreux, S.; Ravaine, V. *Biomacromolecules* 2006, 7, 3356–3363.
- (10) Ancla, C.; Lapeyre, V.; Gosse, I.; Catargi, B.; Ravaine, V. *Langmuir* 2011, 27, 12693–12701.
- (11) Gupta, S.; Tyagi, R.; Parmar, V. S.; Sharma, S. K.; Haag, R. *Polymer*. 2012, 53, 3053–3078.
- (12) Piemonte, V. *Polylactic acid: Synthesis, properties and applications*; Nova Science Publishers, Inc., 2012; pp. 1–340.
- (13) Xu, J.; Feng, E.; Song, J. J. *Appl. Polym. Sci.* 2014, 131.
- (14) Khan, W.; Muthupandian, S.; Farah, S.; Kumar, N.; Domb, A. J. *Macromol. Biosci.* 2011, 11, 1625–1636.
- (15) Fasman, G. *Poly a-amino acids*; Dekker: New York, 1967.
- (16) De La Rosa, V. R.; Bouten, P. J. M.; Hoogenboom, R. *Macromol. Chem. Phys.* 2012, 213, 2669–2673.
- (17) Sedlacek, O.; Monnery, B. D.; Filippov, S. K.; Hoogenboom, R.; Hruby, M. *Macromol. Rapid Commun.* 2012, 33, 1648–1662.
- (18) Serina therapeutics Inc. <http://www.serinatherapeutics.com> (accessed Jul 22, 2014).

CHAPTER 1

- (1) Schlaad, H.; Diehl, C.; Gress, A.; Meyer, M.; Levent Demirel, A.; Nur, Y.; Bertin, A. *Macromol. Rapid Commun.* 2010, 31, 511–525.
- (2) Hoogenboom, R. *Macromol. Chem. Phys.* 2007, 208, 18–25.
- (3) Hoogenboom, R. *Angew. Chemie, Int. Ed.* 2009, 48, 7978–7994.
- (4) Warchol, J. F.; Walton, C. D. Creping adhesives containing oxazoline polymer blends and use in paper product applications. US 97-795911, 1998.
- (5) Frechet, J. M. ; Yui, K. Polymerizable polyoxazolines and hyperbranched polymers prepared therefrom. US 96-660684, 1997.
- (6) Brinkhuis, R. H. G. Hyperbranched ester-oxazoline polymers as binders for coatings, inks and adhesives. WO 2002-EPI3898, 2003.
- (7) Ma, S.-H.; Rodriguez-Parada, J. N. Preparation of block copolymers of oxazolines and/or oxazines and their use in ink-jet inks as pigment dispersants. US 97-963839, 1998.
- (8) Moreadith, R.; Bentley, M. D.; Yoon, K.; Weimer, R.; Dizman, B.; Viegas, T. Subcutaneous delivery of poly(oxazoline) conjugates. US 8383093 B1, 2013.

- (9) Yoon, K.; Benthley, M. D.; Harris, J. M.; Fung, Z.; Viegas, T. Multifunctional forms of polyoxazoline copolymers and drug compositions comprising the same. US 8101706 B2, 2012.
- (10) Food and Drug Administration website, List of indirect additives used in food contact substances <http://www.accessdata.fda.gov/scripts/fcn/fcnDetailNavigation.cfm?rpt=iaListing&id=2151> (accessed Jul 31, 2014).
- (11) Luxenhofer, R.; Sahay, G.; Schulz, A.; Alakhova, D.; Bronich, T. K.; Jordan, R.; Kabanov, A. V. *J. Control. Release* **2011**, *153*, 73–82.
- (12) Bauer, M.; Lautenschlaeger, C.; Kempe, K.; Tauhardt, L.; Schubert, U. S.; Fischer, D. *Macromol. Biosci.* **2012**, *12*, 986–998.
- (13) Kronek, J.; Kroneková, Z.; Lustoň, J.; Paulovičová, E.; Paulovičová, L.; Mendrek, B. *J. Mater. Sci. Mater. Med.* **2011**, *22*, 1725–1734.
- (14) Viegas, T. X.; Bentley, M. D.; Harris, J. M.; Fang, Z.; Yoon, K.; Dizman, B.; Weimer, R.; Mero, A.; Pasut, G.; Veronese, F. M. *Bioconjug. Chem.* **2011**, *22*, 976–986.
- (15) Bauer, M.; Schroeder, S.; Tauhardt, L.; Kempe, K.; Schubert, U. S.; Fischer, D. *J. Polym. Sci. Part A Polym. Chem.* **2013**, *51*, 1816–1821.
- (16) Tauhardt, L.; Pretzel, D.; Kempe, K.; Gottschaldt, M.; Schubert, U. S. *Polym. Chem.* **2014**, DOI: 10.1039/C4PY00434E.
- (17) Goddard, P.; Hutchinson, L. E.; Brown, J.; Brookman, L. J. *J. Control. Release* **1989**, *10*, 5–16.
- (18) Gaertner, F. C.; Luxenhofer, R.; Blechert, B.; Jordan, R.; Essler, M. *J. Control. release* **2007**, *119*, 291–300.
- (19) Veronese, F. M.; Mero, A.; Pasut, G.; Fang, Z.; T. X. Viegas. In *36th Ann. Meeting & Exposition CRS*; 2009.
- (20) Knop, K.; Hoogenboom, R.; Fischer, D.; Schubert, U. S. *Angew. Chemie, Int. Ed.* **2010**, *49*, 6288–6308.
- (21) Knop, K.; Pretzel, D.; Urbanek, A. *Biomacromolecules* **2013**, *14*, 2536–2548.
- (22) Wang, C.-H.; Fan, K.-R.; Hsiue, G.-H. *Biomaterials* **2005**, *26*, 2803–2811.
- (23) Jeong, J. H.; Song, S. H.; Lim, D. W.; Lee, H.; Park, T. G. *J. Control. Release* **2001**, *73*, 391–399.
- (24) Hsiue, G.-H.; Chiang, H.-Z.; Wang, C.-H.; Juang, T.-M. *Bioconjug. Chem.* **2006**, *17*, 781–786.
- (25) Van Kuringen, H. P. C.; Lenoir, J.; Adriaens, E.; Bender, J.; De Geest, B. G.; Hoogenboom, R. *Macromol. Biosci.* **2012**, *12*, 1114–1123.
- (26) Ulbricht, J.; Jordan, R.; Luxenhofer, R. *Biomaterials* **2014**, *35*, 4848–4861.
- (27) Woodle, M. C.; Engbers, C. M.; Zalipsky, S. *Bioconjug. Chem.* **1994**, *5*, 493–496.
- (28) Zalipsky, S.; Hansen, C. B.; Oaks, J. M.; Allen, T. M. *J. Pharm. Sci.* **1996**, *85*, 133–137.
- (29) Konradi, R.; Acikgoz, C.; Textor, M. *Macromol. Rapid Commun.* **2012**, *33*, 1663–1676.
- (30) Barz, M.; Luxenhofer, R.; Zentel, R.; Vicent, M. J. *Polym. Chem.* **2011**, *2*, 1900–1918.
- (31) Knop, K.; Hoogenboom, R.; Fischer, D.; Schubert, U. S. *Angew. Chemie, Int. Ed.* **2010**, *49*, 6288–6308.
- (32) Mero, A.; Pasut, G.; Dalla Via, L.; Fijten, M. W. M.; Schubert, U. S.; Hoogenboom, R.; Veronese, F. M. *J. Control. Release* **2008**, *125*, 87–95.
- (33) Pasut, G.; Veronese, F. M. *J. Control. Release* **2012**, *161*, 461–472.
- (34) Guillerm, B.; Darcos, V.; Lapinte, V.; Monge, S.; Coudane, J.; Robin, J. *Chem. Commun.* **2012**, *48*, 2879–2881.
- (35) Konradi, R.; Pidhatika, B.; Mühlebach, A.; Textor, M. *Langmuir* **2008**, *24*, 613–616.
- (36) Bauer, M.; Lautenschlaeger, C.; Kempe, K.; Tauhardt, L.; Schubert, U. S.; Fischer, D. *Macromol. Biosci.* **2012**, *12*, 986–998.
- (37) Zhang, N.; Pompe, T.; Amin, I.; Luxenhofer, R.; Werner, C.; Jordan, R. *Macromol. Biosci.* **2012**, *12*, 926–936.
- (38) Kempe, K.; Ng, S. L.; Noi, K. F.; Mu, M.; Gunawan, S. T.; Caruso, F. *ACS Macro Lett.* **2013**, *2*, 1069–1072.

- (39) Farrugia, B. L.; Kempe, K.; Schubert, U. S.; Hoogenboom, R.; Dargaville, T. R. *Biomacromolecules* **2013**, *14*, 2724–2732.
- (40) Zhu, Z.; Li, X. *J. Appl. Polym. Sci.* **2013**, *131*, 39867–39874.
- (41) Naka, K.; Nakamura, T. *Macromol. Chem. Phys.* **1997**, *198*, 101–116.
- (42) Kelly, A. M.; Kaltenhauser, V.; Mühlbacher, I.; Rametsteiner, K.; Kren, H.; Slugovc, C.; Stelzer, F.; Wiesbrock, F. *Macromol. Biosci.* **2013**, *13*, 116–125.
- (43) Sedlacek, O.; Monnery, B. D.; Filippov, S. K.; Hoogenboom, R.; Hruby, M. *Macromol. Rapid Commun.* **2012**, *33*, 1648–1662.
- (44) Tomalia, D. A.; Sheetz, D. P. *J. Polym. Sci. Part A Polym. Chem.* **1966**, *4*, 2253–2265.
- (45) Seeliger, W.; Aufderhaar, E.; Diepers, W.; Feinauer, R.; Nehring, R.; Thier, W.; Hellmann, H. *Angew. Chemie, Int. Ed.* **1966**, *5*, 875–888.
- (46) Kagiya, T.; Narisawa, S.; Maeda, T.; Fukui, K. *Polym. Lett.* **1966**, *4*, 441–445.
- (47) Bassiri, T. G.; Levy, A.; Litt, M. H. *Polym. Lett.* **1967**, *5*, 871–879.
- (48) Kobayashi, S. *Prog. Polym. Sci.* **1990**, *15*, 751–823.
- (49) Aoi, K.; Okada, M. *Prog. Polym. Sci.* **1996**, *21*, 151–208.
- (50) Kobayashi, S.; Uyama, H. *J. Polym. Sci. Part A Polym. Chem.* **2002**, *40*, 192–209.
- (51) Kobayashi, S. *Polymerization of Oxazolines*; Elsevier B.V., 2012; Vol. 4, pp. 397–426.
- (52) Rudolph, T.; Kempe, K.; Crotty, S.; Paulus, R. M.; Schubert, U. S.; Krossing, I.; Schacher, F. H. *Polym. Chem.* **2013**, *4*, 495–505.
- (53) Aoi, K.; Miyamoto, M.; Chujo, Y.; Saegusa, T. *Macromol. Symp.* **2002**, *183*, 53–64.
- (54) Litt, M.; Levy, A.; Herz, J.; Allied, L. J. *Macromol. Sci. Part A - Chem.* **1975**, *9*, 703–727.
- (55) Cai, G.; Litt, M. *J. Polym. Sci. Part A Polym. Chem.* **1992**, *30*, 649–657.
- (56) Warakomski, J. M.; Thill, B. P. *Polymer.* **1990**, *28*, 3551–3563.
- (57) Hoogenboom, R.; Paulus, R. M.; Fijten, M. W. M.; Schubert, U. S. *J. Polym. Sci. Part A Polym. Chem.* **2005**, *43*, 1487–1497.
- (58) Hoogenboom, R.; Fijten, M. W. M.; Brändli, C.; Schroer, J.; Schubert, U. S. *Macromol. Rapid Commun.* **2003**, *24*, 98–103.
- (59) Hoogenboom, R.; Fijten, M. W. M.; Meier, M. A. R.; Schubert, U. S. *Polymer.* **2003**, *24*, 92–97.
- (60) Hoogenboom, R.; Fijten, M. W. M.; Schubert, U. S. *Macromol. Rapid Commun.* **2004**, *25*, 339–343.
- (61) Park, J. S.; Kataoka, K. *Macromolecules* **2006**, *39*, 6622–6630.
- (62) Hoogenboom, R.; Fijten, M. W. M.; Schubert, U. S. *J. Polym. Sci. Part A Polym. Chem.* **2004**, *42*, 1830–1840.
- (63) Goossens, H.; Catak, S.; Glassner, M.; De La Rosa, V. R.; Monnery, B. D.; De Proft, F.; Van Speybroeck, V.; Hoogen. *ACS Macro Lett.* **2013**, *2*, 651–654.
- (64) Brissault, B.; Kichler, A.; Leborgne, C.; Danos, O.; Cheradame, H.; Gau, J.; Auvray, L.; Guis, C. *Biomacromolecules* **2006**, *7*, 2863–2870.
- (65) Wiesbrock, F.; Hoogenboom, R.; Abeln, C. H.; Schubert, U. S. *Macromol. Rapid Commun.* **2004**, *25*, 1895–1899.
- (66) Wiesbrock, F.; Hoogenboom, R.; Leenen, M. A. M.; Meier, M. A. R.; Schubert, U. S. *Macromolecules* **2005**, *38*, 5025–5034.
- (67) Hoogenboom, R.; Wiesbrock, F.; Huang, H.; Leenen, M. a. M.; Thijs, H. M. L.; van Nispen, S. F. G. M.; van der Loop, M.; Fustin, C.-A.; Jonas, A. M.; Gohy, J.-F.; Schubert, U. S. *Macromolecules* **2006**, *39*, 4719–4725.
- (68) Kempe, K.; Becer, C. R.; Schubert, U. S. *Soft Matter* **2011**, *44*, 5825–5842.
- (69) Wiesbrock, F.; Hoogenboom, R.; Leenen, M.; Nispen, S. F. G. M. Van; Loop, M. Van Der; Abeln, C. H.; Berg, A. M. J. Van Den; Schubert, U. S. *Macromolecules* **2005**, *38*, 7957–7966.
- (70) Lambermont-Thijs, H. M. L.; Heuts, J. P. A.; Hoepfener, S.; Hoogenboom, R.; Schubert, U. S. *Polym. Chem.* **2011**, *2*, 313–322.
- (71) Kagiya, T.; Matsuda, T.; Nakato, M.; Hirata, R. *Macromolecules* **1972**, *6*, 1631–1652.

- (72) Brissault, B.; Kichler, A.; Leborgne, C.; Danos, O.; Cheradame, H.; Gau, J.; Auvray, L.; Guis, C. *Biomacromolecules* **2006**, *7*, 2863–2870.
- (73) Taubmann, C.; Luxenhofer, R.; Cesana, S.; Jordan, R. *Macromol. Biosci.* **2005**, *5*, 603–612.
- (74) Hoogenboom, R.; Lambermont-Thijs, H. M. L.; Jochems, M. J. H. C.; Hoepfener, S.; Guerlain, C.; Fustin, C. A.; Gohy, J. F.; Schubert, U. S. *Soft Matter* **2009**, *5*, 3590–3592.
- (75) Guillermin, B.; Monge, S.; Lapinte, V.; Robin, J.-J. *Macromol. Rapid Commun.* **2012**, *3*, 1600–1612.
- (76) Harris, J. M.; Bentley, M. D.; Yoon, K.; Fang, Z.; Veronese, F. M. Activated polyoxazolines and compositions comprising the same. US 2010/0069579 AA, May 17, 2010.
- (77) Kempe, K.; Lobert, M.; Hoogenboom, R.; Schubert, U. S. *J. Comb. Chem.* **2009**, *11*, 274–280.
- (78) Takahashi, S.; Togo, H. *Synthesis* **2009**, *14*, 2329–2332.
- (79) Levy, A.; Litt, M. J. *Polym. Sci. Part A-1 Polym. Chem.* **1968**, *6*, 1883–1894.
- (80) Kronek, J.; Luston, J.; Kroneková, Z.; Paulovicová, E.; Farkas, P.; Petrencíková, N.; Paulovicová, L.; Janigová, I. *J. Mater. Sci. Mater. Med.* **2010**, *21*, 879–886.
- (81) Cortez, M. A.; Grayson, S. M. *Macromolecules* **2010**, *43*, 4081–4090.
- (82) Zarka, M. T.; Nuyken, O.; Weberskirch, R. *Chemistry* **2003**, *9*, 3228–3234.
- (83) Cesana, S.; Auernheimer, J.; Jordan, R.; Kessler, H.; Nuyken, O. *Macromol. Chem. Phys.* **2006**, *207*, 183–192.
- (84) Hartlieb, M.; Pretzel, D.; Englert, C.; Hentschel, M.; Kempe, K.; Gottschaldt, M.; Schubert, U. S. *Biomacromolecules* **2014**, *15*, 1970–1978.
- (85) Cesana, S.; Kurek, A.; Baur, M. A.; Auernheimer, J.; Nuyken, O. *Macromol. Rapid Commun.* **2007**, *28*, 608–615.
- (86) Hawker, C. J.; Wooley, K. L. *Science* **2005**, *309*, 1200–1205.
- (87) Gauthier, M. A.; Gibson, M. I.; Klok, H.-A. *Angew. Chemie Int. Ed.* **2009**, *48*, 48–58.
- (88) Odian, G. *Principles of polymerization, Fourth edition*; Wiley-interscience John Wiley & Sons, Inc.: Hoboken, New Jersey, 2004; p. 832.
- (89) Hartlieb, M.; Pretzel, D.; Kempe, K.; Fritzsche, C.; Paulus, R. M.; Gottschaldt, M.; Schubert, U. S. *Soft Matter* **2013**, *9*, 4693–4704.
- (90) Kolb, H. C.; Finn, M. G.; Sharpless, K. B. *Angew. Chemie, Int. Ed.* **2001**, *40*, 2004–2021.
- (91) Becer, C. R.; Hoogenboom, R.; Schubert, U. S. *Angew. Chemie, Int. Ed.* **2009**, *48*, 4900–4908.
- (92) Luxenhofer, R.; Jordan, R. *Macromolecules* **2006**, *39*, 3509–3516.
- (93) Lav, T.; Lemechko, P.; Renard, E.; Amiel, C.; Langlois, V.; Volet, G. *React. Funct. Polym.* **2013**, *73*, 1001–1008.
- (94) Del Rio, E.; Lligadas, G.; Ronda, J. C.; Galia, M.; Cadiz, V. J. *Polym. Sci. Part A Polym. Chem.* **2011**, *49*, 3069–3079.
- (95) Kempe, K.; Hoogenboom, R.; Schubert, U. S. *Macromol. Rapid Commun.* **2011**, *32*, 1484–1489.
- (96) Gress, A.; Völkel, A.; Schlaad, H. *Macromolecules* **2007**, *40*, 7928–7933.
- (97) Work, W. J.; Horie, K.; Hess, M.; Stepto, R. F. T. *Pure Appl. Chem.* **2004**, *76*, 1985–2007.
- (98) Diehl, C.; Schlaad, H. *Macromol. Biosci.* **2009**, *9*, 157–161.
- (99) De Espinosa, L. M.; Kempe, K.; Schubert, U. S.; Hoogenboom, R.; Meier, M. A. R. *Macromol. Rapid Commun.* **2012**, *33*, 2023–2028.
- (100) Pánek, J.; Filippov, S. K.; Hrubý, M.; Rabyk, M.; Bogomolova, A.; Kučka, J.; Stěpánek, P. *Macromol. Rapid Commun.* **2012**, *33*, 1683–1689.
- (101) Atilkan, N.; Schlaad, H.; Nur, Y.; Hacaloglu, J. *Macromol. Chem. Phys.* **2014**, *215*, 148–152.
- (102) Kedracki, D.; Maroni, P.; Schlaad, H.; Vebert-Nardin, C. *Adv. Funct. Mater.* **2014**, *24*, 1133–1139.
- (103) Diehl, C.; Schlaad, H. *Macromol. Biosci.* **2009**, *9*, 157–161.
- (104) Schenk, V.; Ellmaier, L.; Rossegger, E.; Edler, M.; Griesser, T.; Weidinger, G.; Wiesbrock, F. *Macromol. Rapid Commun.* **2012**, *33*, 396–400.
- (105) Cai, G.; Litt, M. H. *J. Polym. Sci. Part A Polym. Chem.* **1996**, *34*, 2701–2709.
- (106) Hoogenboom, R. *Eur. J. Lipid Sci. Technol.* **2011**, *113*, 59–71.
- (107) Kempe, K.; Hoogenboom, R.; Jaeger, M.; Schubert, U. S. *Macromolecules* **2011**, *44*, 6424–6432.

- (108) Dargaville, T. R.; Forster, R.; Farrugia, B. L.; Kempe, K.; Voorhaar, L.; Schubert, U. S.; Hoogenboom, R. *Macromol. Rapid Commun.* **2012**, *33*, 1695–1700.
- (109) Hoogenboom, R.; Thijs, H. M. L.; Fijten, M. W. M.; Schubert, U. S. *J. Polym. Sci. Part A Polym. Chem.* **2007**, *45*, 5371–5379.
- (110) Huang, H.; Hoogenboom, R.; Leenen, M. A. M.; Guillet, P.; Jonas, A. M.; Schubert, U. S.; Gohy, J. F. *J. Am. Chem. Soc.* **2006**, *128*, 3784–3788.
- (111) Hoogenboom, R.; Leenen, M. A. M.; Huang, H.; Fustin, C.-A.; Gohy, J.-F.; Schubert, U. S. *Colloid Polym. Sci.* **2006**, *284*, 1313–1318.
- (112) Einzmann, M.; Binder, W. H. *J. Polym. Sci. Part A Polym. Chem.* **2001**, *39*, 2821–2831.
- (113) Yang, Y.; Kataoka, K.; Winnik, F. M. *Macromolecules* **2005**, *38*, 2043–2046.
- (114) Giardi, C.; Lapinte, V. *Polymer* **2010**, *48*, 4027–4035.
- (115) Park, J.; Akiyama, Y.; Winnik, F. *Macromolecules* **2004**, *37*, 6786–6792.
- (116) Reif, M.; Jordan, R. *Macromol. Chem. Phys.* **2011**, *212*, 1815–1824.
- (117) Rueda, J. C.; Komber, H.; Cedrón, J. C.; Voit, B.; Shevtsova, G. *Macromol. Chem. Phys.* **2003**, *204*, 947–953.
- (118) Fijten, M. W. M.; Haensch, C.; Van Lankvelt, B. M.; Hoogenboom, R.; Schubert, U. S. *Macromol. Chem. Phys.* **2008**, *209*, 1887–1895.
- (119) Guillerm, B.; Monge, S.; Lapinte, V.; Robin, J.-J. *J. Polym. Sci. Part A Polym. Chem.* **2013**, *51*, 1118–1128.
- (120) Kempe, K.; Onbulak, S.; Schubert, U. S.; Sanyal, A.; Hoogenboom, R. *Polym. Chem.* **2013**, *4*, 3236.
- (121) Isaacman, M. J.; Barron, K. A.; Theogarajan, L. S. *J. Polym. Sci. Part A Polym. Chem.* **2012**, *50*, 2319–2329.
- (122) Caponi, P.-F.; Qiu, X.-P.; Vilela, F.; Winnik, F. M.; Ulijn, R. V. *Polym. Chem.* **2011**, *2*, 306–308.
- (123) Kim, J.; Lee, E.; Park, J.; Kataoka, K.; Jang, W. *Chem. Commun.* **2012**, *48*, 3662–3664.
- (124) Guillerm, B.; Monge, S.; Lapinte, V.; Robin, J. J. *J. Polym. Sci. Part A Polym. Chem.* **2013**, *51*, 1118–1128.
- (125) Hespel, L.; Morandi, G.; Grossel, M.; Lecamp, L.; Picton, L.; Burel, F. *Polym. Chem.* **2014**, *5*, 4009–4015.
- (126) Fijten, M. W. M.; Haensch, C.; van Lankvelt, B. M.; Hoogenboom, R.; Schubert, U. S. *Macromol. Chem. Phys.* **2008**, *209*, 1887–1895.
- (127) Yuan, J.; Ten Brummelhuis, N.; Junginger, M.; Xie, Z.; Lu, Y.; Taubert, A.; Schlaad, H. *Macromol. Rapid Commun.* **2011**, *32*, 1157–1162.
- (128) Kobayashi, S.; Iijima, S.; Igarashi, T.; Saegusa, T. *Macromolecules* **1987**, *20*, 2–7.
- (129) Stemmelen, M.; Travelet, C.; Lapinte, V.; Borsali, R.; Robin, J.-J. *Polym. Chem.* **2013**, *4*, 1445–1458.
- (130) Giardi, C.; Lapinte, V.; Charnay, C.; Robin, J. J. *React. Funct. Polym.* **2009**, *69*, 643–649.
- (131) Volet, G.; Chanthavong, V.; Wintgens, V.; Amiel, C. *Macromolecules* **2005**, *38*, 5190–5197.
- (132) Volet, G.; Amiel, C. *Colloids Surf. B. Biointerfaces* **2012**, *91*, 269–273.
- (133) Chujo, Y.; Sada, K.; Kawasaki, T.; Saegusa, T. *Polym. J.* **1992**, *24*, 1301–1306.
- (134) Weber, C.; Czaplowska, J. A.; Baumgaertel, A.; Altuntas, E.; Gottschaldt, M.; Hoogenboom, R.; Schubert, U. S. *Macromolecules* **2012**, *45*, 46–55.
- (135) Aoi, K.; Suzuki, H.; Okada, M. *Macromolecules* **1992**, *25*, 7073–7075.
- (136) Paulus, R. M.; Becer, C. R.; Hoogenboom, R.; Schubert, U. S. *Macromol. Chem. Phys.* **2008**, *209*, 794–800.
- (137) Bühler, J.; Muth, S.; Fischer, K.; Schmidt, M. *Macromol. Rapid Commun.* **2013**, *34*, 588–594.
- (138) Chujo, Y.; Sada, K.; Kawasaki, T.; Ihara, E.; Saegusa, T. *Polym. Bull.* **1993**, *31*, 311–316.
- (139) Mero, A.; Fang, Z.; Pasut, G.; Veronese, F. M.; Viegas, T. X. *J. Control. Release* **2012**, *159*, 353–361.
- (140) Konieczny, S.; Fik, C. P.; Aversch, N. J. H.; Tiller, J. C. *J. Biotechnol.* **2012**, *159*, 195–203.
- (141) Krumm, C.; Konieczny, S.; Dropalla, G. J.; Milbradt, M.; Tiller, J. C. *Macromolecules* **2013**, *46*, 3234–3245.

- (142) Kobayashi, S.; Masuda, E.; Shoda, S.; Shimano, Y. *Macromolecules* **1989**, *22*, 2878–2884.
- (143) Miyamoto, M.; Naka, K.; Tokumizu, M.; Saegusa, T. *Macromolecules* **1989**, *22*, 1604–1607.
- (144) Weber, C.; Wagner, M.; Baykal, D.; Hoepfener, S.; Paulus, R. M.; Festag, G.; Altuntas, E.; Schacher, F. H.; Schubert, U. S. *Macromolecules* **2013**, *46*, 5107–5116.
- (145) Wang, C.-H.; Hsiue, G.-H. *J. Polym. Sci. Part A Polym. Chem.* **2002**, *40*, 1112–1121.
- (146) Kempe, K.; Killups, K. L.; Poelma, J. E.; Jung, H.; Bang, J.; Hoogenboom, R.; Tran, H.; Hawker, C. J.; Schubert, U. S.; Campos, L. M. *ACS Macro Lett.* **2013**, *2*, 677–682.
- (147) David, G.; Alupeii, V.; Simionescu, B. C. *Eur. Polym. J.* **2001**, *37*, 1353–1358.
- (148) Volet, G.; Lav, T.-X.; Babinot, J.; Amiel, C. *Macromol. Chem. Phys.* **2011**, *212*, 118–124.
- (149) Glassner, M.; Kempe, K.; Schubert, U. S.; Hoogenboom, R.; Barner-Kowollik, C. *Chem. Commun.* **2011**, *47*, 10620–10622.
- (150) Marx, L.; Volet, G.; Amiel, C. *J. Polym. Sci. Part A Polym. Chem.* **2011**, *49*, 4785–4793.
- (151) Waschinski, C. J.; Herdes, V.; Schueler, F.; Tiller, J. C. *Macromol. Biosci.* **2005**, *5*, 149–156.
- (152) Waschinski, C. J.; Tiller, J. C. *Biomacromolecules* **2005**, *6*, 235–243.
- (153) Krumm, C.; Harmuth, S.; Hijazi, M.; Neugebauer, B.; Kampmann, A.-L.; Geltenpoth, H.; Sickmann, A.; Tiller, J. C. *Angew. Chemie Int. Ed.* **2014**, *53*, 1–6.
- (154) Alemán, J.; Chadwick, a.; He, J.; Hess, M.; Horie, K.; Jones, R. G.; Kratochvíl, P.; Meisel, I.; Mita, I.; Moad, G.; Penczek, S.; Stepto, R. F. T. *Pure Appl. Chem.* **2007**, *79*, 1801–1829.
- (155) Kelly, A. M.; Wiesbrock, F. *Macromol. Rapid Commun.* **2012**, *33*, 1632–1647.
- (156) Chujo, Y.; Sada, K.; Matsumoto, K.; Saegusa, T. *Polym. Bull.* **1989**, *21*, 353–356.
- (157) Chujo, Y.; Sada, K.; Matsumoto, K.; Saegusa, T. *Macromolecules* **1990**, *23*, 1234–1237.
- (158) Kelly, A. M.; Hecke, A.; Wirnsberger, B.; Wiesbrock, F. *Macromol. Rapid Commun.* **2011**, *32*, 1815–1819.
- (159) Park, I.; Han, I.; Kim, D.; Saegusa, T. *Angew. Makromol. Chem.* **1991**, *190*, 165–176.
- (160) Brissault, B.; Kichler, A.; Guis, C.; Leborgne, C.; Danos, O.; Cheradame, H. *Polymer.* **2003**, *14*, 581–587.
- (161) Litt, M. H.; Lin, C. S. *J. Polym. Sci. Part A Polym. Chem.* **1992**, *30*, 779–786.
- (162) Tauhardt, L.; Kempe, K.; Schubert, U. S. *J. Polym. Sci. Part A Polym. Chem.* **2012**, *50*, 4516–4523.
- (163) De La Rosa, V. R.; Bauwens, E.; Monnery, B. D.; De Geest, B. G.; Hoogenboom, R. *Polym. Chem.* **2014**.
- (164) Van Kuringen, H. P. C.; De La Rosa, V. R.; Fijten, M. W. M.; Heuts, J. P. A.; Hoogenboom, R. *Macromol. Rapid Commun.* **2012**, *33*, 827–832.
- (165) Tanaka, R.; Ueoka, I.; Takaki, Y.; Kataoka, K.; Saito, S. *Macromolecules* **1983**, *16*, 849–853.
- (166) Lambermont-Thijs, H. M. L.; Van Der Woerd, F. S.; Baumgaertel, A.; Bonami, L.; Du Prez, F. E.; Schubert, U. S.; Hoogenboom, R. *Macromolecules* **2010**, *43*, 927–933.
- (167) Tauhardt, L.; Kempe, K.; Knop, K.; Altuntaş, E.; Jäger, M.; Schubert, S.; Fischer, D.; Schubert, U. S. *Macromol. Chem. Phys.* **2011**, *212*, 1918–1924.
- (168) Hachemaoui, A.; Yahiaoui, A.; Belbachir, M. *J. Appl. Polym. Sci.* **2006**, *102*, 3741–3750.
- (169) Chujo, Y.; Yoshifuji, Y.; Sada, K.; Saegusa, T. *Macromolecules* **1989**, *22*, 1074–1077.
- (170) Chujo, Y.; Sada, K.; Naka, A.; Nomura, R.; Saegusa, T. *Macromolecules* **1993**, *26*, 883–887.
- (171) Chujo, Y.; Sada, K.; Saegusa, T. *Macromolecules* **1990**, *23*, 2693–2697.
- (172) Chujo, Y.; Sada, K.; Nomura, R.; Naka, A.; Saegusa, T. *Macromolecules* **1993**, *26*, 5611–5614.
- (173) Chujo, Y.; Sada, K.; Saegusa, T. *Macromolecules* **1990**, *23*, 2636–2641.
- (174) Wang, C.; Hwang, Y.; Chiang, P.; Shen, C.; Hong, W.; Hsiue, G. *Biomacromolecules* **2012**, *13*, 40–48.
- (175) Fijten, M.; Kranenburg, J.; Thijs, H. M. L.; Paulus, R. M.; van Lankvelt, B. M.; De Hullu, J.; Springintveld, M.; Thielen, D. J. G.; Tweedie, C. A.; Hoogenboom, R.; Van Vliet, K. J.; Schubert, U. S. *Macromolecules* **2007**, *40*, 5879–5886.
- (176) Rettler, E. F.-J.; Kranenburg, J. M.; Lambermont-Thijs, H. M. L.; Hoogenboom, R.; Schubert, U. S. *Macromol. Chem. Phys.* **2010**, *211*, 2443–2448.

- (177) Weber, C.; Hoogenboom, R.; Schubert, U. S. *Prog. Polym. Sci.* **2011**, *37*, 686–714.
- (178) Erik, F.; Lambermont-Thijs, H.; Kranenburg, J. J. *Mater. Chem.* **2011**, *21*, 17331–17337.
- (179) Rettler, E. F.; Unger, M. V.; Hoogenboom, R.; Siesler, H. W. *Appl. Spectrosc.* **2012**, *66*, 1145–1155.
- (180) Lambermont-Thijs, H. M. L.; Kuringen, H. P. C. Van; Put, J. P. W. Van Der; Schubert, U. S.; Hoogenboom, R. *Polymers* **2010**, *2*, 188–199.
- (181) Lambermont-Thijs, H. M. L.; Hoogenboom, R.; Fustin, C. A.; Bomal-D’Haese, C.; Gohy, J. F.; Schubert, U. S. *J. Polym. Sci. Part A Polym. Chem.* **2009**, *47*, 515–522.
- (182) Hoogenboom, R.; Thijs, H. M. L.; Wouters, D.; Hoepfener, S.; Schubert, U. S. *Soft Matter* **2008**, *4*, 103–107.
- (183) Aseyev, V.; Tenhu, H.; Winnik, F. M. *Adv. Polym. Sci.* **2011**, *242*, 29–89.
- (184) Bloksma, M. M.; Bakker, D. J.; Weber, C.; Hoogenboom, R.; Schubert, U. S. *Macromol. Rapid Commun.* **2010**, *31*, 724–728.
- (185) Huber, S.; Hutter, N.; Jordan, R. *Colloid Polym. Sci.* **2008**, *286*, 1653–1661.
- (186) Kempe, K.; Rettler, E. F.-J.; Paulus, R. M.; Kuse, A.; Hoogenboom, R.; Schubert, U. S. *Polymer* **2013**, *54*, 2036–2042.
- (187) Huber, S.; Jordan, R. *Colloid Polym. Sci.* **2007**, *286*, 395–402.
- (188) Zhang, N.; Luxenhofer, R.; Jordan, R. *Macromol. Chem. Phys.* **2012**, *213*, 1963–1969.
- (189) Weber, C.; Remzi Becer, C.; Guenther, W.; Hoogenboom, R.; Schubert, U. S. *Macromolecules* **2010**, *43*, 160–167.
- (190) Weber, C.; Krieg, A.; Paulus, R. M.; Lambermont-Thijs, H. M. L.; Becer, C. R.; Hoogenboom, R.; Schubert, U. S. *Macromol. Symp.* **2011**, *308*, 17–24.
- (191) Kempe, K.; Neuwirth, T.; Czaplewska, J.; Gottschaldt, M.; Hoogenboom, R.; Schubert, U. S. *Polym. Chem.* **2011**, *2*, 1737–1743.
- (192) Litt, M.; Rhal, F.; Roldan, L. G. *J. Polym. Sci. Part A-2 Polym. Phys.* **1969**, *7*, 463–473.
- (193) Rettler, E. F.-J.; Lambermont-Thijs, H. M. L.; Kranenburg, J. M.; Hoogenboom, R.; Unger, M. V.; Siesler, H. W.; Schubert, U. S. *J. Mater. Chem.* **2011**, *21*, 17331–17337.
- (194) Diehl, C.; Dambowsky, I.; Hoogenboom, R.; Schlaad, H. *Macromol. Rapid Commun.* **2011**, *32*, 1753–1758.
- (195) Güner, P. T.; Mikó, A.; Schweinberger, F. F.; Demirel, A. L. *Polym. Chem.* **2012**, *3*, 322–324.
- (196) Bloksma, M. M.; Hendrix, M. M. R. M.; Schubert, U. S.; Hoogenboom, R. *Macromolecules* **2010**, *43*, 4654–4659.
- (197) Bloksma, M. M.; Weber, C.; Perevyazko, I. Y.; Kuse, A.; Baumgartel, A.; Vollrath, A.; Hoogenboom, R.; Schubert, U. S. *Macromolecules* **2011**, *44*, 4057–4064.
- (198) Hocine, S.; Li, M. *Soft Matter* **2013**, *9*, 5839–5861.
- (199) Diab, C.; Akiyama, Y.; Kataoka, K.; Winnik, F. M. *Macromolecules* **2004**, *37*, 2556–2562.
- (200) Uyama, H.; Kobayashi, S. *Chem. Lett.* **1992**, *9*, 1643–1646.
- (201) Zhao, J.; Hoogenboom, R.; Van Assche, G.; Van Mele, B. *Macromolecules* **2010**, *43*, 6853–6860.
- (202) Meyer, M.; Antonietti, M.; Schlaad, H. *Soft Matter* **2007**, *3*, 430–431.
- (203) Demirel, A. L.; Meyer, M.; Schlaad, H. *Angew. Chem. Int. Ed. Engl.* **2007**, *46*, 8622–8624.
- (204) Katsumoto, Y.; Tsuchiizu, A.; Qiu, X.; Winnik, F. M. *Macromolecules* **2012**, *45*, 3531–3541.
- (205) Diehl, C.; Schlaad, H. *Chem. Eur. J.* **2009**, *15*, 11469–11472.
- (206) Morimoto, N.; Obeid, R.; Yamane, S.; Winnik, F. M.; Akiyoshi, K. *Soft Matter* **2009**, *5*, 1597–1600.
- (207) Luxenhofer, R.; Han, Y.; Schulz, A.; Tong, J.; He, Z.; Kabanov, A. V.; Jordan, R. *Macromol. Rapid Commun.* **2012**, *33*, 1613–1631.
- (208) Adams, N.; Schubert, U. S. *Adv. Drug Deliv. Rev.* **2007**, *59*, 1504 – 1520.
- (209) Claeys, B.; Vervaeck, A.; Vervaeet, C.; Remon, J. P.; Hoogenboom, R.; De Geest, B. G. *Macromol. Rapid Commun.* **2012**, *33*, 1701–1707.
- (210) Serina therapeutics Inc. <http://www.serinatherapeutics.com> (accessed Jul 22, 2014).
- (211) Lammers, T.; Kiessling, F.; Hennink, W. E.; Storm, G. *J. Control. Release* **2012**, *161*, 175–187.
- (212) Kelkar, S. S.; Reineke, T. M. *Bioconjug. Chem.* **2011**, *22*, 1879–1903.

- (213) Ma, X.; Zhao, Y.; Liang, X. J. *Acc. Chem. Res.* **2011**, *44*, 1114–1122.
- (214) Nystrom, A. M.; Wooley, K. L. *Acc. Chem. Res.* **2011**, *44*, 969–978.
- (215) Kamaly, N.; Xiao, Z.; Valencia, P. M.; Radovic-Moreno, A. F.; Farokhzad, O. C. *Chem. Soc. Rev.* **2012**, *41*, 2971–3010.
- (216) Farokhzad, O. C.; Langer, R. *ACS Nano* **2009**, *3*, 16–20.
- (217) Doane, T. L.; Burda, C. *Chem. Soc. Rev.* **2012**, *41*, 2885–2911.
- (218) Hamidi, M.; Shahbazi, M.-A.; Rostamizadeh, K. *Macromol. Biosci.* **2012**, *12*, 144–164.
- (219) Upadhyay, K. K.; Agrawal, H. G.; Upadhyay, C.; Schatz, C.; Le Meins, J. F.; Misra, A.; Lecommandoux, S. *Crit. Rev. Ther. Drug Carrier Syst.* **2009**, *26*, 157–205.
- (220) Khandare, J.; Calderón, M.; Dagia, N. M.; Haag, R. *Chem. Soc. Rev.* **2012**, *41*, 2824–2848.
- (221) Sultana, F.; Arafat, M.; Sharmin, S. J. *Appl. Pharm. Sci.* **2013**, *3*, 95–105.
- (222) Devadasu, V. R.; Bhardwaj, V.; Kumar, M. N. V. R. *Chem. Rev.* **2013**, *113*, 1686–1735.
- (223) Ganta, S.; Devalapally, H.; Shahiwala, A.; Amiji, M. J. *Control. Release* **2008**, *126*, 187–204.
- (224) Elsabahy, M.; Wooley, K. L. *Chem. Soc. Rev.* **2012**, *41*, 2545–2561.
- (225) Jain, R. K.; Stylianopoulos, T. *Nat. Rev. Clin. Oncol.* **2010**, *7*, 653–664.
- (226) Deshayes, S.; Kasko, A. J. *Polym. Sci. Part A Polym. Chem.* **2013**, *51*, 3531–3566.
- (227) De Las Heras Alarcon, C.; Pennadam, S.; Alexander, C. *Chem. Soc. Rev.* **2005**, *34*, 276–285.
- (228) Alvarez-Lorenzo, C.; Concheiro, A. *Chem. Commun.* **2014**, *50*, 7743–7765.
- (229) Abulateefeh, S. R.; Spain, S. G.; Aylott, J. W.; Chan, W. C.; Garnett, M. C.; Alexander, C. *Macromol. Biosci.* **2011**, *11*, 1722–1734.
- (230) Binauld, S.; Stenzel, M. H. *Chem. Commun.* **2013**, *49*, 2082–2102.
- (231) Nowag, S.; Haag, R. *Angew. Chemie Int. Ed.* **2014**, *53*, 49–51.
- (232) Huo, M.; Yuan, J.; Tao, L.; Wei, Y. *Polym. Chem.* **2014**, *5*, 1519–1528.
- (233) Gracia, R.; Mecerreyes, D. *Polym. Chem.* **2013**, *4*, 2206–2214.
- (234) Lallana, E.; Tirelli, N. *Macromol. Chem. Phys.* **2013**, *214*, 143–158.
- (235) Meng, F.; Hennink, W. E.; Zhong, Z. *Biomaterials* **2009**, *30*, 2180–2198.
- (236) Ravichandran, R.; Sundarrajan, S.; Venugopal, J. R.; Mukherjee, S.; Ramakrishna, S. *Macromol. Biosci.* **2012**, *12*, 286–311.
- (237) Tong, R.; Tang, L.; Ma, L.; Tu, C.; Baumgartner, R.; Cheng, J. *Chem. Soc. Rev.* **2014**, DOI: 10.1039/c4cs00133h.
- (238) Jackson, A. W.; Fulton, D. a. *Polym. Chem.* **2013**, *4*, 31–45.
- (239) Nicolas, J.; Mura, S.; Brambilla, D.; Mackiewicz, N.; Couvreur, P. *Chem. Soc. Rev.* **2013**, *42*, 1147–1235.
- (240) Moyano, D. F.; Rotello, V. M. *Langmuir* **2011**, *27*, 10376–10385.
- (241) Dawidczyk, C. M.; Kim, C.; Park, J. H.; Russell, L. M.; Lee, K. H.; Pomper, M. G.; Searson, P. C. J. *Control. Release* **2014**, *187*, 133–144.
- (242) Velander, W. H.; Madurawe, R. D.; Subramanian, A.; Kumar, G.; Sinai-zingde, G.; Rifflet, J. S. *Biotechnol. Bioeng.* **1992**, *39*, 1024–1030.
- (243) Tong, J.; Yi, X.; Luxenhofer, R.; Banks, W. a; Jordan, R.; Zimmerman, M. C.; Kabanov, A. V. *Mol. Pharm.* **2013**, *10*, 360–377.
- (244) Tong, J.; Luxenhofer, R.; Yi, X.; Jordan, R. *Mol. Pharm.* **2010**, *7*, 984–992.
- (245) Kempe, K.; Vollrath, A.; Schaefer, H. W.; Poehlmann, T. G.; Biskup, C.; Hoogenboom, R.; Hornig, S.; Schubert, U. S. *Macromol. Rapid Commun.* **2010**, *31*, 1869–1873.
- (246) Milonaki, Y.; Kaditi, E.; Pispas, S.; Demetzos, C. J. *Polym. Sci. Part A Polym. Chem.* **2011**, *50*, 1226–1237.
- (247) Hruby, M.; Filippov, S. K.; Panek, J.; Novakova, M.; Mackova, H.; Kucka, J.; Vetvicka, D.; Ulbrich, K. *Macromol. Biosci.* **2010**, *10*, 916–924.
- (248) Luxenhofer, R.; Schulz, A.; Roques, C.; Li, S.; Bronich, T. K.; Batrakova, E. V.; Jordan, R.; Kabanov, A. V. *Biomaterials* **2010**, *31*, 4972–4979.

- (249) Han, Y.; He, Z.; Schulz, A.; Bronich, T. K.; Jordan, R.; Luxenhofer, R.; Kabanov, A. V. *Mol. Pharm.* **2012**, *9*, 2302–2313.
- (250) Schulz, A.; Jaksch, S.; Schubel, R.; Wegener, E.; Di, Z.; Han, Y.; Meister, A.; Kressler, J.; Kabanov, A. V.; Luxenhofer, R.; Papadakis, C. M.; Jordan, R. *ACS Nano* **2014**, *8*, 2686–2696.
- (251) Nardin, C.; Hirt, T.; Leukel, J.; Meier, W. *Langmuir* **2000**, *16*, 1035–1041.
- (252) Broz, P.; Benito, S. M.; Saw, C. L.; Burger, P.; Heider, H.; Pfisterer, M.; Marsch, S.; Meier, W.; Hunziker, P. *J. Control. release* **2005**, *102*, 475–488.
- (253) Egli, S.; Nussbaumer, M. G.; Balasubramanian, V.; Chami, M.; Bruns, N.; Palivan, C.; Meier, W. *J. Am. Chem. Soc.* **2011**, *133*, 4476–4483.
- (254) Jaskiewicz, K.; Larsen, A.; Lieberwirth, I.; Koynov, K.; Meier, W.; Fytas, G.; Kroeger, A.; Landfester, K. *Angew. Chemie, Int. Ed.* **2012**, *51*, 1–6.
- (255) Jaskiewicz, K.; Larsen, A.; Schaeffel, D.; Koynov, K.; Lieberwirth, I.; Fytas, G.; Landfester, K.; Kroeger, A. *ACS Nano* **2012**, *6*, 7254–7262.
- (256) Pippa, N.; Kaditi, E.; Pispas, S.; Demetzos, C. *J. Nanoparticle Res.* **2013**, *15*, 1685.
- (257) Chen, L.; Zhang, L.; Chen, J.; Yang, J.; Li, R. *Chinese Sci. Bull.* **2010**, *55*, 4187–4196.
- (258) Peng, K.; Wang, S.; Lee, R. *J. Polym. Sci. Part A Polym. Chem.* **2013**, *51*, 2769–2781.
- (259) Lin, C.; Sung, Y.-C.; Hsiue, G.-H. *J. Med. Biol. Eng.* **2011**, *32*, 365–372.
- (260) An, Z.; Qiu, Q.; Liu, G. *Chem. Commun.* **2011**, *47*, 12424–12440.
- (261) He, C.; Zhuang, X.; Tang, Z.; Tian, H.; Chen, X. *Adv. Healthc. Mater.* **2012**, *1*, 48–78.
- (262) Dai, Z.; Ngai, T. *J. Polym. Sci. Part A Polym. Chem.* **2013**, *51*, 2995–3003.
- (263) Liu, G.; An, Z. *Polym. Chem.* **2014**, *5*, 1559–1565.
- (264) Seiffert, S. *J. Polym. Sci. Part A Polym. Chem.* **2014**, *52*, 435–449.
- (265) Taton, D. In *Macromolecular Engineering: precise synthesis, materials properties, application*; Matyjaszewski, K.; Gnanou, Y.; Leibler, L., Eds.; Wiley-VCH Verlag GmbH & Co. KGaA: Weinheim, Germany, 2007.
- (266) Kabanov, A. V.; Vinogradov, S. V. *Angew. Chemie, Int. Ed.* **2009**, *48*, 5418–5429.
- (267) Hendrickson, G. R.; Lyon, L. A. *Angew. Chemie, Int. Ed.* **2010**, *49*, 2193–2197.
- (268) Merkel, T. J.; Jones, S. W.; Herlihy, K. P.; Kersey, F. R.; Shields, A. R.; Napier, M.; Luft, J. C.; Wu, H.; Zamboni, W. C.; Wang, A. Z.; Bear, J. E.; DeSimone, J. M. *Proc. Natl. Acad. Sci.* **2011**, *108*, 586–591.
- (269) Elsbahy, M.; Wooley, K. L. *J. Polym. Sci. Part A Polym. Chem.* **2012**, *50*, 1869–1880.
- (270) Chang, D. H. C.; Johnston, A. P. R.; Wark, K. L.; Breheny, K.; Caruso, F. *Angew. Chemie, Int. Ed.* **2011**, 1–6.
- (271) Oh, J. K.; Drumright, R.; Siegwart, D. J.; Matyjaszewski, K. *Prog. Polym. Sci.* **2008**, *33*, 448–477.
- (272) Oh, J. K.; Lee, D. I.; Park, J. M. *Prog. Polym. Sci.* **2009**, *34*, 1261–1282.
- (273) Sasaki, Y.; Akiyoshi, K. *Chem. Rec. Rec.* **2010**, *10*, 366–376.
- (274) Oh, J. K.; Tang, C.; Gao, H.; Tsarevsky, N. V.; Matyjaszewski, K. *J. Am. Chem. Soc.* **2006**, *128*, 5578–5584.
- (275) Poly, J.; Ibarboure, E.; Le Meins, J.-F.; Rodriguez-Hernandez, J.; Taton, D.; Papon, E. *Langmuir* **2011**, *27*, 4290–4295.
- (276) Huang, H.; Hoogenboom, R.; Leenen, M. A. M.; Guillet, P.; Jonas, A. M.; Schubert, U. S.; Gohy, J. F. *J. Am. Chem. Soc.* **2006**, *128*, 3784–3788.
- (277) Brummelhuis, N. Ten; Schlaad, H. *Polym. Chem.* **2011**, *2*, 1180–1184.
- (278) Ten Brummelhuis, N.; Secker, C.; Schlaad, H. *Macromol. Rapid Commun.* **2012**, 1–5.
- (279) Zschoche, S.; Rueda, J.; Boyko, V.; Krahl, F.; Arndt, K.-F.; Voit, B. *Macromol. Chem. Phys.* **2010**, *211*, 1035–1042.
- (280) Zschoche, S.; Rueda, J. C.; Binner, M.; Komber, H.; Janke, A.; Arndt, K.-F.; Lehmann, S.; Voit, B. *Macromol. Chem. Phys.* **2011**, *213*, 215–226.
- (281) David, G.; Simionescu, B. C.; Albertsson, A.-C. *Biomacromolecules* **2008**, *9*, 1678–1683.
- (282) Adams, N.; Schubert, U. S. *Adv. Drug Deliv. Rev.* **2007**, *59*, 1504–1520.

CHAPTER 2

- (1) Hennink, W. E.; van Nostrum, C. F. *Adv. Drug Deliv. Rev.* **2012**, *64*, 223–236.
- (2) Qiu, Y.; Park, K. *Adv. Drug Deliv. Rev.* **2012**, *64*, 49–60.
- (3) Hoffman, A. S. *Adv. Drug Deliv. Rev.* **2012**, *64*, 18–23.
- (4) Kharkar, P.; Kiick, K.; Kloxin, A. *Chem. Soc. Rev.* **2013**, *42*, 7335–7372.
- (5) Alemán, J.; Chadwick, a. V.; He, J.; Hess, M.; Horie, K.; Jones, R. G.; Kratochvíl, P.; Meisel, I.; Mita, I.; Moad, G.; Penczek, S.; Stepto, R. F. T. *Pure Appl. Chem.* **2007**, *79*, 1801–1829.
- (6) Kabanov, A. V; Vinogradov, S. V. *Angew. Chemie, Int. Ed.* **2009**, *48*, 5418–5429.
- (7) Chacko, R. T.; Ventura, J.; Zhuang, J.; Thayumanavan, S. *Adv. Drug Deliv. Rev.* **2012**, *64*, 836–851.
- (8) Oh, J. K.; Drumright, R.; Siegwart, D. J.; Matyjaszewski, K. *Prog. Polym. Sci.* **2008**, *33*, 448–477.
- (9) Gaulding, J. C.; Smith, M. H.; Hyatt, J. S.; Fernandez-Nieves, A.; Lyon, L. A. *Macromolecules* **2012**, *45*, 39–45.
- (10) Nayak, S.; Lyon, L. A. *Angew. Chemie, Int. Ed.* **2005**, *44*, 7686–7708.
- (11) Oh, J. K.; Lee, D. I.; Park, J. M. *Prog. Polym. Sci.* **2009**, *34*, 1261–1282.
- (12) Sasaki, Y.; Akiyoshi, K. *Chem. Rec.* **2010**, *10*, 366–376.
- (13) Pich, A.; Richtering, W. *Adv. Polym. Sci.* **2011**, *234*, 1–37.
- (14) Hawker, C. J.; Wooley, K. L. *Science* **2005**, *309*, 1200–1205.
- (15) Gauthier, M. A.; Gibson, M. I.; Klok, H.-A. *Angew. Chemie Int. Ed.* **2009**, *48*, 48–58.
- (16) Odian, G. *Principles of polymerization, Fourth edition*; Wiley-interscience John Wiley & Sons, Inc.: Hoboken, New Jersey, 2004; p. 832.
- (17) Albrecht, K.; Moeller, M.; Groll, J. *Adv. Polym. Sci.* **2011**, *234*, 65–93.
- (18) Aoi, K.; Suzuki, H.; Okada, M. *Macromolecules* **1992**, *25*, 7073–7075.
- (19) Barz, M.; Luxenhofer, R.; Zentel, R.; Vicent, M. J. *Polym. Chem.* **2011**, *2*, 1900–1918.
- (20) Knop, K.; Hoogenboom, R.; Fischer, D.; Schubert, U. S. *Angew. Chemie, Int. Ed.* **2010**, *49*, 6288–6308.
- (21) Bauer, M.; Lautenschlaeger, C.; Kempe, K.; Tauhardt, L.; Schubert, U. S.; Fischer, D. *Macromol. Biosci.* **2012**, *12*, 986–998.
- (22) Sedlacek, O.; Monnery, B. D.; Filippov, S. K.; Hoogenboom, R.; Hruby, M. *Macromol. Rapid Commun.* **2012**, *33*, 1648–1662.
- (23) Konradi, R.; Pidhatika, B.; Mühlebach, A.; Textor, M. *Langmuir* **2008**, *24*, 613–616.
- (24) Zhang, N.; Pompe, T.; Amin, I.; Luxenhofer, R.; Werner, C.; Jordan, R. *Macromol. Biosci.* **2012**, *12*, 926–936.
- (25) Konradi, R.; Acikgoz, C.; Textor, M. *Macromol. Rapid Commun.* **2012**, *33*, 1663–1676.
- (26) Waschinski, C. J.; Herdes, V.; Schueler, F.; Tiller, J. C. *Macromol. Biosci.* **2005**, *5*, 149–156.
- (27) Luxenhofer, R.; Han, Y.; Schulz, A.; Tong, J.; He, Z.; Kabanov, A. V; Jordan, R. *Macromol. Rapid Commun.* **2012**, *33*, 1613–1631.
- (28) Kelly, A. M.; Wiesbrock, F. *Macromol. Rapid Commun.* **2012**, *33*, 1632–1647.
- (29) Guillermin, B.; Monge, S.; Lapinte, V.; Robin, J.-J. *Macromol. Rapid Commun.* **2012**, *33*, 1600–1612.
- (30) Chujo, Y.; Sada, K.; Matsumoto, K.; Saegusa, T. *Polym. Bull.* **1989**, *21*, 353–356.
- (31) Chujo, Y.; Sada, K.; Matsumoto, K.; Saegusa, T. *Macromolecules* **1990**, *23*, 1234–1237.
- (32) Hoogenboom, R. *Macromol. Chem. Phys.* **2007**, *208*, 18–25.
- (33) Schenk, V.; Ellmaier, L.; Rossegger, E.; Edler, M.; Griesser, T.; Weidinger, G.; Wiesbrock, F. *Macromol. Rapid Commun.* **2012**, *33*, 396–400.
- (34) Chujo, Y.; Sada, K.; Kawasaki, T.; Ihara, E.; Saegusa, T. *Polym. Bull.* **1993**, *31*, 311–316.
- (35) Rueda, J. C.; Komber, H.; Cedrón, J. C.; Voit, B.; Shevtsova, G. *Macromol. Chem. Phys.* **2003**, *204*, 947–953.
- (36) Wang, C.-H.; Hsiue, G.-H. *J. Polym. Sci. Part A Polym. Chem.* **2002**, *40*, 1112–1121.

- (37) Hartlieb, M.; Pretzel, D.; Kempe, K.; Fritzsche, C.; Paulus, R. M.; Gottschaldt, M.; Schubert, U. S. *Soft Matter* **2013**, *9*, 4693–4704.
- (38) Dargaville, T. R.; Forster, R.; Farrugia, B. L.; Kempe, K.; Voorhaar, L.; Schubert, U. S.; Hoogenboom, R. *Macromol. Rapid Commun.* **2012**, *33*, 1695–1700.
- (39) Chujo, Y.; Sada, K.; Naka, A.; Nomura, R.; Saegusa, T. *Macromolecules* **1993**, *26*, 883–887.
- (40) Chujo, Y.; Yoshifuji, Y.; Sada, K.; Saegusa, T. *Macromolecules* **1989**, *22*, 1074–1077.
- (41) Chujo, Y.; Sada, K.; Saegusa, T. *Macromolecules* **1990**, *23*, 2693–2697.
- (42) Chujo, Y.; Sada, K.; Nomura, R.; Naka, A.; Saegusa, T. *Macromolecules* **1993**, *26*, 5611–5614.
- (43) Chujo, Y.; Sada, K.; Saegusa, T. *Macromolecules* **1990**, *23*, 2636–2641.
- (44) Huang, H.; Hoogenboom, R.; Leenen, M. A. M.; Guillet, P.; Jonas, A. M.; Schubert, U. S.; Gohy, J. F. *J. Am. Chem. Soc.* **2006**, *128*, 3784–3788.
- (45) Brummelhuis, N. Ten; Schlaad, H. *Polym. Chem.* **2011**, *2*, 1180–1184.
- (46) Aoi, K.; Okada, M. *Prog. Polym. Sci.* **1996**, *21*, 151–208.
- (47) Kobayashi, S. *Prog. Polym. Sci.* **1990**, *15*, 751–823.
- (48) Lambermont-Thijs, H. M. L.; van der Woerd, F. S.; Baumgaertel, A.; Bonami, L.; Du Prez, F. E.; Schubert, U. S.; Hoogenboom, R. *Macromolecules* **2010**, *43*, 927–933.
- (49) Van Kuringen, H. P. C.; De La Rosa, V. R.; Fijten, M. W. M.; Heuts, J. P. A.; Hoogenboom, R. *Macromol. Rapid Commun.* **2012**, *33*, 827–832.
- (50) Lambermont-Thijs, H. M. L.; Heuts, J. P. a.; Hoepfener, S.; Hoogenboom, R.; Schubert, U. S. *Polym. Chem.* **2011**, *2*, 313–322.
- (51) Singh, S.; Blöbbaum, J.; Möller, M.; Pich, A. *J. Polym. Sci. Part A Polym. Chem.* **2012**, *50*, 4288–4299.
- (52) Hermanson, G. T. *Bioconjugate techniques, 2nd Ed.*; Elsevier, 2008.
- (53) Steinhilber, B. D.; Sisson, A. L.; Mangoldt, D.; Welker, P.; Licha, K.; Haag, R. *Adv. Funct. Mater.* **2010**, *20*, 4133–4138.
- (54) Kuringen, H. P. C. Van; Lenoir, J.; Adriaens, E.; Bender, J.; Geest, B. G. De; Hoogenboom, R. *Macromol. Biosci.* **2012**, *12*, 1114–1123.
- (55) Pidhatika, B.; Möller, J.; Benetti, E. M.; Konradi, R.; Rakhmatullina, E.; Mühlebach, A.; Zimmermann, R.; Werner, C.; Vogel, V.; Textor, M. *Biomaterials* **2010**, *31*, 9462–9472.
- (56) Kok, C. M.; Rudin, A. *Macromol. Rapid Commun.* **1981**, *2*, 655–659.

CHAPTER 3

- (1) Lazzari, M.; Liu, G.; Lecommandoux, S. *Block copolymers in nanoscience*; Wiley-VCH Verlag GmbH & Co. KGaA: Weinheim, Germany, 2007.
- (2) Schacher, F. H.; Rutar, P. a.; Manners, I. *Angew. Chem. Int. Ed. Engl.* **2012**, *51*, 7898–7921.
- (3) Mai, Y.; Eisenberg, A. *Chem. Soc. Rev.* **2012**, *41*, 5969–5985.
- (4) Blanz, A.; Armes, S. P.; Ryan, A. J. *Macromol. Rapid Commun.* **2009**, *30*, 267–277.
- (5) Gohy, J. *Adv. Polym. Sci.* **2005**, *190*, 65–136.
- (6) Huang, H.; Chung, B.; Jung, J.; Park, H.-W.; Chang, T. *Angew. Chem. Int. Ed. Engl.* **2009**, *48*, 4594–4597.
- (7) Discher, D. E.; Eisenberg, A. *Science* **2002**, *297*, 967–973.
- (8) Huang, J.; Bonduelle, C.; Thévenot, J.; Lecommandoux, S.; Heise, A. *J. Am. Chem. Soc.* **2012**, *134*, 119–122.
- (9) De Oliveira, H.; Thevenot, J.; Lecommandoux, S. *WIREs Nanomed. nanobiotechnol.* **2012**, *4*, 525–546.
- (10) Harada, A.; Kataoka, K. *Macromolecules* **1995**, *28*, 5294–5299.
- (11) Lim, D. W.; Park, T. G. *J. Appl. Polym. Sci.* **2000**, *75*, 1615–1623.

- (12) Molev, G.; Lu, Y.; Kim, K. S.; Majdalani, I. C.; Guerin, G.; Petrov, S.; Walker, G.; Manners, I.; Winnik, M. A. *Macromolecules* **2014**, *47*, 2604–2615.
- (13) Hsiao, M.; Yusoff, S.; Winnik, M. A.; Manners, I. *Macromolecules* **2014**, *47*, 2361–2372.
- (14) McGrath, N.; Schacher, F. H.; Qiu, H.; Mann, S.; Winnik, M. A.; Manners, I. *Polym. Chem.* **2014**, *5*, 1923.
- (15) Gilroy, J. B.; Lunn, D. J.; Patra, S. K.; Whittell, G. R.; Winnik, M. A.; Manners, I. *Macromolecules* **2012**, *45*, 5806–5815.
- (16) Petzetakis, N.; Dove, A. P.; O'Reilly, R. K. *Chem. Sci.* **2011**, *2*, 955.
- (17) Petzetakis, N.; Robin, M. P.; Patterson, J. P.; Kelley, E. G.; Cotanda, P.; Bomans, P. H. H.; Sommerdijk, N. a J. M.; Dove, A. P.; Epps, T. H.; O'Reilly, R. K. *ACS Nano* **2013**, *7*, 1120–1128.
- (18) Petzetakis, N.; Walker, D.; Dove, A. P.; O'Reilly, R. K. *Soft Matter* **2012**, *8*, 7408.
- (19) Sun, L.; Petzetakis, N.; Pitto-barry, A.; Schiller, T. L.; Kirby, N.; Keddie, D. J.; Boyd, B. J.; Reilly, R. K. O.; Dove, A. P. *Macromolecules* **2013**, *46*, 9074–9082.
- (20) Schlaad, H.; Diehl, C.; Gress, A.; Meyer, M.; Levent Demirel, A.; Nur, Y.; Bertin, A. *Macromol. Rapid Commun.* **2010**, *31*, 511–525.
- (21) Hoogenboom, R. *Macromol. Chem. Phys.* **2007**, *208*, 18–25.
- (22) Hoogenboom, R. *Angew. Chemie, Int. Ed.* **2009**, *48*, 7978–7994.
- (23) Adams, N.; Schubert, U. S. *Adv. Drug Deliv. Rev.* **2007**, *59*, 1504 – 1520.
- (24) Luxenhofer, R.; Schulz, A.; Roques, C.; Li, S.; Bronich, T. K.; Batrakova, E. V.; Jordan, R.; Kabanov, A. V. *Biomaterials* **2010**, *31*, 4972–4979.
- (25) Aoi, K.; Suzuki, H.; Okada, M. *Macromolecules* **1992**, *25*, 7073–7075.
- (26) Barz, M.; Luxenhofer, R.; Zentel, R.; Vicent, M. J. *Polym. Chem.* **2011**, *2*, 1900–1918.
- (27) Knop, K.; Hoogenboom, R.; Fischer, D.; Schubert, U. S. *Angew. Chemie, Int. Ed.* **2010**, *49*, 6288–6308.
- (28) Bauer, M.; Lautenschlaeger, C.; Kempe, K.; Tauhardt, L.; Schubert, U. S.; Fischer, D. *Macromol. Biosci.* **2012**, *12*, 986–998.
- (29) Aseyev, V.; Tenhu, H.; Winnik, F. M. *Adv. Polym. Sci.* **2011**, *242*, 29–89.
- (30) Diab, C.; Akiyama, Y.; Kataoka, K.; Winnik, F. M. *Macromolecules* **2004**, *37*, 2556–2562.
- (31) Uyama, H.; Kobayashi, S. *Chem. Lett.* **1992**, *9*, 1643–1646.
- (32) Abulateefeh, S. R.; Spain, S. G.; Aylott, J. W.; Chan, W. C.; Garnett, M. C.; Alexander, C. *Macromol. Biosci.* **2011**, *11*, 1722–1734.
- (33) Katsumoto, Y.; Tsuchiizu, A.; Qiu, X.; Winnik, F. M. *Macromolecules* **2012**, *45*, 3531–3541.
- (34) Meyer, M.; Antonietti, M.; Schlaad, H. *Soft Matter* **2007**, *3*, 430–431.
- (35) Demirel, A. L.; Meyer, M.; Schlaad, H. *Angew. Chem. Int. Ed. Engl.* **2007**, *46*, 8622–8624.
- (36) Diehl, C.; Černoch, P.; Zenke, I.; Runge, H.; Pitschke, R.; Hartmann, J.; Tiersch, B.; Schlaad, H. *Soft Matter* **2010**, *6*, 3784–3788.
- (37) Diehl, C.; Schlaad, H. *Chem. Eur. J.* **2009**, *15*, 11469–11472.
- (38) Morimoto, N.; Obeid, R.; Yamane, S.; Winnik, F. M.; Akiyoshi, K. *Soft Matter* **2009**, *5*, 1597–1600.
- (39) Bloksma, M. M.; Hendrix, M. M. R. M.; Schubert, U. S.; Hoogenboom, R. *Macromolecules* **2010**, *43*, 4654–4659.
- (40) Güner, P. T.; Mikó, A.; Schweinberger, F. F.; Demirel, A. L. *Polym. Chem.* **2012**, *3*, 322–324.
- (41) Rettler, E. F.-J.; Lambermont-Thijs, H. M. L.; Kranenburg, J. M.; Hoogenboom, R.; Unger, M. V.; Siesler, H. W.; Schubert, U. S. *J. Mater. Chem.* **2011**, *21*, 17331–17337.
- (42) Aoi, K.; Okada, M. *Prog. Polym. Sci.* **1996**, *21*, 151–208.
- (43) Kobayashi, S. *Prog. Polym. Sci.* **1990**, *15*, 751–823.
- (44) Odian, G. *Principles of polymerization, Fourth edition*; Wiley-interscience John Wiley & Sons, Inc.: Hoboken, New Jersey, 2004; p. 832.
- (45) Kobayashi, S. *Polymerization of Oxazolines*; Elsevier, 2012; Vol. 4, pp. 397–426.

- (46) Wiesbrock, F.; Hoogenboom, R.; Leenen, M. A. M.; Meier, M. A. R.; Schubert, U. S. *Macromolecules* **2005**, *38*, 5025–5034.
- (47) Aseyev, V.; Tenhu, H.; Winnik, F. M. *Adv. Polym. Sci.* **2011**, *242*, 29–89.
- (48) Park, J. S.; Kataoka, K. *Macromolecules* **2006**, *39*, 6622–6630.
- (49) Huber, S.; Jordan, R. *Colloid Polym. Sci.* **2007**, *286*, 395–402.
- (50) Weber, C.; Hoogenboom, R.; Schubert, U. S. *Prog. Polym. Sci.* **2011**, *37*, 686–714.
- (51) Mirabella, F. M. *J. Polym. Sci. Part B Polym. Phys.* **2001**, *39*, 2800–2818.
- (52) Lee, Y.; Porter, R. S. *Macromolecules* **1987**, *20*, 1336–1341.
- (53) Blundell, D. J. *Polymer*. **1987**, *28*, 2248–2251.
- (54) Yu, T.; Bu, H.; Hu, J.; Zhang, W.; Gu, Q. *Polym. Commun.* **1983**, *1*, 83–91.
- (55) Qiu, J. I. E.; Xu, D.; Zhao, J.; Niu, Y.; Wang, Z. *J. Polym. Sci. Part B Polym. Phys.* **2008**, *46*, 2100–2115.
- (56) Rettler, E. F.-J.; Unger, M. V.; Hoogenboom, R.; Siesler, H. W.; Schubert, U. S. *Appl. Spectrosc.* **2012**, *66*, 1145–1155.
- (57) Erik, F.; Lambermont-Thijs, H.; Kranenburg, J. J. *Mater. Chem.* **2011**, *21*, 17331–17337.
- (58) Litt, M.; Rhal, F.; Roldan, L. G. *J. Polym. Sci. Part A-2 Polym. Phys.* **1969**, *7*, 463–473.
- (59) Chandler, D. *Nature* **2005**, *437*, 640–647.
- (60) Neradovic, D.; Soga, O.; Nostrum, C. Van; Hennink, W. *Biomaterials* **2004**, *25*, 2409–2418.
- (61) Meyer, M.; Schlaad, H. *Macromolecules* **2006**, *39*, 3967–3970.
- (62) Rudin, A.; Choi, P. *The elements of polymer science and engineering, 2nd Edition*; Elsevier: Waltham, USA, 2012; p. 584.

CHAPTER 4

- (1) Hawker, C. J.; Wooley, K. L. *Science* **2005**, *309*, 1200–1205.
- (2) Gauthier, M. A.; Gibson, M. I.; Klok, H.-A. *Angew. Chemie Int. Ed.* **2009**, *48*, 48–58.
- (3) Odian, G. *Principles of polymerization, Fourth edition*; Wiley-interscience John Wiley & Sons, Inc.: Hoboken, New Jersey, 2004; p. 832.
- (4) Boanen, N. K.; Hillmyer, M. A. *Chem. Soc. Rev.* **2005**, *34*, 267–275.
- (5) Tempelaar, S.; Mespouille, L.; Coulembier, O.; Dubois, P.; Dove, A. P. *Chem. Soc. Rev.* **2013**, *42*, 1312–1336.
- (6) Heo, G. S.; Cho, S.; Wooley, K. L. *Polym. Chem.* **2014**, *5*, 3555–3558.
- (7) Ke, X.; Coady, D. J.; Yang, C.; Engler, A. C.; Hedrick, J. L.; Yang, Y. Y. *Polym. Chem.* **2014**, *5*, 2621–2628.
- (8) Singha, N.; Schlaad, H. In *Functional Polymers by Post-Polymerization Modification*; Theato, P.; Klok, H., Eds.; Wiley-VCH Verlag GmbH & Co. KGaA: Weinheim, Germany, 2012; pp. 65–86.
- (9) Gevrek, T. N.; Arslan, M.; Sanyal, A. In *Functional Polymers by Post-Polymerization Modification*; Theato, P.; Klok, H., Eds.; Wiley-VCH Verlag GmbH & Co. KGaA, 2012.
- (10) Kakuchi, R.; Theato, P. In *Functional Polymers by Post-Polymerization Modification*; Theato, P.; Klok, H., Eds.; Wiley-VCH Verlag GmbH & Co. KGaA: Weinheim, Germany, 2012.
- (11) Günay, K. A.; Theato, P.; Klok, H. In *Functional Polymers by Post-Polymerization Modification*; Theato, P.; Klok, H., Eds.; Wiley-VCH Verlag GmbH & Co. KGaA: Weinheim, Germany, 2012; pp. 1–42.
- (12) Mansfeld, U.; Pietsch, C.; Hoogenboom, R.; Becer, C. R.; Schubert, U. S. *Polym. Chem.* **2010**, *1*, 1560–1598.
- (13) Whitmore, F. C.; Herr, C. H.; Clarke, D. G.; Rowland, C. S.; Schiessler, R. W. *J. Am. Chem. Soc.* **1945**, *67*, 2059–2061.
- (14) Klein, D. R. In *Organic chemistry, 2nd edition*; John Wley & Sons Ltd., 2014; p. 1344.

- (15) Liu, N.; Martin, A.; Robert, F.; Vincent, J.-M.; Landais, Y.; Vignolle, J.; Cramail, H.; Taton, D. *Macromolecules* **2014**, *47*, 525–533.
- (16) Hirao, A.; Nakahama, S. *Macromolecules* **1987**, *20*, 2968–2972.
- (17) Taubmann, C.; Luxenhofer, R.; Cesana, S.; Jordan, R. *Macromol. Biosci.* **2005**, *5*, 603–612.
- (18) Yang, S. K.; Weck, M. *Macromolecules* **2008**, *41*, 346–351.
- (19) Alconcel, S.; Kim, S.; Tao, L.; Maynard, H. D. *Macromol. Rapid Commun.* **2013**, *34*, 983–989.
- (20) Sun, G.; Cheng, C.; Wooley, K. L. *Macromolecules* **2007**, *40*, 793–795.
- (21) Li, R. C.; Hwang, J.; Maynard, H. D. *Chem. Commun.* **2007**, 3631–3633.
- (22) Hwang, J.; Li, R. C.; Maynard, H. D. *J. Control. Release* **2007**, *122*, 279–286.
- (23) Wang, S.; Oommen, O.; Yan, H.; Varghese, O. *Biomacromolecules* **2013**, *14*, 2427–2432.
- (24) Lu, C.; Wang, X.; Wu, G.; Wang, J.; Wang, Y.; Gao, H.; Ma, J. *J. Biomed. Mater. Res. A* **2013**, *102*, 628–638.
- (25) Patenaude, M.; Hoare, T. *Biomacromolecules* **2012**, *13*, 369–378.
- (26) Patenaude, M.; Hoare, T. *ACS Macro Lett.* **2012**, *1*, 409–413.
- (27) Patenaude, M.; Campbell, S.; Kinio, D.; Hoare, T. *Biomacromolecules* **2014**, *15*, 781–790.
- (28) Kesselman, L. R. B.; Shinwary, S.; Selvaganapathy, P. R.; Hoare, T. *Small* **2012**, *8*, 1092–1098.
- (29) Hu, X.; Tian, J.; Liu, T.; Zhang, G.; Liu, S. *Macromolecules* **2013**, *46*, 6243–6256.
- (30) Karagoz, B.; Esser, L.; Duong, H. T.; Basuki, J. S.; Boyer, C.; Davis, T. P. *Polym. Chem.* **2014**, *5*, 350.
- (31) Kakuchi, R.; Theato, P. *ACS Macro Lett.* **2014**, *3*, 329–332.
- (32) Aoi, K.; Suzuki, H.; Okada, M. *Macromolecules* **1992**, *25*, 7073–7075.
- (33) Barz, M.; Luxenhofer, R.; Zentel, R.; Vicent, M. J. *Polym. Chem.* **2011**, *2*, 1900–1918.
- (34) Knop, K.; Hoogenboom, R.; Fischer, D.; Schubert, U. S. *Angew. Chemie, Int. Ed.* **2010**, *49*, 6288–6308.
- (35) Bauer, M.; Lautenschlaeger, C.; Kempe, K.; Tauhardt, L.; Schubert, U. S.; Fischer, D. *Macromol. Biosci.* **2012**, *12*, 986–998.
- (36) Aoi, K.; Okada, M. *Prog. Polym. Sci.* **1996**, *21*, 151–208.
- (37) Kobayashi, S. *Prog. Polym. Sci.* **1990**, *15*, 751–823.
- (38) Schlaad, H.; Diehl, C.; Gress, A.; Meyer, M.; Levent Demirel, A.; Nur, Y.; Bertin, A. *Macromol. Rapid Commun.* **2010**, *31*, 511–525.
- (39) Hoogenboom, R. *Macromol. Chem. Phys.* **2007**, *208*, 18–25.
- (40) Hoogenboom, R. *Angew. Chemie, Int. Ed.* **2009**, *48*, 7978–7994.
- (41) Guillerm, B.; Monge, S.; Lapinte, V.; Robin, J.-J. *Macromol. Rapid Commun.* **2012**, *3*, 1600–1612.
- (42) Sedlacek, O.; Monnery, B. D.; Filippov, S. K.; Hoogenboom, R.; Hruby, M. *Macromol. Rapid Commun.* **2012**, *33*, 1648–1662.
- (43) Luxenhofer, R.; Jordan, R. *Macromolecules* **2006**, *39*, 3509–3516.
- (44) Gress, A.; Völkel, A.; Schlaad, H. *Macromolecules* **2007**, *40*, 7928–7933.
- (45) Kempe, K.; Hoogenboom, R.; Schubert, U. S. *Macromol. Rapid Commun.* **2011**, *32*, 1484–1489.
- (46) Cesana, S.; Auernheimer, J.; Jordan, R.; Kessler, H.; Nuyken, O. *Macromol. Chem. Phys.* **2006**, *207*, 183–192.
- (47) Levy, A.; Litt, M. *J. Polym. Sci. Part A-1 Polym. Chem.* **1968**, *6*, 1883–1894.
- (48) Godin, G.; Levrant, B.; Trachsel, A.; Lehn, J.-M.; Herrmann, A. *Chem. Commun.* **2010**, *46*, 3125–3127.
- (49) Levrant, B.; Ruff, Y.; Lehn, J.-M.; Herrmann, A. *Chem. Commun.* **2006**, *28*, 2965–2967.
- (50) Borch, R. F.; Bernstein, M. D.; Dupont Durst, H. *J. Am. Chem. Soc.* **1971**, *93*, 2897–2904.
- (51) Moses, J. E.; Moorhouse, A. D. *Chem. Soc. Rev.* **2007**, *36*, 1249–1262.
- (52) Litt, M.; Levy, A.; Herz, J.; Allied, L. *J. Macromol. Sci. Part A - Chem.* **1975**, *9*, 703–727.
- (53) Cai, G.; Litt, M. *J. Polym. Sci. Part A Polym. Chem.* **1992**, *30*, 649–657.
- (54) Warakomski, J. M.; Thill, B. P. *Polymer.* **1990**, *28*, 3551–3563.

- (55) Hoogenboom, R.; Paulus, R. M.; Fijten, M. W. M.; Schubert, U. S. *J. Polym. Sci. Part A Polym. Chem.* **2005**, *43*, 1487–1497.
- (56) Wiesbrock, F.; Hoogenboom, R.; Abeln, C. H.; Schubert, U. S. *Macromol. Rapid Commun.* **2004**, *25*, 1895–1899.
- (57) Kobayashi, S.; Iijima, S.; Igarashi, T.; Saegusa, T. *Macromolecules* **1987**, *20*, 2–7.

CHAPTER 5

- (1) Devadasu, V. R.; Bhardwaj, V.; Kumar, M. N. V. R. *Chem. Rev.* **2013**, *113*, 1686–1735.
- (2) Dawidczyk, C. M.; Kim, C.; Park, J. H.; Russell, L. M.; Lee, K. H.; Pomper, M. G.; Searson, P. C. *J. Control. Release* **2014**, *187*, 133–144.
- (3) Al-Jamal, W. T.; Kostarelos, K. *Acc. Chem. Res.* **2011**, *44*, 1094–1104.
- (4) Farokhzad, O. C.; Langer, R. *ACS Nano* **2009**, *3*, 16–20.
- (5) Doane, T. L.; Burda, C. *Chem. Soc. Rev.* **2012**, *41*, 2885–2911.
- (6) Muller, R. H.; Keck, C. M. *J. Biotechnol.* **2004**, *113*, 151–170.
- (7) Elsabahy, M.; Wooley, K. L. *Chem. Soc. Rev.* **2012**, *41*, 2545–2561.
- (8) Nicolas, J.; Mura, S.; Brambilla, D.; Mackiewicz, N.; Couvreur, P. *Chem. Soc. Rev.* **2013**, *42*, 1147–1235.
- (9) Smeets, N.; Hoare, T. *J. Polym. Sci. Part A Polym. Chem.* **2013**, *51*, 3027–3043.
- (10) Upadhyay, K. K.; Agrawal, H. G.; Upadhyay, C.; Schatz, C.; Le Meins, J. F.; Misra, A.; Lecommandoux, S. *Crit. Rev. Ther. Drug Carrier Syst.* **2009**, *26*, 157–205.
- (11) De Oliveira, H.; Thevenot, J.; Lecommandoux, S. *WIREs Nanomed nanobiotechnol* **2012**, *4*, 525–546.
- (12) Khandare, J.; Calderón, M.; Dagia, N. M.; Haag, R. *Chem. Soc. Rev.* **2012**, *41*, 2824–2848.
- (13) Liu, G.; An, Z. *Polym. Chem.* **2014**, *5*, 1559–1565.
- (14) Carlsen, A.; Lecommandoux, S. *Curr. Opin. Colloid Interface Sci.* **2009**, *14*, 329–339.
- (15) Aoi, K.; Suzuki, H.; Okada, M. *Macromolecules* **1992**, *25*, 7073–7075.
- (16) Luxenhofer, R.; Sahay, G.; Schulz, A.; Alakhova, D.; Bronich, T. K.; Jordan, R.; Kabanov, A. V. *J. Control. Release* **2011**, *153*, 73–82.
- (17) Kronek, J.; Kroneková, Z.; Lustoň, J.; Paulovičová, E.; Paulovičová, L.; Mendrek, B. *J. Mater. Sci. Mater. Med.* **2011**, *22*, 1725–1734.
- (18) Tong, J.; Luxenhofer, R.; Yi, X.; Jordan, R. *Mol. Pharm.* **2010**, *7*, 984–992.
- (19) Gaertner, F. C.; Luxenhofer, R.; Blechert, B.; Jordan, R.; Essler, M. *J. Control. Release* **2007**, *119*, 291–300.
- (20) Barz, M.; Luxenhofer, R.; Zentel, R.; Vicent, M. *J. Polym. Chem.* **2011**, *2*, 1900–1918.
- (21) Knop, K.; Hoogenboom, R.; Fischer, D.; Schubert, U. S. *Angew. Chemie, Int. Ed.* **2010**, *49*, 6288–6308.
- (22) Bauer, M.; Lautenschlaeger, C.; Kempe, K.; Tauhardt, L.; Schubert, U. S.; Fischer, D. *Macromol. Biosci.* **2012**, *12*, 986–998.
- (23) Sedlacek, O.; Monnery, B. D.; Filippov, S. K.; Hoogenboom, R.; Hruby, M. *Macromol. Rapid Commun.* **2012**, *33*, 1648–1662.
- (24) Luxenhofer, R.; Han, Y.; Schulz, A.; Tong, J.; He, Z.; Kabanov, A.; Jordan, R. *Macromol. Rapid Commun.* **2012**, *33*, 1613–1631.
- (25) Guillerm, B.; Darcos, V.; Lapinte, V.; Monge, S.; Coudane, J.; Robin, J. *Chem. Commun.* **2012**, *48*, 2879–2881.
- (26) Bauer, M.; Lautenschlaeger, C.; Kempe, K.; Tauhardt, L.; Schubert, U. S.; Fischer, D. *Macromol. Biosci.* **2012**, *12*, 986–998.

- (27) Alemán, J.; Chadwick, a.; He, J.; Hess, M.; Horie, K.; Jones, R. G.; Kratochvíl, P.; Meisel, I.; Mita, I.; Moad, G.; Penczek, S.; Stepto, R. F. T. *Pure Appl. Chem.* **2007**, *79*, 1801–1829.
- (28) An, Z.; Qiu, Q.; Liu, G. *Chem. Commun.* **2011**, *47*, 12424–12440.
- (29) Hendrickson, G. R.; Lyon, L. A. *Angew. Chemie, Int. Ed.* **2010**, *49*, 2193–2197.
- (30) Aoi, K.; Okada, M. *Prog. Polym. Sci.* **1996**, *21*, 151–208.
- (31) Kobayashi, S. *Prog. Polym. Sci.* **1990**, *15*, 751–823.
- (32) Legros, C.; De Pauw-Gillet, M.-C.; Tam, K. C.; Lecommandoux, S.; Taton, D. *Polym. Chem.* **2013**, *4*, 4801–4808.
- (33) Lambermont-Thijs, H. M. L.; Van Der Woerd, F. S.; Baumgaertel, A.; Bonami, L.; Du Prez, F. E.; Schubert, U. S.; Hoogenboom, R. *Macromolecules* **2010**, *43*, 927–933.
- (34) Torchilin, V. P. *Handb. Exp. Pharmacol.* **2010**, 3–53.
- (35) Wood, K. C.; Little, S. R.; Langer, R.; Hammond, P. T. *Angew. Chem. Int. Ed. Engl.* **2005**, *44*, 6704–6708.
- (36) Alvarez-Lorenzo, C.; Concheiro, A. *Chem. Commun.* **2014**, *50*, 7743–7765.
- (37) Ramos, J.; Forcada, J.; Hidalgo-Alvarez, R. *Chem. Rev.* **2014**, *114*, 367–428.
- (38) Urakami, H.; Hentschel, J.; Seetho, K.; Zeng, H.; Chawla, Z.; Guan, Z. *Biomacromolecules* **2013**, *14*, 3682–3688.
- (39) Englert, C.; Tauhardt, L.; Hartlieb, M.; Kempe, K.; Gottschaldt, M.; Schubert, U. S. *Biomacromolecules* **2014**, *15*, 1124–1131.
- (40) Lin, C.; Sung, Y.-C.; Hsiue, G.-H. *J. Med. Biol. Eng.* **2011**, *32*, 365–372.
- (41) Knop, K.; Hoogenboom, R.; Fischer, D.; Schubert, U. S. *Angew. Chemie, Int. Ed.* **2010**, *49*, 6288–6308.
- (42) Mero, A.; Pasut, G.; Dalla, L.; Fijten, M. W. M.; Schubert, U. S.; Hoogenboom, R.; Veronese, F. M. *J. Control. Release* **2008**, *125*, 87 – 95.
- (43) Viegas, T. X.; Bentley, M. D.; Harris, J. M.; Fang, Z.; Yoon, K.; Dizman, B.; Weimer, R.; Mero, A.; Pasut, G.; Veronese, F. M. *Bioconjug. Chem.* **2011**, *22*, 976–986.
- (44) Tong, J.; Yi, X.; Luxenhofer, R.; Banks, W. a.; Jordan, R.; Zimmerman, M. C.; Kabanov, A. V. *Mol. Pharm.* **2013**, *10*, 360–377.
- (45) Luxenhofer, R.; Schulz, A.; Roques, C.; Li, S.; Bronich, T. K.; Batrakova, E. V.; Jordan, R.; Kabanov, A. V. *Biomaterials* **2010**, *31*, 4972–4979.
- (46) Peng, K.; Wang, S.; Lee, R. J. *Polym. Sci. Part A Polym. Chem.* **2013**, *51*, 2769–2781.
- (47) Knop, K.; Pretzel, D.; Urbanek, A. *Biomacromolecules* **2013**, *14*, 2536–2548.
- (48) Kempe, K.; Vollrath, A.; Schaefer, H. W.; Poehlmann, T. G.; Biskup, C.; Hoogenboom, R.; Hornig, S.; Schubert, U. S. *Macromol. Rapid Commun.* **2010**, *31*, 1869–1873.
- (49) Lv, H.; Zhang, S.; Wang, B.; Cui, S.; Yan, J. *J. Control. Release* **2006**, *114*, 100–109.
- (50) Moghimi, S. M.; Symonds, P.; Murray, J. C.; Hunter, a C.; Debska, G.; Szewczyk, A. *Mol. Ther.* **2005**, *11*, 990–995.
- (51) Fischer, D.; Bieber, T.; Li, Y.; Elsässer, H. P.; Kissel, T. A novel non-viral vector for DNA delivery based on low molecular weight, branched polyethylenimine: effect of molecular weight on transfection efficiency and cytotoxicity. *Pharmaceutical research*, **1999**, *16*, 1273–1279.
- (52) Van Kuringen, H. P. C.; Lenoir, J.; Adriaens, E.; Bender, J.; De Geest, B. G.; Hoogenboom, R. *Macromol. Biosci.* **2012**, *12*, 1114–1123.
- (53) Van Vlerken, L. E.; Duan, Z.; Seiden, M. V.; Amiji, M. M. *Cancer Res.* **2007**, *67*, 4843–4850.
- (54) Gessner, A.; Lieske, A.; Paulke, B.-R.; Müller, R. H. *J. Biomed. Mater. Res. A* **2003**, *65*, 319–326.
- (55) Gessner, a; Waicz, R.; Lieske, a; Paulke, B.; Mäder, K.; Müller, R. H. *Int. J. Pharm.* **2000**, *196*, 245–249.
- (56) Gessner, A.; Lieske, A.; Paulke, B.; Müller, R. *Eur. J. Pharm. Biopharm.* **2002**, *54*, 165–170.
- (57) Nuhn, L.; Gietzen, S.; Mohr, K.; Fischer, K.; Toh, K.; Miyata, K.; Matsumoto, Y.; Kataoka, K.; Schmidt, M.; Zentel, R. *Biomacromolecules* **2014**, *15*, 1526–1533.
- (58) Woodle, M. C.; Engbers, C. M.; Zalipsky, S. *Bioconjug. Chem.* **1994**, *5*, 493–496.

- (59) Zalipsky, S.; Hansen, C. B.; Oaks, J. M.; Allen, T. M. *J. Pharm. Sci.* **1996**, *85*, 133–137.
- (60) Konradi, R.; Acikgoz, C.; Textor, M. *Macromol. Rapid Commun.* **2012**, *33*, 1663–1676.
- (61) Zhang, N.; Pompe, T.; Amin, I.; Luxenhofer, R.; Werner, C.; Jordan, R. *Macromol. Biosci.* **2012**, *12*, 926–936.
- (62) Kempe, K.; Ng, S. L.; Noi, K. F.; Mu, M.; Gunawan, S. T.; Caruso, F. *ACS Macro Lett.* **2013**, *2*, 1069–1072.
- (63) Farrugia, B. L.; Kempe, K.; Schubert, U. S.; Hoogenboom, R.; Dargaville, T. R. *Biomacromolecules* **2013**, *14*, 2724–2732.
- (64) Zhu, Z.; Li, X. *J. Appl. Polym. Sci.* **2013**, *131*, 39867–39874.
- (65) Naka, K.; Nakamura, T. *Macromol. Chem. Phys.* **1997**, *198*, 101–116.
- (66) Dobrovolskaia, M. a.; McNeil, S. E. *Nat. Nanotechnol.* **2007**, *2*, 469–478.
- (67) Hume, D. A. *Curr. Opin. Immunol.* **2006**, *18*, 49–53.
- (68) Van Furth, R.; Cohn, Z. A.; Hirsch, J. G.; Humphrey, J. H.; Spector, W. G.; Langevoort, H. L. *Bull. World Health Organ.* **1972**, *46*, 845–852.
- (69) Szebeni, J. *Eur. J. Nanomedicine* **2012**, *4*, 33–53.
- (70) Kazatchkine, D.; Cameno, P. *Biomaterials* **1988**, *9*, 30–35.
- (71) Oikonomopoulou, K.; Edimara, S.; Lambris, J. D. In *Encyclopedia of life science*; John Wiley & Sons Ltd.: Chichester, 2012.
- (72) Janeway, C. J.; Travers, P.; Walport, M. *Immunobiology: the immune system in health and disease. 5th edition*; Garland sc.; New York, 2001.
- (73) Gessner, A.; Lieske, A.; Paulke, B. R.; Müller, R. H. *Eur. J. Pharm. Biopharm.* **2002**, *54*, 165–170.
- (74) Harboe, M.; Thorgersen, E. B.; Mollnes, T. E. *Adv. Drug Deliv. Rev.* **2011**, *63*, 976–987.
- (75) Mosqueira, F. C. V.; Legrand, P.; Gulik, A.; Bourdon, O.; Gref, R.; Labarre, D.; Barratt, G. *Biomaterials* **2001**, *22*, 2967–2979.
- (76) Jaskowski, T. D.; Martins, T. B.; Litwin, C. M.; Hill, H. R. *Clin. Diagn. Lab. Immunol.* **1999**, *6*, 137–139.
- (77) North, J.; Whaley, K. In *Encyclopedia of life science*; John Wiley & Sons Ltd.: Chichester, 2001; pp. 1–7.
- (78) Lück, M.; Schröder, W.; Paulke, B.-R.; Blunk, T.; Müller, R. *Biomaterials* **1999**, *20*, 2063–2068.
- (79) Cajot, S.; Lautram, N.; Passirani, C.; Jérôme, C. *J. Control. Release* **2011**, *152*, 30–36.
- (80) Aqil, A.; Vasseur, S.; Duguet, E.; Passirani, C.; Benoît, J. P.; Roch, A.; Müller, R.; Jérôme, R.; Jérôme, C. *Eur. Polym. J.* **2008**, *44*, 3191–3199.
- (81) Vittaz, M.; Bazile, D.; Spenlehauer, G.; Verrecchia, T.; Veillard, M.; Puisieux, F.; Labarre, D. *Biomaterials* **1996**, *17*, 1575–1581.
- (82) Mizrahy, S.; Raz, S. R.; Hasgaard, M.; Liu, H.; Soffer-Tsur, N.; Cohen, K.; Dvash, R.; Landsman-Milo, D.; Bremer, M. G. E. G.; Moghimi, S. M.; Peer, D. *J. Control. Release* **2011**, *156*, 231–238.
- (83) Arpicco, S.; De Rosa, G.; Fattal, E. *J. Drug Deliv.* **2013**, *2013*.
- (84) Dufay Wojcicki, A.; Hillaireau, H.; Nascimento, T. L.; Arpicco, S.; Taverna, M.; Ribes, S.; Bourge, M.; Nicolas, V.; Bochot, A.; Vauthier, C.; Tsapis, N.; Fattal, E. *J. Control. Release* **2012**, *162*, 545–552.
- (85) Wetterö, J.; Askendal, A.; Bengtsson, T.; Tengvall, P. *Biomaterials* **2002**, *23*, 981–991.
- (86) Andersson, J.; Ekdahl, K. N.; Lambris, J. D.; Nilsson, B. *Biomaterials* **2005**, *26*, 1477–1485.
- (87) Hirsh, S. L.; McKenzie, D. R.; Nosworthy, N. J.; Denman, J. a; Sezerman, O. U.; Bilek, M. M. M. *Colloids Surf. B. Biointerfaces* **2013**, *103*, 395–404.
- (88) Vauthier, C.; Persson, B.; Lindner, P.; Cabane, B. *Biomaterials* **2011**, *32*, 1646–1656.
- (89) Alexis, F.; Pridgen, E.; Molnar, L. K.; Farokhzad, O. C. *Mol. Pharm.* **2008**, *5*, 505–515.
- (90) Laemmli, U. *Nature* **1970**, *227*, 680–685.
- (91) De St. Groth, S. F.; Webster, R. G.; Datyner, A. *Biochim. Biophys. Acta* **1963**, *71*, 377–391.
- (92) Danhier, F.; Lecouturier, N.; Vroman, B.; Jérôme, C.; Marchand-Brynaert, J.; Feron, O.; Préat, V. *J. Control. Release* **2009**, *133*, 11–17.

- (93) Garinot, M.; Fiévez, V.; Pourcelle, V.; Stoffelbach, F.; des Rieux, A.; Plapied, L.; Theate, I.; Freichels, H.; Jérôme, C.; Marchand-Brynaert, J.; Schneider, Y.-J.; Préat, V. *J. Control. Release* **2007**, *120*, 195–204.
- (94) Upadhyay, K. K.; Le Meins, J.-F.; Misra, A.; Voisin, P.; Bouchaud, V.; Ibarboure, E.; Schatz, C.; Lecommandoux, S. *Biomacromolecules* **2009**, *10*, 2802–2808.
- (95) Bonduelle, C.; Mazzaferro, S.; Huang, J.; Lambert, O.; Heise, A.; Lecommandoux, S. *Faraday Discuss.* **2013**, *166*, 137–150.
- (96) Physico Filter - iGEM Team TU-Munich <http://2013.igem.org/wiki/index.php?title=Team:TU-Munich/Results/GM-Moss&oldid=361404>.
- (97) Technical bulletin CH50 - Wako Pure Chemical Industries, Ltd. http://www.wako-chemicals.de/DWD/_111327/upload/media_132768.pdf.